2012

Improved performance of alkaline batteries via magnetic modification and voltammetric detection of breath acetone at platinum electrodes

Perry Nelson Motsegood
University of Iowa

IMPROVED PERFORMANCE OF ALKALINE BATTERIES VIA MAGNETIC MODIFICATION AND VOLTAMMETRIC DETECTION OF BREATH ACETONE AT PLATINUM ELECTRODES

by

Perry Nelson Motsegood

An Abstract

Of a thesis submitted in partial fulfillment
of the requirements for the Doctor of
Philosophy degree in Chemistry
in the Graduate College of
The University of Iowa

July 2012

Thesis Supervisor: Associate Professor Johna Leddy

ABSTRACT

Incorporation of magnetic microparticles ($\sim$ 1 μm) at electrode structures increases electron transfer efficiency, observed as increased current, for multiple electrochemical systems. Current increases occur with magnetic field. Inclusion of magnetic materials into the cathode matrix of alkaline MnO_2 batteries requires the materials to be stable in the strong base electrolyte, typically 6 to 9 M KOH. Samarium cobalt magnetic particles sustain strong permanent magnetic fields and are stable in base without surface modification. Studies were undertaken at fast (C/2), moderate (C/3), and slow (C/5) constant current discharges.

Here, alkaline MnO_2 batteries generated increased power and energy when magnetic microparticles are incorporated into the cathode of the battery. Because of anode limitations in the battery, total coulombic output is not increased for the first electron discharge, but the available power and energy is significantly higher compared to nonmagnetic batteries at voltages above 0.9V. Constant current discharge curves of magnetic batteries demonstrate higher voltages than nonmagnetic batteries at a given time, which translates to greater power output. This effect is also observed by electrochemical impedance spectroscopy, where charge transfer resistance is less for magnetically modified cells.

This work also developed voltammetric measurement protocols for acetone concentration collected in the liquid and vapor phase and measured in solution. Acetone on the breath is an indicator for physiological dysregulation. Measurements are demonstrated for acetone concentrations across the human physiological range, 1 μM to 10 mM at platinum electrodes in 0.5 M H_2SO_4. Effects arise through

adsorption of acetone from the gas phase onto a platinum surface and hydrogen in acidic solution within the voltammetric butterfly region. The protocol is demonstrated to yield breath acetone concentration on a human subject within the physiological range and consistent with ketone urine test strip.

Abstract Approved: _____
Thesis Supervisor

_____
Title and Department

_____
Date

IMPROVED PERFORMANCE OF ALKALINE BATTERIES VIA MAGNETIC MODIFICATION AND VOLTAMMETRIC DETECTION OF BREATH ACETONE AT PLATINUM ELECTRODES

by

Perry Nelson Motsegood

A thesis submitted in partial fulfillment
of the requirements for the Doctor of
Philosophy degree in Chemistry
in the Graduate College of
The University of Iowa

July 2012

Thesis Supervisor: Associate Professor Johna Leddy

Graduate College
The University of Iowa
Iowa City, Iowa

CERTIFICATE OF APPROVAL

PH.D. THESIS

This is to certify that the Ph.D. thesis of

Perry Nelson Motsegood

has been approved by the Examining Committee for the thesis requirement for the Doctor of Philosophy degree in Chemistry at the July 2012 graduation.

Thesis Committee:

Johna Leddy, Thesis Supervisor

Mark A. Arnold

Edward G. Gillan

Claudio J. Margulis

Michelle M. Scherer

Always bear in mind that your own resolution to
succeed is more important than any other thing.
~Abraham Lincoln

OR

Success is not final, failure is not fatal:
it is the courage to continue that counts.
~Winston Churchill

ACKNOWLEDGMENTS

I would like to ardently thank Prof. Johna Leddy for her guidance and encouragment to transform a horrible situation into a new opportunity. Without her, I probably would have left The University of Iowa and never have earned the opportunities I now face. I would like to acknowledge the undergraduate students who worked on the battery project: Jen Augello, Jessica Jewett, Jacob Robbins, and Darren Youngs. Recognition goes to Nate Coleman and Andrew Zimmerman for their conversations and assistance with SEM and XRD data acquisition. Gratitude is expressed toward Prof. Petr Vanysek (Northern Illinois University Department of Chemistry) for conversations and instruction on impedance spectroscopy. Resounding thanks goes to the Leddy Group as a whole and specifically toward fellow departmental graduate students Tim Paschkewitz, Mike Ivanov, David Rotsch, Arundhuti Sen, and Kreso Bucar for their friendship and support during my graduate career. For financial assistance, The University of Iowa Graduate College, National Science Foundation, and GM Nameplate (Seattle, WA) are greatly appreciated.

I would like to humbly thank my entire family, especially my wife Jennifer. It is by her grace, patience, and support that I am able to achieve this goal. Finally, to my children Aleksander and Natalia for making me laugh and being a continuous reminder of why this is important.

TABLE OF CONTENTS

LIST OF TABLES

Table

LIST OF FIGURES

Figure

CHAPTER 1

INTRODUCTION

The work presented here covers two different areas of research, alkaline batteries and acetone breath detection. Consequently, this dissertation is written so the reader may easily identify the topics and sections accordingly. The bulk of this work is the development of alkaline batteries and will constitute the majority of this dissertation, while the acetone breath detection is a preliminary effort and is intended as a starting point for future development.

1.1 Alkaline Batteries

Demands for portable power have increased greatly over the past several decades as personal electronic devices proliferate and have become ubiquitous. Batteries serve as the primary power source for such devices. Since its debut in the 1960's, the alkaline $Zn|MnO_2$ battery has become the best selling battery and dominates a multi-billion dollar battery market. Energizer Holdings, Inc., manufacturer of Energizer alkaline batteries, reported the average combined sales of all alkaline batteries over the course of 2009 through 2011 at \$1.3B [1]. Reasons for the success of the alkaline battery are: 1) a long shelf-life, measurable in years, 2) good power output capability, and 3) low production cost. Since the ban on the use of mercury in the 1990's, these batteries are regarded as low toxicity and are consequently considered disposable.

Although the alkaline battery has remained in active production for half a century, active research is on going in all aspects of the battery. Work commonly

focuses on additives for the cathode, porosity control, and better separators [2–4]. Mechanical implementations to vent any evolved hydrogen gas are necessary to better prevent the casing from rupture [5–7]. Research into a rechargeable alkaline battery commonly focuses on the rechargability of the MnO_2 cathode [8–12].

Electrons possess both charge and spin. During an electron transfer, only charge is typically considered. However, the presence of a magnetic field can improve electron transfer kinetics through spin polarization. Leddy and coworkers have demonstrated magnetically enhanced electron transfer events between paramagnetic species as between paramagnetic and diamagnetic species [13–15].

Here, improvements to the alkaline battery via magnetic modification of the MnO_2 cathode are discussed. Incorporation of magnetic material enhances the MnO_2 homogeneous self exchange and heterogeneous electron transfer reactions, which translates to greater electron transfer efficiency in the form of increased current, or energy, and power output.

1.1.1 Basic Electrochemistry Of Zn|MnO_2 Battery

The electrochemistry of the alkaline battery is based on a MnO_2 cathode and a Zn anode. The cathode accepts electrons from the anode and typically consists of MnO_2, graphite, a binder, and KOH electrolyte. The anode donates electrons to the cathode and typically consists of a zinc alloy (that commonly contains some combination of bismuth, indium, and other elements such as calcium and aluminum), a gelling agent, and KOH electrolyte. Concentrations for the KOH electrolyte range between 6 and 9 M. In this battery, zinc is the electron source and is oxidized at the

anode, while MnO_2 is the electron sink and is reduced at the cathode.

There are many allotropes of MnO_2, but the most common form used in commercial battery production is γ-MnO_2. This is a synthetic material generated by electrolytically reducing $MnSO_4$ from hot sulfuric acid [16]. Because of the process by which it is produced, the gamma allotrope is commonly called electrolytic manganese dioxide (EMD).

Reduction of EMD is performed through a two step process [17, 18]. However, the cell voltage is set by the first reduction of MnO_2 to manganese oxyhydroxide, MnOOH, and the oxidation of zinc metal to the zincate ion (Equations 1 and 3).

$$MnO_2 + H_2O + e \rightleftharpoons MnOOH + OH^- \tag{1}$$

$$MnOOH + H_2O + e \rightleftharpoons Mn(OH)_2 + OH^- \tag{2}$$

Zinc is oxidized at the anode.

$$Zn(OH)_2 + 2e \rightleftharpoons Zn + 2OH^- \tag{3}$$

In high pH environments, $Zn(OH)_2$ undergoes transformation to the zincate ion.

$$Zn\left(OH\right)_2 + 2OH^- \rightleftharpoons Zn\left(OH\right)_4^{2-}$$

The overall chemical equation is

$$MnO_2 + Zn + 2H_2O \rightleftharpoons Mn(OH)_2 + Zn(OH)_2 \tag{4}$$

and provides a battery voltage of 1.5 V in commercial batteries. Although the theoretical voltage is actually greater, >1.5 V, this practical value is lower because of nominal self discharge. Consequently, the voltage value often reported commercially

is 1.5 V and allows for voltage loss due to self discharge over the course of a possibly long shelf life. Addition of magnetic particles does not effect the theoretical output voltage or capacity of the battery from a stoichiometric perspective. A more thorough explanation of the electrochemistry of the alkaline battery is found in Chapter 2.

1.1.2 Magnetic Field Effects on Electrochemical Systems

Magnetic fields affect chemical systems through magnetohydrodynamics, which influence mass transport and redox processes [19–23]. Externally applied magnetic fields have been shown to influence systems through gradient fields effects [24–27]. Here, inclusion of permanent magnets into the electrode or applied to the electrode surface minimizes the complexity of such a system and provides a sustained magnetic field at or in close proximity to the electron transfer site.

Redox reactions in electrochemistry involve the transfer of an electron, which fundamentally is a tiny magnet. The presence of a magnetic field prealigns electron spins as the magnetic interacts with the spin polarity of the tiny magnet. This results in improved flux to the electrode surface, observed as greater current. In diffusional systems, the presence of magnetic fields enhances electron transfer kinetics that manifests as increased current [13, 28].

1.1.3 Self Exchange Reactions

A self exchange reaction is an electron transfer reaction between two molecularly

identical species that differ only in their oxidation state.

$$M^n + M^{n+1} \rightleftarrows M^{n+1} + M^n \tag{5}$$

The ionic species, M^n, is an ionic species with a charge n. An electron transfer occurs between M^n and M^{n+1} that results in an effective transposition in space of M^n and M^{n+1}. Many electrochemical reactions involve the transfer of an electron across two phases, called a heterogeneous electron transfer. Self exchange reactions occur within a single phase, called homogeneous reactions. The self exchange reaction rate, k_{ex}, is symmetric in that the forward and reverse rates are equal and the energy of the products and reactants are equal. At high concentration and slow physical transport, self exchange or electron hopping between adjacent moieties enhances current. Electron hopping between manganese species in a confined, near solid state matrix contributes directly to the EMD cathode of an alkaline battery. Here, the effect of increased current based on magnetically enhanced electron transfer kinetics results in greater power output when compared to analogous nonmagnetic systems.

1.2 Acetone Detection on Human Breath

A summary physiological acetone is offered along with a brief discussion of detection methods and electrochemistry.

1.2.1 Brief history

Acetone is a common metabolic byproduct and serves an indicator for various physiological states related to ketosis, such as diabetes, low carbohydrate diet,

and weight loss. In diabetic status, acetone can provide an alternative to glucose monitoring. In hospital settings, the preferred blood measurement is not for glucose but for one of the three ketone bodies, 3-hydroxy-butyrate. The main ketone bodies, 3-hydroxy-butyrate, acetoacetic acid, and acetone are in equilibrium; acetone is the only ketone body that partitions to appreciable extent into the breath from blood. Detection is commonly performed in urine, where acetone concentration in urine lags blood, which tends to skew measurements.

Human breath analysis commonly involves complex instrumentation and sample handling, that includes gas chromatography and mass spectrometry techniques. Here, we report the direct electrochemical detection of acetone at a platinum surface via cyclic voltammetry by competitive acetone adsorption in 0.5 M H_2SO_4.

1.2.2 Conventional Detection Techniques

Detection of acetone is routinely performed by gas chromatography (GC) in lab or clinical quantization. These methods require costly instrumentation and time intensive sample preparation. Blood analysis is often used in clinical settings and offers good accuracy, but is also time intensive. Over the counter methods, such as urine sticks, are quick but generate results that are broadly categorized because visual analysis relies on colorimetric indications.

1.2.3 Electrochemical Acetone Reduction on Platinum

The adsorption of acetone onto a platinum surface has been used to track the mechanistic reduction of acetone to isopropanol and propane [29–31]. Based on these

voltammetric responses, it is reported here that voltammetric breath measurements for acetone provide a calibration curve with over five orders of magnitude in acetone concentration (1 μM to 10 mM). Calibrations were made with head space gases and in solution phase over a range of acetone concentrations. In a healthy, stationary adult, acetone is the sixth most common component on breath and one of the very few that are electroactive under these reductive conditions. The observation of competitive reduction of adsorbed proton versus acetone in the butterfly region of platinum provides a rapid response for the detection of acetone on human breath. Proof of concept measurements are provided with further development needed.

CHAPTER 2

ALKALINE BATTERY SYSTEMS AND MAGNETIC PROPERTIES

A battery is a self contained electrochemical system with finite energy and capacity. They are defined thermodynamically by cell voltage (V), based on the battery redox chemistry, and by electrochemical capacity in amp hours (Ah) or milliamp hours (mAh), that quantifies the electroactive reagents. Thermodynamically, all batteries are governed by the Nernst equation (Equation 6),

$$E = E^{o}_{cell} - \frac{RT}{nF} \ln \left(\frac{C_R}{C_O} \right) \tag{6}$$

where E^{o}_{cell} is the standard cell potential (V), R is the molar gas constant ($J/\left(mol \times K\right)$), T is temperature in Kelvin, n is the number of electrons involved in the reaction, F is Faraday's constant (C/mol), C_O and C_R are the the concentration of oxidized and reduced species, respectively. Capacity of the battery is governed by physical size, where a larger battery contains more electroactive reagents than a smaller battery. For example, a D size battery does not provide greater voltage than a AA size battery of similar chemistry, but lasts longer because it has greater capacity (mAh).

2.1 Alkaline Battery Electrochemistry

As mentioned earlier, the cell voltage is set by thermodynamics and the capacity of the battery is determined by the amount of material present. The following sections explain this relationship in greater detail.

2.1.1 Cell Voltage

For the alkaline battery, the oxidation occurs at the zinc anode and the reduction occurs at the EMD cathode. Characterization of the EMD standard potentials and two step reduction process was performed by Kozawa and coworkers [17, 18, 32–34].

$$\gamma - MnO_2 + e + H_2O \rightleftarrows MnOOH + OH^- \qquad E^0 = 0.36\ V \text{ vs NHE} \tag{7}$$

$$MnOOH + e + H_2O \rightleftharpoons Mn(OH)_2 + OH^- \tag{8}$$

Reduction of EMD occurs in a two step process, where Mn is reduced from the +4 to +3 oxidation state and then to the +2 oxidation state. The first reduction is the more energetic process and the preferred reaction in a commercial battery. The second reduction is made more complex because of multiple allotropes and complexes of manganese(III) oxides, hence the nonspecific allotrope declaration in Equation 7. The allotropes of MnO_2 have different standard potentials for the second electron reduction. A generic electrochemical equation is reported here.

Zinc, under strong alkaline conditions, is oxidized at the anode to form a zincate [35].

$$Zn\,(OH)_4^{2-} + 2e \rightleftarrows Zn + 4OH^- \qquad E^0 = -1.285\ V \text{ vs NHE} \tag{9}$$

Maximum theoretical voltage of a battery can be determined by tabulated half cell reactions.

$$E^o_{cell} = E^o_{cathode} - E^o_{anode} \tag{10}$$

The standard reduction potentials from Equations 7−9 yield the standard cell voltages for the first and second reductions, $E^o_{cell} = +1.645\ V$ and $E^o_{cell} = +0.987\ V$,

respectively. Because of the diminished energy for the second electron reduction of EMD versus zinc, commercial alkaline batteries are designed with zinc as the limiting reagent. This restricts the EMD oxidation to the first electron transfer, as shown in Equation 7.

2.1.2 Battery Capacity

Faraday's Law describes the relationship between the number of electrons (charge) and amount of active material involved in an electrochemical reaction. The passage of 96485.3 C causes 1 equivalent of reaction, meaning 1 mole of reactant is consumed or 1 mole of product is formed during a one electron reaction [35]. This means the relationship between available charge and amount of material is dependent on the molecular weight of the material and the number of electrons transferred during the reaction. Available capacity (Ah) is calculated by

$$\frac{96485.3\ C \times n\ electrons}{molecular\ weight\ \left(\frac{g}{mol}\right)} \times \frac{1\ h}{3600\ s} = \frac{Ah}{g} \tag{11}$$

where n is the number of electrons transferred in the reaction and one Coulomb is one amp second ($A \cdot s$). Charge and capacity values per gram for zinc and MnO_2 electrodes are listed in Table 1.

Table 1. Charge (C/g) and capacity (Ah/g) values for EMD and zinc

Material	n	Molar Mass $\left(\frac{g}{mol}\right)$	Charge $\left(\frac{C}{g}\right)$	Capacity $\left(\frac{Ah}{g}\right)$
MnO_2	1	86.93	1110	0.308
Zinc	2	65.38	2952	0.820

2.1.3 Discharge Current (C rate)

Constant current discharge is used to gauge battery performance. The rate at which the capacity of a battery is discharge over time is called a C rate or capacity rate and is defined by the theoretical capacity of a battery (Ah) per unit time in hours.

$$C \text{ rate} = \frac{theoretical\ capacity\ \ (Ah)}{time\ \ (h)} = A \tag{12}$$

The capacity of each battery varies with the mass of the electroactive active materials. Experimental discharge currents must be individually calculated based on the mass of the electroactive material. Use of C rates allows for batteries with different sizes to be compared in a uniform manner. Notation for C rates is designated by C_n or C/n, where C is the theoretical capacity and n is the number of hours. For example, C/2 means the constant current demand is set so that the theoretical capacity of the battery would discharge in two hours.

For alkaline batteries described here, the total capacity is based on the ratio of zinc and MnO_2 and their respective energetics. As an example, the ratio of EMD in the cathode is 85% by weight (% w/w), with a target cathode mass of 1.0 g. Based on the capacity of MnO_2 in Table 1, the cathode capacity is 0.236 Ah

$$\frac{0.85\ g\ MnO_2}{1\ g\ cathode} \times 0.9 \times \frac{0.308\ Ah}{g\ MnO_2} \times 1.0\ g\ cathode = 0.236\ Ah \tag{13}$$

where the 0.9 term is a purity factor for EMD, which typically contains 90 % MnO_2 and 10 % impurities such as $MnSO_4$ from the manufacturing process.

The anode mass is then back calculated based on the cathode capacity value from Equation 13. Here, the amount of zinc within the anode is set by a stoichiometric

ratio of 10:1 zinc to MnO_2 to ensure the batteries are cathode limited. Based upon the capacity for zinc in Table 1, the mass of an anode containing 70% w/w zinc is

$$0.236\ Ah \times \frac{g\ Zn}{0.820\ Ah} \times \frac{1\ g\ anode}{0.70\ g\ Zn} \times 10 = 4.1\ g\ anode \tag{14}$$

The total capacity is based on the energetics and ratio of the mass of zinc and EMD.

Finally, a battery with an EMD cathode weighing 1.0 g discharged over 5 hours has a $C/5$ rate and the discharge current is calculated based on cathode capacity from Equation 13.

$$\text{Discharge Current} = \frac{0.236\ Ah}{5\ h} = 0.0472\ A = 47.2\ mA \tag{15}$$

Batteries discharged in this work are cathode limited, which means MnO_2 is the limiting reagent and zinc is in excess. This is in direct contrast to commercial batteries where zinc is the limiting reagent. Because MnO_2 is the limiting reagent, here all C rates are calculated based on the capacity of the EMD cathode.

2.1.4 Energy versus Power

Other characteristics of battery performance include energy and power. Energy is an amount of total work available within a system and has units of joules (J). Power is the *rate* at which energy is used and has units of joules per second (J/s). Because the discharge is performed at a constant rate (constant current), the shape of paired voltage and power transients are scaled differently but the curve shapes are the same. Energy is calculated by integrating the area under the curve of a voltage

versus discharge time (Equation 16)

$$Energy\ (J) = \int V(t) \times i dt \tag{16}$$

$$= i \int V(t)\, dt \tag{17}$$

where $V(t)$ is the voltage (J/C) at time t and i is the current in amps (C/s). Equation 17 represents energy versus voltage over time for a constant current discharge. The units reported here are actually J/g EMD or mWh/g EMD because the discharge current is normalized for the mass of EMD (A/g).

2.2 Magnetic Impacts on Electrochemical Systems

Magnetic fields influence electrochemical systems. Leddy and coworkers first reported the enhancement of self exchange rates in the presence of a magnetic field [13]. Increases in the self exchange rates were found to be proportional to the magnetic properties of the redox couple and the strength of the magnetic field. This effect occurs through spin polarization pathways that affect electron transfer rates.

Redox reactions in electrochemistry commonly involve a paramagnetic or radical species as either a reagent, intermediate, or product. Electrons have both spin and charge. During an electron transfer event, both spin and charge must be passed. The magnetic field alters energy and pre-aligns spins, which facilitates electron transfer. The magnetic field couples to the electron spin in processes of electron spin polarization and electron nuclear spin polarization. Electron spin polarization occurs when the spins of unpaired electrons interact with a magnetic field so as to couple; unpaired electrons are on distinct chemical moieties. Electron nuclear

spin polarization occurs when the magnetic field of an unpaired electron induces polarization in the nucleus of an adjacent species. Both spin polarization events are facilitated in an externally applied magnetic field.

From classical transition state theory, the overall rate of reaction is expressed by the Arrhenius equation for a single molecule

$$k = A \exp\left[-\frac{\Delta G^{\ddagger}}{k_b T}\right] \tag{18}$$

where k is the rate (s^{-1}), A is the pre-exponential factor, $\Delta G^{\ddagger}$ is the free energy of activation associated with forming a complex. For example, the reaction of two moieties, A and B to form products is represented on a reaction coordinate diagram as reactants $A + B$ form a complex $[AB]$ at the top of an energy barrier and the complex dissociates and products can be formed.

From the Gibbs equation for an activated complex,

$$\Delta G^{\ddagger} = \Delta H^{\ddagger} - T\Delta S^{\ddagger} \tag{19}$$

where $\Delta H^{\ddagger}$ is the enthalpy of activation and $\Delta S^{\ddagger}$ is the entropy of activation. The height of the barrier is the enthalpy and the width of the barrier is set by the entropy. The classical transition state model can be extended to include magnetic effects on the rates. There are impacts on the enthalpy and the entropy for the rate.

Consider an example of a generic singlet doublet self exchange reaction that relies on electron nuclear spin polarization as provided in Figure 1.

In a self exchange reaction, two charge states of a single species exchange an electron such that the product and reactants are the same but there is a

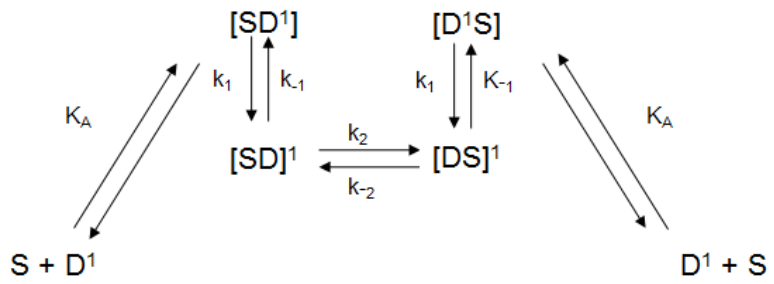

Figure 1. A self exchange reaction includes electron spin polarization between a singlet (S) and a doublet (D). The magnetic field of the electron on the doublet couples to the nuclear spin of the singlet. After the cage complex forms (denoted in square brackets) the complex undergoes electron nuclear spin polarization at rates k_1 and k_{-1}. The rate of the instantaneous electron transfer, k_2 and k_{-2}, is rapid because it is isoenergetic.

transposition in space of the species involved. A singlet (S) and a doublet $\left(\mathrm{D}^{\uparrow}\right.$, where the superscript $\uparrow$ represents the unpaired electron$\left.\right)$ combine to form a complex $\left[\mathrm{SD}^{\uparrow}\right]$ according to a classically defined, electrostatic pre-equilbrium constant, K_A. To account for magnetic effects, it is noted that $\left[\mathrm{SD}^{\uparrow}\right]$ forms at energy slightly above $\Delta H^{\ddagger}$ at $\Delta H^{\ddagger} + gHS\beta$. The Zeeman energy is $gHS\beta$, where the magnetic properties of the electron on the doublet are described by the Lande g-value and the spin of the electron, $S = 1/2$ for the doublet. The magnetic intensity, H, is the magnetic field in a nonmagnetizable matrix and β is the Bohr magneton, a constant. Once formed, the spin of the electron on the doublet polarizes the nuclear spin of the singlet to form $[\mathrm{SD}]^{\uparrow}$ where the notation indicates the electron and nuclear spins are now polarized (coupled) together. The energy of the complex $[\mathrm{SD}]^{\uparrow}$ is lower than the enthalpy of activation by the Zeeman energy as $\Delta H^{\ddagger} - gHS\beta$. The process of conversion by electron nuclear spin polarization $\left[\mathrm{SD}^{\uparrow}\right] \rightleftarrows [\mathrm{SD}]^{\uparrow}$ is expressed with forward and backward rate constants k_1 and k_{-1}, as denoted in

Figure 1. The Figure is a reaction coordinate diagram where the reaction coordinate is the x axis and energy increases up on the y axis. The instant of electron transfer, embedded in rates k_2 and k_{-2}, occurs isoenergetically and thus $k_2 = k_{-2} = 1$. To model self exchange reactions, only steps from the pre-equilibrium to the instant of electron transfer are considered. The rates for k_1 and k_{-1} are explicit rates such that the net rate for electron transfer process is proportional to

$$rate \propto k_1 - k_{-1} \tag{20}$$

where the rates for the electron nuclear spin polarization step are

$$k_1 \propto \exp\left[-\frac{\Delta H^{\ddagger} - gHS\beta}{k_b T}\right] \exp\left[\frac{\Delta S_1^{\ddagger}}{k_b T}\right] \tag{21}$$

$$k_{-1} \propto \exp\left[-\frac{\Delta H^{\ddagger} + gHS\beta}{k_b T}\right] \exp\left[\frac{\Delta S_{-1}^{\ddagger}}{k_b T}\right] \tag{22}$$

Such that, for the entropy unchanged for the forward and reverse steps consistent with electron spins fixed as the cage forms, $\Delta S_1^{\ddagger} = \Delta S_{-1}^{\ddagger}$

$$rate \propto k_1 - k_{-1} \tag{23}$$

$$\propto \exp\left[-\frac{\Delta H^{\ddagger} - gHS\beta}{k_b T}\right] \exp\left[\frac{\Delta S_1^{\ddagger}}{k_b T}\right] - \exp\left[-\frac{\Delta H^{\ddagger} + gHS\beta}{k_b T}\right] \exp\left[\frac{\Delta S_{-1}^{\ddagger}}{k_b T}\right] \tag{24}$$

$$\propto \exp\left[-\frac{\Delta H^{\ddagger}}{k_b T}\right] \exp\left[\frac{\Delta S_1^{\ddagger}}{k_b T}\right] \left(\exp\left[\frac{gHS\beta}{k_b T}\right] - \exp\left[-\frac{gHS\beta}{k_b T}\right]\right) \tag{25}$$

The Zeeman energy is much less than $k_b T$ where k_b is Boltzmann's constant $\left(1.3806568 \times 10^{-23}\,\mathrm{J\,K^{-1}}\right)$, and T is temperature in Kelvin. β is the Bohr magneton $\left(9.2740154 \times 10^{-24}\,\mathrm{J\,T^{-1}}\right)$. Then expansion of the exponentials as

$\lim_{x \longrightarrow 0} e^x \longrightarrow 1 + x$ yields

$$rate \propto k_1 - k_{-1} \tag{26}$$

$$\propto \exp\left[-\frac{\Delta H^{\ddagger}}{k_b T}\right] \exp\left[\frac{\Delta S_1^{\ddagger}}{k_b T}\right] \left(\exp\left[\frac{gHS\beta}{k_b T}\right] - \exp\left[-\frac{gHS\beta}{k_b T}\right]\right) \tag{27}$$

$$\propto \exp\left[-\frac{\Delta H^{\ddagger}}{k_b T}\right] \exp\left[\frac{\Delta S_1^{\ddagger}}{k_b T}\right] \left(1 + \frac{gHS\beta}{k_b T} - \left(1 - \frac{gHS\beta}{k_b T}\right)\right) \tag{28}$$

$$rate \propto \frac{2gHS\beta}{k_b T} \exp\left[-\frac{\Delta H^{\ddagger}}{k_b T}\right] \exp\left[\frac{\Delta S_1^{\ddagger}}{k_b T}\right] \tag{29}$$

Because $k_1 - k_{-1}$ is explicitly included, the net rate for the electron transfer is proportional to the Zeeman energy. Thus, the rates are strongly impacted by magnetic properties of the redox probe and the applied field. There are additional prepolarization steps that occur before the formation of the complex. These effect both entropy and enthalpy for the electron transfer process. Increases in self exchange rates with magnetic field and magnetic properties of the redox species are well established experimentally [13, 15].

2.2.1 Dahms Ruff Model

Every electrochemical reaction involves the exchange of at least one electron between molecular or ionic species. Reactants that are the same species but differ only in oxidation states undergo a self exchange reaction, $M^n + M^{n+1} \rightleftarrows M^{n+1} + M^n$ [36]. Self exchange reactions enhance measured diffusion coefficients under conditions of high concentration and slow physical diffusion. The increase in observed diffusion coefficient arises from an electron passed between M^n and M^{n+1} such that the two species are spatially transposed. Enhanced diffusion coefficients are observed for

self exchange reactions for transition metal complexes concentrated in ion exchange polymers, such as Nafion® (DuPont), where physical mobility is constrained and ion cation concentrations are high [13–15, 37, 38].

Dahms and Ruff developed a model for enhanced current observed in diffusion limited systems [39–42]. In such systems, the observed diffusion coefficient is set by the physical diffusion, D_{phys}, and the self exchange diffusion coefficient, D_{et} (Equation 30).

$$D_{obs} = D_{phys} + D_{et} \tag{30}$$

The self exchange diffusion coefficient is described as

$$D_{et} = \frac{1}{6} k_{ex} \delta^2 C_o^* \tag{31}$$

where k_{ex} is the self exchange rate, δ is the center to center distance of the reactants, C_o^* is the concentration of the redox couple. D_{et} is also described as a hopping diffusion coefficient. The Dahms Ruff Model for a self exchange reaction is

$$D_{obs} = D_{phys} + \frac{1}{6} k_{ex} \delta^2 C_o^* \tag{32}$$

In slow transport systems, physical diffusion becomes highly constrained, such that $D_{phys} \rightarrow 0$, and the observed diffusion coefficient becomes more dependent upon the self exchange rate.

$$D_{obs} \longrightarrow \frac{1}{6} k_{ex} \delta^2 C_o^* \tag{33}$$

In high concentration systems, the impact of self exchanged is further enhanced. Because k_{ex} is proportional to $gHS\beta$ (Equation 29), an externally applied magnetic

field manifests as higher diffusion coefficients and thus larger current.

2.3 MnO_2 Allotropes and Lattice Structures

There are multiple allotropes for MnO_2, but the three types referred in this work are pyrolusite (β-MnO_2), ramsdellite, and electrolytic MnO_2, EMD, (γ-MnO_2). The latter is so named because of the manufacturing process for which it's named. EMD is generated by electrochemically reducing $MnSO_4$ in hot, dilute H_2SO_4 [16]. Although a naturally occurring γ-MnO_2 is available, it is generally not used in commercial processes because of its lower purity. The gamma form is comprised of ramsdellite and pyrolusite structures. De Wolff described the lattice structure of nsutite as predominately being ramsdellite with random intergrowth of pyrolusite formations [43] See Figure 2.

2.3.1 Pyrolusite

Pyrolusite is a rutile compound essentially comprised of infinite MnO_6 octahedral chains and the most stable form of MnO_2 [44]. Unit cells align along the c axis by connecting opposite edges of octahedra. Extension of this lattice is performed by sharing O atoms. The extended chains form 1×1 channels within the crystal lattice (Figure 2A) creating narrow channels or cavities, which are generally not large enough for adequate permeation by water or hydrated ions.

2.3.2 Ramsdellite

Ramsdellite is a dimorph of pyrolusite and is an unstable form of MnO_2, which

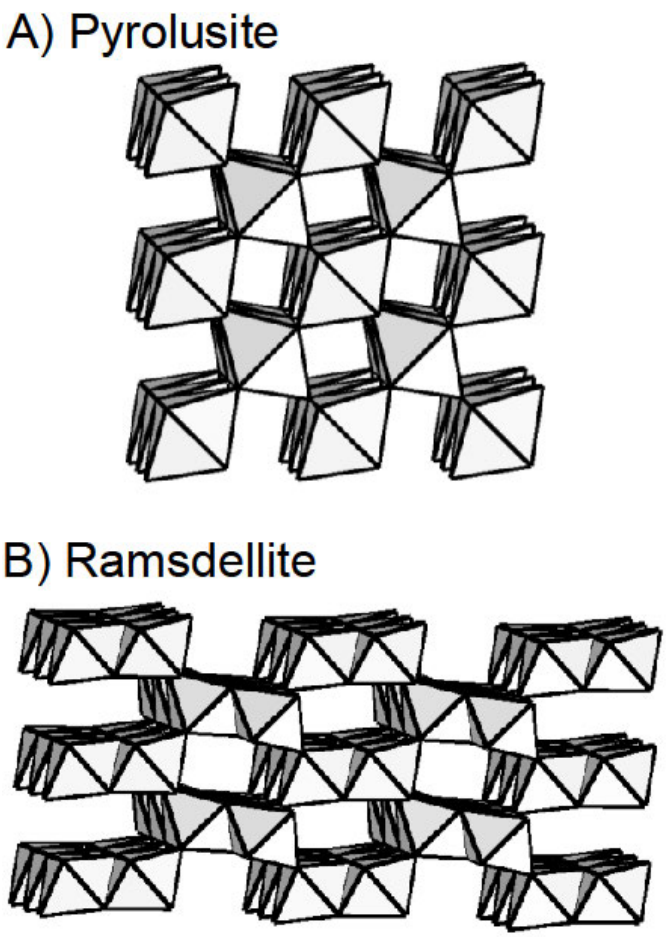

Figure 2. Space filling drawings of MnO_2 allotropes. The pyrolusite (A) lattice contains a 1×1 channel while the ramsdellite (B) lattice is comprised of a 1×2 channel. EMD (γ-MnO_2) is predominately the ramsdelite form with random insertions of pyrolusite.

easily converts to pyrolusite by heating at $\sim 300\ ^oC$ [45, 46]. Unit cells consist of MnO_6 octahedra but are double in width to pyrolusite (Figure 2B). Extension of the lattice is still performed by sharing O atoms at the corners similar to pyrolusite. The extended chains for 2×1 channels that form channels suitable for water permeation. Ramsdellite is chemically reversible between MnO_2 $\left(Mn^{+4}\right)$ and MnOOH $\left(Mn^{+3}\right)$. Unfortunately, ramsdellite is a rare allotrope.

2.3.3 Nsutite and Electrolytic MnO_2

Nsutite is a naturally occurring form of γ-MnO_2, named for the Nsuta region of Ghana in Western Africa. Electrolytic MnO_2 is a synthetic form of γ-MnO_2 generated from the electrochemical reduction of $MnSO_4$ in hot dilute H_2SO_4 [47]. Because of global industrial requirements, generation of the electrolytic form is the major production process. The crystal structure is predominately ramsdellite with random intergrowth of pyrolusite [43, 48]. EMD contains 2×1 channels that serve as permeation pathways for water as observed in ramsdellite. Electrochemical reduction of EMD involves proton insertion into the lattice to form MnOOH (Equation 7) [18, 33]. Consequently, permeation of water in the wider ion channels is essential to obtain the higher conversion of bulk cathode material.

2.3.4 Magnetic Susceptibility

Manganese dioxide contains a Mn^{+4} ion, which has a d^3 electron configuration. In the reduction of MnO_2 to MnOOH (Equation 7), manganese is reduced to Mn^{+3} and has a d^4 electron configuration. Magnetic properties of the various manganese

oxides in various oxidation states are reported in Table 2. All reported species are paramagnetic. They respond to an external magnetic field, but will not maintain a magnetic field for extended periods once the external field dissipates.

Table 2. Magnetic susceptibilities of manganese dioxides allotropes.

Common Name	Compound	Structure Type	n in $3d^n$	χ_m $\frac{\times 10^{-6}}{(cm^3 mol^{-1})}$	Reference
Pyrolusite	β-MnO_2	Rutile	3	2280	[49]
EMD	γ-MnO_2	Intergrowth	3	3440	[50]
Hausmannite	Mn_3O_4	Spinel (normal)	4.5	12400	[49]
	Mn_2O_3		4	14100	[49]
Pyrochroite	$Mn(OH)_2$	$Cd(OH)_2$	5	13500	[49]

Recreated from [51].

2.4 Experimental

This section discusses the general procedures and parameters employed for the alkaline batteries presented in this work. Specific detail that account for alterations in procedure, composition, or configuration specifications are found in Chapters 3 and 4.

2.4.1 Materials

Battery grade materials were used when available, with major components, EMD and zinc, being obtained from leading battery material suppliers. Data presented in Chapters 3 and 4 represent two different configurations. Although the active reagents were the same in both cases, supplemental materials, such as gelling and binding agents and graphite, differ. The goal was to generate batteries similar to industrial products. All reagents were in powder form and used as received. Powders

were mixed together in a vial and then rotated in a tumbler to ensure homogeneity.

EMD (TXL grade) was obtained from Delta EMD (South Africa). Powder X-ray diffraction was used to confirm composition (Figure 3) as a quantitative method to demonstrate the existence of ramsdellite and pyrolusite domains. Battery grade zinc alloy was obtained from Umicore (p/n BIA 100 200 65 d175, Belgium), which contains small amounts of bismuth (100 ppm), indium (200 ppm), and aluminum (65 ppm). Zinc oxide was obtained from Strem Chemicals (p/n 93-3017). Potassium hydroxide, 40% w/w with deionized water, was mixed fresh from solid, flaked technical grade stock purchased from Fisher Scientific (p/n P246-3). Deionized water was generated with a Milli-Q Plus filtration system from Millipore. REacton® grade samarium cobalt ($SmCo_5$) was obtained from Alfa Aesar (p/n 42732). Graphite was obtained from Sigma-Aldrich (p/n 282863) and Alfa Aesar (conductive grade, p/n 40798). Cathode binding agents used in this work included polytetrafluoroethylene (PTFE) and a polyvinylidene fluoride (PVDF) and were obtained from Sigma-Aldrich (p/n 43-0935) and Arkema Inc $\left(\text{Kynar}^{®}\ \text{HSV900}\right)$, respectively. Two anodic gelling agents were used, carboxymethyl cellulose (Sigma-Aldrich p/n 4192373) and Carbopol® 940 (Lubrizol), a powder polyacrylate.

2.4.2 Powder X-ray Diffraction

Characterization EMD was performed by powder x-ray diffractometry merely to verify the presence of ramsdellite and pyrolusite domains. See Figure 3. Data was collected with a Siemens D5000 Powder X-ray Diffractometer scanning with

Cu Kα radiation (40kV and 30 mA) from 10^o to 80^o 2Θ, with a step size of 0.05^o and a step scan time of 6 seconds. Simulated data was generated with PowderCell (version 2.3), which is a free shareware X-ray powder diffraction software package capable of structure visualization and modification. Experimental powder diffraction data are compared to simulated powder diffraction data generated from tabulated crystal structure data [52]. Characteristics of both ramsdellite and pyrolusite are observed, with more ramsdellite character present. This material was used without modification for all battery experiments.

2.4.3 Scanning Electron Microscopy

Images of the particle sizes for EMD and zinc were obtained with a Hitachi 3400N scanning electron microscope. Particle sizes were verified to the certificate of analysis specifications. These materials were used as received.

2.4.4 Battery Assembly Procedure

Battery assembly involved mixing and pressing the cathode powder into a pellet and mixing the anode reagents to form a gel. The half cell components were then assembled into a whole cell battery.

2.4.4.1 Cathode Formation

Cathodic materials including KOH were mixed in a 20 mL scintillation vial for each configuration. See Chapters 3 and 4 for specific ratios. Because KOH clumps the powdered mixture together, two borosilicate glass beads, 0.25 inch diameter,

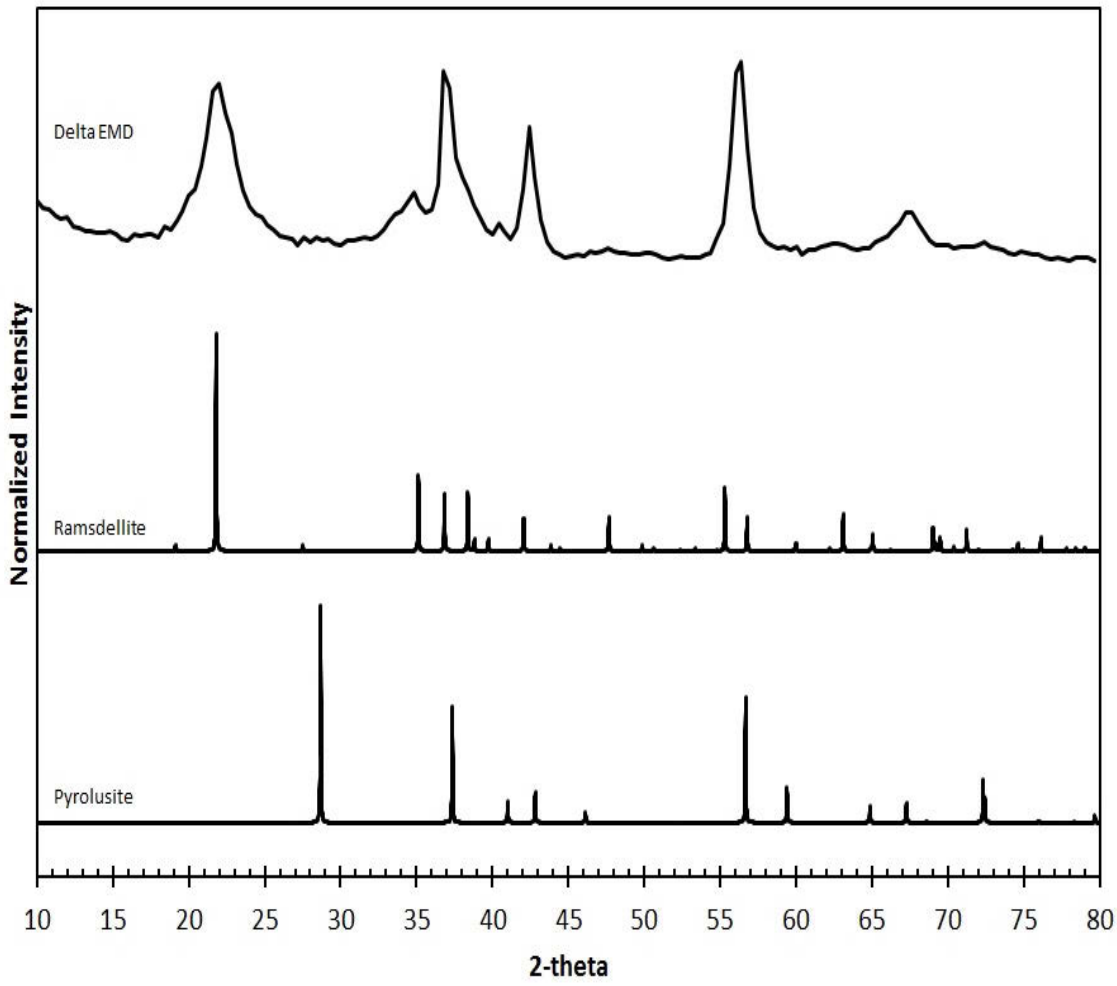

Figure 3. Powder X-ray diffraction (Cu K_α) overlay of experimental and simulated patterns for MnO_2 allotropes. Data for Delta EMD were signal averaged over 6 seconds and normalized to the maximum peak intensity. Simulated data was generated with the program Powder Cell (version 2.3). The Delta EMD shows characteristics of both ramsdelite and pyrolusite, which was used without modification. No evidence of crystalline $MnSO_4$ (anhydrous) or $MnSO_4 \bullet 5H_2O$ was observed within this pattern based on respective crystal structure data [53, 54].

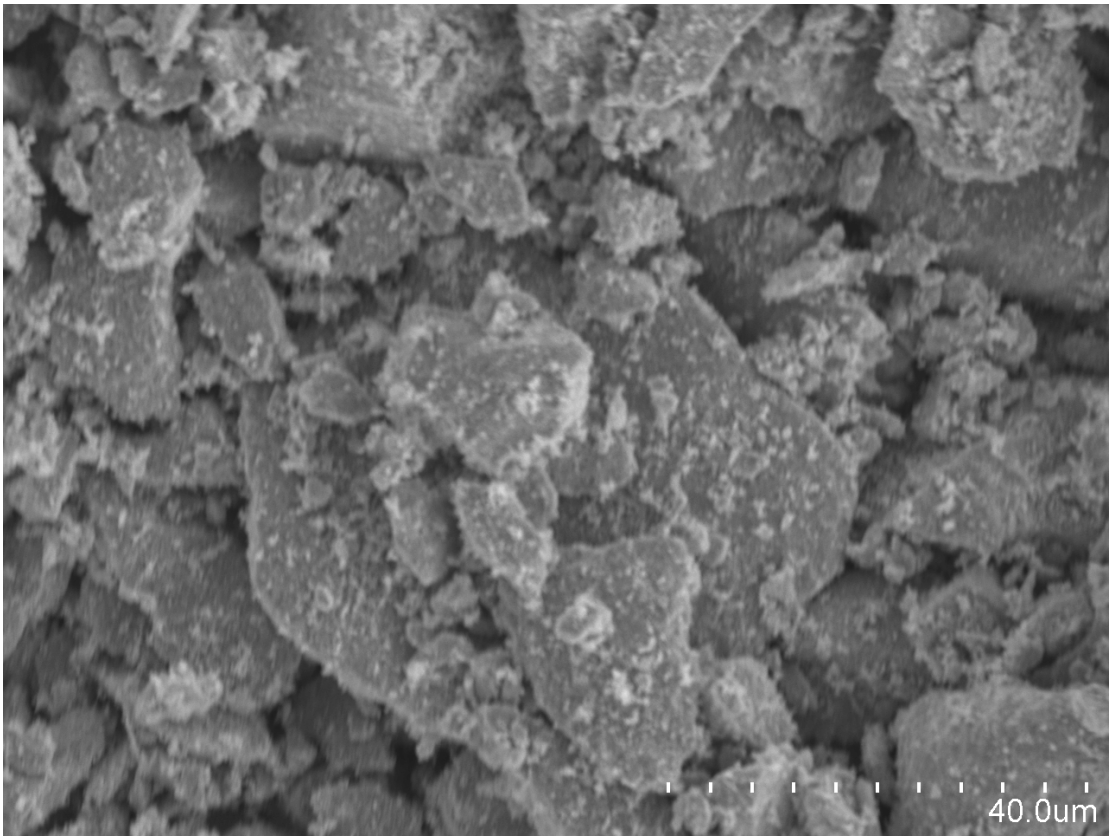

Figure 4. Scanning electron microscopic image of EMD obtained from Delta EMD, TXL grade.

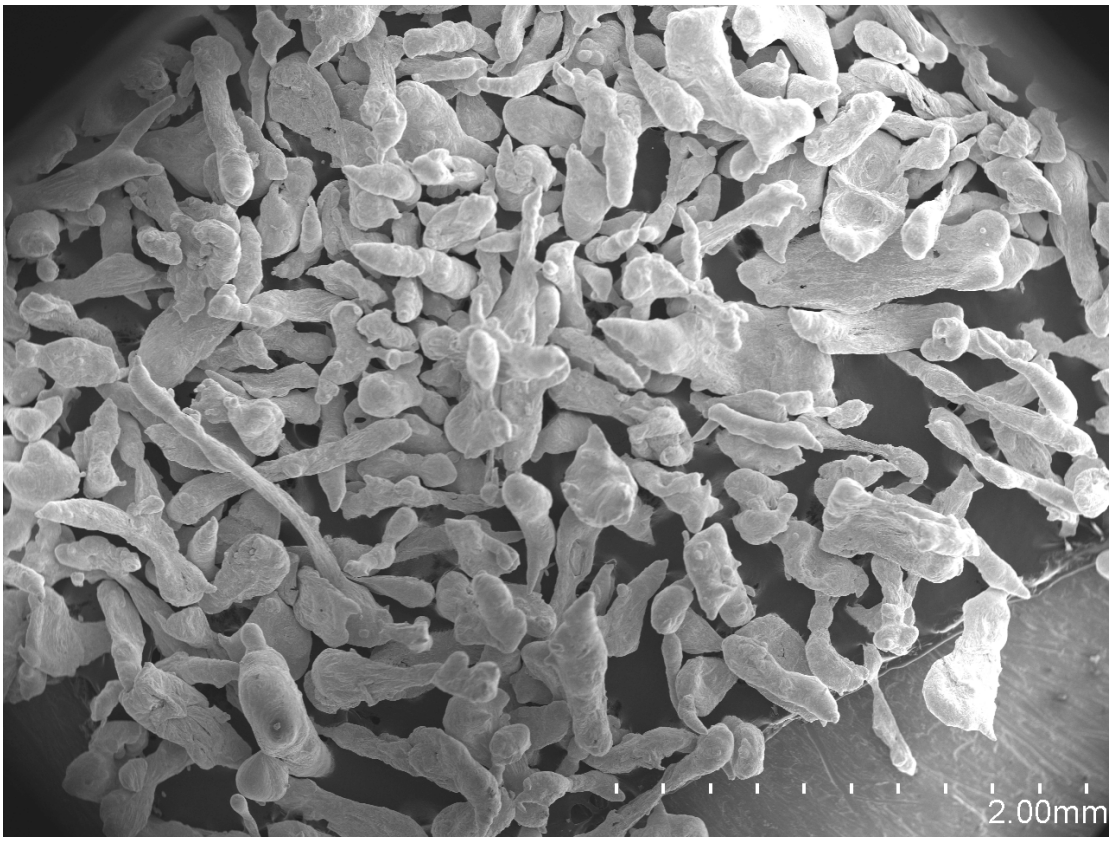

Figure 5. Scanning electron microscopic image of battery grade zinc obtained from Umicore.

(McMaster-Carr, p/n 8996K25) were placed into the vial. The vial was then placed in an in-house built tumbler and rotated for 24 hours at $\sim 60\ rpm$. Cathode powder was then allowed to rest up to an additional 24 hours to allow for permeation of KOH into the EMD crystal lattice. A pellet was formed by placing a weighed aliquot of cathode powder into a pressing die, machined in house (Figure 6). The die is placed in a hydraulic press (Carver, Inc., Model C) and a force is applied. Pressure was then released and the newly formed pellet was removed from the die, weighed, and magnetized (if applicable) prior to use. Two different pressing procedures were developed and are specified in Chapters 3.1.1 and 4.1.1.

2.4.4.2 Cathodic Magnetization

A magnetic field was sustained within the cathode with samarium cobalt ($SmCo_5$) particles, which were blended into the cathode powder mixture as described in the previous section. The pressed pellet was magnetized by centering the pellet within a magnetic field from a NdFeB ring magnet ($3"o.d. \times 2"i.d. \times 0.5"height$). The $SmCo_5$ particles were magnetically saturated for 5 minutes and the pellet was assembled with a zinc anode to complete the battery.

2.4.4.3 Anode Formation

A zinc paste was mixed from battery grade zinc alloy, zinc oxide, gelling agent, and KOH. The specific composition of the anode gels used for discharge experiments are listed in Chapters 3 and 4.

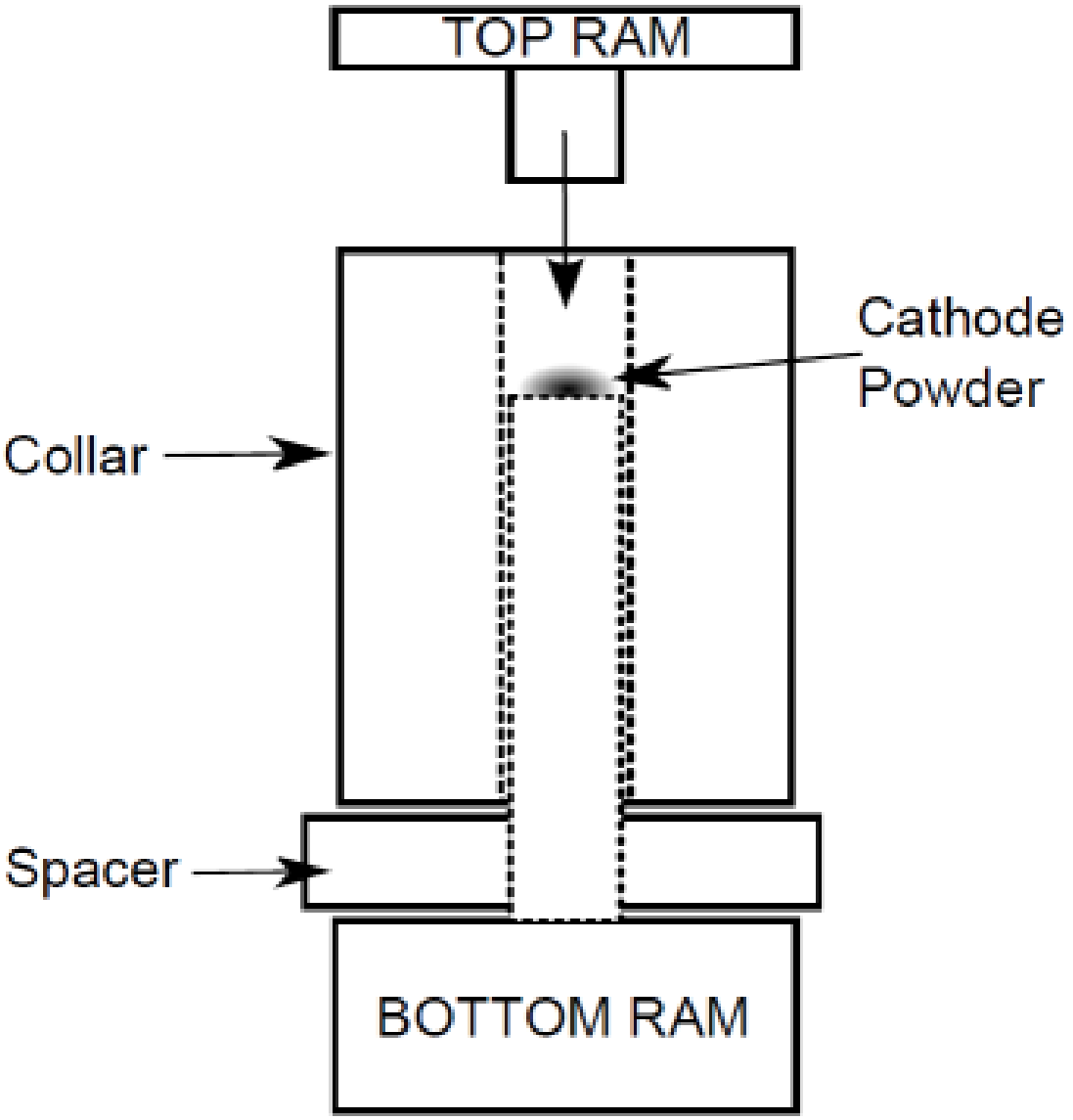

Figure 6. Diagram of the pressing die used to generate EMD cathode pellets. Cathode powder is placed in the chamber between the top and bottom ram. A pellet is formed when the die is placed within a hydraulic press and an external force applied. Removal of the pellet occurs by removal of the top ram and spacer, then the collar is lowered to expose the newly formed pellet. Dimensions are: 8 mm i.d., 24.5 mm o.d., 9.2 mm top ram piston length, 36.7 mm bottom ram piston length, and a spacer height of 9.5 mm.

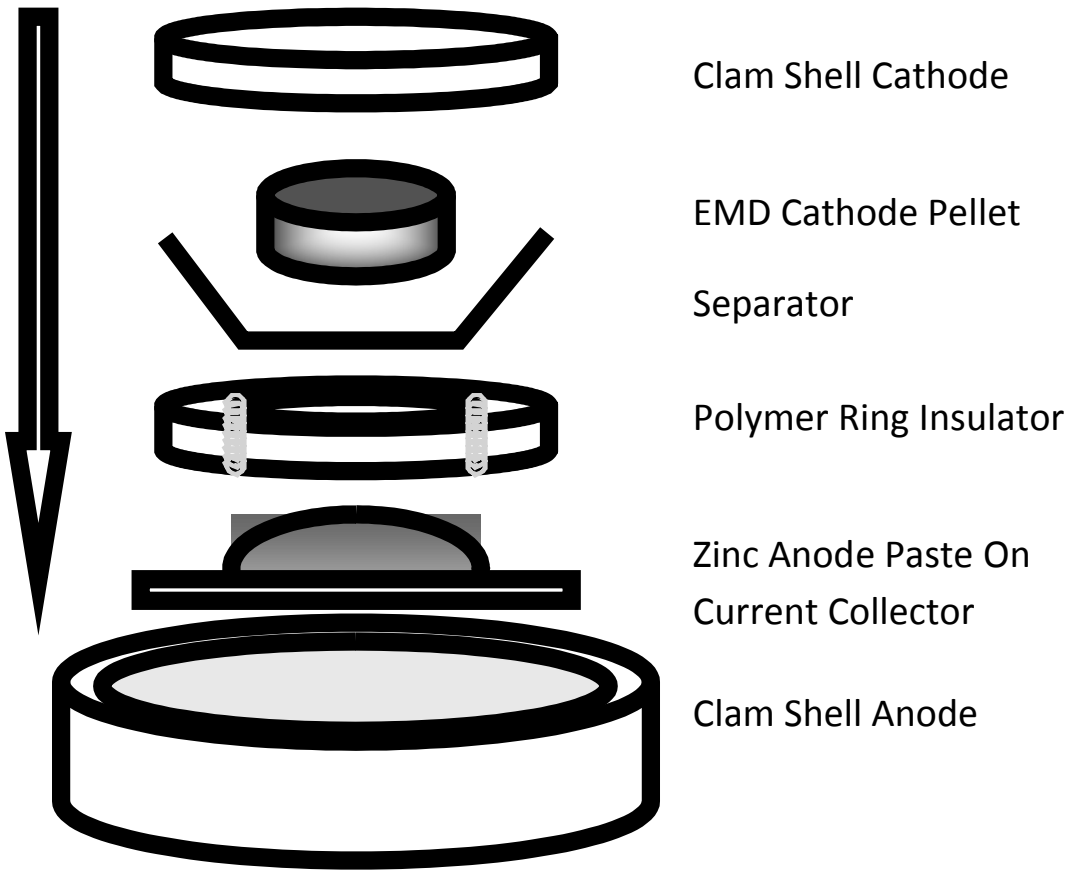

Figure 7. Exploded diagram of an alkaline battery assembled within a stainless steel clamshell casing. The outer diameter of the nylon insulator ring is 29 mm and matches the inner diameter of the anode. The inner diameter of the insulator ring is is 19 mm and matches the outer diameter of the cathode current collector. The entire assembly is held intact by wing nuts torqued to finger tightness.

2.4.4.4 Assembly and Testing Apparatus

A clam shell style battery cannister (MTI Corporation) was used to house the two half cells. Assembly (illustrated in Figure 7) consisted of a stainless steel apparatus insulated to maintain electrical separation of the anode and cathode. A thin disposable copper plate (0.127 mm thick, Strem Chemicals) served as the anodic current collector and electrical contact to the clam shell. The zinc paste rested directly on a copper plate and completed the anode portion of the battery. A nylon ring (29 mm $o.d.$ $\times$ 19 mm $i.d.$) was then placed around the anode to maintain electrical insulation. Two layers of a cellulose based separator were wetted with 100 μL of KOH electrolyte and served as the charge separator between the anode and cathode. The EMD cathode pellet was placed on top of the separator and then forced inside the insulating ring to achieve contact with the separator. The clam shell cathode was then secured into place to complete the battery. A computer-controlled battery analyzer (MTI Corporation), with independent channel capability, measured voltage and current separately for up to eight batteries. Batteries were discharged at constant C-rates based on individual theoretical maximum capacity according to the amount of EMD within the cathode. To ensure the system quantified only cathodic effects, battery capacities were controlled by designating the cathode (EMD specifically) as the limiting reagent. Excess zinc in the anode was stoichiometrically ten times greater than the amount of EMD in the cathode.

2.5 Techniques

Two techniques were employed to analyze the batteries. Primary evaluation was performed under constant current discharge, also called constant current chronopotentiometry. Secondary evaluation was performed with electrochemical impedance spectroscopy. The following section provides a brief summary of each.

2.5.1 Chronopotentiometry

Batteries are commonly discharged by chronopotentiometric methods, where current is demanded (i.e., circuit load) and the voltage response recorded. Constant current chronopotentiometry is used to monitor discharge performance of a battery by demanding a set discharge value and monitoring the voltage output. This technique can also be applied to charge a battery over time when applicable. All work presented here utilizes chronopotentiometry to provide a constant current discharge.

During a constant current chronopotentiometric step (Figure 8), current is initially set to zero and no electrons are transferred, meaning no reaction occurs. A current is then either applied or demanded, which begins to charge or discharge a battery, respectively. For the primary alkaline battery, a negative current is demanded and the battery is discharged.

Performance of a battery is then evaluated as voltage vs time (Figure 9) Under zero current conditions ($t < 0$), a battery sits at rest and no reaction occurs. The potential measured is called the open circuit voltage (OCV), and is a metric to

evaluate whether the cell approaches its thermodynamic value. At $t = 0$, a current is demanded and the battery begins to discharge. The potential measured when the circuit is closed at $t = 0$ is called the closed circuit voltage (CCV) and is a metric to evaluate the kinetic capabilities of the system for the demanded current. A small gap between the CCV and the OCV indicates better battery performance. At values of $t > 0$, the voltage is roughly approximated by the Nernst equation (Equation 6). The dashed line at +0.8 V represents the stoichiometric cutoff voltage between the first and second electron transfers for Mn^{+4} to Mn^{+3} and Mn^{+3} to Mn^{+2} (Equations 7 and 8). A commercial battery generally considered spent at values below +1.0 V.

2.5.2 Impedance Spectroscopy

Electrochemical impedance spectroscopy (EIS) is an electrical measurement capable of evaluating the electrochemical behavior of an electrode or system. Impedance is measured by applying a single frequency voltage to an interface or system and measuring the phase shift and amplitude of the resulting current at that frequency [55]. An alkaline battery contains multiple categories commonly found in electrochemical systems: electrode-electrolyte interfaces, reaction kinetics, mass transport, and electrode passivation. Because this technique is often employed to study electrochemical interfaces, corrosion, and system impedance, it is has become a valuable tool for the power generation community.

Application towards battery performance involves several key aspects: solution (electrolyte) resistance, charge transfer kinetics, double layer capacitance, and mass transport (diffusion). These components are present in every battery and impact

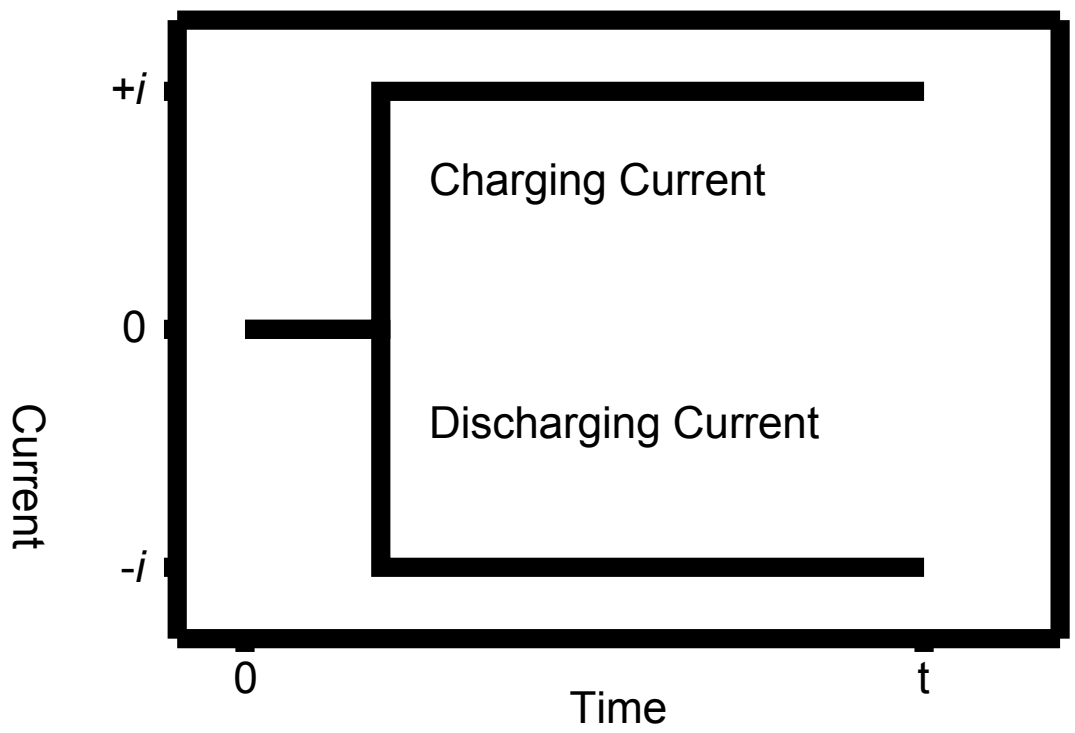

Figure 8. Illustration of current wave form for chronopotentiometry. Current is demanded from the battery during discharge and applied to a battery during charging. Because of electrical circuit convention, the signs for current are negative for discharging and positive for charging.

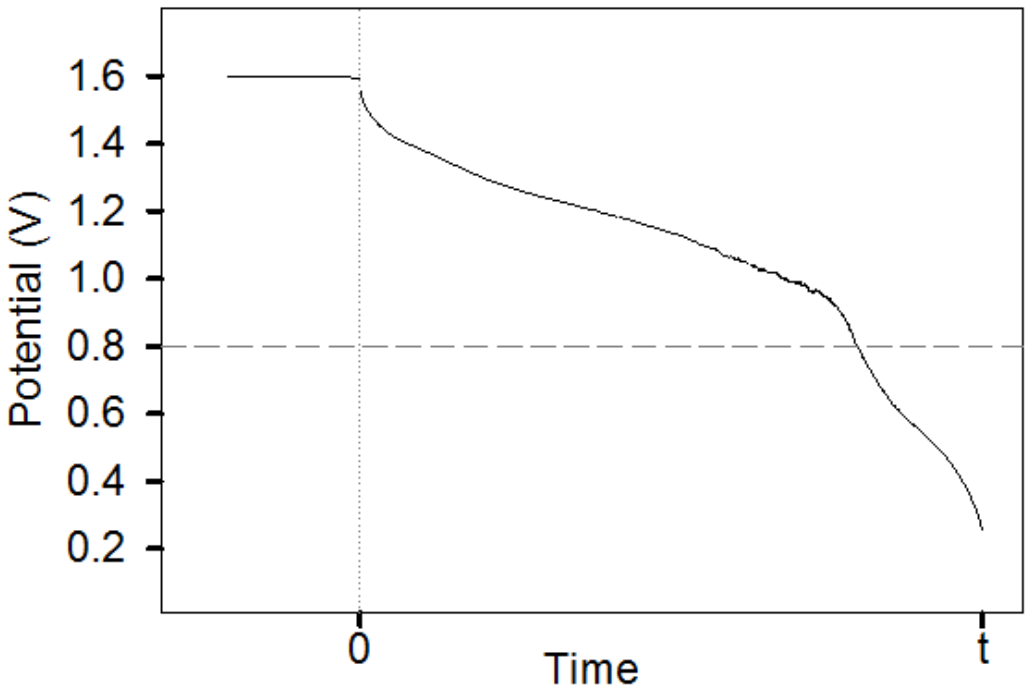

Figure 9. Example discharge curve for alkaline batteries. Prior to $t = 0$ (vertical dotted line), no current is demanded and the system is at rest and an open circuit voltage is measured. At $t = 0$, a current is demanded (closed circuit voltage) and the voltage decreases over time. The horizontal dashed line (gray) represents the voltage cutoff of the first electron reduction of Mn^{+4} to Mn^{+3} and the beginning of the second electron transfer of Mn^{+3} to Mn^{+2}.

battery performance differently over the course of a discharge. The Randles circuit is an equivalent circuit model for a single step charge transfer reaction that involves diffusion, Figure 10A [56]. The components of a Randles circuit include: solution resistance, R_s, double layer capacitance, C_{dl}, charge transfer resistance, R_{ct}, and mass transport behavior represented by the Warburg component, Z_w. A Nyquist plot represents the complex plane (-Z") versus the real plane (Z') measurements, Figure 10B. This technique was used to characterize batteries in order to understand magnetic effects on the kinetics within the battery. It is thought that magnetic modification influences electron transfer events, which should manifest in the charge transfer component, R_{ct}, and is discussed further in Section 4.2.3.

2.5.3 Summary of Statistical Tests

Statistical assessment of the data are appropriate to vett a magnetic effect. The methods used are summarized here.

2.5.3.1 Propagation of Error

The first statistical evaluations are propagation of error and relative error. For division and multiplication steps, the relative error is found from the relative error of the data, as for example,

$$rel\ error = \sqrt{rel\ error_1^2 + rel\ error_2^2} \tag{34}$$

The $rel\ error_i$ is calculated from the corresponding standard deviation $st\ dev_i$ and

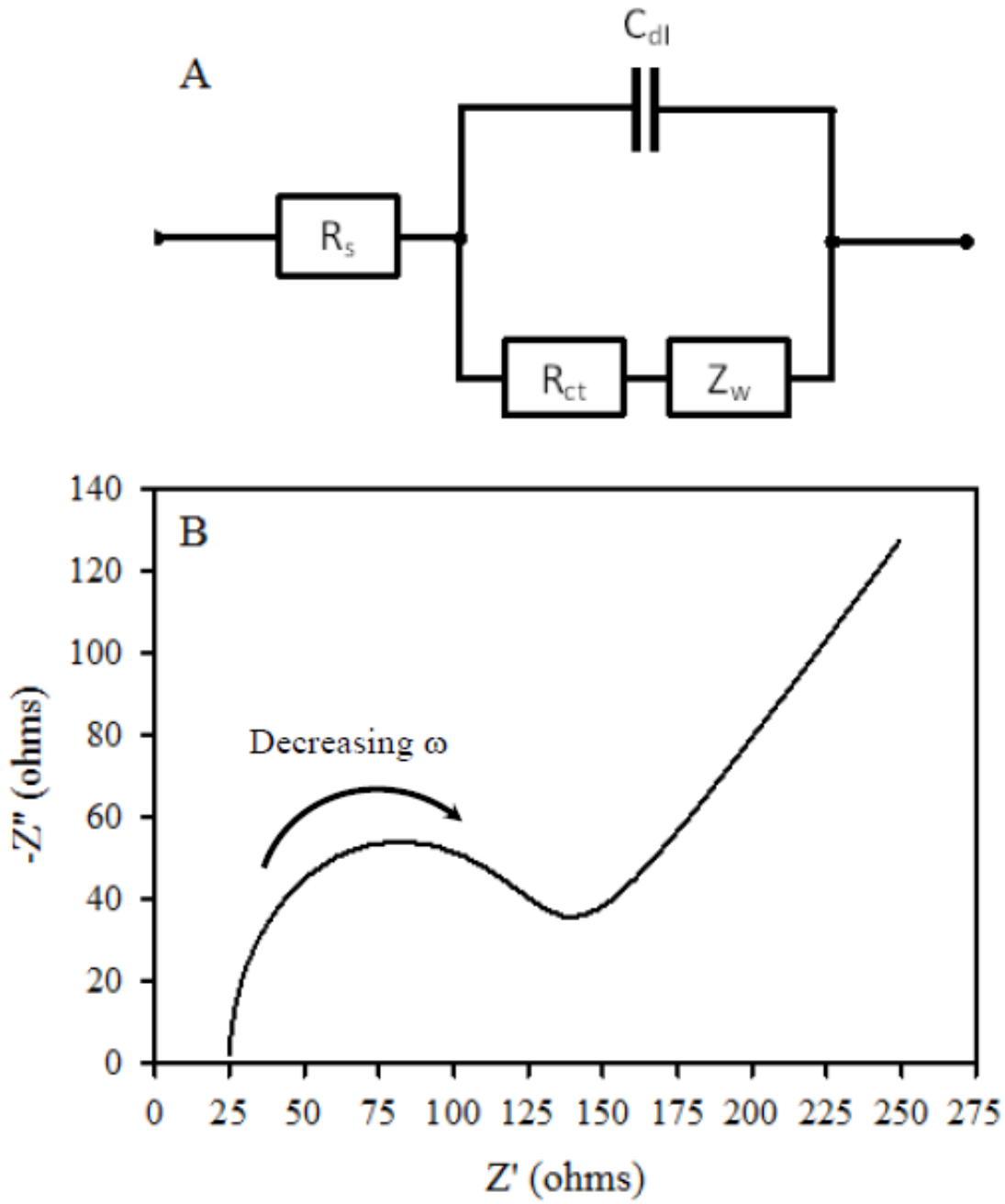

Figure 10. A Randles equivalent circuit model and simulated impedance spectroscopy output. Values for the simulation are: $R_s = 25\ \Omega$, $C_{dl} = 1\ \mu F$, $R_{ct} = 100\ \Omega$, and $Z_w = 0.001\ \Omega\ s^{-0.5}$.

mean x_i of the parameter.

$$rel\ error_i = \frac{st\ dev}{x_i} \tag{35}$$

Throughout, the relative errors are large. Ratios of parameters are used to assess relative merits of different systems. In the ratios, the relative errors propagate to yield similarly large relative errors. When the ratios $\pm$ the relative errors are large, the results have limited statistical significance. To evaluate the significance of the ratios, t-tests were generated under the null hypothesis that the means used to calculate the ratios were not different This is outlined below.

2.5.3.2 Student t-test

Statistical evaluation by the t-test is useful in assessment of small data sets ($n \leq 40$) as reported here. The t-test is a statistical method to compare data for two different experimental conditions where multiple replicates are available for each condition. The t-test establishes whether the averages, given the standard deviations, are different. A confidence level is reported as to whether the values are different. Confidence levels range from zero to approaching 100 %: the larger the confidence level, the higher the statistical confidence that the means are different. Confidence levels are higher with larger numbers of samples and smaller standard deviations. A calculated t value, t_{calc}, includes a pooled standard deviation, s_{pooled},derived from the two sample standard deviations. Expressions are taken from [Harris, Quantitative Analysis, 7th edition] for $n_1 + n_2 - 2$ degrees of freedom.

$$t_{calc} = \frac{|x_1 - x_2|}{s_{pooled}} \sqrt{\frac{n_1 n_2}{n_1 + n_2}} \tag{36}$$

$$s_{pooled} = \sqrt{\frac{s_1^2 (n_1 - 1) + s_2^2 (n_2 - 1)}{n_1 + n_2 - 2}} \tag{37}$$

A statistical value, t_{table}, is established for $n_1 + n_2 - 2$ degrees of freedom and a specified confidence interval. For the specified level of confidence, if $t_{calc} > t_{table}$, then the two means are considered to be different.

2.5.3.3 Comments on the F-test and Application of the t-test

The equations 36 and 37 are based on the assumption of equally populated standard deviations for the two data sets ($n_1 = n_2$). Whether s_1 and s_2 are the same is determined by the F-test, where

$$F_{calc} = \frac{s_1^2}{s_2^2} \tag{38}$$

If $F_{calc} > F_{table}$, then the difference in standard deviations is significant. F_{table} is given in terms of the degrees of freedom for s_1 and s_2. If the standard deviations are different, then the t-test equations are replaced with

$$t_{calc} = \frac{|x_1 - x_2|}{\sqrt{\frac{s_1^2}{n_1} + \frac{s_2^2}{n_2}}} \tag{39}$$

for

$$degrees\ of\ freedom = \frac{\left(\frac{s_1^2}{n_1} + \frac{s_2^2}{n_2}\right)^2}{\frac{\left(\frac{s_1^2}{n_1}\right)^2}{n_1+1} + \frac{\left(\frac{s_2^2}{n_2}\right)^2}{n_2+1}} - 2 \tag{40}$$

Given the variation in battery systems, good statistical assessment is critical.

CHAPTER 3

HIGH ELECTROLYTE CONTENT ALKALINE BATTERIES

The batteries discussed here were the first full batteries made in this lab. Previous work from Leddy and coworkers on EMD cathodes was performed by Tesene and Ünlü [51, 57, 58]. These studies focused exclusively on flooded half cells and all measurements were made galvanically. In a flooded half cell, one battery electrode is studied in bulk electrolyte (KOH) solution. The electrodes were alkaline MnO_2 cathodes, but as flooded electrodes, they would not be appropriate for a "dry cell" of industrial standards.

3.1 Battery Formation

Batteries were prepared according to the general procedure from Section 2.4.4 with specific parameters and configurations describe in this Section.

3.1.1 Magnetic Cathode Preparation

Cathode mixing was performed as specified in Section 2.4.4. The specific parameter for this battery type are described as follows. Cathode components, mixed daily as per Table 3, were blended with KOH to form a paste. The paste was allowed to hydrate for 12 to 48 hours. Aliquots of the paste were weighed to the specified quantity and transferred into the pressing die. Application of 0.75 metric tons of force for 30 seconds was performed with a hydraulic press, pressure was released, and the process was repeated two more times. Pressure was applied for

a total of 90 seconds. Magnetic saturation of the cathode pellet was performed by centering the pellet in a small plastic weigh dish the corners of which rested on the top of a hollow cylinder NdFeB permanent magnet (3" $o.d.$ × 2" $i.d.$ × 0.5" ht) for 60 seconds. In this configuration, the pellet was near the center of the cylinder and field lines of the magnet are normal to the pellet face.

Table 3. Cathode formulations for high electrolyte content batteries.

Reagent	Non-modified (% w/w)	Magnetically Modified (% w/w)
MnO_2	68	58
graphite	10	10
PTFE	2	2
$SmCo_5$	–	10
KOH, 9 M	20	20

3.1.2 Nonmagnetic Cathode Preparation

The sole difference for the nonmagnetic cathode was exclusion of samarium cobalt (0 % w/w). The EMD mass difference was increased to 68 % w/w. See 3. All other reagent compositions remained the same. The pressing procedure also remained the same.

For high electrolyte content batteries, blank electrode pellets (i.e., No $SmCo_5$) were examined either as formed or after magnetization. Blank (control) pellets were magnetized in a 2 Tesla electromagnet for 10 seconds between a turn between the 30 second pellet pressing times discussed in the previous Section. These electrodes are identified as e-mag.

3.1.3 Anode Preparation

Anode reagents are as specified in Table 4. All reagents are in powder form and used as received. Anode reagents are initially mixed dry by the same procedure as the cathode materials to ensure matrix homogeneity. The dry components were then mixed with KOH and allowed to gel for 15 minutes prior to use. For these batteries, the stoichiometric ratio of Zn:EMD is 2:1 and is based on total anode capacity versus total cathode capacity as explained in Section 2.1.2.

Table 4. Anode formulation for high electrolyte content batteries.

Reagent	% w/w
Zinc	57
ZnO	1
Carboyxymethyl cellulose (CMC)	4
KOH, $9M$	38

3.2 Discharge Data

Batteries were discharged at two different constant current discharge rates, C/5 and C/3. The discharge rates were calculated based on the mass of EMD of the individual cathode pellet because cathode masses vary slightly. Representative discharge curves for C/5 are shown in Figure 11. Time to complete discharge of the first electron process (Mn^{+4} to Mn^{+3}), is close to the theoretical mark of 300 minutes at 0.8 V. Voltage values are as reported by the instrument.

Energy versus potential data provides insight into the efficiency of a battery by comparison of energy discharged at a given voltage. Batteries with greater efficiency

have more energy. Energy values were calculated by numerically integrating the area under a voltage vs time curve with MS Excel®. Figure 13 illustrates the efficiency of a battery as total energy discharge at a given voltage.

Time to a given voltage is used to evaluate the ability of the battery to sustain a voltage. Longer time to a given voltage is consistent with better performance. A bar graph for the time for a system to sustain a given voltage or better is shown for C/5 in Figure 12. Four battery types are shown: blank unmagnetized, blank magnetized in the electromagnet, $SmCo_5$ pellets without magnetization, and $SmCo_5$ pellets magnetized in the NdFeB ring magnet. Larger impacts are observed at voltages above 0.8 V. The error bars are standard deviations for 1σ and are large. Battery performance was inconsistent and required high numbers of replicates to be statistically persuasive. Batteries were considered poor performers and excluded from analysis when the voltage discharge curve fell below 1.0 V within the first 10 minutes of discharge.

3.2.1 C/5 Data

Representative discharge curves, time to a given voltage, for C/5 and corresponding energy curves, total energy to a given voltage, are found in 11, 12, 13, and 14, respectively.

From the data, C/5 results exhibit a general trend toward improve performance with magnetization and with incorporation of $SmCo_5$. Magnetized blanks (emag) have better performance than nonmagnetized blank. $SmCo_5$ batteries perform better than blanks. Magnetized batteries are better than the nonmagnetized analogs.

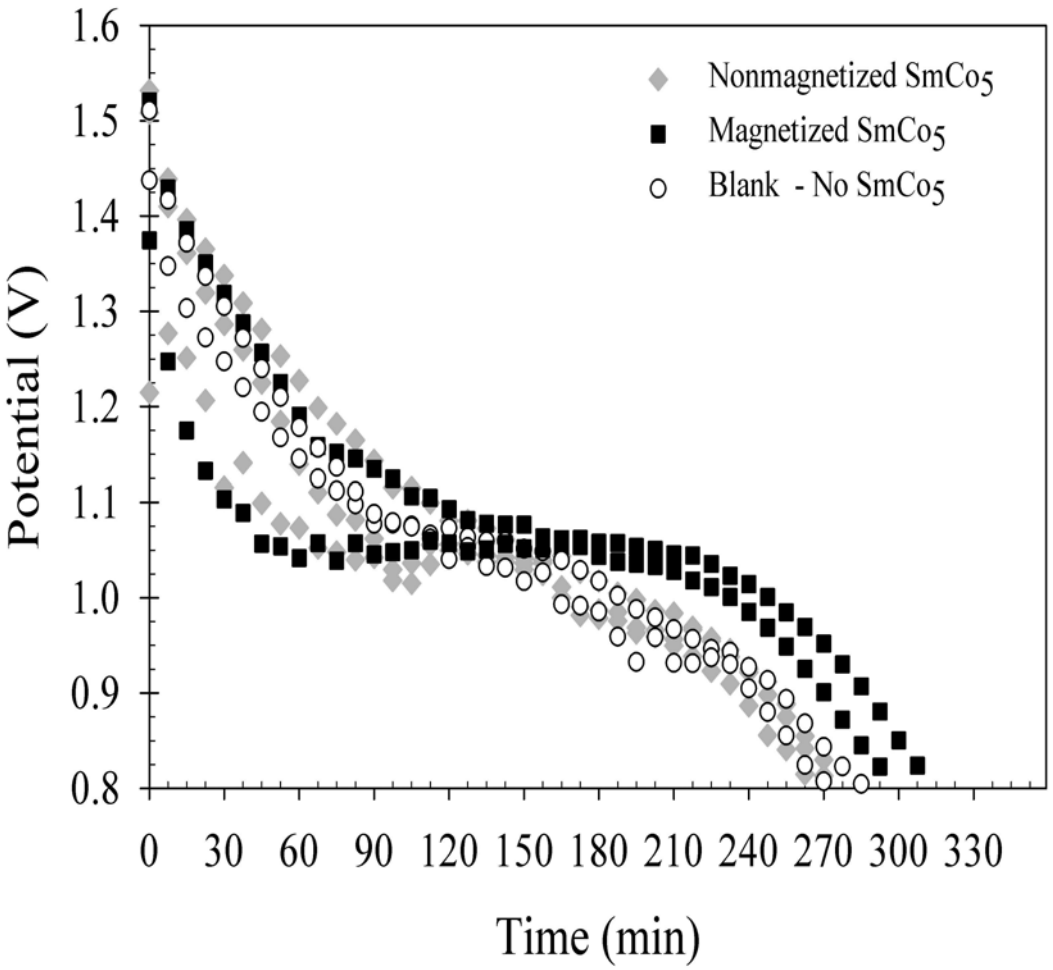

Figure 11. Representative discharge curves using a C/5 rate for a high electrolyte content battery. Discharge to 0.8 V correspond to the first electron discharge. Data was collected on a single day and is typical of the performance observed across all battery types, which manifests itself in the statistical analysis.

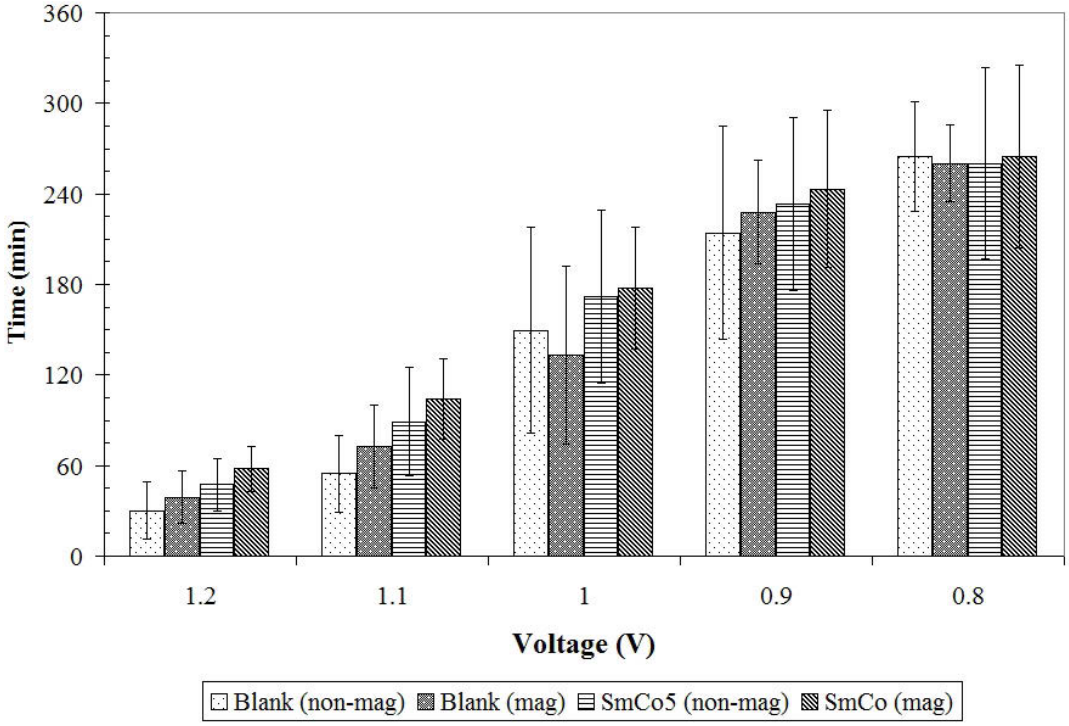

Figure 12. Bar graph representation of time to a given voltage for high electrolyte batteries at a C/5 discharge rate.

Throughout, the error bars are large; however, so the statistical significance is diminished. This is discussed in greater detail in Section 3.3.

3.2.2 C/3 Data

The data C/3 discharge is a higher discharge rate and kinetically more demanding. Results analogous to C/5 are shown for C/3 in Figures 15, 17, 16, and 18. All data were collected on the same day and with the individual cathodes formed from the same corresponding batch mixture for the day. Figure 15 contains representative discharge curves. All electrodes approach the theoretical discharge time of 180 minutes and converge to similar times. Improved performance with $SmCo_5$ is

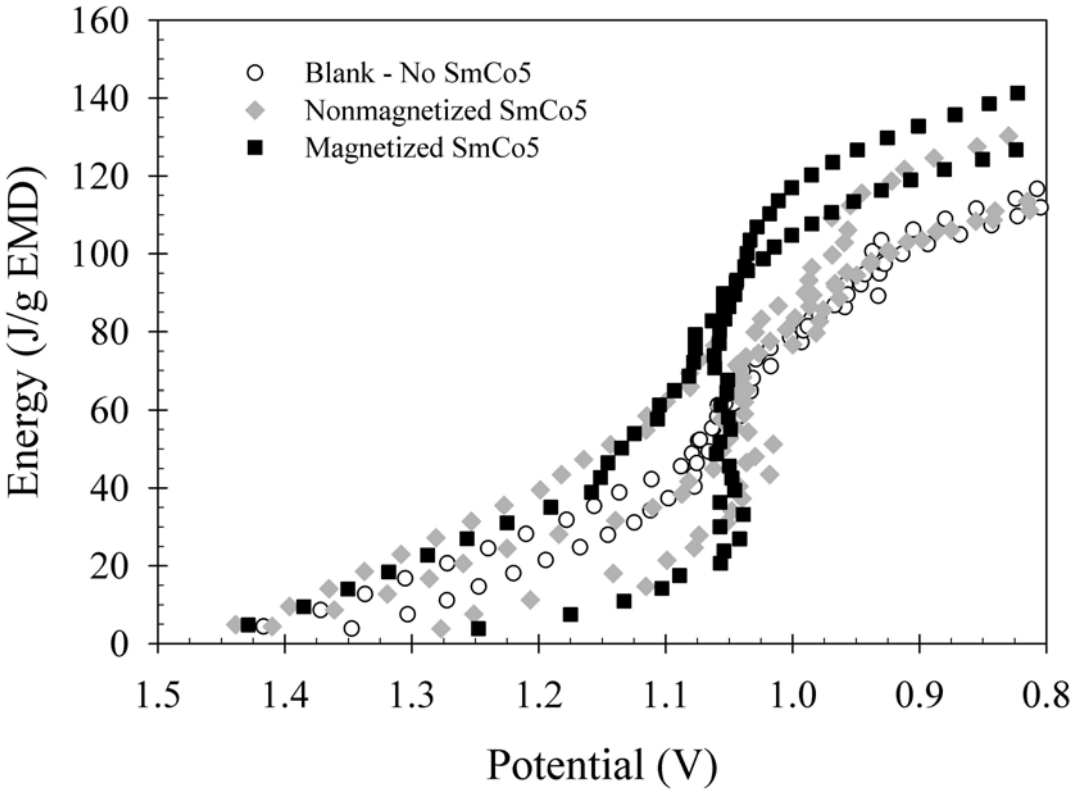

Figure 13. Representative energy versus voltage curves using a C/5 rate for a high electrolyte content battery. Data shown is the integrated values from the corresponding discharge data.

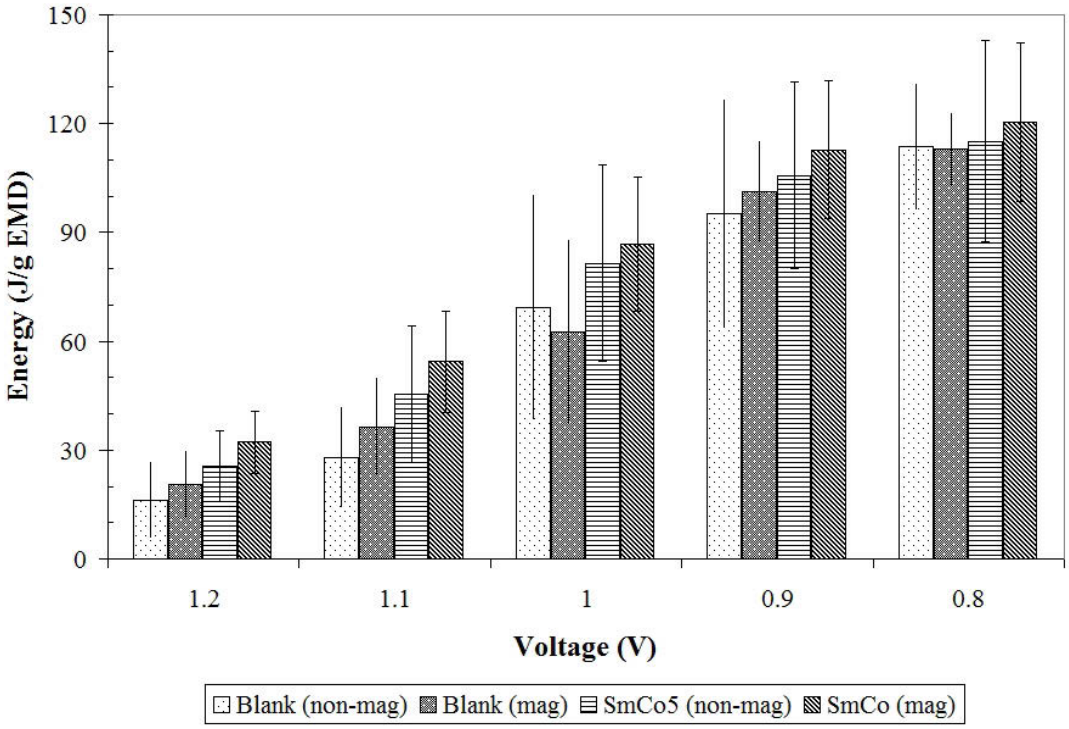

Figure 14. Bar graph representation of total energy at a given voltage for high electrolyte batteries at a C/5 discharge rate.

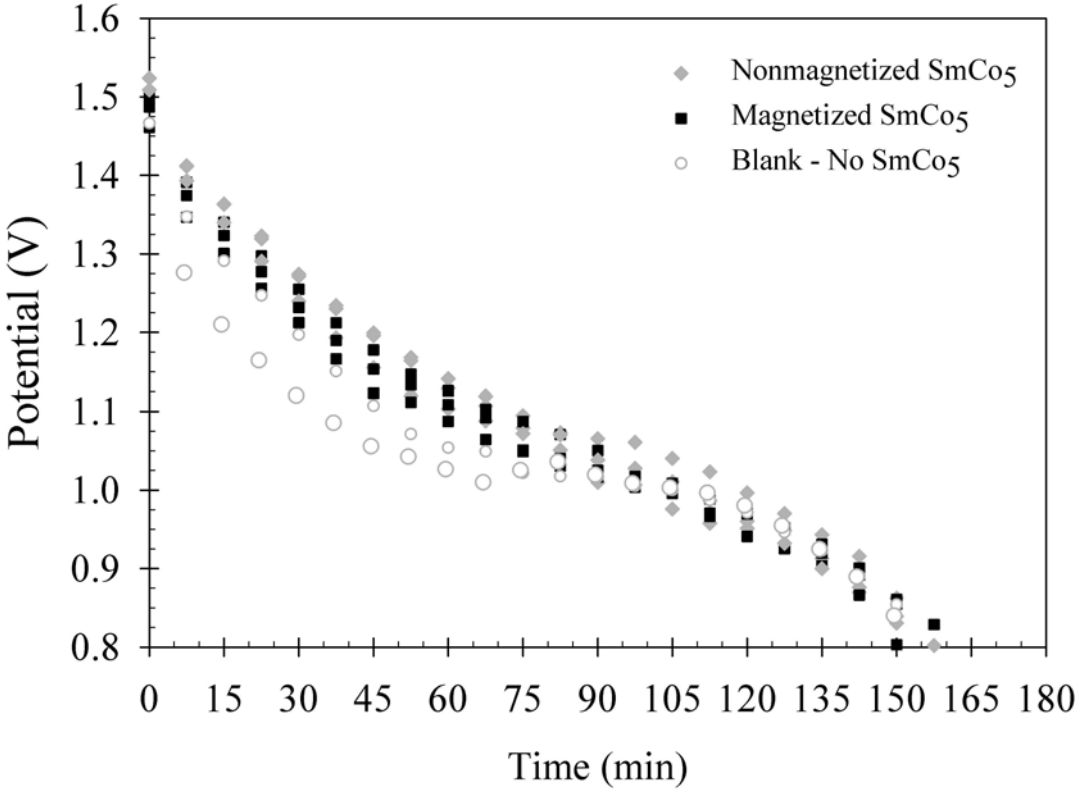

Figure 15. A representative constant current discharge curve using a C/3 rate. Magnetically modified batteries are capable of sustaining higher voltages for longer times than nonmagnetically modified batteries. Data was collected on a single day and is typical of the performance observed across all battery types. The cathode material soaked with electrolyte for 24 hours prior to pressing.

apparent with voltage $\gtrsim 1\,\mathrm{V}$. The profile have better morphology than C/5 data in Figure 11. Figure 16 is a bar graph for time to a given voltage. The $SmCo_5$ modified electrode performed better than the blanks. Evidence of magnetized $SmCo_5$ electrodes perform better than nonmagnetized $SmCo_5$ is less apparent. Standard deviations are shown as error bars on the plot. These figures are included as representative data.

Figures 15-18 are illustrations of the experimental data evaluated at specific points of interest during an experiment. The values are plotted as averages with

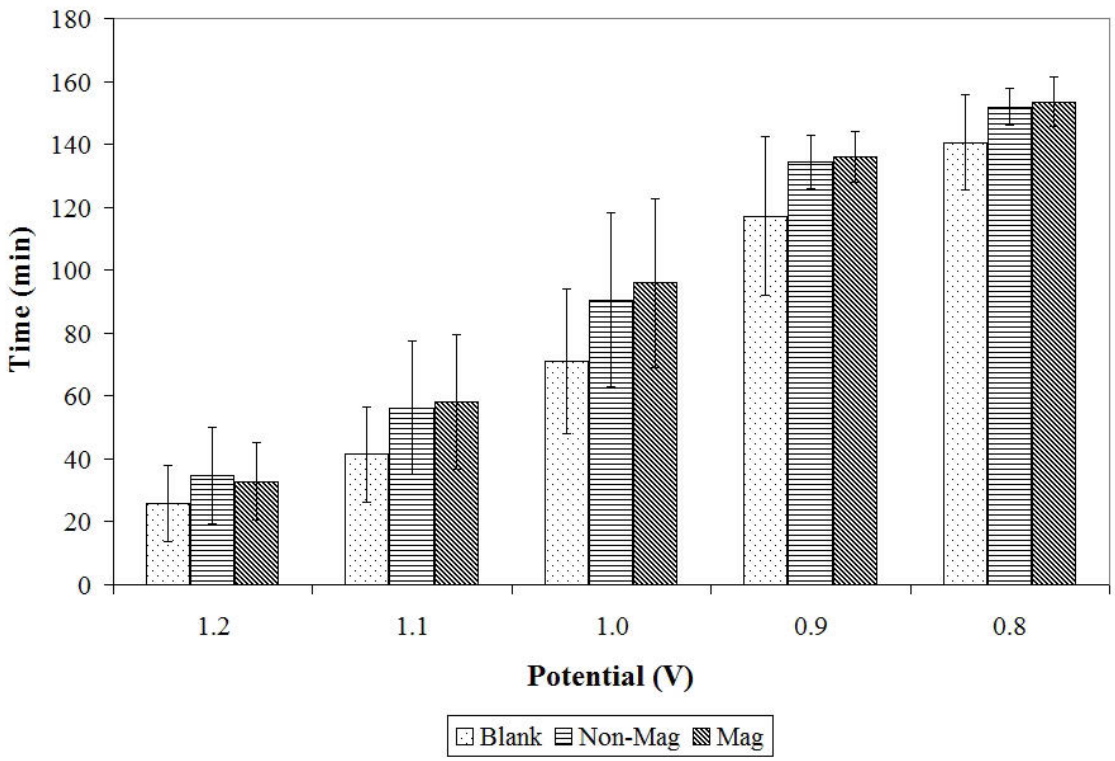

Figure 16. Bar graph representation of time to a given voltage for high electrolyte batteries at a C/3 discharge rate.

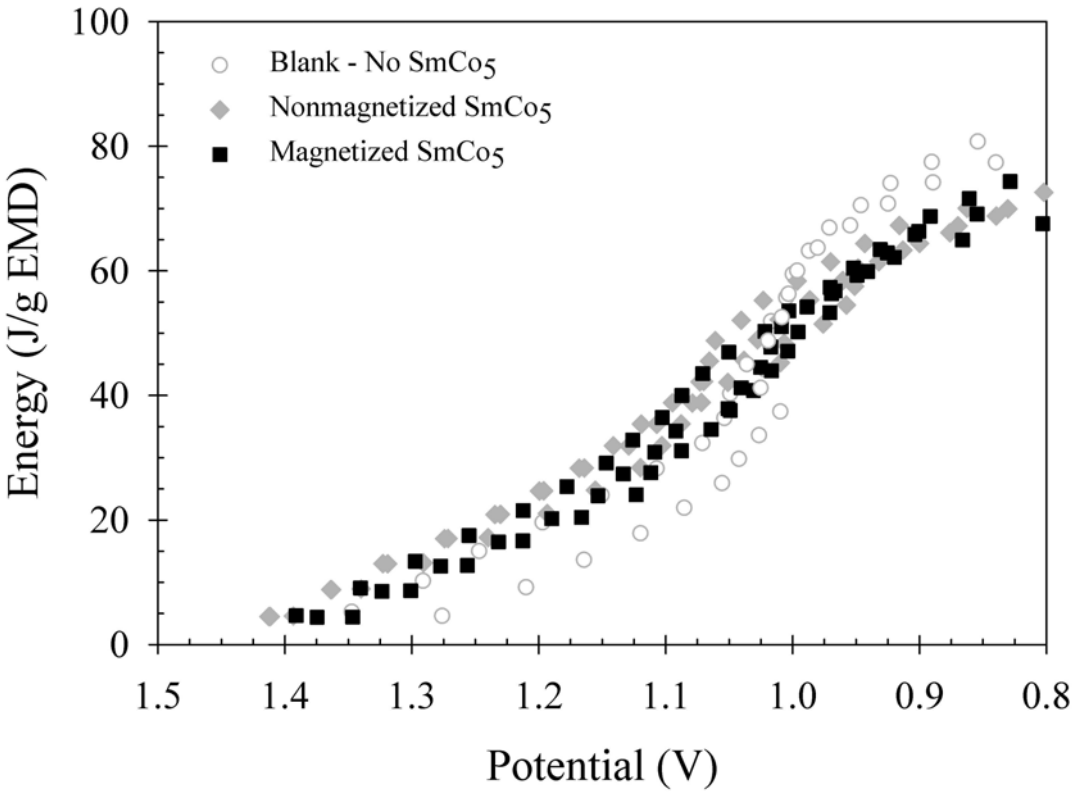

Figure 17. Representative energy versus voltage curves at a C/3 rate. Magnetically modified batteries are capable of generating more energy than nonmagnetically modified batteries at higher potentials. Data shown is the integrated values from the corresponding discharge data.

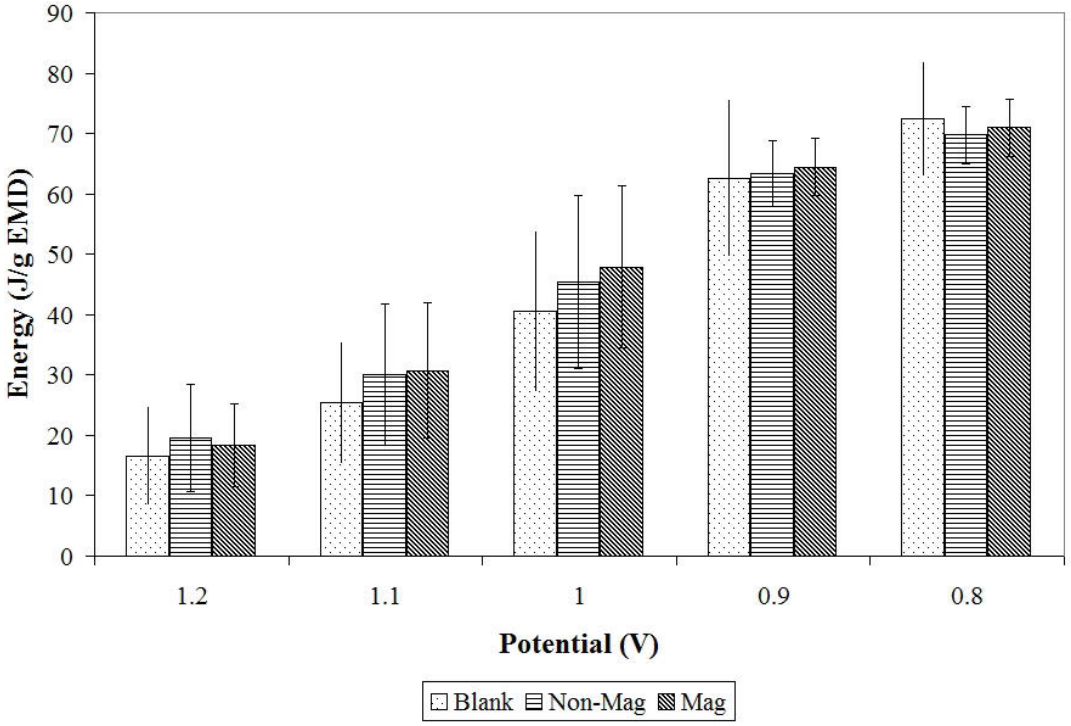

Figure 18. Bar graph representation of total energy at a given voltage for high electrolyte batteries at a C/3 discharge rate.

standard deviations are analyzed more thoroughly in the data analysis section, Section 3.3.

3.3 Data Analysis and Summary with Statistics

Data for C/5 and C/3 discharge rates are summarized in Tables 5 and 6. Data, for n replicates, include average time to a given voltage, average at a given voltage, average capacity at a given voltage, and average fractional capacity at a given voltage. Voltage are expected at 1.2, 1.1, 1.0, 0.9, 0.8 V. Standard deviations are reported for average time and average energy to a given voltage. All other parameters in Table 5 are calculated from average time and average energy. Controls

(blanks) and magnetically modified are shown for C/5 only. Comparable data for C/3 batteries are in Table 6 only. All data are included except batteries where voltage decayed below 1.0 V before ten minutes. The fraction of excluded data sets were approximately 5% and were uniformly distributed across all classes of batteries.

Table 5. Assessment of blanks and $SmCo_5$ nonmagnetized and magnetized at C/5; standard deviations are also shown.

Average Time (min) to a Given Voltage				
Voltage (V)	Control / no field	Control / field applied	Mag Mod / no field	Mag Mod / field applied
	$(n = 24)$	$(n = 9)$	$(n = 31)$	$(n = 11)$
1.2	30.2 ± 19.0	38.8 ± 17.3	47.2 ± 17.5	58.0 ± 14.8
1.1	54.8 ± 25.4	72.4 ± 27.5	88.9 ± 36.0	104 ± 27
1.0	150 ± 69	133 ± 59	172 ± 57	178 ± 40
0.9	214 ± 70	228 ± 34	233 ± 58	243 ± 52
0.8	265 ± 37	260 ± 25	260 ± 63	265 ± 61

Average Energy (J/g) at a Given Voltage				
	Control / no field	Control / field applied	Mag Mod / no field	Mag Mod / field applied
1.2	16.3 ± 10.7	20.7 ± 9.2	25.5 ± 9.8	32.2 ± 8.6
1.1	28.1 ± 14.0	36.5 ± 13.5	45.4 ± 18.9	54.4 ± 14.0
1.0	69.3 ± 31.1	62.6 ± 25.4	81.5 ± 27.2	86.9 ± 18.5
0.9	95.2 ± 31.6	101 ± 14	106 ± 26	113 ± 19
0.8	114 ± 17	113 ± 10	115 ± 28	120 ± 22

Average Capacity (mAh/g) at a Given Voltage				
	Control / no field	Control / field applied	Mag Mod / no field	Mag Mod / field applied
1.2	25.8	33.2	40.4	49.7
1.1	46.9	62.0	76.1	89.2
1.0	128.2	113.8	147.3	152.3
0.9	183.5	195.1	199.8	208.4
0.8	226.7	222.8	222.8	226.7

Average Fractional Capacity at a Given Voltage				
	Control / no field	Control / field applied	Mag Mod / no field	Mag Mod / field applied
1.2	0.10	0.13	0.16	0.19
1.1	0.18	0.24	0.30	0.35
1.0	0.50	0.44	0.57	0.59
0.9	0.71	0.76	0.78	0.81
0.8	0.88	0.87	0.81	0.88

Table 6. Assessment of blanks and $SmCo_5$ nonmagnetized and magnetized at C/3; standard deviations are also shown.

	Average Time (min) to a Given Voltage		
Voltage (V)	Control, no field	Mag Mod, no field	Mag Mod, field applied
	$(n = 9)$	$(n = 17)$	$(n = 17)$
1.2	25.8 ± 11.9	34.8 ± 15.4	32.8 ± 12.3
1.1	41.5 ± 15.1	56.2 ± 21.2	58 ± 21
1.0	71 ± 23	91 ± 28	96 ± 27
0.9	117 ± 25	134 ± 9	136 ± 8
0.8	141 ± 15	152 ± 6	154 ± 8

	Average Energy (J/g) at a Given Voltage		
	Control, no field	Mag Mod, no field	Mag Mod, field applied
1.2	16.6 ± 8.2	19.6 ± 8.9	18.4 ± 6.8
1.1	25.4 ± 10.1	30.0 ± 11.7	30.7 ± 11.2
1.0	40.6 ± 13.3	45.4 ± 14.3	47.9 ± 13.4
0.9	62.7 ± 13.1	63 ± 5	64 ± 5
0.8	72 ± 9	70 ± 5	71 ± 5

	Average Capacity (mAh/g) at a Given Voltage		
	Control, no field	Mag Mod, no field	Mag Mod, field applied
1.2	36.9	49.6	46.8
1.1	59.2	80.2	82.7
1.0	101.4	129.2	136.8
0.9	167.3	191.7	194.0
0.8	200.7	216.9	219.2

	Average Fractional Capacity at a Given Voltage		
	Control, no field	Mag Mod, no field	Mag Mod, field applied
1.2	0.14	0.19	0.18
1.1	0.23	0.31	0.32
1.0	0.39	0.50	0.53
0.9	0.65	0.75	0.76
0.8	0.78	0.84	0.85

3.3.1 Parameters to Evaluate Effectiveness of Modification

Evaluations are based on the discharge curves of voltage with time and the curve for energy with voltage. Data evaluations are tabulated at voltages of 1.2, 1.1, 1.0, 0.9, and 0.8 V. Experiments are reported for C/5 and C/3 where the EMD cathode mixtures were formed and allowed to rest for 24 hr before being pressed into cathode pellets and placed in the battery clam shell with the anode and separator and then tested. The notation C/n means that the theoretical capacity of the battery based on mass of EMD will be discharge in n hours. C/n sets the constant current demanded of the EMD mass. Commercial batteries discharge faster than n hours because of losses and inefficiencies in the battery. Two principal types of data are reported in Tables 5 and 6: time to a given voltage and energy. In this Section, discussion highlights results for blanks and $SmCo_5$, nonmagnetized and magnetized and their ratios. Only the C/5 data includes magnetized blanks, where blanks are magnetized in the electromagnet.

3.3.1.1 Time to a Given Voltage

Time to a given voltage is a measure of power (rate) and of capacity (energy). From the voltage decay curves (Figures 11 and 15), the time is measured at each of five voltages. The average time (minutes) to a given voltage for each class of samples is shown in Table 5 for C/5 and Table 6 for C/3. The standard deviations and number of samples for each average are also shown. The C/5 data includes data for magnetized blanks.

For parameters for C/5 discharges, summarized in Table 5 the average time at a given voltage increases as blank, non-mag < blank, mag < $SmCo_5$, non-mag < $SmCo_5$, mag for all voltages > 0.8 V. All batteries discharge to a similar end time at 0.8 V, independent of composition and magnetization. This indicates the anode behaves as the limiting reagent and as weighed the stoichiometric excess of zinc to EMD of 2:1 is not electrochemically accessible. Relative standard deviations are less for blanks and for $SmCo_5$ when comparison is made of magnetized and nonmagnetized sample. This is consistent with a reduction in entropy under magnetization. Though, the relative standard deviations are large.

For C/3 discharge, summarized in Table 6, the average time at a given voltage increases as blank, non-mag < $SmCo_5$, non-mag $\sim$ $SmCo_5$, mag for all voltages. Relative standard deviations are not clearly smaller with magnetization, but the relative standard deviations are again large.

3.3.1.2 Power Considerations

Power is calculated from the time to a given voltage. Battery voltages at fixed C/n decays with time. The longer a battery remains at a given voltage before decaying, the higher the rate and the higher the power, $P(t)$. Power is defined as:

$$P(t) = i(t)\,V(t) \tag{41}$$

$$= i_{\text{constant}} V(t) \qquad \text{for constant C/n} \tag{42}$$

The constant current i_{constant} is in amps per gram of EMD and is established by C/n. Thus, the discharge curves of voltage ($V(t)$) with time is a measure of power for a

Table 7. Time (minutes) to a given voltage for blanks and $SmCo_5$ nonmagnetized and magnetized at C/5; averages are in bold and corresponding standard deviations are also shown.

Average Time (min) to a Given Voltage				
Voltage (V)	Control / no field	Control / field applied	Mag Mod / no field	Mag Mod / field applied
	$(n = 24)$	$(n = 9)$	$(n = 31)$	$(n = 11)$
1.2	30.2 ± 19.0	38.8 ± 17.3	47.2 ± 17.5	58.0 ± 14.8
1.1	54.8 ± 25.4	72.4 ± 27.5	88.9 ± 36.0	104 ± 27
1.0	150 ± 69	133 ± 59	172 ± 57	178 ± 40
0.9	214 ± 70	228 ± 34	233 ± 58	243 ± 52
0.8	265 ± 37	260 ± 25	260 ± 63	265 ± 61

Average Energy (J/g) at a Given Voltage				
	Control / no field	Control / field applied	Mag Mod / no field	Mag Mod / field applied
1.2	16.3 ± 10.7	20.7 ± 9.2	25.5 ± 9.8	32.2 ± 8.6
1.1	28.1 ± 14.0	36.5 ± 13.5	45.4 ± 18.9	54.4 ± 14.0
1.0	69.3 ± 31.1	62.6 ± 25.4	81.5 ± 27.2	86.9 ± 18.5
0.9	95.2 ± 31.6	101 ± 14	106 ± 26	113 ± 19
0.8	114 ± 17	113 ± 10	115 ± 28	120 ± 22

Average Capacity (mAh/g) at a Given Voltage				
	Control / no field	Control / field applied	Mag Mod / no field	Mag Mod / field applied
1.2	25.8	33.2	40.4	49.7
1.1	46.9	62.0	76.1	89.2
1.0	128.2	113.8	147.3	152.3
0.9	183.5	195.1	199.8	208.4
0.8	226.7	222.8	222.8	226.7

Table 8. Time (minutes) to a given voltage for non-magnetized blanks and $SmCo_5$ and magnetized $SmCo_5$ at C/3; averages are in bold and corresponding standard deviations are also shown.

	Time (min) to a Given Voltage		
Voltage (V)	Control no field	Mag Mod no field	Mag Mod field applied
	($n = 9$)	($n = 17$)	($n = 17$)
1.2	25.8 ± 11.9	34.8 ± 15.4	32.8 ± 12.3
1.1	41.5 ± 15.1	56.2 ± 21.2	58 ± 21
1.0	71 ± 23	91 ± 28	96 ± 27
0.9	117 ± 25	134 ± 9	136 ± 8
0.8	141 ± 15	152 ± 6	154 ± 8

	Energy (J/g) at a Given Voltage		
	Control no field	Mag Mod no field	Mag Mod field applied
1.2	16.6 ± 8.2	19.6 ± 8.9	18.4 ± 6.8
1.1	25.4 ± 10.1	30.0 ± 11.7	30.7 ± 11.2
1.0	40.6 ± 13.3	45.4 ± 14.3	47.9 ± 13.4
0.9	62.7 ± 13.1	63 ± 5	64 ± 5
0.8	72 ± 9	70 ± 5	71 ± 5

	Average Capacity (mAh/g) at a Given Voltage		
	Control no field	Mag Mod no field	Mag Mod field applied
1.2	36.9	49.6	46.8
1.1	59.2	80.2	82.7
1.0	101.4	129.2	136.8
0.9	167.3	191.7	194.0
0.8	200.7	216.9	219.2

given C/n. In general, power is expected to be lower at lower n because higher C/n demands higher current. However, higher discharge rates can be limited kinetics.

Conversion of discharge curves to power curves is expressed as follows. One gram of MnO_2, the electroactive component in EMD equivalent to 0.011503 moles.

$$\frac{1.0000\ g}{MW\ MnO_2} = \frac{1.0000\ g}{86.937\ g/mol} = 0.01150\ mol \tag{43}$$

From Faraday's Law, to complete conversion of 0.01150 moles from MnO_2 to Mn^{3+}, the one electron is transferred. Charge, $Q\,(C/g\ MnO_2)$ is

$$\begin{aligned} Q\,(C/g\ MnO_2) &= nF \times \frac{mol\ MnO_2}{1.0000\ g\ MnO_2} && (44)\\ &= 1 \times \frac{96485\ C}{mol} \times \frac{0.01150\ mol}{1.0000\ g\ MnO_2} && (45)\\ &= \frac{1109.827\ C}{1.0000\ g\ MnO_2} = \frac{1109.827\ As}{g\ MnO_2} && (46)\\ &= \frac{1109.827\ As}{g\ MnO_2} \times \frac{1000\ mA}{A} \times \frac{hr}{3600\ s} && (47)\\ &= \frac{308.385\ mA\ hr}{g\ MnO_2} && (48) \end{aligned}$$

The same lot of EMD was used in all experiments and this was estimated to be of ~ 90 % purity of MnO_2 by mass. Vendor values specify $\gtrsim 90$ % purity.

$$\frac{0.9\ g\ MnO_2}{1.0\ g\ EMD} \times \frac{308.385\ mA\ hr}{g\ MnO_2} = \frac{256.9\ \ mA\ hr}{g\ EMD} \tag{49}$$

For a given C/n or n hours, the constant current, i_{constant}, to discharge 1 g of EMD at a given C/n, for a one electron process and 90 % purity for EMD is defined.

$$i_{\text{constant}} = \frac{256.9\ mA}{n\ g\ EMD} \tag{50}$$

Thus, from equation 42, the voltage discharge curves are converted to power curves.

For i_{constant} in mA and $V(t)$ in volts, the power is in mW or mJ/s. For C/5 and C/3,

$$i_{\text{constant}}(C/5) = \frac{51.38\ mA}{g\ EMD} \quad (51)$$

$$i_{\text{constant}}(C/3) = \frac{85.63\ mA}{g\ EMD} \quad (52)$$

for a given mass of EMD in the battery, the current is specified.

From Equation 42, i_{constant} is then a proportionality between $P(t)$ and $V(t)$. Power with time tracks voltage with time. Just as time to a given voltage indicates the time to which a voltage is sustained, time to a given voltage indicates the time to which a power is sustained. Power at time is the same for as voltage at time where i_{constant} multiplies voltage. In Table 5, the multiplier is 87.38 mA/g EMD and for Table 6, 85.63 mA/g EMD power at time. Thus, power is higher at C/5 for magnetized and $SmCo_5$ counting classes. Power is higher for C/3 for $SmCo_5$.

3.3.1.3 Capacity

Capacity per gram of EMD at a given voltage can be considered in two ways: fraction of theoretical capacity and capacity in mAh/g EMD.

3.3.1.3.1 Fraction of Theoretical Capacity

For a given C/n, the ratio of the time to a given voltage, to the theoretical time n yields the fraction of theoretical capacity at a given voltage. Values for C/5 and C/3 discharge are summarized in Tables 5 and 6. In both cases, fractional capacity increases as voltage decreases. All classes of batteries achieve similar capacities of $\sim$ 80 % or better at 0.8 V. This approaches the theoretical capacity. Fractional

capacities are similar for C/5 and C/3 with higher fractional capacity found for $SmCo_5$ batteries than blanks. For C/5, magnetized blanks have higher capacity than nonmagnetized blanks.

3.3.1.3.2 Capacity in mAh/g EMD

The maximum theoretical capacity for the first electron ($MnO_2 \rightarrow Mn^{3+}$) is 256.9 $mA\ hr/g\ EMD$, Equation 49. From the product of the fractional capacities and 256.9 $mA\ hr/g\ EMD$, the capacity in mAh/g EMD is found, as reported in Tables 5 and 6. For C/5 and C/3, patterns in the average capacities directly map those of the fractional capacities. Under the slower C/5 discharge, slightly more of the battery capacity is harvested at 0.8 V. Capacities at higher voltages tend to be higher for C/3. For C/5, the capacities of the magnetized cells remain higher than analogous non-magnetized cells for voltages > 0.9 V.

3.3.1.4 Energy at a Given Voltage

Integration of the area under a constant current discharge yields energy data. Data for C/5 is summarized in Table 5 and is illustrated in Figure 13 and data for C/3 is listed in Table 6 and illustrated in Figure 17. Average energy at a given voltage increases as blank, non-mag < blank, mag < $SmCo_5$, non-mag < $SmCo_5$, mag for all voltages at C/5. Relative standard deviations C/5 are less for blanks and for $SmCo_5$ when magnetized than non-magnetized, consistent with a reduction in entropy under magnetization. However, the relative standard deviations are large.

Performance for C/3, average energy at a given voltage increases as blank,

non-mag < $SmCo_5$, non-mag ~ $SmCo_5$, mag for all voltages greater than 0.9 V. Relative standard deviations are marginally less for $SmCo_5$ than the blanks, but are large.

3.3.2 Ratios of Parameters to Evaluate Effectiveness of Modification and Their Statistical Significance

The impact of modification is evaluated by examining ratios of the parameters outlined above. Several parameters were evaluated to assess the effectiveness of magnetic modification. These were expressed as ratios of two observables, where multiple replicates for each set of conditions allowed means (x_i), standard deviations ($st\ dev_i$), relative error ($rel\ error_i$), and number of samples ($count$ or n_i) for each data set. Ratios were determined from the values of x_i, and the statistical significance was assessed through propagation of errors and t-tests under the null hypothesis that the ratio was not statistically significant (i.e., for ratio x_1/x_2, the null hypothesis is $x_1 = x_2$). The t-tests required that several other parameters be calculated; this includes t-tests (t_{calc}), pooled standard deviations (s_{pooled}), and F-tests to determine if the standard deviations are the same (F_{calc}). Details of the statistical processing are outlined below in Section 2.5.3.

Batteries are complicated systems. All of these batteries were made individually and by hand. The relative standard deviations are high. This determined the statistical assessments that were used and allowed. Confidence levels of $\geq 95\%$ are most typically considered persuasive, but the uncertainties are sufficiently high in some cases that this level of confidence cannot be ascribed When the null hypothesis

is used to evaluate data, the level of confidence is reported. With more batteries and more automated processing, the confidence levels would likely be higher. In some cases, especially at higher voltages, the confidence levels are higher.

The patterns in the above data are reflected in the time to a given voltage, which also maps capacity and power as above, and energy with voltage. Ratios for time to a give voltage and energy with voltage are evaluated and reported in Table 9 for C/5 and Table 10 for C/3. Confidence levels for each ratio are reported as a subscript.

3.3.2.1 Time to a Given Voltage

Data are compared by discharge rate. The ratios for C/5 data, Table 9, are greater than 1 for all but one case for voltages > 0.8 V. This uniformity of pattern is consistent with magnetization a useful effect. The addition of $SmCo_5$ is also a useful effect, where magnetized is better than nonmagnetized $SmCo_5$. Confidence levels are provided for each ratio. Data at higher voltages has higher confidence levels. As compared to the blank (control) nonmagnetized, both $SmCo_5$ system and the magnetized blanks have higher time to voltage with good confidence above 1 V. Enhancements > 50 % are found for the $SmCo_5$ relative to the blank and ~ 30 % for magnetized blank relative to the nonmagnetized blank, all at 1.1 and 1.2 V. Capacity and power are similarly enhanced. Ratios and confidence level decrease as the battery discharges. At lower voltages the batteries are Zn limited and ratios converge to 1 for all systems.

At high voltages, the magnetized blank is ~ 30 % better than the non-magnetized blank with a high degree of confidence. For voltages of 1.0 V and lower, the

Table 9. Ratios of average time and average energy to a given voltage to assess batteries discharged at C/5.

Ratios of Average Time to a Given Voltage$_{\text{Confidence Level}}$						
Voltage (V)	$\frac{\text{Blank}_{e-mag}}{\text{Control}}$	$\frac{\text{Mag Mod}_{No\ Field}}{\text{Control}}$	$\frac{\text{Mag Mod}_{Field}}{\text{Control}}$	$\frac{\text{Mag Mod}_{Field}}{\text{Mag Mod}_{No\ Field}}$	$\frac{\text{Mag Mod}_{No\ Field}}{\text{Blank}_{e-mag}}$	$\frac{\text{Mag Mod}_{Field}}{\text{Blank}_{e-mag}}$
1.2	$1.29_{\ 76\ \%}$	$1.57_{\ 99.9\ \%}$	$1.92_{\ 100\ \%}$	$1.23_{\ 92\ \%}$	$1.22_{\ 79\ \%}$	$1.50_{\ 99\ \%}$
1.1	$1.32_{\ 91\ \%}$	$1.62_{\ 100\ \%}$	$1.90_{\ 100\ \%}$	$1.17_{\ 80\ \%}$	$1.23_{\ 79\ \%}$	$1.44_{\ 98\ \%}$
1.0	$0.89_{\ 48\ \%}$	$1.15_{\ 81\ \%}$	$1.19_{\ 78\ \%}$	$1.08_{\ 25\ \%}$	$1.29_{\ 92\ \%}$	$1.34_{\ 94\ \%}$
0.9	$1.06_{\ 41\ \%}$	$1.09_{\ 73\ \%}$	$1.14_{\ 39\ \%}$	$1.04_{\ 39\ \%}$	$1.02_{\ 21\ \%}$	$1.07_{\ 55\ \%}$
0.8	$0.98_{\ 26\ \%}$	$0.98_{\ 24.4\ \%}$	$1.00_{\ 0\ \%}$	$1.02_{\ 16\ \%}$	$1.00_{\ 0\ \%}$	$1.02_{\ 16\ \%}$

Ratios of Average Energy at a Given Voltage$_{\text{Confidence Level}}$						
	$\frac{\text{Blank}_{e-mag}}{\text{Control}}$	$\frac{\text{Mag Mod}_{No\ Field}}{\text{Control}}$	$\frac{\text{Mag Mod}_{Field}}{\text{Control}}$	$\frac{\text{Mag Mod}_{Field}}{\text{Mag Mod}_{No\ Field}}$	$\frac{\text{Mag Mod}_{No\ Field}}{\text{Blank}_{e-mag}}$	$\frac{\text{Mag Mod}_{Field}}{\text{Blank}_{e-mag}}$
1.2	$1.27_{\ 71\ \%}$	$1.57_{\ 99.8\ \%}$	$1.97_{\ 100\ \%}$	$1.26_{\ 95\ \%}$	$1.24_{\ 81\ \%}$	$1.56_{\ 99\ \%}$
1.1	$1.30_{\ 87\ \%}$	$1.62_{\ 100\ \%}$	$1.94_{\ 100\ \%}$	$1.20_{\ 85\ \%}$	$1.24_{\ 81\ \%}$	$1.49_{\ 99\ \%}$
1.0	$0.90_{\ 44\ \%}$	$1.18_{\ 87\ \%}$	$1.25_{\ 91\ \%}$	$1.07_{\ 45\ \%}$	$1.30_{\ 98\ \%}$	$1.39_{\ 98\ \%}$
0.9	$1.06_{\ 42\ \%}$	$1.11_{\ 82\ \%}$	$1.19_{\ 90\ \%}$	$1.07_{\ 59\ \%}$	$1.04_{\ 37\ \%}$	$1.11_{\ 85\ \%}$
0.8	$0.99_{\ 9\ \%}$	$1.01_{\ 19\ \%}$	$1.06_{\ 67\ \%}$	$1.05_{\ 43\ \%}$	$1.02_{\ 19\ \%}$	$1.07_{\ 64\ \%}$

Comparison of different electrode performance represented as a ratio of energy at a given voltage for five potentials at C/5. Ratios are in boldface; the level of confidence is also reported as subscripts.

magnetized blank does not improve or hinder performance as compared to the non-magnetized blank. The datum at 1.0V for the magnetized blank is especially poor; there is no known reason. A comparison of the non-magnetized $SmCo_5$ to the magnetized blank yields better performance for the non-magnetized $SmCo_5$ than the magnetized blank at voltages > 0.9 V by ∼20 % with some confidence. Finally, comparison of magnetized $SmCo_5$ to magnetized blank yields better performance by 35 to 50% for voltages from 1.0 to 1.2 V with high confidence. There is little effect at the lower voltages.

Similar ratios for C/3 data are summarized in Table 10. The ratios are greater than 1 for all comparisons to the control with good confidence across the voltage range. This uniformity of pattern is consistent with addition of $SmCo_5$ as a useful effect. The confidence levels also support the utility of adding $SmCo_5$. The effects of adding $SmCo_5$ to the matrix are in the range of 25 to 40% for voltages > 0.9 V with strong degree of confidence. Comparison of magnetized $SmCo_5$ batteries versus nonmagnetized $SmCo_5$ batteries, in the third column, shows there is no statistically significant difference in the responses for the magnetized and nonmagnetized $SmCo_5$ batteries. At lower voltages, all values for C/3 converge to 1, which is consistent Zn limited electrochemistry at lower voltage. There are no experiments undertaken for magnetized blanks at C/3.

3.3.2.2 Energy at a Given Voltage

Ratios in energy at a given voltage are updated for C/5 in Table 9 and for C/3 in Table 10. Trends in energy at a given voltage generally track the trends in time to a

Table 10. Ratios of average time and average energy to a given voltage to assess batteries discharged at C/3.

Ratios of Average Time to a Given Voltage$_{\text{Confidence Level}}$						
Voltage (V)	$\frac{\text{Blank}_{e-mag}}{\text{Control}}$	$\frac{\text{Mag Mod}_{Non}}{\text{Control}}$	$\frac{\text{Mag Mod}_{Field}}{\text{Control}}$	$\frac{\text{Mag Mod}_{Field}}{\text{Mag Mod}_{Non}}$	$\frac{\text{Mag Mod}_{Non}}{\text{Blank}_{e-mag}}$	$\frac{\text{Mag Mod}_{Field}}{\text{Blank}_{e-mag}}$
1.2	$1.29_{\ 76\ \%}$	$1.57_{\ 99.9\ \%}$	$1.92_{\ 100\ \%}$	$1.23_{\ 92\ \%}$	$1.22_{\ 79\ \%}$	$1.50_{\ 99\ \%}$
1.1	$1.32_{\ 91\ \%}$	$1.62_{\ 100\ \%}$	$1.90_{\ 100\ \%}$	$1.17_{\ 80\ \%}$	$1.23_{\ 79\ \%}$	$1.44_{\ 98\ \%}$
1.0	$0.89_{\ 48\ \%}$	$1.15_{\ 81\ \%}$	$1.19_{\ 78\ \%}$	$1.08_{\ 25\ \%}$	$1.29_{\ 92\ \%}$	$1.34_{\ 94\ \%}$
0.9	$1.06_{\ 41\ \%}$	$1.09_{\ 73\ \%}$	$1.14_{\ 39\ \%}$	$1.04_{\ 39\ \%}$	$1.02_{\ 21\ \%}$	$1.07_{\ 55\ \%}$
0.8	$0.98_{\ 26\ \%}$	$0.98_{\ 24.4\ \%}$	$1.00_{\ 0\ \%}$	$1.02_{\ 16\ \%}$	$1.00_{\ 0\ \%}$	$1.02_{\ 16\ \%}$

Ratios of Average Energy at a Given Voltage$_{\text{Confidence Level}}$						
	$\frac{\text{Blank}_{e-mag}}{\text{Control}}$	$\frac{\text{Mag Mod}_{Non}}{\text{Control}}$	$\frac{\text{Mag Mod}_{Field}}{\text{Control}}$	$\frac{\text{Mag Mod}_{Field}}{\text{Mag Mod}_{No\ Field}}$	$\frac{\text{Mag Mod}_{Non}}{\text{Blank}_{e-mag}}$	$\frac{\text{Mag Mod}_{Field}}{\text{Blank}_{e-mag}}$
1.2	$1.27_{\ 71\ \%}$	$1.57_{\ 99.8\ \%}$	$1.97_{\ 100\ \%}$	$1.26_{\ 95\ \%}$	$1.24_{\ 81\ \%}$	$1.56_{\ 99\ \%}$
1.1	$1.30_{\ 87\ \%}$	$1.62_{\ 100\ \%}$	$1.94_{\ 100\ \%}$	$1.20_{\ 85\ \%}$	$1.24_{\ 81\ \%}$	$1.49_{\ 99\ \%}$
1.0	$0.90_{\ 44\ \%}$	$1.18_{\ 87\ \%}$	$1.25_{\ 91\ \%}$	$1.07_{\ 45\ \%}$	$1.30_{\ 98\ \%}$	$1.39_{\ 98\ \%}$
0.9	$1.06_{\ 42\ \%}$	$1.11_{\ 82\ \%}$	$1.19_{\ 90\ \%}$	$1.07_{\ 59\ \%}$	$1.04_{\ 37\ \%}$	$1.11_{\ 85\ \%}$
0.8	$0.99_{\ 9\ \%}$	$1.01_{\ 19\ \%}$	$1.06_{\ 67\ \%}$	$1.05_{\ 43\ \%}$	$1.02_{\ 19\ \%}$	$1.07_{\ 64\ \%}$

Comparison of different electrode performance represented as a ratio of energy at a given voltage for five potentials at C/3. Ratios are in boldface; the level of confidence is also reported as subscripts.

given voltage.

The ratios for C/5 data, Table 9, are greater than 1 for all but one case for voltages > 0.8 V. This uniformity of pattern is consistent with magnetization a useful effect. The addition of $SmCo_5$ is also a useful effect, where magnetized is better than nonmagnetized $SmCo_5$. Comparison of $SmCo_5$ batteries as compared to the nonmagnetized blank, sustain higher energies at a given voltage. With a good confidence > 1 V the $SmCo_5$ batteries perform better than the blank. The largest effects are found in the ratios for the magnetized $SmCo_5$ as compared to the blank non-magnetized at 1.2 and 1.1 V where the time to a given voltage is $\sim 95\%$ higher than for the nonmagnetized blank. For the nonmagnetized $SmCo_5$ at 1.2 and 1.1 V as compared to the nonmagnetized blank, the energy at a voltage is $\sim 60\%$ higher. Ratios and confidence level decrease as the battery discharges. Comparison of magnetized $SmCo_5$ batteries to nonmagnetized $SmCo_5$ batteries show the magnetized $SmCo_5$ is statistically better than the nonmagnetized $SmCo_5$ by $\sim 20\%$ at higher voltages. At lower voltages, effects are not apparent, but this may be because at the lower voltages the batteries are Zn limited.

Consider the behavior of the magnetized blank. At high voltages, the magnetized blank is $\sim 30\%$ better than the nonmagnetized blank with a high degree of confidence. For voltages of 1.0 V and lower, the magnetized blank does not improve or hinder performance as compared to the nonmagnetized blank. The datum at 1.0 V for the magnetized blank is especially poor; there is no known cause. Performance for the nonmagnetized $SmCo_5$ as compared to magnetized blank is better at voltages

> 0.9 V by ~30 % with some confidence. Comparison of magnetized $SmCo_5$ to magnetized blank yields better performance by 40 to 55% for voltages from 1.0 to 1.2 V with high confidence. There is little effect at the lower voltages, again consistent with zinc limited responses at lower voltages.

The statistics for C/3 energy at a given voltage (Table 10) are not strong. Consider $SmCo_5$ batteries as compared to the nonmagnetized blanks. The ratios are ≥ 1 for voltage > 0.9 V. This uniformity of pattern is consistent with addition of $SmCo_5$ as a useful effect, although the confidence levels marginally support the utility of adding $SmCo_5$. The effects of adding $SmCo_5$ to the matrix $\sim$ 20% for voltages > 0.9 V with some confidence. Comparison of magnetized $SmCo_5$ batteries compared with nonmagnetized $SmCo_5$ batteries demonstrate no statistically significant difference in their responses. There were no data taken for the magnetized blank at C/3.

3.3.3 Separate Comments on the Import of the Magnetized Blank in the C/5 Data

Unique to the C/5 data are results that compare two blank electrodes, one magnetized and one not magnetized. The magnetized blank exhibits performance superior to that of the nonmagnetized blank. MnO_2 can be magnetized, but because MnO_2 and MnOOH are paramagnetic, it is not clear how long the magnetization will persist.

The impact of magnetizing a blank and having it perform better than an analogous but nonmagnetized blank is an important result for several reasons. The two blanks are chemically the same and likely structurally the same. The observed

effect can only be ascribed to magnetization because the electrodes are otherwise the same. There is no possibility of introduction of chemical mediators into this system, as there are when adding materials such as $SmCo_5$. This strongly supports the idea that magnetization leads to improved performance, likely through enhanced electron transfer rates.

Challenges of magnetizing EMD in an external field in commercial systems are several. It is unclear whether the magnetization will persist over time and/or under less than gentle handling of the battery. Paramagnetic species lose magnetization outside of an applied field. Commercial batteries have shelf lives of several years. These factors remain to be investigated.

3.4 Summary

In summary, magnetization improves the performance of MnO_2 primary batteries under low (C/5) and moderate (C/3) discharge rates in high electrolyte system. Magnetization by introduction of $SmCo_5$ and by magnetization with an external magnet both improve performance. Statistical assessment supports these claims.

Commercial alkaline batteries are low electrolyte volumes. The high electrolyte volumes in Chapter 3 support ideas that magnetic modification enhances battery performance. In Chapter 4, low electrolyte systems are investigated.

CHAPTER 4

LOW ELECTROLYTE CONTENT ALKALINE PRIMARY BATTERIES

Batteries presented in Chapter 3 differ from work previously conducted in the Leddy Lab [51, 58] because these are whole cell systems, a complete battery, instead of a flooded half cell configuration, a single electrode test. Although the batteries in Chapter 3 demonstrated magnetic modification of the cathode results in improved performance, the batteries are not good commercial analogs. Components do not match industrial composition standards and contain too much electrolyte. Batteries reported here more closely resemble industrially relevant compositions with increased active reagents (EMD and zinc) and minimized electrolyte and inactive reagents (binders, gelling agents, and graphite). In the end, a nongelled anode formulation provided better discharge data while a gelled anode coupled with higher % w/w EMD cathode was better suited for impedance spectroscopy.

4.1 Experimental

Industrially relevant batteries have well defined compositions hidden within broad reagent values contained within patent literature, which makes refining compositions difficult. Throughout these battery studies, the anode was as challenging to form as the cathode. In the full battery, performance is limited by the least effective electrode at each current and voltage. Here, formulations for the two different batteries will be referred to as Battery Type 1 and 2, which correspond to a gelled anode and nongelled anode, respectively. Batteries with gelled anode, type 1, are

based on trial and error compositions within the ranges found in Linden's Handbook of Batteries [59]. Batteries with a nongelled configuration, type 2, are based on work by Manickam, which only used zinc powder and KOH for the anode [60, 61]. Composition values for the cathode and anode are found in Tables 11 and 12. Batteries were produced by the general assembly procedure described in Section 2.4.4 with specific alterations for the cathode and anode as follows.

4.1.1 Cathode Preparation

Compositions for cathodes of battery types 1 and 2 are listed in Table 11. All concentrations are reported as a fractional mass of the total cathode weight. The amount of magnetic material used was set at 5% w/w $SmCo_5$. For magnetically modified batteries, the EMD content was lowered based on the amount of $SmCo_5$ added, meaning a control cathode pellet weighing 1 gram would contain 0.86 g EMD and 0.00 g $SmCo_5$ versus 0.81 g EMD and 0.05 g $SmCo_5$. Similar adjustments were made for type 2 batteries.

Table 11. Cathode formulations for low electrolyte batteries reported as a fractional mass, % w/w.

Type 1			Type 2	
Blank	Mag Mod	Reagent	Blank	Mag Mod
86	81	EMD	75	70
–	5	$SmCo_5$	–	5
–	–	PVDF	5	5
2	2	PTFE	–	–
8	8	Graphite	15	15
5	5	KOH	5	5
Industrial Grade		Separator	Whatman #1	

Cathode materials were mixed as previously described. The pressing procedure here was aimed at increased pellet density to reduce any void spaces within the pellet. The pressing procedure applied 4 tons of force for 60 seconds, slow release of pressure, and reapplication of 4 tons for 30 seconds. Removal of the pellet was easier than batteries from Chapter 3 because of less electrolyte in the system.

4.1.2 Anode Preparation

Preparation of type 1 anode was similar to that in Chapter 3, but the greatest difference involved implementation of a polyacrylate gelling agent, Carbopol 940, in place of carboxymethyl cellulose. Carbopol provided greater gelling efficiency over carboxymethyl cellulose and required less gelling material. The difference in mass allowed for more zinc in the anode.

Table 12. Anode formulation, reported as % w/w, with Carbopol 940.

Type 1	Reagent	Type 2
68.5	Zn	100
1	ZnO	–
0.5	Carbopol 940	–
30	KOH	200 μL

4.1.3 Battery Assembly

Assembly of the battery followed the procedure described in the Section 2.4.4. Battery type 1 used a copper current collector as depicted in Figure 7. Type 2 batteries used no current collector because of current collector oxidation issues,

which will be discussed later. For type 2 batteries, the anode was in direct contact with the stainless steel clamshell.

4.1.4 Instrumentation

All batteries were discharged with a MTI BST8-MA battery analyzer, an independently controlled 8 channel device with 0.1-10 mA current range and up to ± 5 V. Discharge rates were C/5, C/3, and C/2 as calculated in Chapter 2. All impedance measurements were performed with a CH Instruments model 760B potentiostat/galvanostat in a two electrode configuration. The working electrode wire from the instrument was connected to the cathode, while the reference and counter electrode wires were linked together and connected to the anode. Parameters for all impedance measurements were made with an initial voltage set to the open circuit voltage of the battery, a voltage amplitude of 0.01 V, and a frequency range of 1×10^5 to 0.05 Hz. Data were fitted with the embedded simulator function of the control software. Because the open circuit voltage measurement is a separate instrument function, control macros were written to automate the settings adjustment and measurement. See Appendix C for the macro code used to automate the instrument.

4.2 Results and Discussion

The results discussed here are for constant current discharge performance for battery types 1 and 2. Impedance data are presented for battery type 1.

4.2.1 Battery Type 1

Two different discharge rates were used to evaluate battery performance, C/5 and C/3. These rates should be considered as a moderate rate for C/5, while C/3 is considered a fast drain. Both are good determinants for battery performance. Statistical evaluation are not as strong for these low electrolyte type 1 batteries because variances were generally higher. It was never clear what specifically caused the variation and lesser performance, but was clearly related to composition. Because industrially relevant compositions are proprietary and described vaguely at best, great effort was spent on finding an optimized composition. In the end, no such composition was found and the type 1 batteries presented here demonstrated the most consistent performance.

The current collector contributed to performance variation. Generally, the current collector is a piece of metal that is considered inert during discharge because of the preferred thermodynamic process is $Zn|MnO_2$. The purpose of the current collector is to simply pass current from the anode to the circuit. However, oxidation of the copper current collector on the anode was often observed during disassembly of spent alkaline batteries. This indicated a side reaction between copper and EMD and was considered as an indicator of kinetic limitations of the anode. Other materials were tested, such as cartridge brass [59] and zinc metal, but are not reported here. Brass (copper/zinc alloy) was observed to oxidize during discharge and zinc ions from the consumed gel anode would often reduce to zinc metal onto the current collector during discharge. Effectively, zinc would electroplate onto the brass. Use of zinc

metal as the current collector was not useful either. Batteries reported here used a copper current collector.

Discharge performance had rather bimodal performance where magnetically modified batteries underwent a more consistent discharge and control batteries performed with great variance. Statistical analysis of discharge properties for battery type 1 is performed to maintain consistency of analysis, but should be treated lightly as offering anything authoritative. One distince advantage of this configuration was the capability to use impedance spectroscopy to probe the system. This differed from type 2 batteries, which did not generate usable impedance data.

4.2.1.1 C/5 Rate

Representative discharge performance of battery type 1 at a C/5 rate is shown in Figures 19 and 20 for voltage (V) and energy (mWh/g), respectively. There are several points of interest. First, magnetically modified batteries maintain higher voltage for longer duration than nonmodified batteries. This demonstrates more power is produced over time for the constant current discharge. Second, the batteries all eventually converge near the same point before progressing into the second electron reduction below 0.8 V. This behavior was consistent throughout battery type 1 and disallows comparison of overall coulombic efficiency. Even though these batteries have stoichiometric ratios of 10:1 zinc to EMD, they perform as zinc limited systems. Finally, it should be noted that nonmagnetic batteries quickly decrease below 1.0 V and then are shown to sustain a low voltage discharge before progressing to the next reduction. Differences in the closed circuit voltage ($t = 0$)

are significant.

Batteries of this type exhibited rather different discharge behaviors. Nonmodified batteries demonstrated a near Ohm's Law relationship ($V = IR$) during early stages of discharge. Batteries commonly dipped to near $+0.9\ V$ or $+0.8\ V$ and would then increase in voltage. This is thought to correlate to a permeation effect of KOH within the cathode pellet. Magnetically modified batteries were capable of sustaining a higher voltage for a longer period of time. The previously mentioned voltage dip was not observed during discharge for modified batteries and a smooth discharge profile was often observed. Regardless of composition, both the control and modified batteries displayed poor performance with respect to time. For a C/5 rate, the theoretical discharge duration is five hours. These batteries typically finished within a much shorter time frame of three hours.

The corresponding representative energy plot, Figure 20, shows that magnetically modified systems are capable of sustaining more energy than blank (control) systems. However, the peculiarities of the voltage discharge profiles for the control batteries are reflected in the energy plots as well.

Statistical treatment of the data was performed as previously described in Section 2.5.3. Table 13 contains averaged voltage discharge and integrated energy data for battery type 1 with a C/5 discharge rate. Standard deviations are reported for 1σ. Time to a given voltage is an indicator of a battery's ability to sustain power output over the course of the discharge. Higher voltages for longer periods of time indicate greater power output. Magnetically modified batteries were capable of sustaining

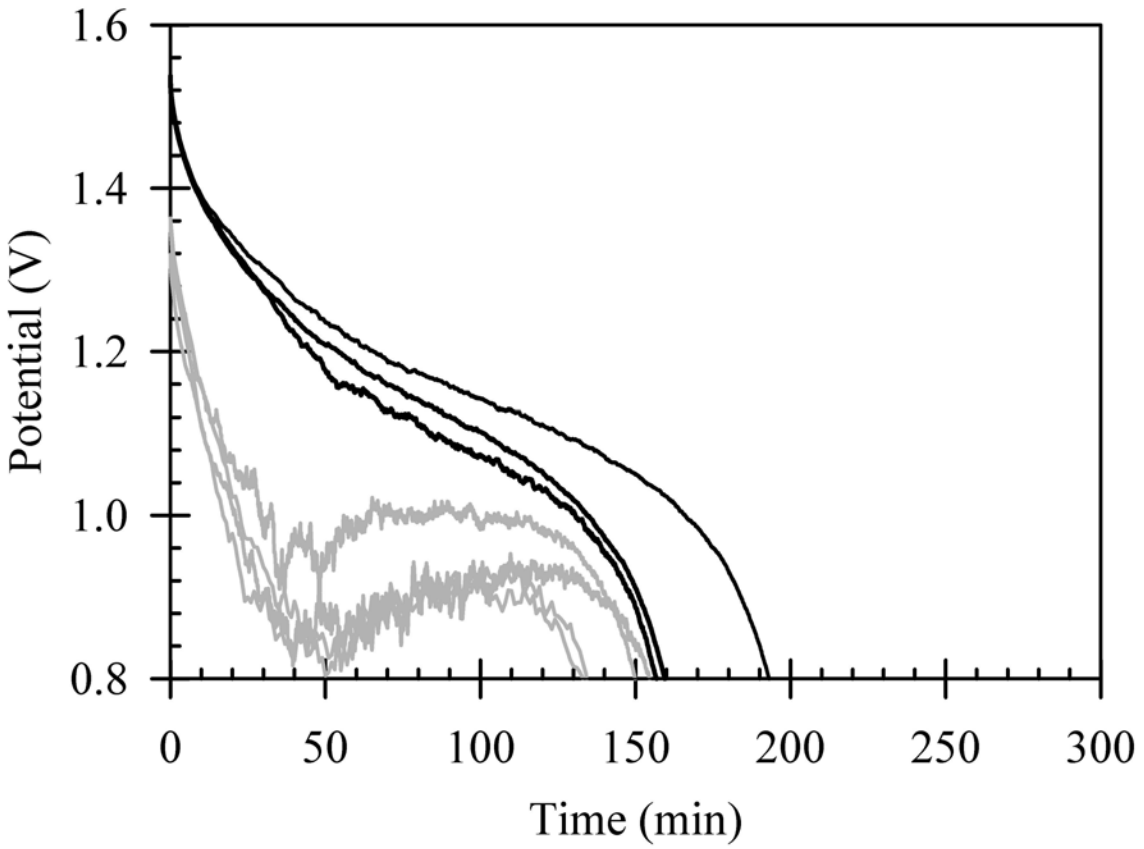

Figure 19. Representative discharge curve for low electrolyte battery type 1 discharged at a C/5 rate. Magnetically modified batteries are in black and nonmodified batteries are in gray. Theoretical discharge time for C/5 is 300 minuets.

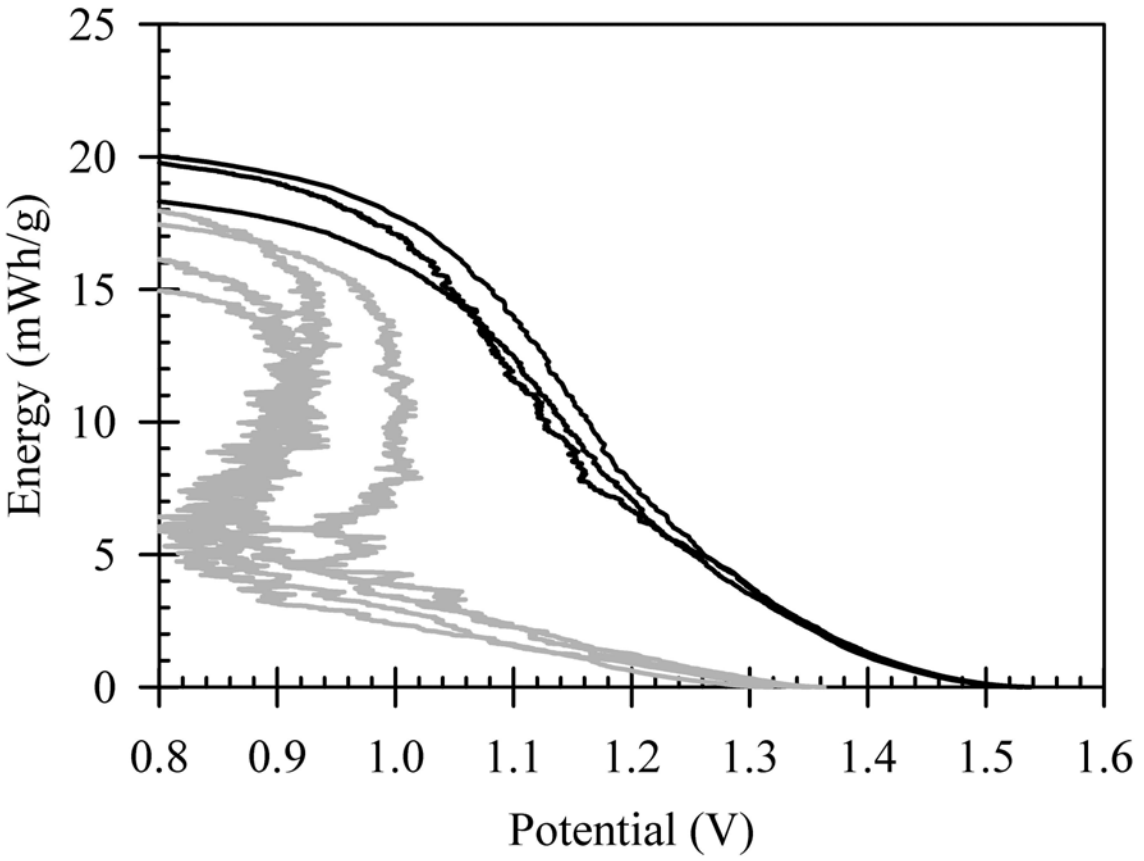

Figure 20. Representative energy curve for low electrolyte battery type 1 discharged at a C/5 rate. Magnetically modified batteries are in black and nonmodified batteries are in gray.

higher voltage longer than control batteries. The enhancement is reported as the ratio of performance for modified/control batteries.

$$enhancement = \left(\frac{modified}{control} - 1\right) * 100\% \tag{53}$$

For C/5 discharge rates, modified batteries outperform control batteries throughout the discharge with an $\sim$ 90% or higher confidence interval for $n = 4$ batteries each. However, this is not a good comparison of battery performance because of the previously mentioned discharge issues of the control batteries. The batteries presented here were the most consistent cells for this category. The data set is limited because the large variance and poor initial performance excluded a large fraction of batteries from statistical consideration. Poor initial performance was particularly significant for the control batteries. Batteries that discharged below 1.2 V in less than 10 minutes were excluded from the data pool. This metric is the same used for statistical treatment of batteries from Chapter 3.

Figures 21 and 22 are column plots for the voltage versus time and energy versus voltage data, respectively. These column plots are visual representations of data in Table 13. From the data, modified batteries provide more energy and power for voltages above 0.9 V. Limitations of the zinc anode are apparent at the lower voltages.

4.2.1.2 C/3 Rate

A faster discharge rate was used to evaluate performance of type 1 batteries. Discharge performance at a C/3 rate is shown in Figures 23 and 24 for voltage versus

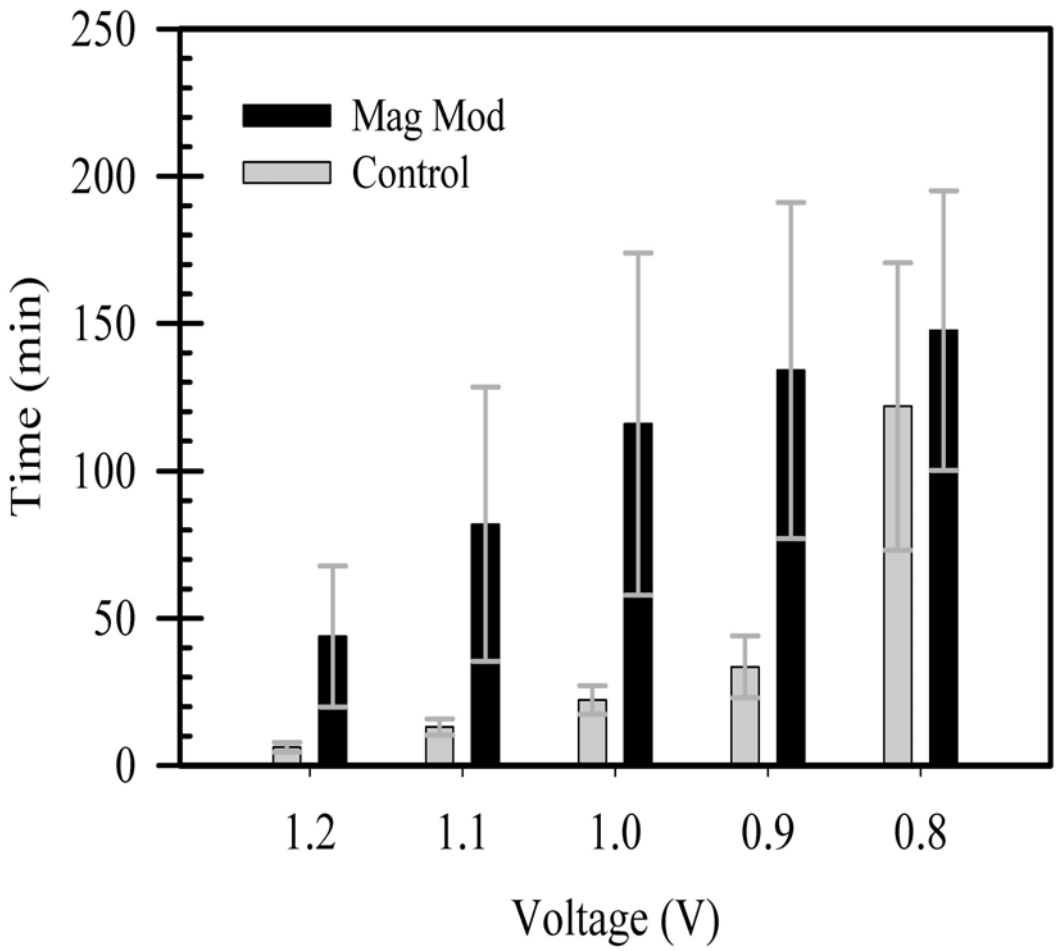

Figure 21. Bar graph representation of time to a given voltage for battery type 1 at a C/5 discharge rate. Magnetically modified batteries are in black and nonmodified batteries are in gray.

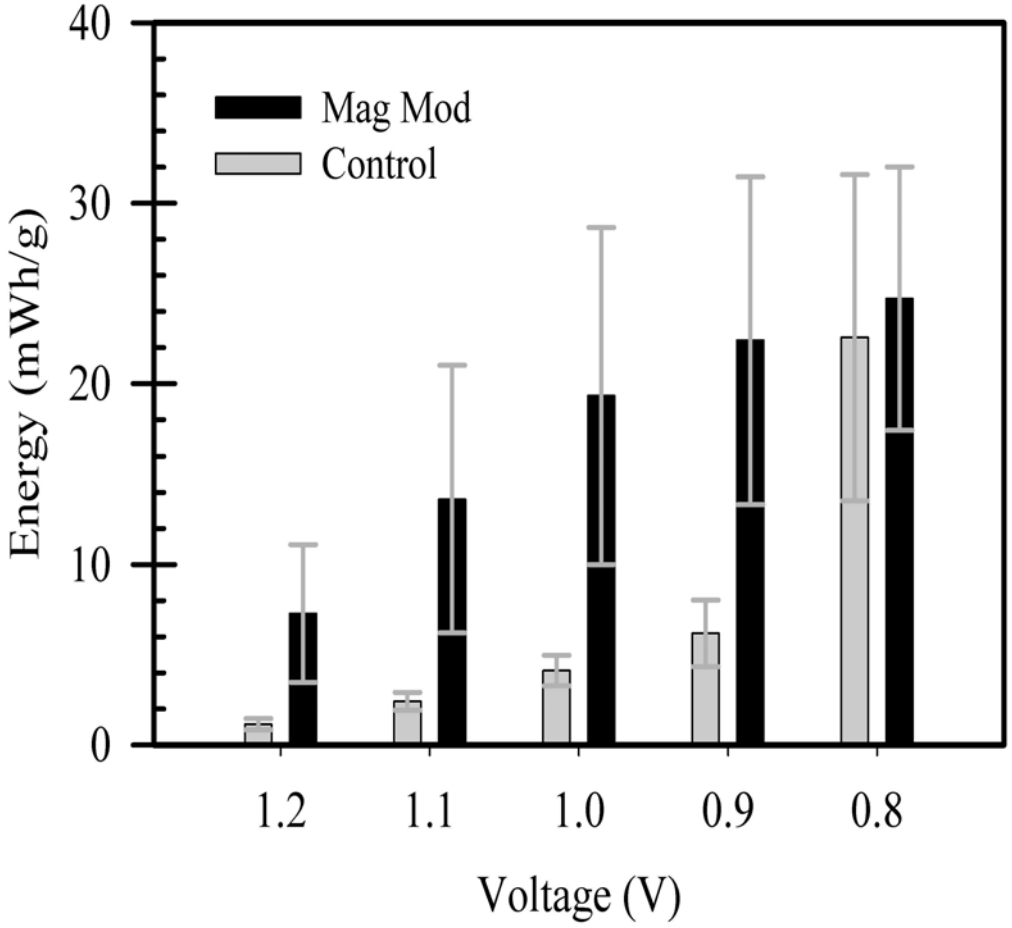

Figure 22. Bar graph representation of total energy at a given voltage for battery type 1 at a C/5 discharge rate. Magnetically modified batteries are in black and nonmodified batteries are in gray.

time and energy versus voltage, respectively. Performance is comparable to C/5 data such that higher voltages are sustained for longer periods of time for magnetically modified batteries over nonmodified batteries. As seen for type 1 C/5 discharge, the control batteries demonstrate a lesser ability to sustain a voltage and demonstrate a similar dip in discharge voltage before stabilizing and sustaining low voltages for the remainder of the discharge. A more distinct linear ohmic profile is observed for both control and modified cells. For the faster C/3 discharge rate, larger impacts of ohmic loss ($V = IR$) are expected. The sharp transition from the first electron to the second electron is observed at roughly the same time ($\sim$ 80 minutes), indicating zinc limited behavior.

From the data in Table 14, modified batteries provide more energy and power for voltages above 0.9 V. Similar limitations of the zinc anode are apparent at the lower voltages were observed.

4.2.2 Battery Type 2

Evaluation of nongelled type 2 batteries were performed with discharge rates of C/5, C/3, and C/2. Compositions of type 2 batteries are listed in Tables 11 and 12 for the cathode and anode, respectively. Type 2 cathodes differed from type 1 cathodes in composition ratios of EMD, and graphite. A different binder was used, PVDF instead of PTFE, to reduce hydrophobicity. However, greater quantities were required to maintain pellet integrity. The mixing and pressing procedures were identical to type 1 batteries. The anode was a nongelled mixture of the

Table 13. Tabulated performance values for battery type 1 at C/5 discharge rates.

Time (min) to a Given Voltage (Figure 21)				
Voltage (V)	Control ($n = 4$)	Modified ($n = 4$)	Enhancement	Confidence Level
1.2	6.2 ± 1.6	43.8 ± 23.9	606%	99%
1.1	13.1 ± 2.7	81.9 ± 46.5	526%	99%
1.0	22.3 ± 4.9	115.9 ± 58.1	420%	99%
0.9	33.5 ± 10.6	134.1 ± 57.0	300%	99%
0.8	121.8 ± 48.8	147.6 ± 47.4	21%	88%

Energy (mWh/g) at a Given Voltage (Figure 22)				
Voltage (V)	Control	Modified	Enhancement	Confidence Level
1.2	1.2 ± 0.3	7.3 ± 3.8	534%	98%
1.1	2.4 ± 0.5	13.6 ± 7.4	462%	99%
1.0	4.1 ± 0.9	19.3 ± 9.3	369%	99%
0.9	6.2 ± 1.9	22.4 ± 9.1	262%	99%
0.8	22.6 ± 9.0	24.7 ± 7.3	9%	99%

Table 14. Tabulated performance values for battery type 1 at C/3 discharge rates.

Time (min) to a Given Voltage (Figure 25)				
Voltage (V)	Control ($n = 4$)	Modified ($n = 4$)	Enhancement	Confidence Level
1.2	10.0 ± 1.0	20.2 ± 3.5	103%	99%
1.1	16.1 ± 1.0	36.0 ± 5.7	123%	99%
1.0	24.5 ± 2.9	58.2 ± 5.7	137%	99%
0.9	53.7 ± 20.4	75.2 ± 2.3	40%	99%
0.8	82.6 ± 2.6	82.6 ± 1.4	0%	99%

Energy (mWh/g) at a Given Voltage (Figure 26)				
Voltage (V)	Control	Modified	Enhancement	Confidence Level
1.2	3.0 ± 0.2	5.9 ± 1.0	98%	89%
1.1	4.8 ± 0.2	10.5 ± 1.5	118%	96%
1.0	7.3 ± 0.7	17.0 ± 1.6	132%	99%
0.9	16.1 ± 6.0	22.0 ± 0.9	37%	99
0.8	24.8 ± 0.9	24.1 ± 1.0	–	–

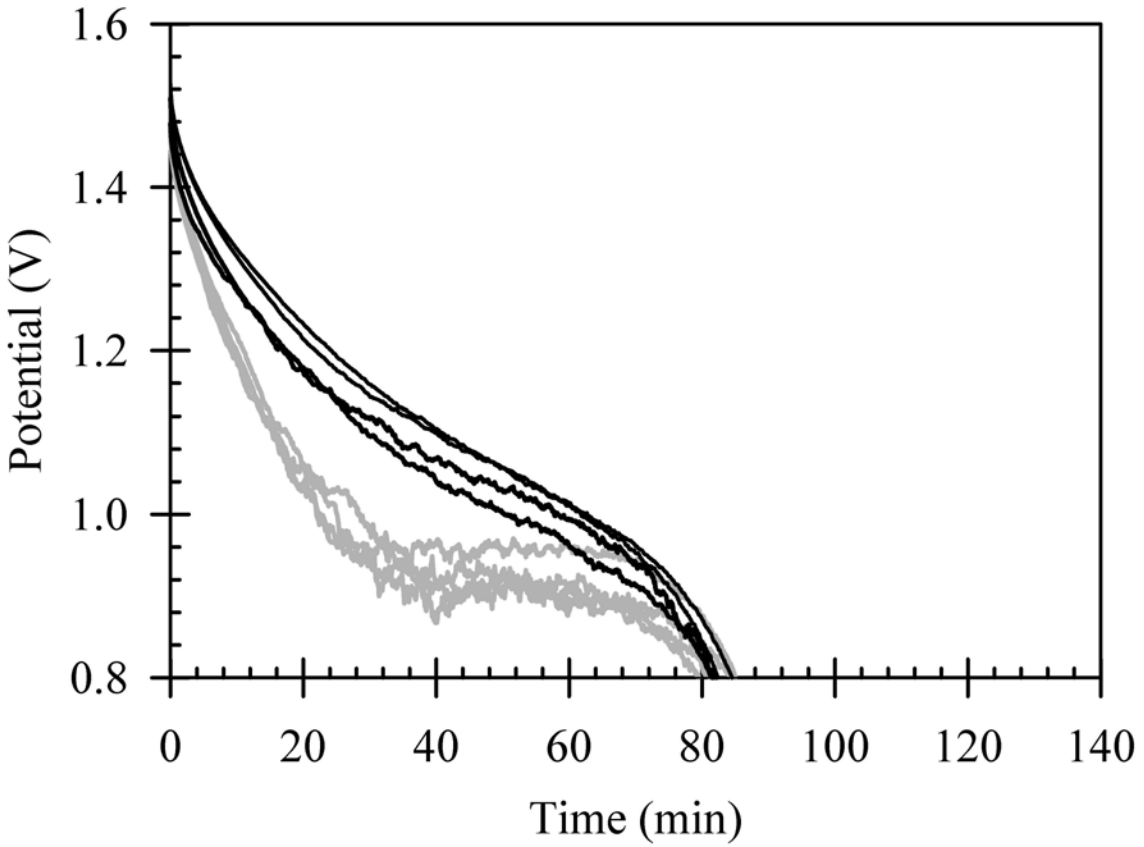

Figure 23. Representative discharge curve for low electrolyte battery type 1 discharged at a C/3 rate. Magnetically modified batteries are in black and nonmodified batteries are in gray. Maximum theoretical discharge time is 180 minutes.

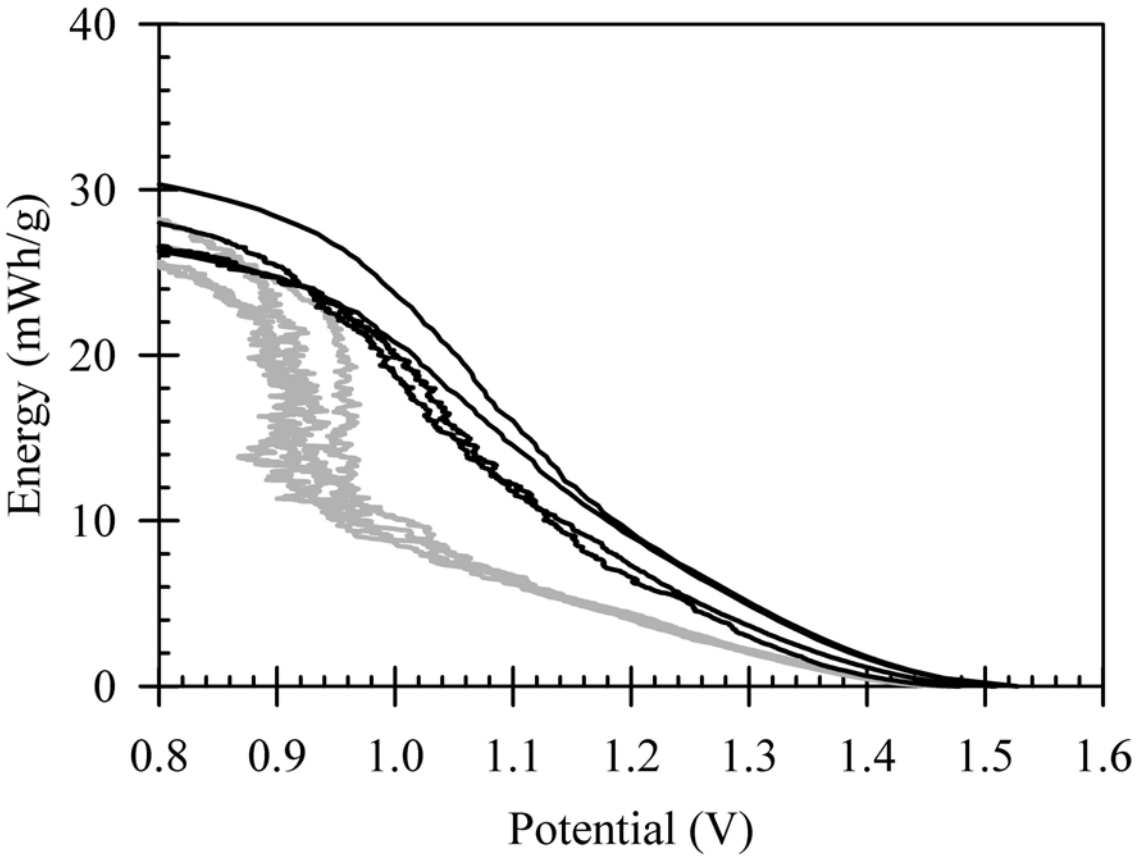

Figure 24. Representative energy curve for low electrolyte battery type 1 discharged at a C/3 rate. Magnetically modified batteries are in black and nonmodified batteries are in gray.

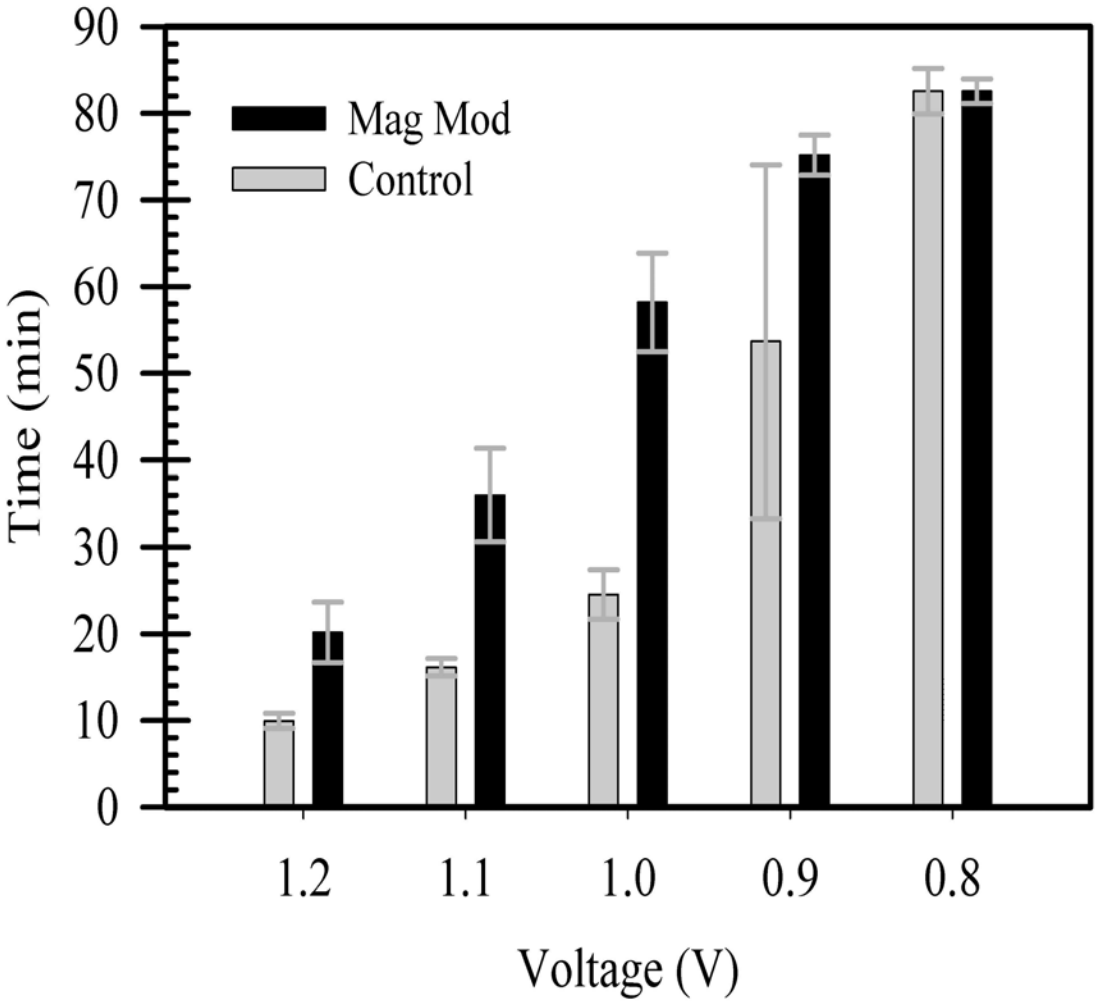

Figure 25. Bar graph representation of time to a given voltage for type 1 batteries at a C/3 discharge rate. Magnetically modified batteries are in black and nonmodified batteries are in gray.

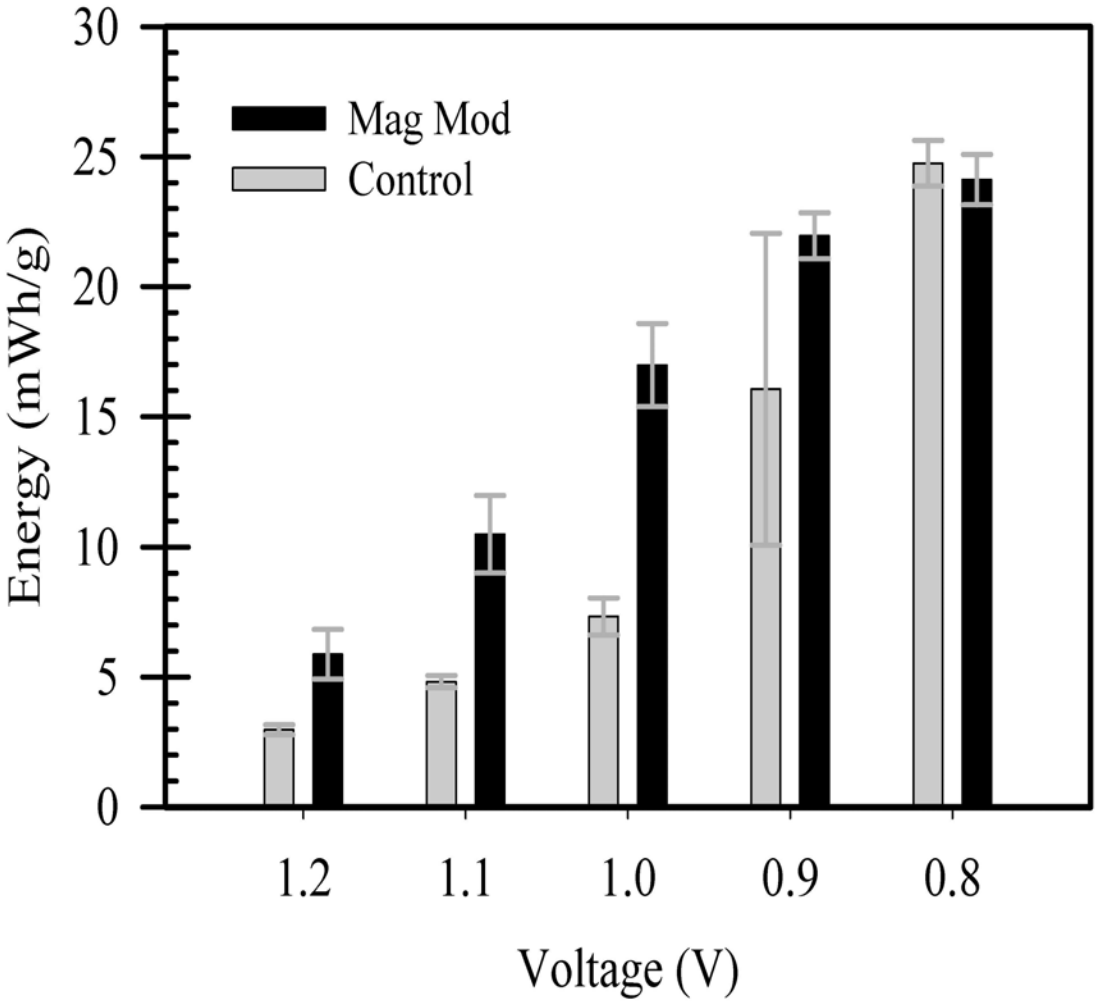

Figure 26. Bar graph representation of energy at a given voltage for type 1 batteries at a C/3 discharge rate. Magnetically modified batteries are in black and nonmodified batteries are in gray.

same granulated zinc used for type 1 batteries and KOH electrolyte. No special preparation was required or performed. Dry zinc was weighed to a desired mass, added to the clamshell, and KOH electrolyte poured over the granulated zinc. The separator used was a cellulose based Whatman #1 filter paper and was saturated in KOH electrolyte prior to assembly. Because of its thickness, only one layer was necessary. The assembly procedure was similar to previously discussed batteries (Figure 7) except the copper current collector was not used. This was an attempt to minimize side reactions within the system. Anodic materials were in direct contact with the stainless steel clamshell.

Overall, type 2 batteries offered a better and more consistent discharge performance. For the first time, data analysis for voltages higher than 1.2 V was possible and offered a more complete view of discharge performance across three different discharge rates. However, these batteries were not well suited for EIS analysis. Nyquist plots for these batteries at best were noisy and typically unusable. Consequently, no equivalent circuit analysis is presented for type 2 batteries.

4.2.2.1 C/5 Rate

Discharge performance of type 2 batteries at the C/5 rate is shown in Figures 27 and 28 for voltage versus time and energy versus voltage, respectively. Performance between control and modified cells was more comparable than for type 1 batteries. Closed circuit voltages, $t = 0$, were much closer to open circuit values for both modified and control batteries. Progression through the discharge still revealed an ohmic (linear) behavior and demonstrated comparable discharge times even though

the amount of zinc within the battery was 10 times greater than MnO_2.

Performance values were statistically analyzed as listed in Table 15. At early times ($V > 1.1$), magnetically modified batteries outperformed control batteries by as much as 34 % for time to 1.2 V and 36 % for energy at 1.2 V. As seen previously, batteries behaved as if zinc limited and ended the discharge at approximately 3.5 hours, which was an hour longer than type 1 batteries. This result could be related to the nongelled anode, the difference in cathode conductivity because of more graphite, or both. Figures 29 and 30 are visual representations of the data listed in Table 15.

Table 15. Tabulated performance values for battery type 2 at C/5 discharge rates. Performance values for enhancement are not reported below 1.1 V because no statistically vetted enhancement was observed.

Time (min) to a Given Voltage (Figure 29)				
Voltage (V)	Control ($n = 10$)	Modified ($n = 11$)	Enhancement	Confidence Level
1.4	22.9 ± 2.8	25.1 ± 4.8	10%	78%
1.3	49.6 ± 4.8	59.3 ± 6.6	20%	99%
1.2	87.9 ± 12.5	117.7 ± 11.6	34%	99%
1.1	158.1 ± 23.7	169.8 ± 13.9	7%	82%
1.0	196.0 ± 27.9	194.5 ± 15.9	–	–
0.9	204.6 ± 30.6	202.5 ± 16.7	–	–
0.8	209.2 ± 32.2	207.3 ± 17.1	–	–

Energy (mWh/g) at a Given Voltage (Figure 30)				
Voltage (V)	Control	Modified	Enhancement	Confidence Level
1.4	2.2 ± 0.2	2.4 ± 0.5	12%	87%
1.3	4.5 ± 0.3	5.5 ± 0.7	22%	99%
1.2	7.6 ± 0.9	10.3 ± 1.3	36%	99%
1.1	12.8 ± 1.6	14.4 ± 2.0	12%	93%
1.0	15.5 ± 1.9	16.1 ± 2.3	–	–
0.9	16.0 ± 2.1	16.6 ± 2.4	–	–
0.8	16.3 ± 2.2	16.9 ± 2.4	–	–

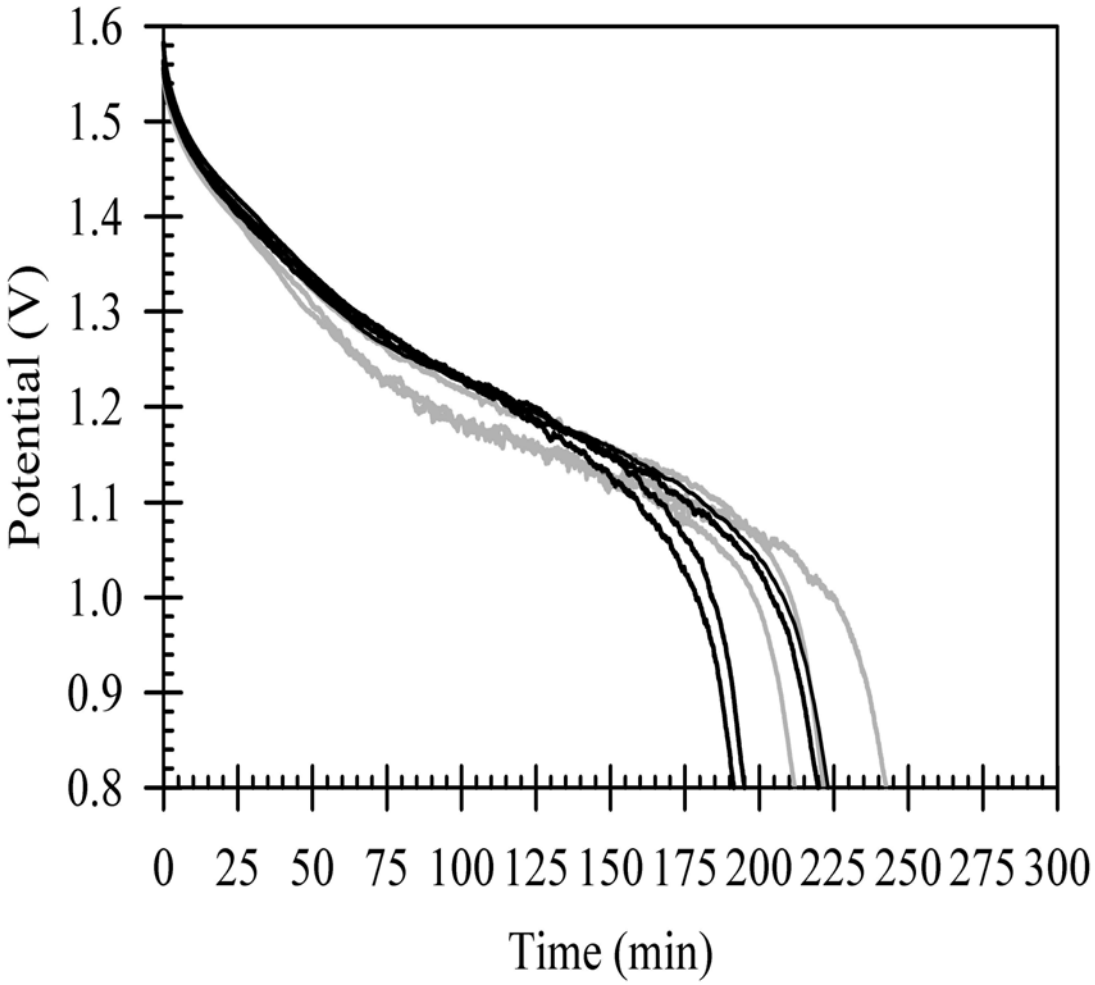

Figure 27. Representative discharge curve for low electrolyte battery type 2 discharged at a C/5 rate. Magnetically modified batteries are in black and nonmodified batteries are in gray. Maximum theoretical discharge time is 300 minutes.

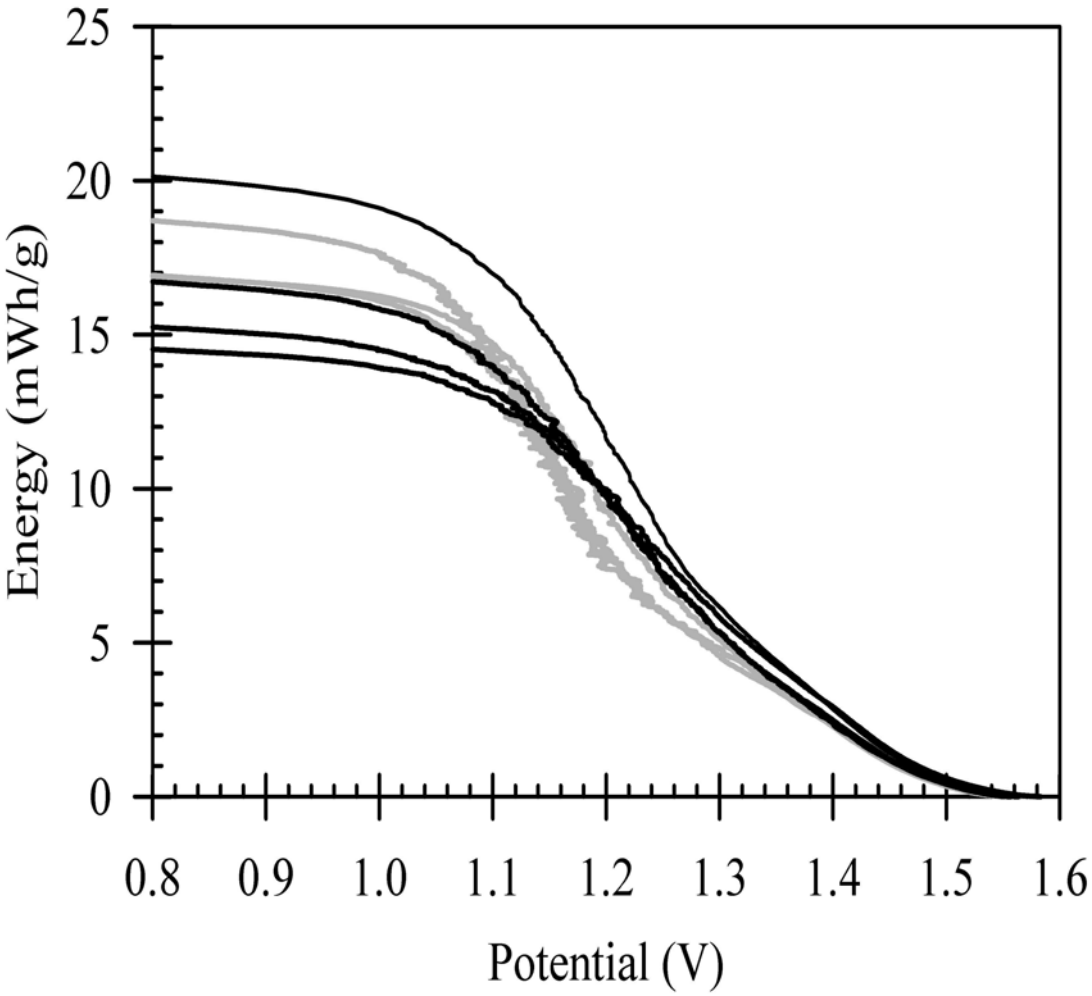

Figure 28. Representative energy curves for low electrolyte battery type 2 discharged at a C/5 rate. Magnetically modified batteries are in black and nonmodified batteries are in gray.

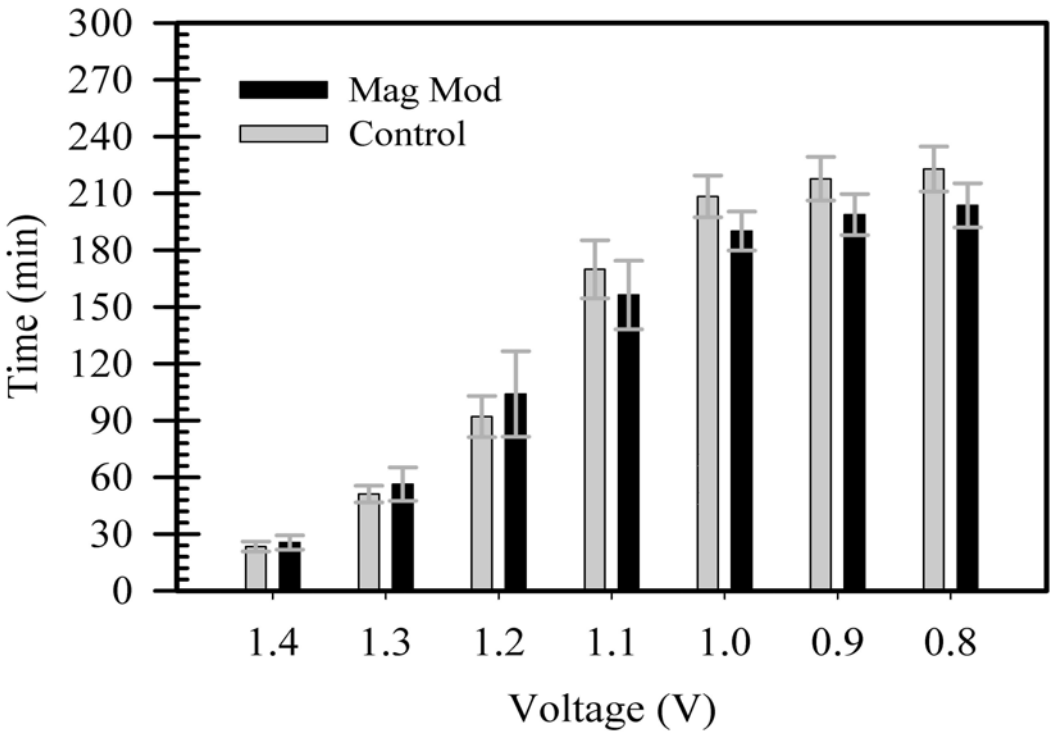

Figure 29. Bar graph representation of time to a given voltage for type 2 batteries at a C/5 discharge rate. Magnetically modified batteries are in black and nonmodified batteries are in gray.

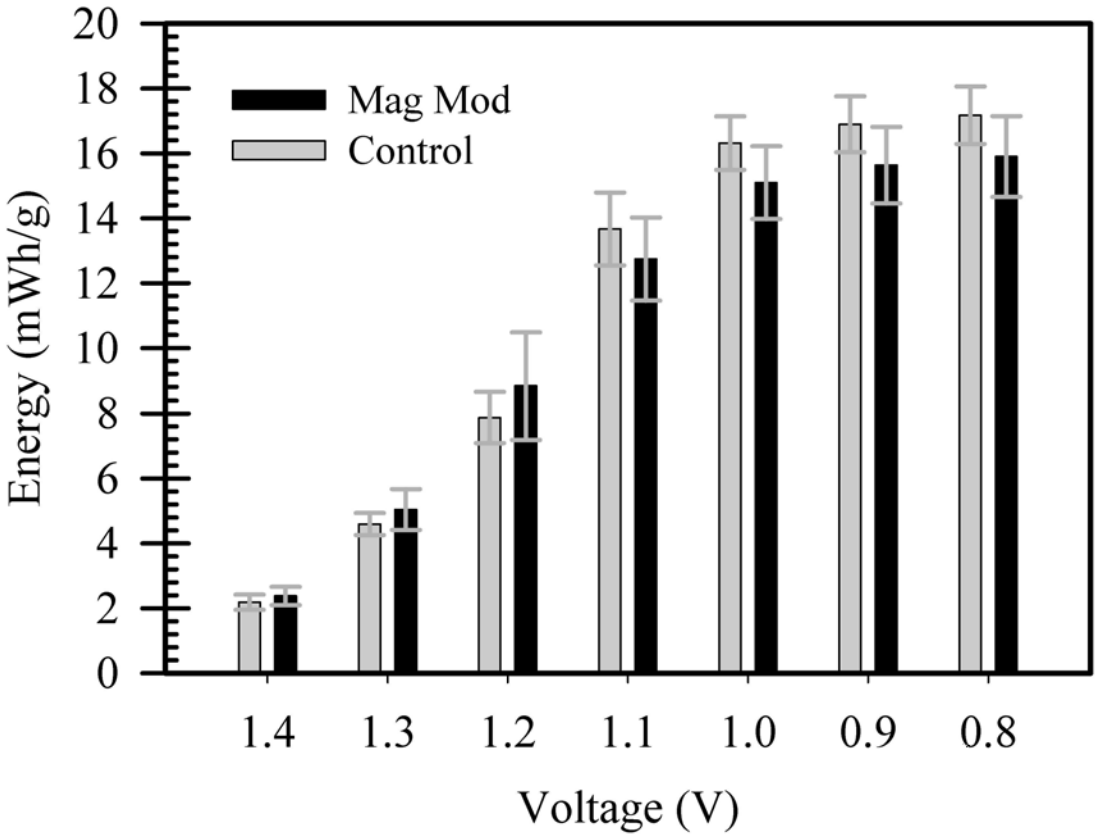

Figure 30. Bar graph representation of total energy at a given voltage for type 2 batteries at a C/5 discharge rate. Magnetically modified batteries are in black and nonmodified batteries are in gray.

4.2.2.2 C/3 Rate

Discharge performance of battery type 2 with a C/3 rate is shown in Figures 31 and 32. Statistical treatment of C/3 discharge data is listed in Table 16. Comparison of discharge profiles shows that modified batteries perform better than control batteries for time to a given voltage. Due to large standard deviations within the energy data, no enhancement is provided at confidence levels higher than 50 %. Comparison of energy averages do show that modified batteries perform better than control batteries. However, a statistically vetted comparison is not available. Visual representations of the data in Table 31 are shown in Figures 33 and 34.

Table 16. Tabulated performance values for battery type 2 at C/3 discharge rates.

Time (min) to a Given Voltage (Figure 33)				
Voltage (V)	Control ($n = 8$)	Modified ($n = 8$)	Enhancement	Confidence Level
1.4	5.4 ± 2.8	10.0 ± 2.8	86%	99%
1.3	15.9 ± 4.8	25.6 ± 3.5	60%	99%
1.2	28.2 ± 7.2	49.9 ± 6.9	77%	99%
1.1	45.1 ± 12.0	83.0 ± 12.4	84%	99%
1.0	72.6 ± 20.6	106.3 ± 6.9	47%	99%
0.9	107.7 ± 6.7	115.3 ± 6.5	7%	96%
0.8	115.3 ± 4.7	119.2 ± 6.7		

Energy (mWh/g) at a Given Voltage (Figure 34)				
Voltage (V)	Control	Modified	Enhancement	Confidence Level
1.4	1.2 ± 0.5	1.3 ± 0.7	–	–
1.3	3.2 ± 0.8	3.3 ± 1.3	–	–
1.2	5.4 ± 1.6	6.1 ± 2.4	–	–
1.1	8.3 ± 3.4	9.7 ± 3.2	–	–
1.0	11.4 ± 3.2	12.6 ± 3.4	–	–
0.9	14.0 ± 2.0	15.0 ± 1.3	–	–
0.8	14.6 ± 1.8	15.5 ± 1.3	–	–

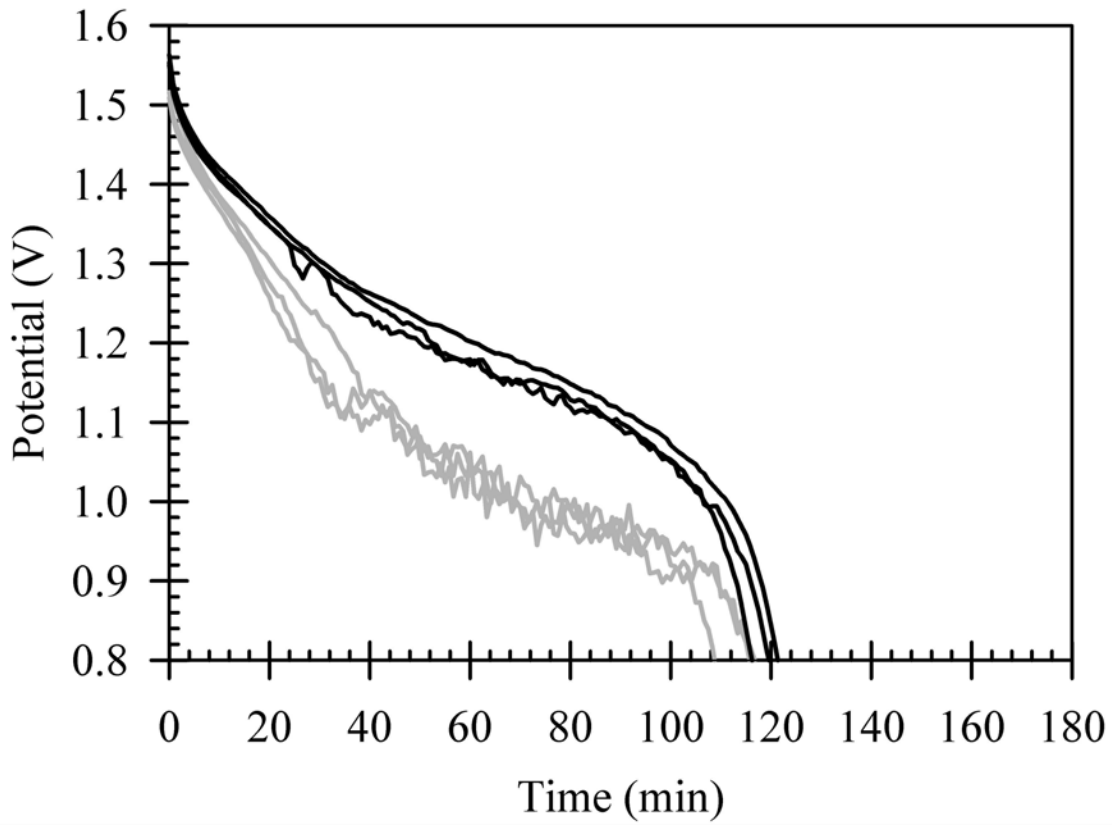

Figure 31. Representative discharge curve for low electrolyte type 2 batteries discharged at a C/3 rate. Magnetically modified batteries are in black and nonmodified batteries are in gray.

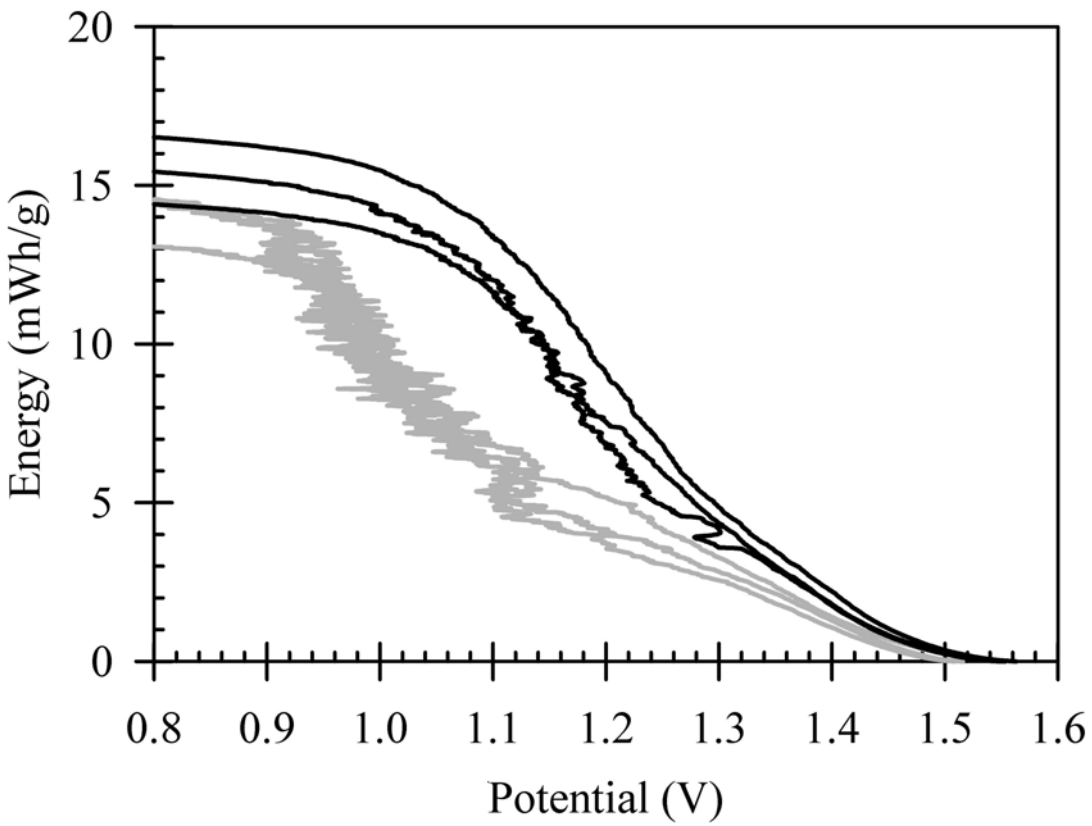

Figure 32. Representative energy curves for low electrolyte type 2 batteries discharged at a C/3 rate. Magnetically modified batteries are in black and nonmodified batteries are in gray.

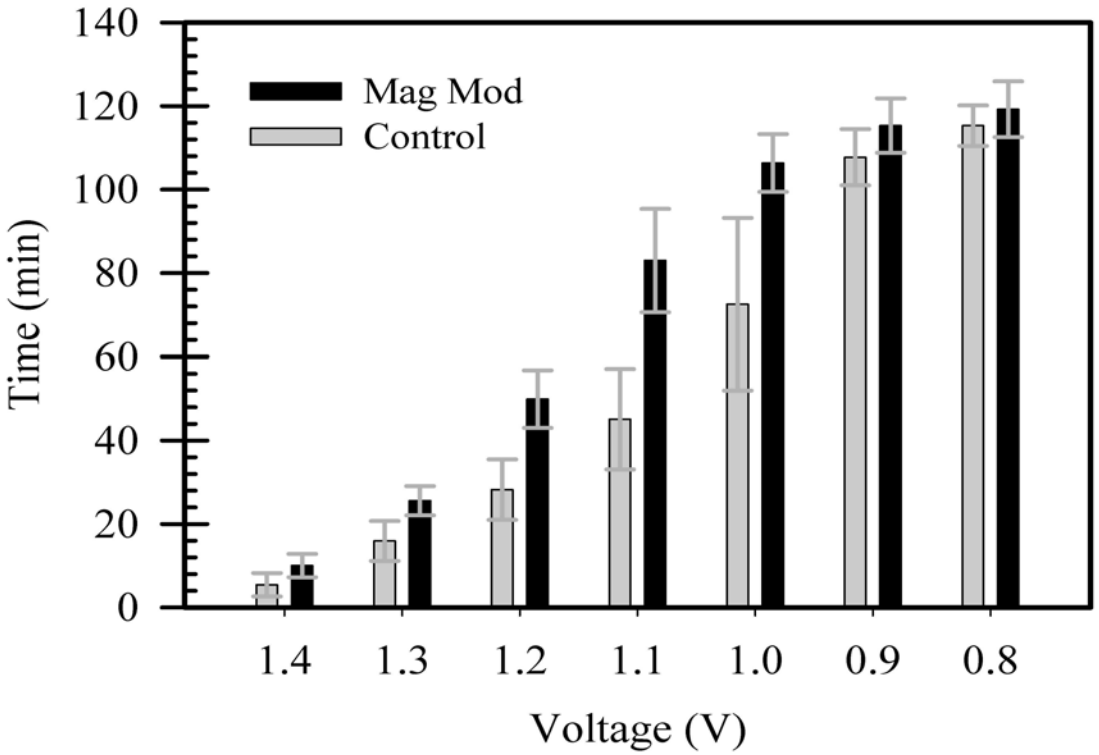

Figure 33. Bar graph representation of time to a given voltage for type 2 batteries at a C/3 discharge rate. Magnetically modified batteries are in black and nonmodified batteries are in gray.

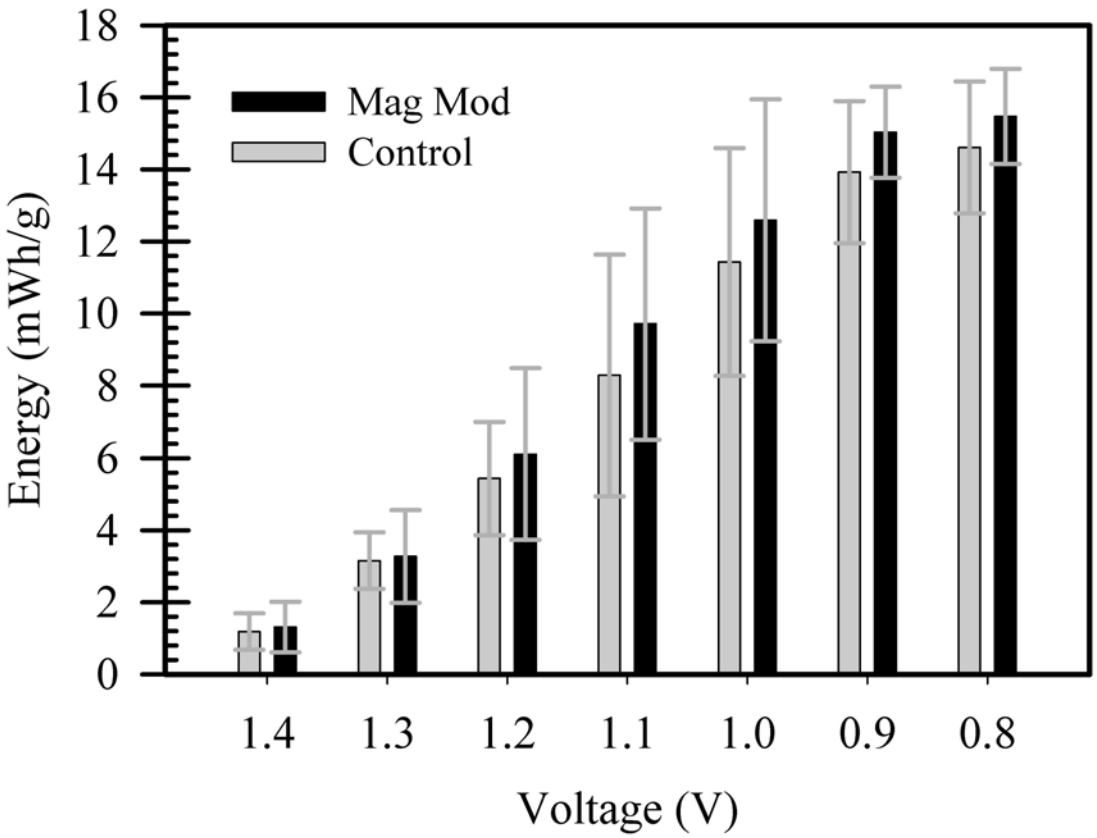

Figure 34. Bar graph representation of energy at a given voltage for type 2 batteries at a C/3 discharge rate. Magnetically modified batteries are in black and nonmodified batteries are in gray.

4.2.2.3 C/2 Data

Data collected at a C/2 discharge rate are shown in Figures 35 and 36 for voltage versus time and energy versus voltage, respectively. The C/2 discharge rate is a very fast rate that is essentially a kinetic stress test of the system. Batteries tested under this discharge rate rapidly consume reagents at a rate that does not allow for any equilibrium conditions to establish. The argument here is to address the assertion that magnetically modified batteries are capable of producing more power. It has been demonstrated the modified batteries do not improve the coulombic efficiency of the system as seen in common end times, likely set by the anode, but do sustain higher voltages for longer periods of time that translates to greater power output.

Similar morphologies are observable in the discharge profile for modified and control batteries. Both batteries were operable for 50 % to 60 % of the maximum theoretical discharge time and demonstrated similar ohmic behavior with a near linear discharge profile. As for the previous C/5 and C/3 rates, the zinc anode plays a large role in dictating discharge time.

Statistical analysis of discharge data is listed in Table 17. A common coulombic efficiency was observed again under these conditions. However, magnetically modified batteries outperformed control batteries under the very fast C/2 discharge rate. Improved performance of modified batteries over controls was observed to be greater than 40% throughout most of the discharge. Visual representations of values in Table 17 are in Figures 37 and 38. Thus, magnetic modification enabled higher rates of discharge, especially above 1.0 V, which is the voltage cut off for high

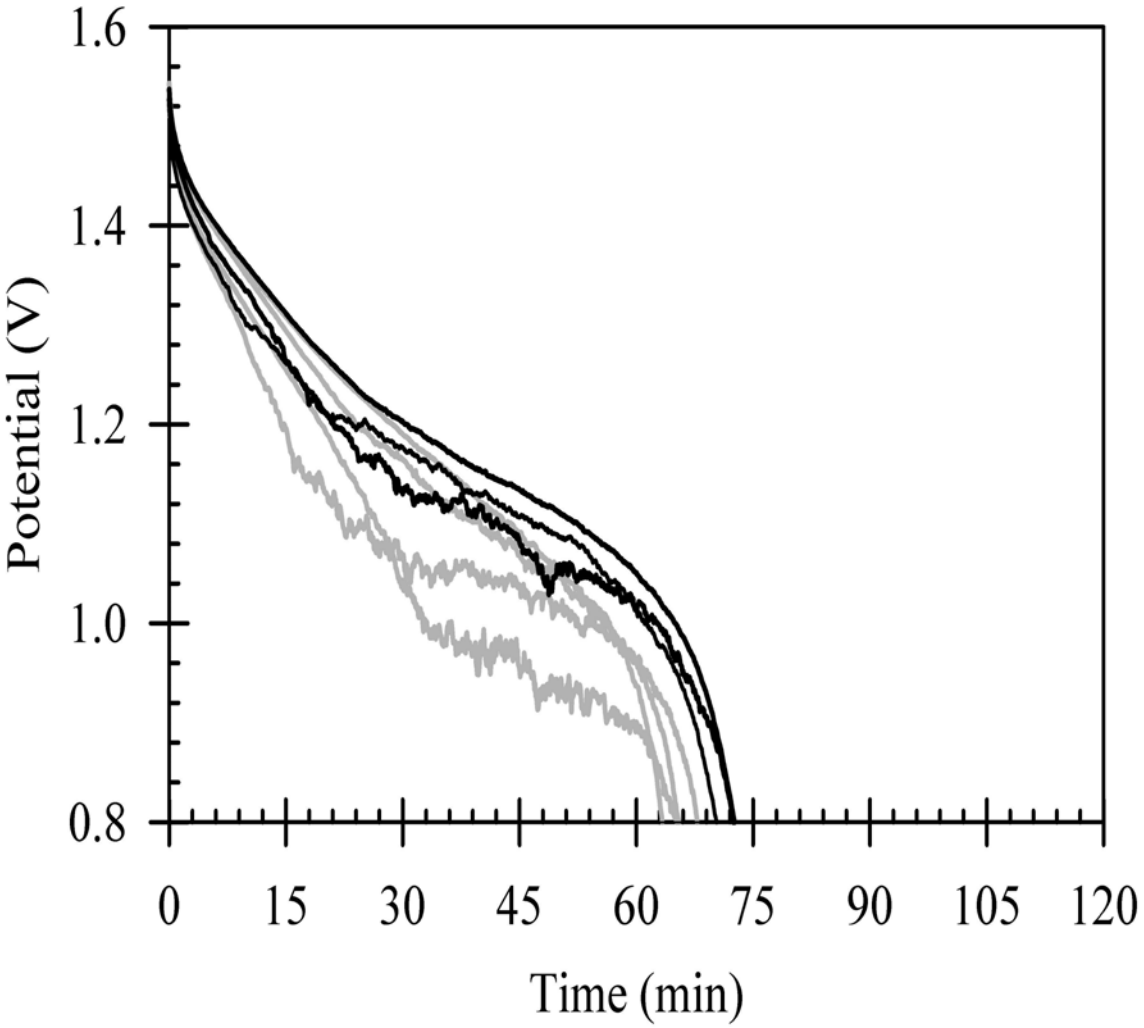

Figure 35. Representative discharge curve for low electrolyte type 2 batteries discharged at a C/2 rate. Magnetically modified batteries are in black and nonmodified batteries are in gray. Maximum theoretical discharge time was 120 minutes.

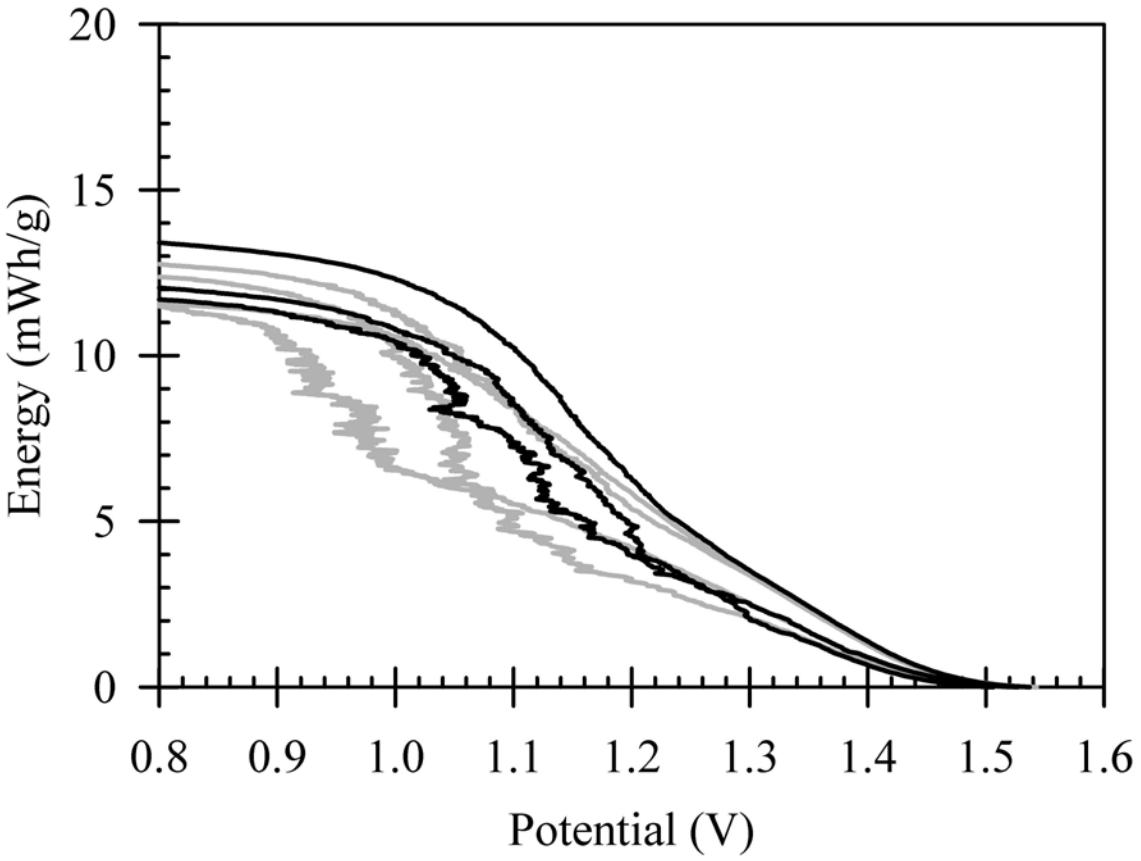

Figure 36. Representative energy versus voltage curve for low electrolyte type 2 batteries discharged at a C/2 rate. Magnetically modified batteries are in black and nonmodified batteries are in gray.

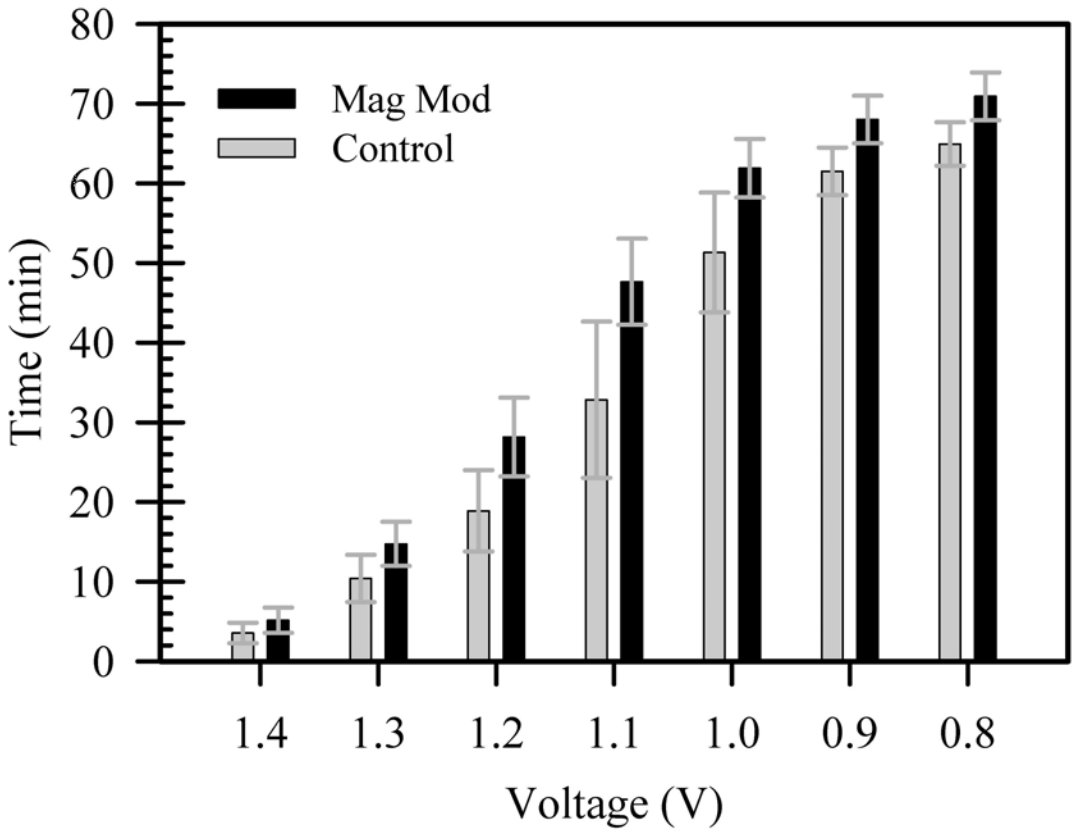

Figure 37. Bar graph representation of time to a given voltage for type 2 batteries at a C/2 discharge rate. Magnetically modified batteries are in black and nonmodified batteries are in gray.

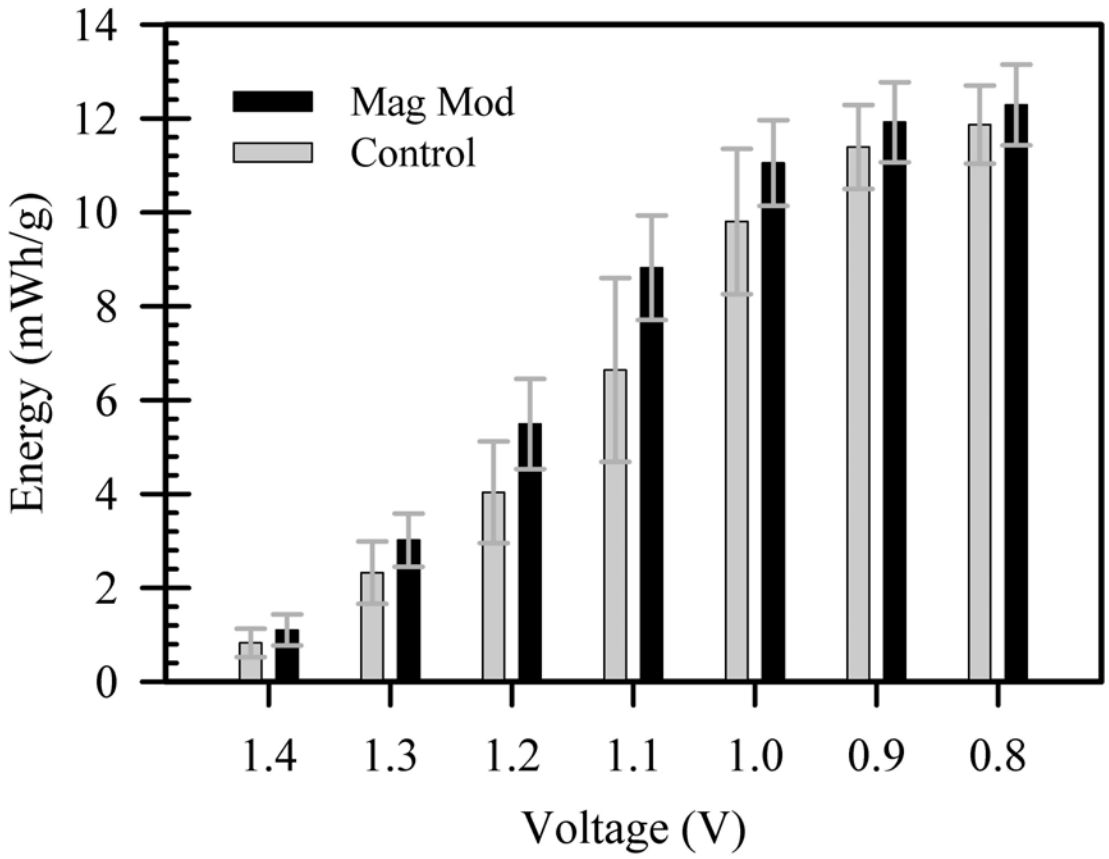

Figure 38. Bar graph representation of energy at a given voltage for type 2 batteries at a C/2 discharge rate. Magnetically modified batteries are in black and nonmodified batteries are in gray.

performance batteries.

Table 17. Tabulated performance values for battery type 2 at C/2 discharge rates.

Time (min) to a Given Voltage (Figure 37)				
Voltage (V)	Control ($n = 12$)	Modified ($n = 12$)	Enhancement	Confidence Level
1.4	3.56 ± 1.29	5.17 ± 1.59	45%	99%
1.3	10.40 ± 2.97	14.75 ± 2.78	42%	99%
1.2	18.89 ± 5.10	28.15 ± 4.95	49%	99%
1.1	32.84 ± 9.80	47.65 ± 5.40	45%	99%
1.0	51.32 ± 7.52	61.90 ± 3.67	21%	99%
0.9	61.51 ± 2.99	68.01 ± 2.99	11%	99%
0.8	64.94 ± 2.73	70.92 ± 3.00	9%	99%

Energy (mWh/g) at a Given Voltage (Figure 38)				
Voltage (V)	Control	Modified	Enhancement	Confidence Level
1.4	0.83 ± 0.30	1.10 ± 0.33	33%	96%
1.3	2.32 ± 0.67	3.02 ± 0.57	30%	99%
1.2	4.04 ± 1.08	5.49 ± 0.96	36%	99%
1.1	6.64 ± 1.96	8.82 ± 1.11	33%	99%
1.0	9.81 ± 1.55	11.05 ± 0.91	13%	98%
0.9	11.39 ± 0.89	11.92 ± 0.85	5%	86%
0.8	11.87 ± 0.83	12.29 ± 0.86	4%	78%

4.2.3 Electrochemical Impedance Spectroscopy

Electrochemical impedance spectroscopy is a nondesctructive test of the battery performed here by applying an equal and opposite open circuit voltage to prevent discharge caused by the instrument. The purpose of this test was to ascertain if magnetic modification would present itself in a manner different from discharge performance. This work has stated magnetic modification enhances charge transfer efficiency. This method allows for the observance of changes in the charge transfer resistance, R_{ct}, and is useful in addressing the benefits of magnetic modification.

Useful data presented here are for type 1 batteries only. Impedance data were

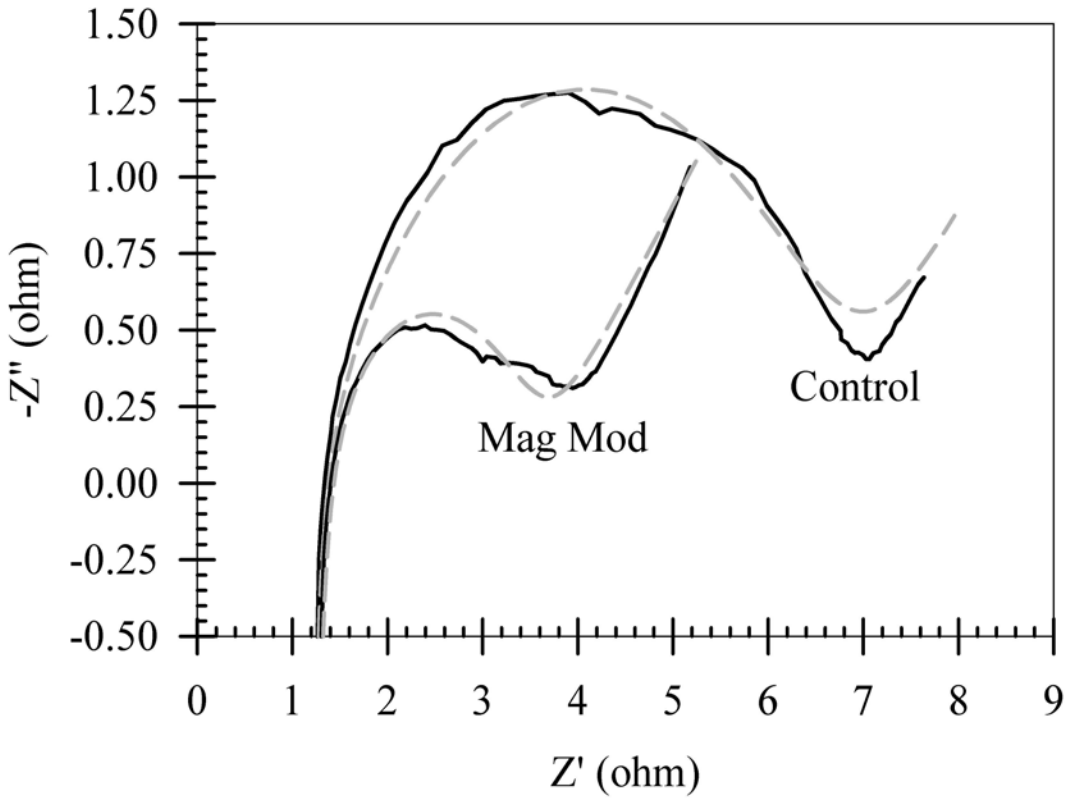

Figure 39. Electrochemical impedance spectroscopy data for type 1 batteries. Equivalent circuit model (dashed line) was fitted to experimental data (solid). Magnetically modified batteries are black and nonmodified batteries are gray. The circuit components represent different aspects of the system. R_s is series (or solution) resistance, L is inductance, R_{ct} is charge transfer resistance, CPE_{dl} and CPE_{dif} correspond to double layer capacitance and diffusion elements, respectively.

collected immediately after assembly of the battery. Once collected, the batteries were then discharged. Figure 39 is a representative Nyquist overlay plot for magnetically modified and nonmodified batteries. Batteries were tested in a two electrode configuration as described in Section 4.1.4. Fitting of the equivalent circuit model, shown in Figure 40, was performed to obtain component values for the batteries, Figure 40. Tabulated data for fitted impedance measurements are

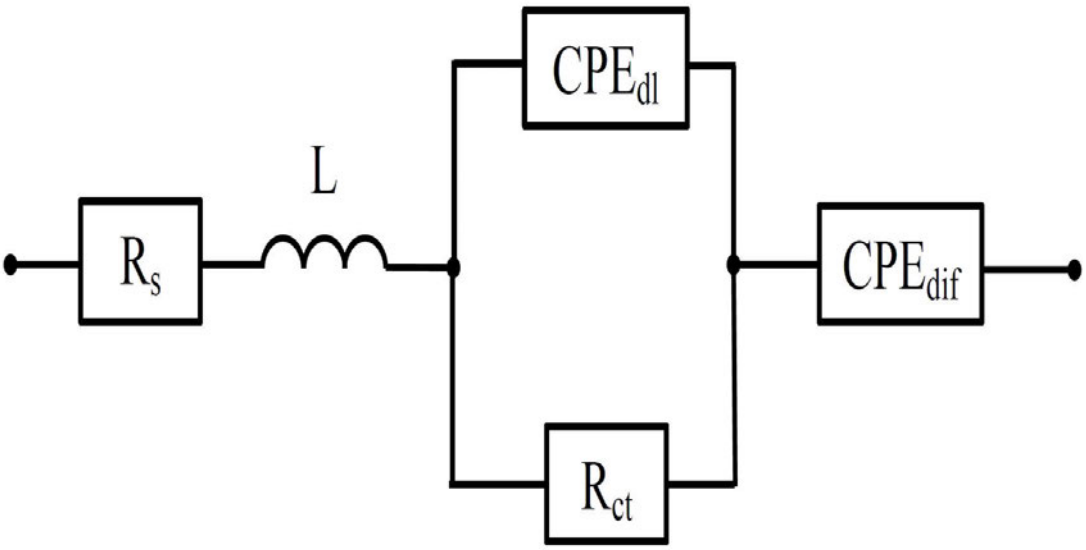

Figure 40. Equivalent circuit used for impedance spectroscopy fitting of alkaline batteries. R_s is solution resistance, R_{ct} is charge transfer resistance, L is inductance, CPE_{dl} is a constant phase element for the charge double layer, and CPE_{diff} is a constant phase element for diffusion. Placement of the CPE_{diff} element outside of the parallel loop helped to fit the more accurately.

reported in Table 18. Values are reported for $n = 4$ samples each.

Tested batteries demonstrated similar characteristics in almost all categories with one exception. Values for R_{ct} (heterogeneous charge transfer resistance) for magnetically modified batteries were smaller than the corresponding value for nonmodified batteries, 3.56 Ω compared to 5.91 Ω, respectively. This is attributed to a change in the charge transfer resistance of the cathode due to the presence of the magnetic field of the $SmCo_5$ particles. The decrease of charge transfer resistance would correspond to more current at the same voltage for voltammetric measurements. However, these batteries are discharged under constant current

conditions and decreased R_{ct} would be expected to sustain higher voltage compared to nonmodified batteries. This is observed in the discharge data.

An inductive component was found to be present in both magnetically modified and nonmodified systems, as seen in the vertical line shape for higher frequencies at $\sim 1.3\ \Omega$. This effect was originally thought to be coupled to the use of magnetic microparticles within the cathode. However, an inductive effect is observed for both conditions (modified and control batteries). The inductive effect could have been due to instrument or cable issues but similar effects were observed on a matching instrument in another part of the lab. Because inductance values for L_{conrol} and L_{mag} are similar and small in magnitude, no impact of the inductance is not observed. This observation is most likely associated with characteristics of the electrode itself. The batteries displayed comparable R_s values indicating the series resistance attributed to electrolyte and separator behavior is comparable.

A constant phase element is an adjustable factor that numerically represent deviations from ideal capactiance or resistance behavior

$$Z_{CPE} = \frac{1}{Q_0 (iw)^n} \tag{54}$$

where Q_0 is the phase element constant $\left(S \cdot s^{-1/2}\right)$, i is the imaginary number $(\sqrt{-1})$, w is the angular frequency (Hz), and n is the exponential term corresponds to the relationship between capacitance and resistance. When $n = 0.5$, a linear relationship between charge transfer resistance and double layer capacitance is observed. When $n > 0.5$, the component represents more capacitive behavior, while $n < 0.5$ represents more resistive behavior. Use of a constant phase element for

CPE_{dl} and CPE_{diff} indicates nonideal behavior for double layer capacitance and diffusion within the system. This can be attributed to porosity and conductivity variation within the batteries, along with nonideal diffusion characteristics. Values for these components are tabulated in Table 18.

Table 18. Equivalent circuit values for fitted impedance spectroscopy data of type 1 low electrolyte batteries.

Tabulated Equivalent Circuit Values					
Control ($n = 4$)			Mag Mod ($n = 4$)		
Average	StDev	Component	Average	StDev	Confidence Interval
1.10	0.05	R_s	1.11	0.04	–
2.23×10^{-6}	5×10^{-8}	L	2.24×10^{-6}	1.5×10^{-7}	–
5.91	0.42	R_{ct}	3.56	1.49	97%
0.00388	0.00117	$(Q_0)_{CPE_{dl}}$	0.00702	0.00622	–
0.583	0.043	$n_{CPE_{dl}}$	0.564	0.074	–
1.38	0.33	$(Q_0)_{CPE_{dif}}$	1.30	0.41	–
0.413	0.047	$n_{CPE_{dif}}$	0.394	0.073	–

4.3 Model Considerations

The working model described in Section 2.2 is expanded here to consider the alkaline MnO_2 system.

Consider the reaction sequence for the MnO_2 electrode.

$$MnO_2 + H^+ + e \rightleftharpoons MnOOH \tag{55}$$

$$MnOOH + H^+ + e \rightleftharpoons Mn(OH)_2 \tag{56}$$

For the first reaction, the basic process is $Mn^{4+} \longrightarrow Mn^{3+}$. The electron is propagated in the EMD matrix by exchange of an electron between Mn^{4+} and Mn^{3+} as the EMD is reduced. This is a homogeneous exchange reaction. It may be thought

of as electron conductivity in the manganese dioxide cathode matrix. Mn^0 is s^2d^5 such that Mn^{4+} is d^3 and Mn^{3+} is d^4. In an octahedral environment,Mn^{4+} is then a quartet Q with 3 unpaired spins and Mn^{3+} as d^4 is a triplet T with 2 unpaired spins. The electron transfer reaction is $T + Q$ with 3 + 2 unpaired electrons.

The Zeeman energy is $gHS\beta$, where the magnetic parameters g and spin S are appropriate to the paramagnetic species, H is the magnetic field, and β is the Bohr magneton, a constant,. The Zeeman energy can be approximated from the number of unpaired electrons. The spin, $S = m/2$. Roughly, $g \sim 2m$, such that $gS \sim m^2$. For a triplet and a quartet, the number of unpaired electrons are $m_T = 2$ and $m_Q = 3$, such that $g_T S_T \sim 4$ and $g_Q S_Q \sim 9$. Thus, a triplet and a quartet have substantial magnetic character and will respond more strongly than singlets ($gS \sim 0$) and doublets ($g_D S_D \sim 1$) to an imposed magnetic field. EMD is a highly appropriate environment to increase electron exchange by application of a magnetic field within the matrix.

Based on the model outlined in Section 2.2, conduction of the electron in the EMD matrix involves formation of the complex, $[Mn^{3+}Mn^{4+}]$. The Zeeman energy for the complex is $(g_T S_T \pm g_Q S_Q)\, H\beta$. In the absence of a magnetic field, the complex may be more likely to form with the spins paired whereas in a sufficient field, the spins may be aligned in a single direction. The magnetic fields in the batteries are not sufficiently large to flip all spins into a single orientation but it is sufficient to impact the rate of conduction or exchange.

Modeling and experimental evaluations of self exchange rates has shown that the rate is proportional to the Zeeman energy. Let the rate of exchange in the

EMD matrix be k_{mag} in the presence of the magnetic microparticles and k_{non} in the nonmagnetic controls. Then, for the average magnetic field of the microparticles in the matrix, H_{mag}, and the earth's magnetic field, H_{non},

$$k_{mag} \propto (g_T S_T \pm g_Q S_Q) H_{\mathrm{mag}} \beta \tag{57}$$

$$k_{non} \propto (g_T S_T \pm g_Q S_Q) H_{\mathrm{non}} \beta \tag{58}$$

The rate determining factor, for electron exchange in discharge of EMD, is set by the current and voltage reflects the efficiency of the electron exchange process. For the experiments here, the electron exchange is largely rate determining at voltages above 1.0 V. Ohm's law is a simple means to consider this behavior; $R_{CT} = V/I$ where V is the measured voltage for a constant current I. The resistance to charge transfer, $R_{CT} = RT/Fi_0$; because the exchange current i_0 is proportional to the rate of exchange (k_{mag} or k_{non}), the ratio of voltages measured at a fixed discharge rate C/n for magnetic and nonmagnetic batteries, approximates the relative efficiency and the ratio of rates. For the same conditions for magnetized and nonmagnetized,

$$\frac{V_{mag}}{V_{non}} = \frac{k_{mag}}{k_{non}} \propto \frac{(g_T S_T \pm g_Q S_Q) H_{mag} \beta}{(g_T S_T \pm g_Q S_Q) H_{non} \beta} \tag{59}$$

$$\propto \frac{H_{mag}}{H_{non}} \tag{60}$$

For the earth's field, $H_{non} = 1\ G$. H_{mag} is roughly the average field in the matrix.

$$\frac{V_{mag}}{V_{non}} \propto H_{mag} \tag{61}$$

For example, if the magnetically modified batteries are showing 40 % enhancement in a range where both batteries are limited by electron exchange, then the average magnetic field in the battery matrix is $H_{mag} \propto 1.4$.

4.4 Conclusions

Addition of magnetic microparticles improves power output of $Zn|MnO_2$ alkaline batteries. The addition of 5 % w/w $SmCo_5$ to the EMD cathode generated greater than 20 % power for magnetically modified batteries over comparable nonmagnetic batteries. Higher voltages were observed for magnetically modified batteries with greater performance observed regardless of discharge rate. Analysis of electrochemical impedance spectroscopy data resulted in a lower charge transfer resistance for modified batteries versus comparable control batteries. Formulation issues still need to be addressed. Regardless of composition, all batteries demonstrated comparable discharge times for their respective categories. This is suspected to be related to the zinc anode. Although effort was spent to optimize the gelled anode, more work needs to be done. Formulation issues still need to be better addressed. Improved performance is found across a total of three different systems (Chapters 3 and 4) with two designed to resemble industrial batteries (Chapter 4).

CHAPTER 5

BREATH ACETONE ELECTROCHEMISTRY

5.1 Physiological Acetone

Acetone is a metabolite of fat catabolism and serves as an indicator for various physiological states related to ketosis, such as diabetes, low carbohydrate diet, and weight loss [62]. Acetone can provide an alternative to glucose monitoring. Under these ketogenic conditions, fat consumption increases within cells and ketone levels increase in the blood. There are three primary ketone bodies generated during ketogenesis: 3-hydroxy-butyrate (3-HB), acetoacetic acid (AcAc), and acetone [63]. They are commonly used as ketotic markers for clinical analysis and over the counter testing. Of these, acetone is the only ketone body that appreciably partitions from the blood into the breath.

Human breath is a complex gas mixture comprised of numerous organic small molecules. A report by Phillips lists the relative abundance for the top three most abundant volatile organic compounds (VOCs) to be isoprene (48.60 %), 1,2-pentadiene (15.00%), and acetone (14.59 %) [64]. Although multiple thiols fill the top ten, the reported relative abundances are lower than acetone by a factor of seven or greater.

Ketogenesis is the generic term for the generation of ketone bodies. Ketosis arises from the metabolic process of converting fats into energy, which in turn generate ketone bodies. This is considered a nonpreferred or abnormal physiological process,

but is not indicative of harmful levels within the blood. Ketosis is routinely achieved during exercise and on a ketogenic (low carbohydrate) diet. Ketoacidosis is a ketotic state (ketosis) where excessive levels in the blood affect pH. Chronic ketoacidosis is typically observed under diabetic conditions.

Ketogenesis under diabetic ketoacidotic conditions is well describe in a review by Laffel [62]. Cells require glucose to generate energy, as illustrated in Figure 41. Transport of glucose from the blood stream into the cells is facilitated by insulin. Diabetic conditions occur when either insulin levels within the blood are too low (type 1) or when insulin is ineffective (type 2). Consequently, glucose is not transported into cells and blood levels of glucose begin to increase. Because cells are starved for glucose, cells begin to convert triglycerides (fatty acids) to acetoacetate (AcAc) and energy. AcAc interconverts with 3-hydroxybutyrate (3HB) under equilibrium conditions. AcAc also undergoes spontaneous, irreversible decarboxylation to form acetone (Me_2O). Together these three products are known as the ketone bodies. For normal human subjects, the concentration ratio of 3HB:AcAc is 1:1 and the total concentration of ketone bodies is well below 0.5 mM. All three ketone bodies can partition across the cell wall into the blood. For Me_2O, a second partition occurs at the blood/air interface in the alveoli. The partition coefficient, K, for Me_2O at this interface [65–68] is reported as almost a factor of ten more favored than for ethanol. (Commercial *potentiometric* breathalyzers for ethanol exploit this partition.) K for acetone at the water/air interface is comparable the blood/air interface [65] and is invariant with concentration [69]. Of the three ketone bodies, only acetone is sufficiently volatile to partition significantly into alveolar air. It is

this acetone that generates the sweet smell characteristic of diabetic ketoacidosis. Ketoacidosis occurs as the fatty acids are consumed and the concentration of ketone bodies rise and blood pH drops. Under ketoacidotic conditions, 3HB:AcAc in the plasma increases to 3:1 or even as high as 10:1 [62] and the concentration of the ketone bodies increases from two to ten fold. See Table 19.

Table 19. Ketone Body Concentrations in Plasma (mM) [70].

	Normal Subject	Treated Diabetic	Ketoacidotic Diabetic	Treated Diabetic / Normal Subject	Ketoacidotic Diabetic / Treated Diabetic
Acetone (Me_2O)	0.015 ± 0.005	1.69 ± 0.78	3.26 ± 0.79	110	1.9
Acetoacetate (AcAc)	0.114 ± 0.029	0.306 ± 0.05	2.84 ± 0.40	2.68	9.3
3-Hydroxy-butyrate (3HB)	0.160 ± 0.050	0.810 ± 0.171	8.23 ± 1.48	5.1	10.

5.1.1 Acetone on the Breath

Acetone is present on the breath of 92 % of healthy subjects [71]. From gas chromatography mass spectrometry, acetone is the third most common compound found in breath of normal subjects [64]. (This is measured as a "positive gradient" that measures volatile organic compound manufactured in the body relative to compounds present in the ambient air.) The integrated area of the chromatogram measures the fraction of the compound in the sample in [64]. Acetone occupies 14.6 % of the area whereas isoprene and 1,2-pentadiene are 48.6 % and 15.0 % for normal subjects [64]. Four species have fractions above 0.7 %: 1-methyl-4-(1-methylethenyl)-cyclohexene (8.4 %), dl-Limonene (2.3 %), 3-(methylthio)-1-propene (2.1 %), and 1-(methylthio)-cis-1-propene (1.6 %). Of these species, the four pure

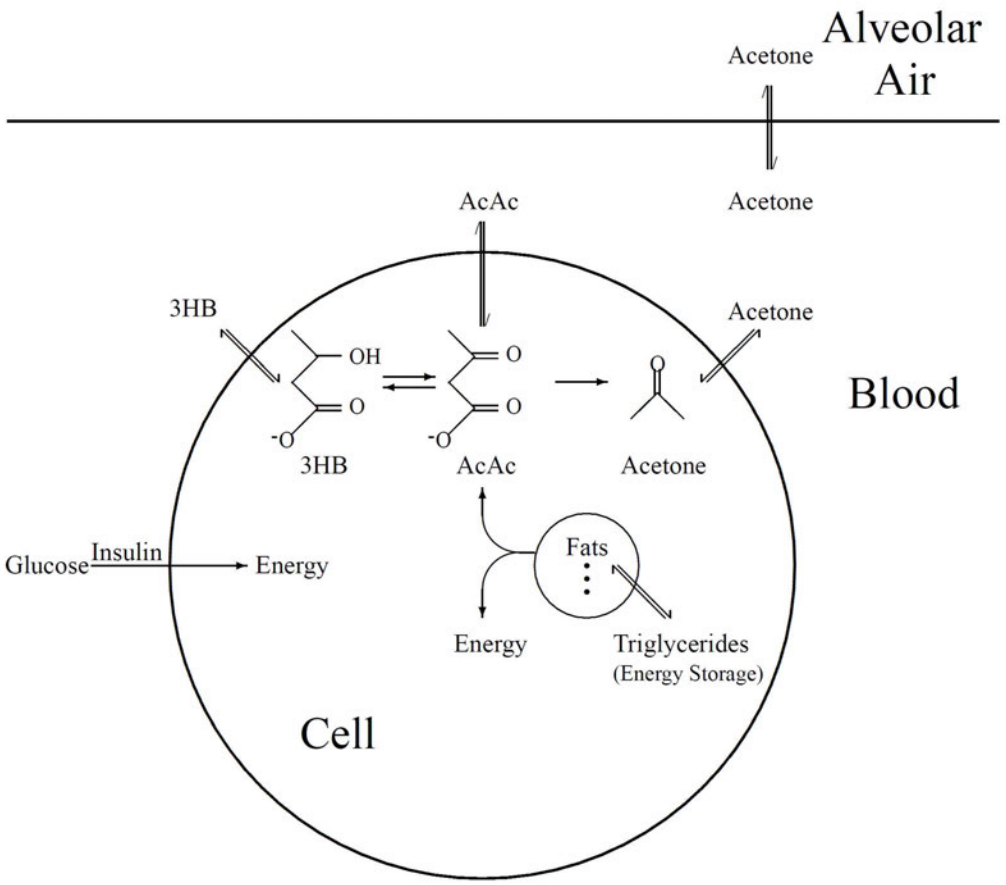

Figure 41. Illustration of the ketone cycle during ketoacidotic conditions. When transport of glucose into the cell fails, triglycerides are converted to energy and acetoacetate (AcAc) is a byproduct. Conversion of AcAc generates 3-hydroxybutyrate (3HB) in equilibrium or acetone during decarboxylation. Acetone enters the blood stream and then be exhaled through the lungs.

hydrocarbons, which include all but the two thio compounds and acetone, are not expected to have voltammetric activity under aqueous conditions. Isoprene is known to adsorb to platinum [72] and could be an interferant. It is not known if the two thio compounds are surface active, but their concentrations are almost an order of magnitude lower than acetone in normal subjects and could be a form of selectivity. Acetone is anticipated to be the dominant, perhaps only, signal on breath that will be determined voltammetrically for normal subjects. Under physiologic conditions when ketone bodies are increased, acetone will have yet higher relative concentration.

Concentrations for ketone bodies in different populations are noted in Table 19. For treated diabetics, the concentration of acetone on the breath is > 100 fold higher than for normal subjects and > 200 for ketoacidotic diabetics. For diabetics, the acetone levels will be higher than for the other components on the breath.

For those exercising effectively, acetone on the breath will be above those of normal subjects. Acetone is generated by fat catabolism and serves as a measure of exercise efficacy as well as low carbohydrate and ketogenic diets. A metabolic rate consistent with a weight loss of 1 lb/week (500 kcal/day, where colloquially, kcal are "calories"), acetone levels on the *breath* will be 7.1 ppm = 0.14 μM [73]. From the ideal gas law

$$P = nRT/V \tag{62}$$

$$= RT\left[Me_2O\right]_{air} \tag{63}$$

$$= 0.082 \times 298 \times 0.14 \times 10^{-6} = 3.4 \times 10^{-6} atm \tag{64}$$

For the Henry's law constant for acetone in water,

$$k_{Me_2O} = 27\ M/atm = \left(\frac{[Me_2O]}{P_{Me_2O}}\right)_{in\ H_2O} \tag{65}$$

the concentration of acetone in water will be $[Me_2O]_{H_2O} = 27\,(3.4 \times 10^{-6}) = 9.2 \times 10^{-5} M = 0.092\ mM$. This corresponds to about six times the concentration of acetone in plasma of normal subjects, with the approximation that the Henry's law coefficient is comparable for plasma and water.

5.2 Voltammetric Sensors Background

The two most common types of electrochemical sensors are potentiometric and voltammetric. A potentiometric sensor measures electrical potential of an electrode where no current flows, so that no electrolysis occurs. Voltammetric sensors measure the passage of current to the electrode as a result of an electrochemical reaction. For acetone, voltammetric sensors are more sensitive and more stable than potentiometric sensors.

5.2.1 Potentiometric Sensors

Potentiometric measurement is based on the concentrations of the halves of a redox couple and the standard potential or formal potential. The standard potential is the thermodynamic potential under standard conditions that include unit activity of protons. The formal potential is analogous to the standard potential except one or more conditions is not standard, such as physiological pH. For the redox reaction $O + ne \rightleftharpoons R$, the standard potential, E^0, relates the activities of the oxidized and

reduced forms of the redox pair O and R through the Nernst equation

$$E = E^0 - \frac{RT}{nF} \ln \frac{a_R}{a_O} \tag{66}$$

where E is the measured potential (V), R is the gas constant ($L \cdot atm \cdot mol^{-1} \cdot K^{-1}$), T is temperature in degrees Kelvin, F is Faraday's constant (96485.3 C), and a_R and a_O are the activities of the reduced and oxidized forms of the couple. At 25 $^{\circ}C$ and only small changes in concentration allow the approximation that activity coefficients for the oxidized and reduced forms are constant in the domain of the measurement. The Nernst equation is expressed in terms of the formal potential, $E^{0'}$,

$$E = E^{0'} - \frac{0.05916\ V}{n} \log \frac{[C_R]}{[C_O]} \tag{67}$$

where the formal potential embeds the activity coefficients, and $[C_R]$ and $[C_O]$ are the concentration of the reduced and oxidized forms. The concentrations are at the electrode surface and reflect either the concentrations in the bulk coverage of adsorbates.

Potentiometric sensors are nondestructive, but for a 1 mV uncertainty in the measured potential, there is a corresponding precision of ± 4 %.

The most common commercially available potentiometric sensors are breathalyzers, which serve as ignition locks on automobiles for those convicted of driving while intoxicated. These devices are based on a fuel cell, where breath is introduced on one electrode and the other electrode is exposed to the air. When a breath sample is introduced at the first electrode, the change in concentration or activity of ethanol at the electrode surface generates a small voltage across the two electrodes. This

change in voltage across the two electrodes in the fuel cell is measured and converted to breath ethanol concentration through the Nernst equation. Because no potential is applied across the electrodes, no reaction occurs and therefore no current is measured. This process is similar to a hydrogen ion concentration measured with a pH electrode.

Work by Leddy and Haverhals has demonstrated the analysis of ethanol, smoking by-products (specifically hydrogen), and acetone are all possible with a potentiometric sensor [74–76]. All measurements are made with *potentiometric* sensors. Here, *voltammetric* sensors are described. As follows, there are significant advantages in the voltammetric sensors as compared to the potentiometric sensors, especially for acetone that is at a lower concentration on the breath than ethanol and smoking by-products for those who have been drinking and/or smoking.

5.2.2 Voltammetric Sensors

The more selective and sensitive electrochemical measurement protocol is a voltammetric sensor. In a voltammetric sensor, potential is applied across the working and counter electrodes and the current is measured. Current arises from the direct electrolysis of the electroactive species and occurs near the formal potential, $E^{0'}$, for $O + ne \rightleftharpoons R$. Because potential is controlled, selectivity is enhanced as compared to potentiometric measurements. Although applied potentials near the formal potential enhance selectivity, the formal potential is not a parameter unique to each compound and it remains possible for several compounds to electrolyze at similar potentials. By control of the current measurement protocol and the rate of

the applied potential, additional advantages in selectivity and sensitivity can be finessed as compared to potentiometric measurements.

For the situation where the oxidized and reduced forms can dissolve in solution and do not adsorb, allow only O initially present in solution. Upon application of an appropriate potential relative to the formal potential, O diffuses toward the electrode, undergoes electrolysis to form R, and then R diffuses away from the electrode. During the electrolysis, n electrons are transferred from the electrode to O. The measurement of current counts the number of electrons transferred, which is directly related to the number of O that are electrolyzed. Faraday's law relates the measured current to the moles of O electrolyzed.

$$\frac{i}{nFA} = \frac{\text{moles of } O \text{ electrolyzed}}{\text{cm}^2 \text{ s}} \tag{68}$$

where A is the area of the electrode (cm^2) and i is the current in amps (C/s). This example describes a reduction reaction, but the transposition to the oxidation where R surrenders n electrons to the electrode to form O is immediate. The moles of O electrolyzed are directly related to the concentration of the analyte O initially present in solution. It is also possible to measure the charge (C) instead of the current (C/s). Mathematical integration of the current calculates the total amount of charge passed, which directly translates to moles of analyte involved in the reaction. For the reduction process,

$$Q(t) = \int_0^t i(\tau)\, d\tau \tag{69}$$

such that

$$\frac{Q\left(t\right)}{nFA} = \frac{\text{moles of } O \text{ electrolyzed}}{\text{cm}^2} \tag{70}$$

For the situation where a species adsorbs to the electrode surface, considerations are similar. Consider the redox process where both the oxidized and reduced forms are absorbed to the electrode surface.

$$O_{ads} + ne \rightleftharpoons R_{ads} \qquad E^{0'} \tag{71}$$

The current is again proportional to the moles electrolyzed. When more than one species is electrolyzed at similar potentials, the total current measured is the sum of the individual current of each species electrolyzed.

In voltammetric measurements, there are several common schemes for how a potential is applied to the electrode: steps, sweeps, or combinations of steps and sweeps. If a potential step is used, then the experiment is referred to as potential step or more correctly as chronoamperometry. If the charge is measured instead of the current, then the technique is chronocoulometry. If the potential is swept, then the technique is referred to as sweep voltammetry or linear sweep voltammetry. If the potential is swept out and back, then the process is referred to as cyclic voltammetry. Another common voltammetric perturbation would be square wave voltammetry where the potential is both stepped and swept.

5.2.3 Cyclic Voltammetry Review

Cyclic voltammetry (CV) is a linear sweep technique and a fundamental technique of electrochemistry. It is extremely versatile and capable of providing information

regarding diffusion, kinetics, and electrode interactions of a redox probe. Although voltammetric interpretation can often be complex, fundamental operation is not.

Instrumentation typically consists of a potentiostat, which applies a potential (voltage) and measures the current response, and a computer to control instrument function and record data. There are three electrodes in the standard configuration: 1) the working electrode, where all targeted reactions occur, 2) the auxiliary or counter electrode, which is designed complete the circuit with the working electrode and electrolyte, and 3) the reference electrode, which serves as a metric to monitor applied voltage at the working electrode.

An excellent description of cyclic voltammetry is explained by Kissinger and Heineman [77]. A CV is obtained by applying a potential (V) and measuring the current (A). There are several components to a voltammogram. See Figure 42. A triangle waveform is applied at the working electrode (Figure 42A). The initial potential, E_i (V), is ramped at a constant rate, called the scan rate (V/s), toward a switching potential, E_s (V), and then ramped toward the final potential, E_f (V). In this example, the initial and final potentials are equal. The instrument measures current as a function of time, Figure 42B. However, potential varies linearly with time and a more useful correlation is made by plotting current vs potential, Figure 42C.

Consider the reaction shown in Figure 42C for a glassy carbon working electrode in a solution containing 2 mM $K_3Fe(CN)_6$ with 0.5 M KNO_3 as the electrolyte.

$$Fe\,(CN)_6^{3-} + e \rightleftharpoons Fe\,(CN)_6^{4-} \qquad E^o = 0.361\ V\ vs\ \text{NHE} \tag{72}$$

The initial potential, E_i, is set at a value where no current is passed, such that no reaction occurs. The potential is ramped and current begins to be passed as the potential is sufficient to begin to electrolyze reactants at the electrode surface. Eventually, available species of $Fe(CN)_6^{3-}$ are depleted at the electrode surface and diffusion of reactant is the rate determining process. Consequently, the current begins to diminish as the potential continues to ramp toward the switching potential and a cathodic peak is formed, $i_{p,c}$. The potential is reversed at E_s and ramped toward the final potential, E_f. The return wave generates an anodic peak at $i_{p,a}$ as the $Fe(CN)_6^{4-}$ species is oxidized to regenerate $Fe(CN)_6^{3-}$ and becomes limited by the diffusion of $Fe(CN)_6^{4-}$ in the same manner. As explained in Section 5.2.2, current is directly related to moles of electrolyzed molecules, which converts to concentration.

5.2.4 Square Wave Voltammetry Review

Square wave voltammetry is a pulsed voltammetric method that provides suppression of nonfaradaic responses. The technique offers increased sensitivity and easier data extraction than cyclic voltammetry. However, the method and sampling mechanism are more complex. An introductory explanation is offered by Bard and Faulker [35], while a more detailed review is offered by Osteryoung and O'Dea [78].

The waveform, Figure 43, is a symmetrical square wave superimposed on a staircase with a wave amplitude of ΔE_p. Incremental changes in the potential, akin to a staircase riser, are designated as ΔE_s. The pulse width, t_p, corresponds to one half the pulse width over a time period, τ, and translates to the frequency $(1/\tau)$ of the pulse.

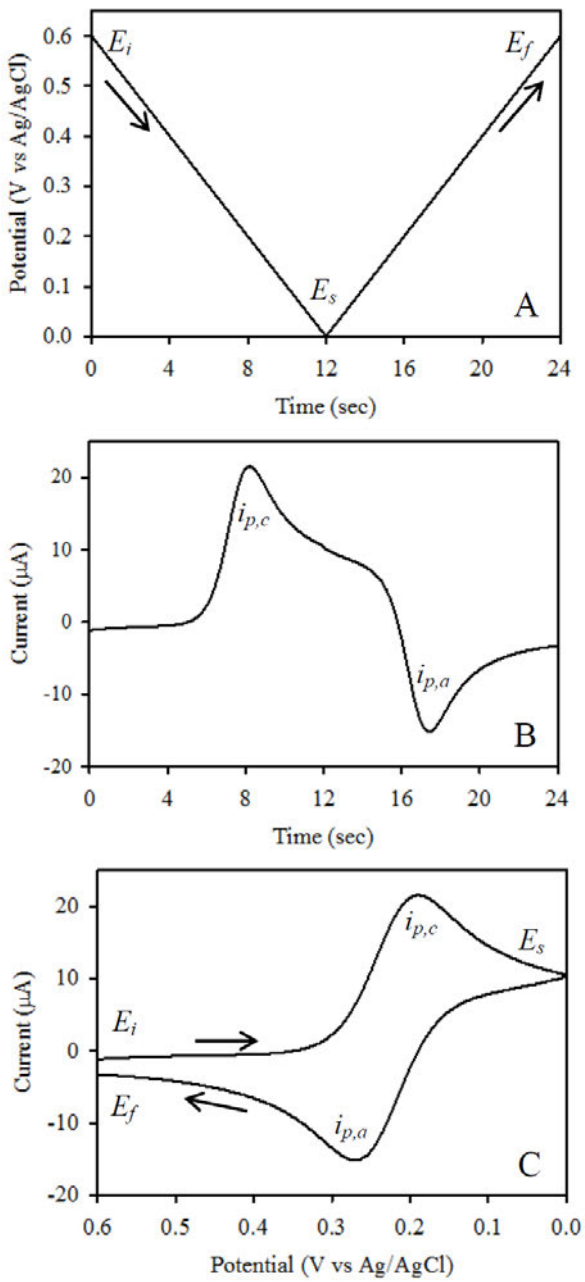

Figure 42. Cyclic voltammetric component waveform output for potential vs time (A), current vs time (B), and current vs potential (C). The data presented are for 2 mM $Fe(CN)_6^{3-}$ in 0.5 mM KNO_3, with a scan rate of 50 mV/s, and an electrode area of 0.071 cm^2.

Consider a single electron reduction

$$O + e \rightleftharpoons R$$

where O is a species in solution that undergoes reduction to R. A change in the applied potential is made at the working electrode and creates a current transient, Figure 44. A large portion of the nonfaradaic current transient (charging current) is ignored because of the data sampling occurs at t_p after most of the nonfaradaic charging current has decayed. Thess current transients are initially small at early times because the applied staircase potential is not sufficient to drive an electron transfer. However, as the potential is incremented (the staircase climbed), the applied potential becomes sufficient to drive an electron transfer. The forward pulse the current, Figure 45, as the applied potential approaches the standard potential of species O and the reverse pulse regenerates the species O and creates an anodic current as the R generated on the forward step is oxidized on the reverse step. Further potential increments past the standard potential generate applied potentials sufficient to electrolyze all the species near the electrode surface, which eventually results in equal rates of electron transfer for the oxidation and reduction such that a zero current difference in the voltammetric outputs is found [35, 78].

Square wave voltammetry is similar to other pulsed techniques, such as differential pulse voltammetry, normal pulse voltammetry, and reverse pulse voltammetry [35]. However, it has a wider range of application because of the frequency dependence ($1/\tau$) embedded within the applied waveform. Rapid measurements can be made that allow the exploration of systems with low concentrations, fast

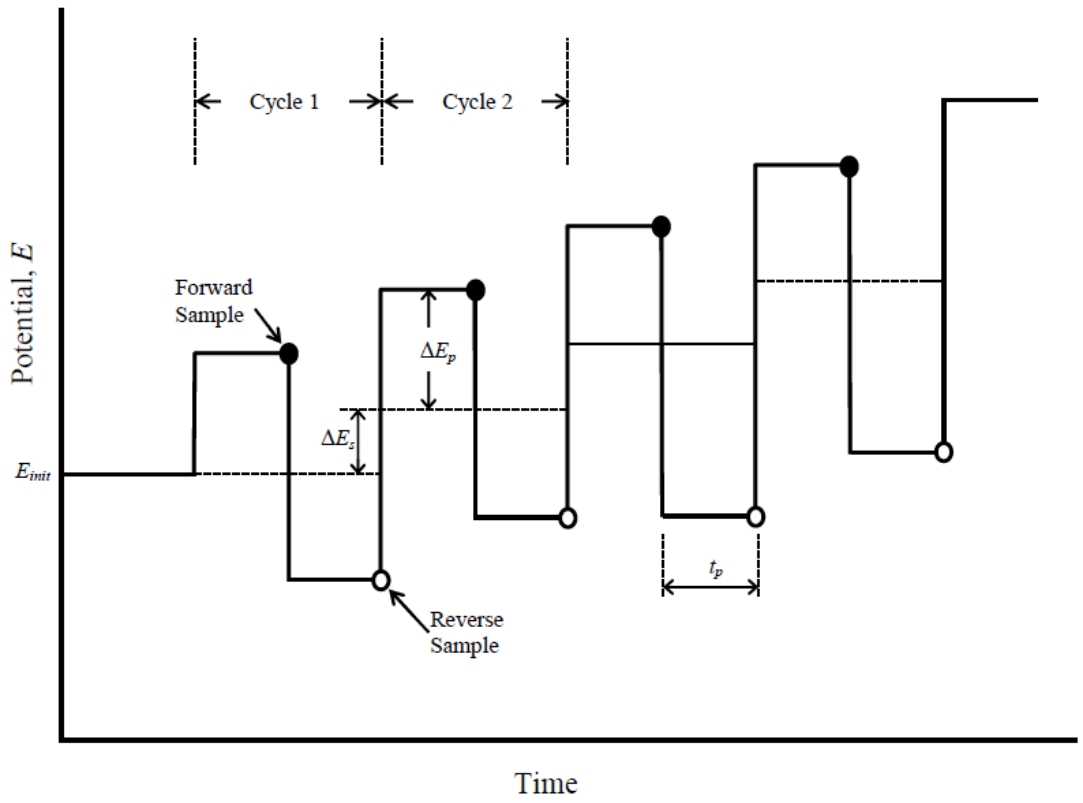

Figure 43. Waveform and data measurement protocol for square wave voltammetry. The solid line represents the applied potential, while the dashed lines represent the superimposed staircase parameters. The large solid dots indicate the time of data sampling on the forward wave, whereas the hollow dots indicate the corresponding sampling for the reverse wave. A time delay at an initial potential, E_{init}, is illustrated prior to the experiment. Recreated from [35].

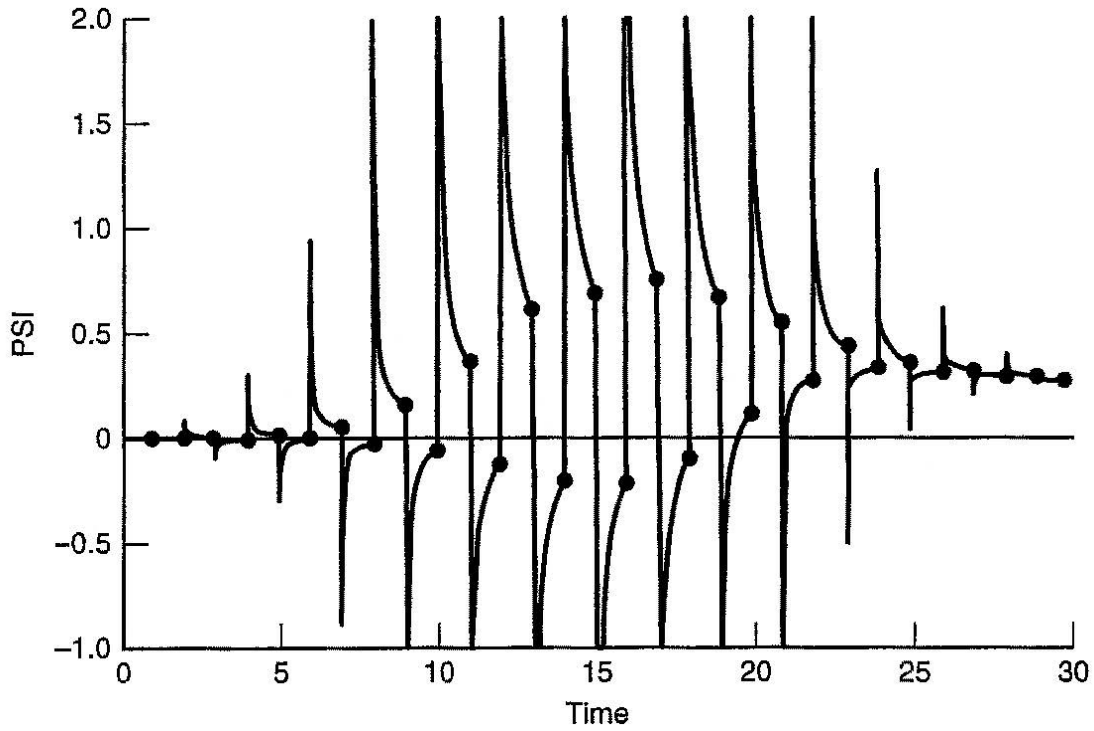

Figure 44. Dimensionless current reponse to the square wave voltammetry experiment of Figure 43. The solid dots represent sampled current. $n\Delta E_p = 50\ mV$ and $n\Delta E_s = 30\ mV$ [78].

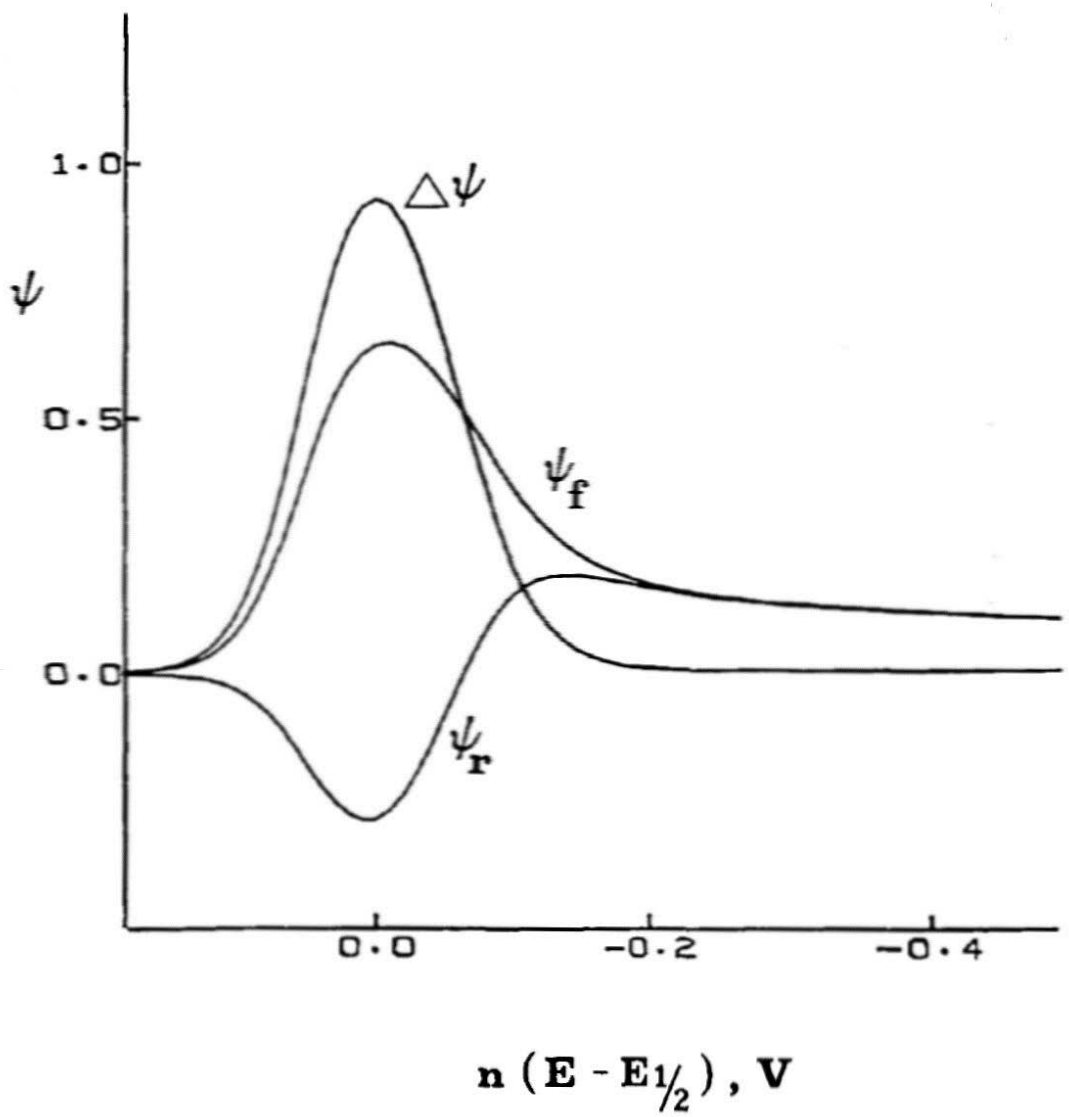

Figure 45. Dimensionless square wave voltammogram for a reversible, single electron reduction ($O + e \rightleftharpoons R$) under semi-infinite linear diffusion, $n\Delta E_p = 50\ mV$ and $n\Delta E_s = 10\ mV$. Forward (Ψ_f), reverse (Ψ_r), and difference ($\Delta\Psi$) dimensionless currents versus the potential axis $n\left(E_m - E_{1/2}\right)$ in volts, where E_m is the potential of the sampled current for the forward and reverse waves. Image source: [78].

kinetics, species with similar standard potentials and electrode processes, and square wave voltammetry can be used to study species that adsorb from solution because of similarities with stripping voltammetry [79–84]. Consequently, square wave voltammetry has significant advantages in the detection of adsorbed acetone on platinum. The balance of frequency, ΔE_p, and ΔE_s are important in optimization of the measurement. When a kinetic process establishes the current over time, other factors may become critical to a good measurement; this includes time and polarization of the electrode between measurements.

5.3 Platinum and Adsorption Reactions in Acidic Media

To describe the electrochemistry of adsorbed acetone on platinum, the electrochemistry of adsorbed hydrogen must be described first.

5.3.1 Hydrogen Electrochemistry on Platinum

Reduction of hydrogen at platinum occurs as a two step adsorption process [85–87]. The reaction involves platinum metal and free protons in solution, Equations 73 and 74.

$$Pt + H^+ + e \rightleftharpoons Pt\text{-}H \tag{73}$$

$$2Pt\text{-}H \rightleftharpoons H_2 + 2Pt \tag{74}$$

During this reaction, hydrogen ions diffuse to the platinum electrode and are reduced during a single electron process to form a chemisorbed Pt-H product. Hydrogen gas is then generated when two adjacent adsorbed hydrogens react to form hydrogen

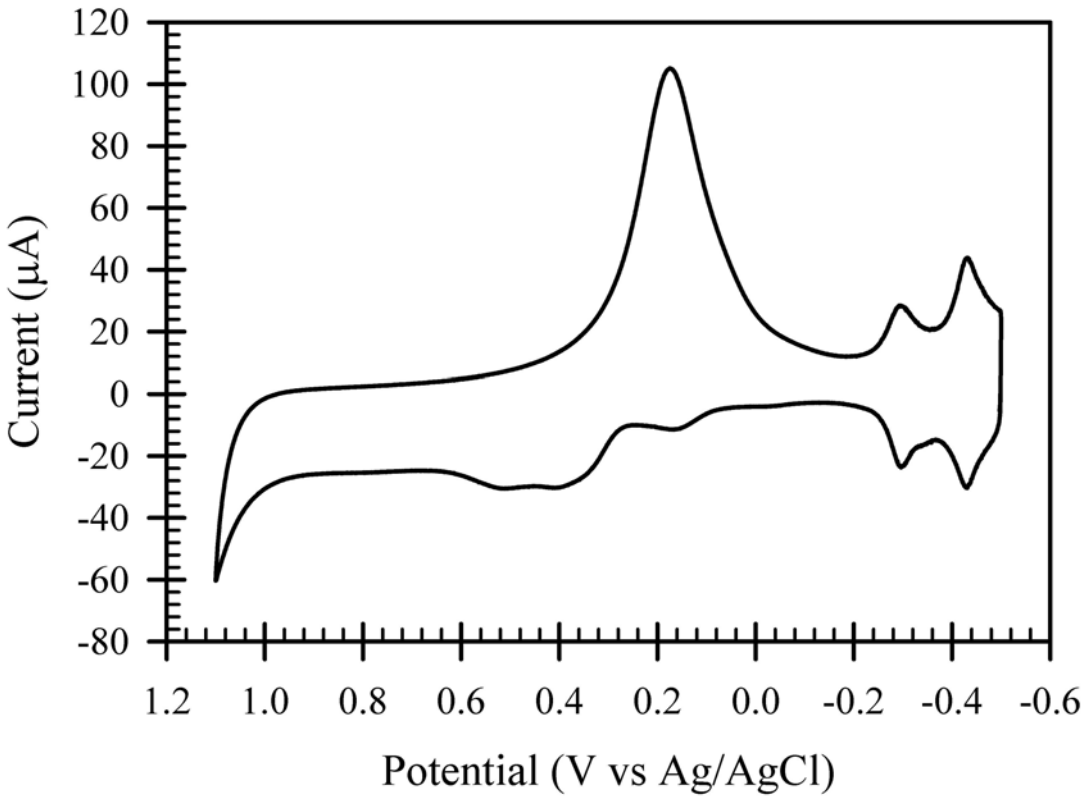

Figure 46. The characteristic butterfly lineshape of a cyclic voltammogram for a platinum working electrode in 0.5 M H_2SO_4 is shown between -0.1 V and -0.5 V vs Ag/AgCl. Data were collected at 100 mV/s. The cell was a standard three electrode configuration with a platinum working electrode (2 mm dia), a platinum counter electrode, and a Ag|AgCl reference electrode. It should be noted the Ag|AgCl reference electrode behaved more like a $Ag|Ag_2SO_4$ reference electrode ($+0.686$ V vs NHE) because of the acidic solution.

gas, desorb, and diffuse away. The voltammetric response of hydrogen reduction at platinum has a characteristic lineshape and is commonly used as a metric for a clean platinum surface. Figure 46 illustrates a cyclic voltammogram for hydrogen in an acidic environment at a platinum surface. The portion of the voltammogram between -0.1 V and -0.5 V is the hydrogen reduction region or butterfly region. This signature lineshape is so named because of the resemblance to a butterfly's

wings.

Work by Will first demonstrated the contribution of the three main crystal faces of platinum (111, 110, and 100) for the adsorption of hydrogen on platinum [87]. Figure 47 represents the current density response of the three crystal faces. Hydrogen was demonstrated to adsorb with similar reductive potentials for each of the crystal faces. For a polycrystalline surface, the two peak maxima between $-0.1\ V$ and $-0.5\ V$ in Figure 46 correspond to the same peaks observed for single crystal surfaces. The data in Figure 46 were collected at a polycrystalline surface. The pronounced maxima in the butterfly region are essentially the same as those reported by Will, when adjusted for a Ag/AgCl reference ($+0.197\ V\ vs\ NHE$). The electrochemistry of hydrogen on platinum relates to that of acetone because adsorbed acetone occupies or is capable of blocking access to hydrogen adsorption sites. Acetone adsorption alters the hydrogen voltammogram morphology as discussed in the next section.

5.3.2 Acetone Electrochemistry on Platinum

The adsorption and electrochemical reactions of acetone have been studied by radiotracer methods [29] and by coupling mass spectrometry to a voltammetric cell [30, 31]. In these papers, acetone adsorption is examined by cyclic voltammetry to observe the oxidation and reduction of acetone within the hydrogen butterfly region. The overall mechanism involves the π electrons of the carbonyl in the surface bonding of adsorption and are involved in a chemisorption process [29]. Reduction to isopropanol and propane involves protons from solution, where propane is a lesser

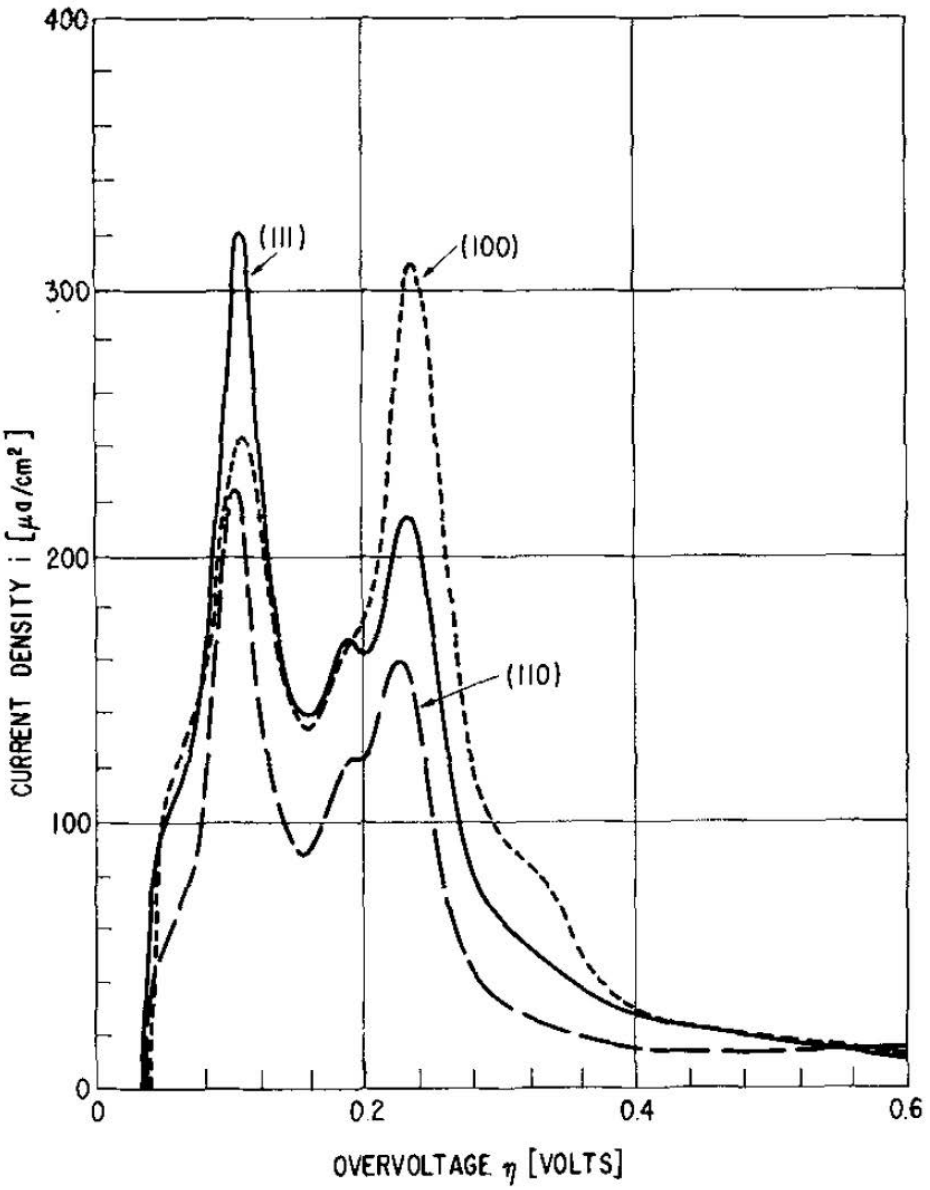

Figure 47. Overlay of linear sweep voltammograms of three platinum crystal faces (111, 110, 100). Data, collected in 8 N H_2SO_4 versus a hydrogen reference electrode (NHE) and a platinum counter electrode, are taken from reference [87]. Note that in the figure, reductive potential is to the left.

product [29, 31]. Reduction reactions based on stoichiometry are as follows.

$$C_3H_6O + 2H^+ + 2e \rightleftharpoons C_3H_7OH \tag{75}$$

$$C_3H_6O + 4H^+ + 4e \rightleftharpoons C_3H_8 + H_2O \tag{76}$$

During the voltammetric scans, adsorbed acetone can be reduced electrochemically or desorb. The products or desorbed species diffuse away and adsorption sites that were previously blocked by acetone are now available for hydrogen adsorption. This results in two different voltammetric waveforms with shifted peak potentials and intensities, Figure 48. The overlaid wave forms show the butterfly region in 0.5 M H_2SO_4 for conditions where no acetone is present (dashed line) and two scans through the butterfly region when acetone is adsorbed to the platinum surface (solid line). Acetone was deposited onto the working electrode from a separate bulk solution, rinsed, and then transferred to a sulfuric acid solution, which contained no acetone.

The impact of acetone on the cyclic voltammetry of the butterfly region is marked. The second reduction wave is enhanced whereas the first wave is suppressed by the presence of acetone. The basic process is that in the absence of acetone, hydrogen decorates the surface of the polycrystalline Pt. When acetone is introduced, it displaces some of the adsorbed hydrogen and this leads to the suppression of the first wave and the augmentation of the second wave as the adsorbed acetone has different voltammetric characteristics from the adsorbed hydrogen. On the second scan in blank electrolyte, the acetone has been electrolyzed and only the adsorbed hydrogen remains to re-establish the pristine butterfly pattern, which typically

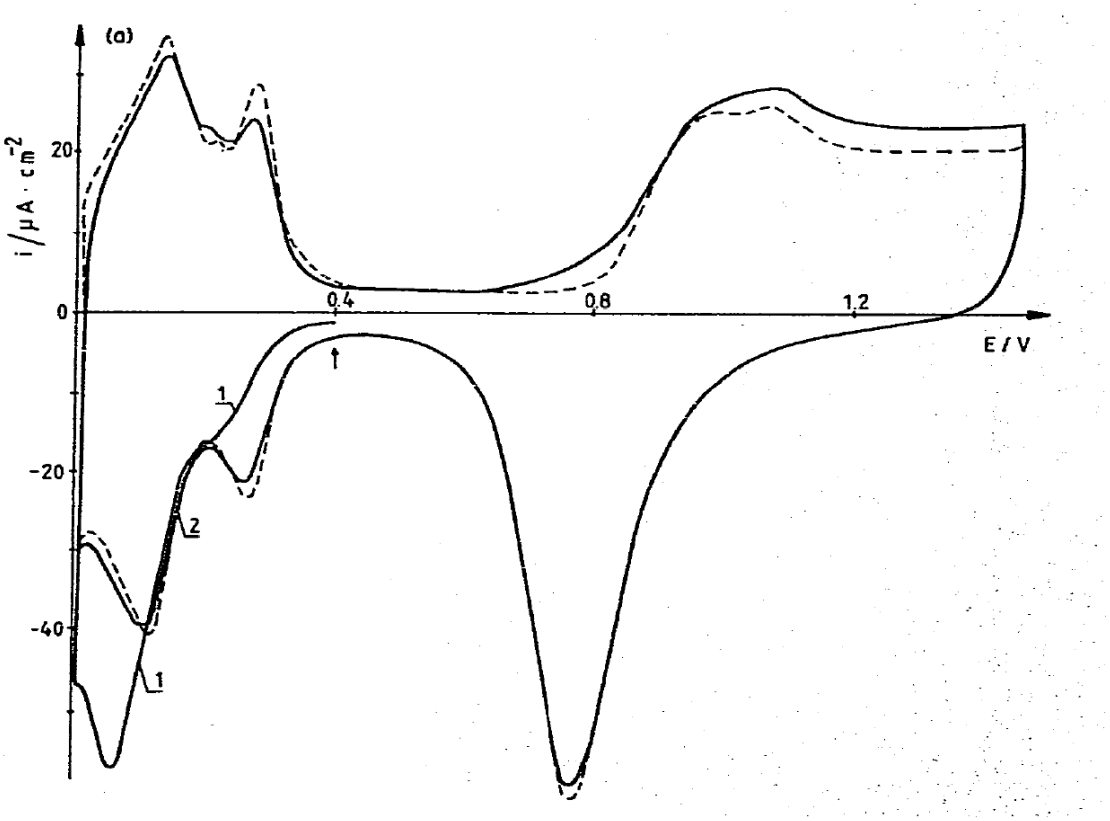

Figure 48. Overlay of acetone and hydrogen reduction voltammograms. The difference in signal between 0 V to 0.4 V demonstrates the reduction of acetone for curve 1 with the return of hydrogen reduction for curve 2 and the dashed line. The electrochemical cell consisted of a platinum working and counter electrode and a hydrogen reference electrode. Note that reduction is shown as potential is swept to the left. Figure and data taken from reference [29].

requires multiple voltammetric scans.

5.3.2.1 Acetone Voltammetric Sensor

The works reported here represent mechanistic studies to understand adsorption phenomena at a platinum electrode. These studies were performed with 10 mM acetone in bulk solution and target full coverage of the platinum surface by adsorbed acetone. Because adsorption establishes a surface concentration measurement, there is a possibility surface adsorption of acetone could be used to generate a calibration

curve for acetone in the gas phase. Concentrations on human breath approach single mM values in treated diabetics and unregulated diabetics, Table 19. Consequently, this method was pursued with the intent of developing an acetone sampling method for possible use in the development of a noninvasive acetone breathalyzer.

It is possible that voltammetric breath sensors exist for analytes besides acetone, but commercial availability of voltammetric type breath sensors for either acetone or other analytes is unknown. The method development for a voltammetric sensor is intended to allow noninvasive *quantization of acetone* associated with various physiologic states that include exercise and diet status as well as medical dysregulation. Possible application includes monitoring of diabetic status, effective management of a ketogenic diet, and as a screening tool for the diabetic state.

CHAPTER 6

VOLTAMMETRIC DETECTION OF BREATH ACETONE AT PLATINUM ELECTRODES

Qualitative methods for detection of acetone are available for blood, urine, and breath [62]. In clinical settings for monitoring of diabetic status, the preferred blood measurement is not for glucose but for one of three ketone bodies, specifically 3-hydroxybutyrate (3-HB), whereas over the counter urine test strips, such as Ketostix® (Bayer), monitor acetoacetate (AcAc). Breath analysis typically involves a gas chromatograph and mass spectrometer, which makes for a rapid measurement, but an infeasible portable device. Electrochemistry offers the possibility of an acetone breath sensor that is portable and would not require heavy, costly equipment. Cyclic voltammetry is used to examine competitive adsorption between acetone and free protons in 0.5 M H_2SO_4. As discussed in the previous chapter, the adsorption of acetone in a 0.5 M H_2SO_4 electrolyte solution alters the line shape of the butterfly region by blocking adsorption sites normally available to hydrogen. During voltammetric perturbation, adsorbed acetone is reduced or desorbs from the surface. The previously blocked adsorption sites are then occupied by hydrogen and the signature hydrogen reduction wave is regenerated on the second and subsequent sweeps. This effect on lineshape correlate with concentration of acetone on breath.

Here, the direct electrochemical reduction of adsorbed breath acetone on platinum in 0.5 M H_2SO_4 electrolyte is reported, a calibration plot is generated, and a human breath sample tested.

6.1 Experimental

Details of the experiments and voltammetric protocols follow.

6.1.1 Reagents

Deionized water from a Milli-Q plus water filtration system (Millipore) was used. Acetone calibration solutions were prepared from HPLC grade stock and serial dilution. Concentrated H_2SO_4 was diluted to 0.5 M. All reagents were purchased from Fisher Scientific and used as received. Artificial lungs were prepared by mixing 500 mL acetone:water solutions in a 1 L glass bottle with a Teflon/silicone septa (Industrial Glassware, Millville, NJ). Gas samples are generated by partition of acetone from solution into the headspace above the sealed vessel. The partition is done from equal volumes of acetone solution and headspace. The acetone solution contained a physiologically appropriate acetone:water concentration. Acetone and water were allowed to partition into the headspace of the container at room temperature for two hours prior to use. The resultant vapor sample simulated humidified breath samples. Because the partition of acetone into the headspace is directly proportional to solution concentration, all concentrations of vapor phase samples used in the calibration process are reported as the acetone solution concentration (mol/L) in water.

6.1.2 Electrode Preparation

Two different electrochemical cells were used, both of which involved a three

electrode configuration. The cells consisted of a platinum working electrode, platinum counter electrode, and a Ag/AgCl reference electrode, but were of different configurations. The first cell consisted of a conventional solid platinum disk electrode (2 mm dia, CH Instruments), a platinum mesh counter electrode (1 cm^2), and a conventional Ag/AgCl reference electrode. The first cell was always used in bulk acidic solution ($\sim 10\ mL$). The second cell was a screen printed electrode (SPE) array from Pine Instruments (p/n RRPE2001PT) comprised of a Pt disk electrode (2 mm dia.), a platinum counter, and a Ag/AgCl reference electrode printed onto a ceramic substrate, shown in Figure 49. The SPE could be used in a thin layer or bulk electrolyte. A computer controlled CH Instruments model 760B bipotentiostat was used to make all measurements.

Electrodes were prepared by different methods. For cyclic voltammetry experiments, The solid working electrode was mechanically polished with successive 1, 0.3, and 0.05 μm alumina polish for 30 seconds each on a micropolishing cloth (Buehler, p/n 40-7218), rinsed with water, and then electrochemically cleaned in 0.5 M H_2SO_4 by scanning between -0.2 V and +1.5 V at 500 mV/s for 25 cycles to generate the signature hydrogen reduction butterfly wave on platinum. The screen printed array could not be polished and was only cycled in acid for the same 25 cycles.

Electrode preparation for square wave experiments was similar in that the electrode was mechanically polished at prior to initial use and then electrochemically cleaned in 0.5 M H_2SO_4 for 25 cycles. Sample collection was performed by scanning between 0.0 V and $-0.5\ V$ with a $\Delta E_s = 0.004\ V$, $\Delta E_p = 0.025\ V$, and a frequency

of 15 Hz for all square wave experiments. Data was collected by electrochemically cleaning the electrode first, then a blank (acetone free) scan performed, and the electrode transfered immediately to an acetone/acid solution for the sample scan. The only time the electrodes were rinsed with water was after the acetone sample scan. Once rinsed, the electrodes were returned to an acid only solution and the process was repeated. Because the butterfly region was easily reacquirable, no mecahnical polishing was performed after the inital polish. The potential limits for electrode cleaning and sampling scans are summarized in Table 20.

Table 20. Cyclic and square wave voltammetric parameters for electrochemical cleaning and acetone sample scans.

CV Parameter	Cleaning Scan	Sample Scan	SWV Parameter	Sample Scan
$E_{initial}$ (V)	+0.2	+0.2	$E_{initial}$ (V)	0.0
$E_{low/final}$ (V)	-0.2	-0.2	E_{final} (V)	-0.5
E_{high} (V)	+1.5	+1.5	ΔE_s (V) (step height)	0.004
Scan rate (V/s)	0.5	0.1	ΔE_p (V) (amplitude)	0.025
Segments	51	3	Frequency (Hz)	15

Although the electrochemical cells involve the same chemistries, the working electrodes are different physically. The solid electrode is a conventional lab electrode (CLE) made with a platinum disk encased in black Delrin®. The solid metal working electrode requires more electrolyte solution volume, measured in mL, to complete the circuit between the working, reference, and counter electrodes in the cell. The screen printed array is capable of conducting an experiment with much less volume, hundreds of μL, because all electrodes are closely spaced and are contained on a single substrate and in one plane. The screen printed array is fabricated by

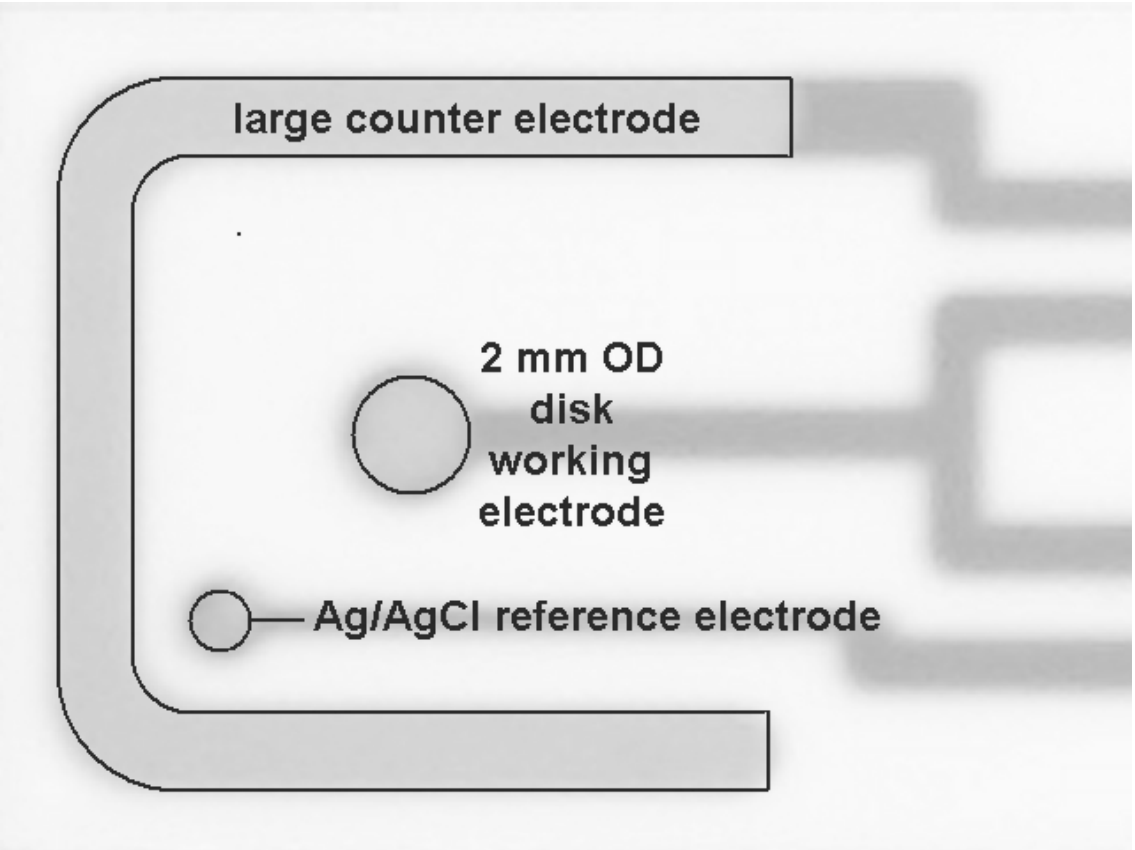

Figure 49. Schematic diagram of the platinum screen printed array. The working and counter electrodes are platinum with a Ag/AgCl reference electrode. Total array area is ~ 6 cm^2. The array is printed on a ceramic substrate and baked to cure the electrodes. Photo courtesy of Pine Instruments, Inc.

dispensing platinum ink on a ceramic substrate and baking at high temperatures to drive organics from the ink. By the nature of the production process, the SPE has a network of platinum resembling a mesh, as shown in Figure 50. Consequently, it has much higher surface area than the solid electrode. Figure 49 is a schematic of the screen printed array used in this work.

6.1.3 Gas Sample Procedure

Once the electrode is electrochemically cleaned, a blank (acid only) scan is

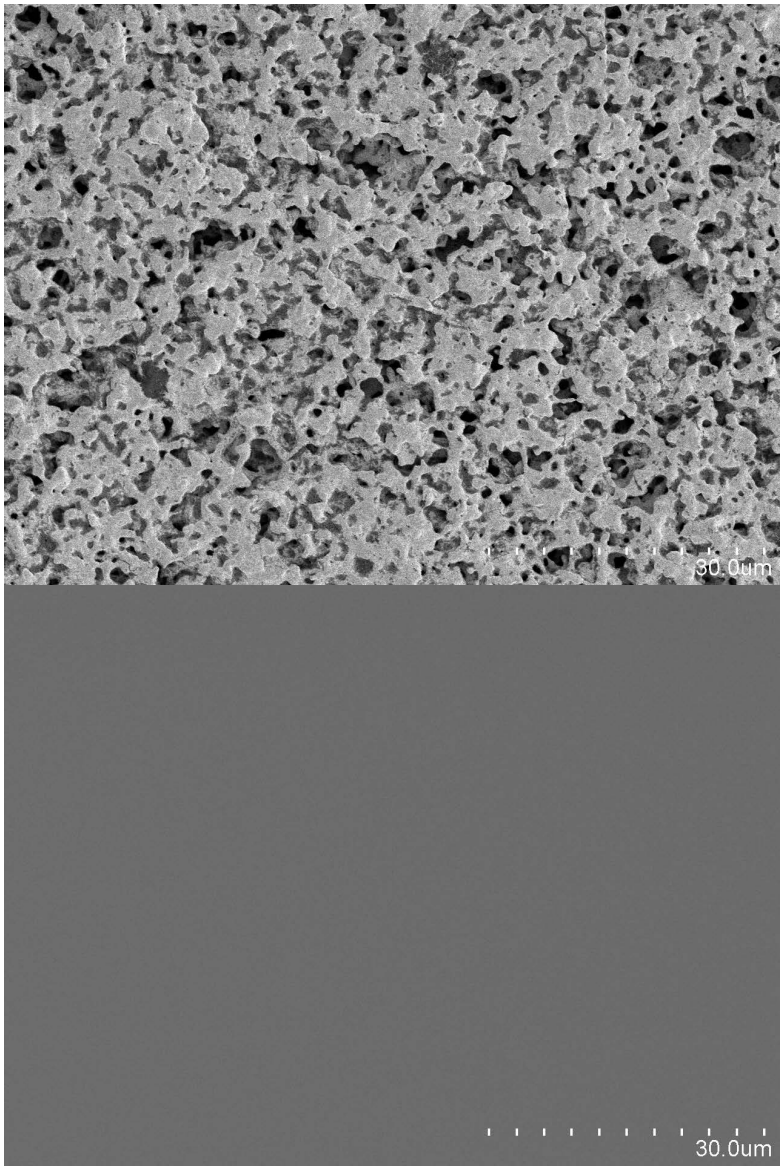

Figure 50. Scanning electron microscopic images of a platinum screen printed electrode (top, Pine Instruments) and a platinum solid working electrode (bottom, CH Instruments) at 1500× magnification.

performed to generate a baseline. The electrode is removed from the acid solution, rinsed with DI water, and dried with ultrahigh purity dry nitrogen for $\sim$ 5 to 10 seconds. An acetone vapor sample is manually delivered directly to the platinum surface with a valved polypropylene syringe at a height of 3-5 mm above the electrode surface with a flow rate of $\sim 0.5\ mL/s$. The electrode is reinserted to the 0.5 M H_2SO_4 electrolyte solution and rescanned with the same parameters as the blank scan.

End breath samples were generated by exhaling for a total of 40 seconds. The first 30 seconds of breath were discarded and the last ten seconds were delivered directly to the electrode surface. Breath was focused onto the electrode surface with a common plastic straw (6 mm i.d. $\times$ 20 cm length). Once the breath sample was delivered, the electrode was reinsterted into acid solution for analysis. Approval for the use of human subjects was received from the University of Iowa Internal Review Board. The subject had been fasting for 14 hours prior to sample collection.

6.2 Results and Discussion

Data and analysis for calibrants and breath sample follow.

6.2.1 Cyclic Voltammetry

The following reports on calibration and breath sample data for measurements acquired with cyclic voltammtry.

6.2.1.1 Solid Platinum Electrode

The following data were collected at a solid platinum electrode.

6.2.1.1.1 Solution Phase Acetone Test

Initial test of platinum as a substrate for acetone electroreduction is presented in Figure 51. The data were collected in 0.5 M H_2SO_4 as a recreation of the protocol from the Wieckowski work [29]. This data showed that acetone could be adsorbed to the surface by electrode prepolarization of acidic electrolyte solutions with and without 10 mM acetone included. Generation of the butterfly lineshape with and without acetone present provided a basis of understanding for moving forward with gas phase measurements.

6.2.1.1.2 Headspace Analysis

In Figure 52, the cyclic voltammetric response in 0.5 M H_2SO_4 is shown for analysis of headspace gas of a low concentration (1 μM) solution immediately after the sample is introduced. The scan starts at 0.4 V and sweeps negative and then positive to 1.5 V. The final sweep segment is then negative back to -0.2 V. On the third segment, the well resolved butterfly region for hydrogen adsorption is apparent. There is a final oxidative sweep. In Figure 53, an enlargement of the reductive portion of the butterfly region is shown. On the initial reductive sweep, the waves for hydrogen are disrupted by the acetone adsorbed from the vapor sample. Thus, on the first sweep, acetone adsorption is apparent. After the full oxidative and the

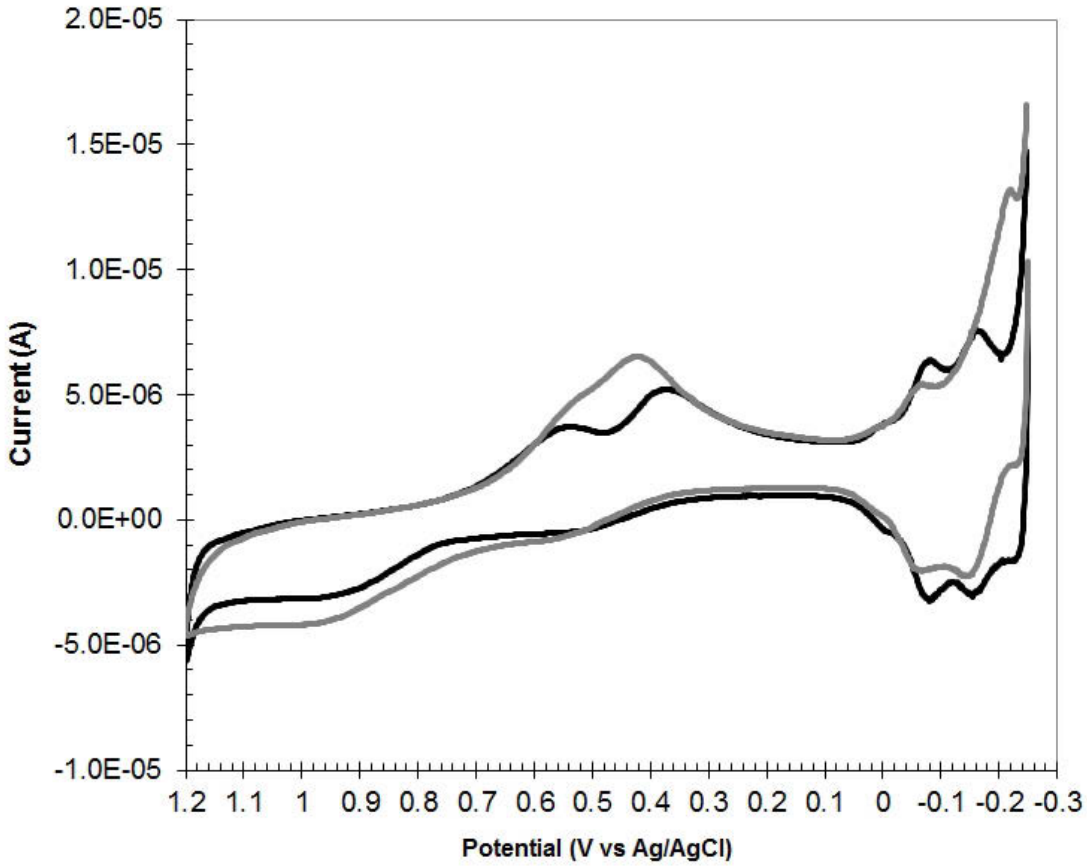

Figure 51. Overlay polot of voltammograms collected in 0.5 M H_2SO_4 with (gray) and without (black) acetone present. Data were collected with a solid Pt working electrode, a Pt counter electrode, and calomel reference electrode. The scan rate was 100 mV/s. The working electrode in both cases was polarized for 15 minutes prior to scanning.

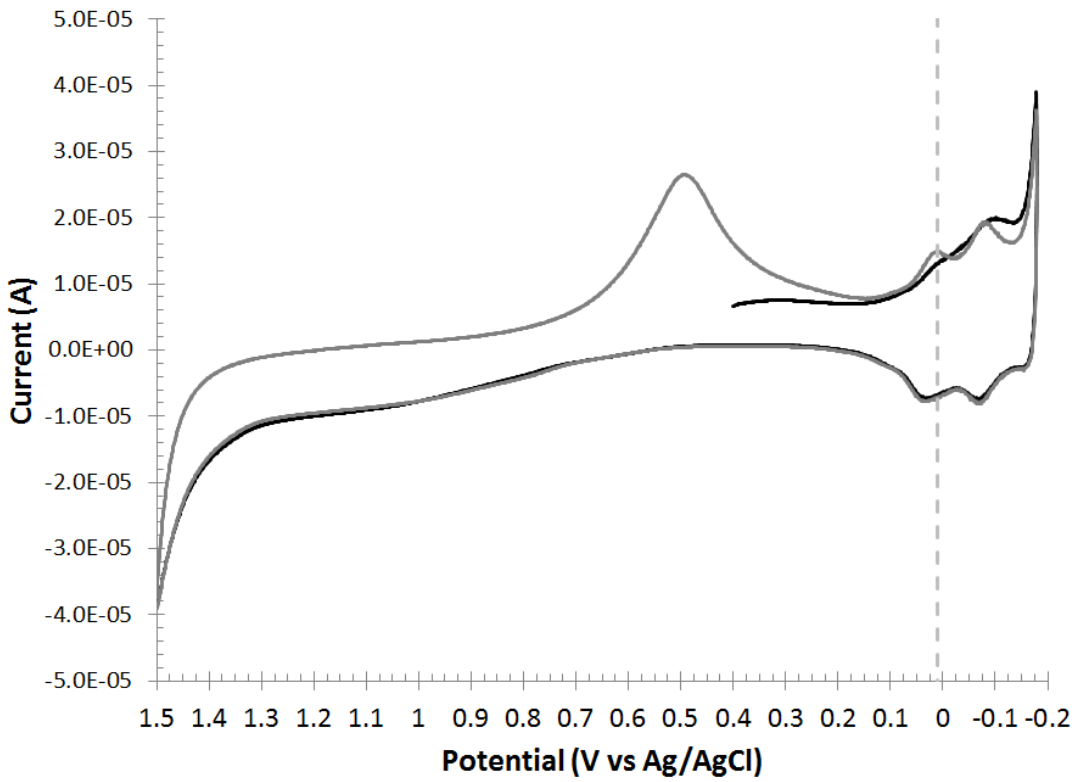

Figure 52. Overlay of headspace analysis scans in 0.5 M H_2SO_4 for 1 μM acetone in water solution over the full sample scan range. Scanning twice through the hydrogen reduction region provides acetone headspace data (black) followed by hydrogen reduction (gray). The vertical dotted line at +0.05 V depicts where the sample data is extracted.

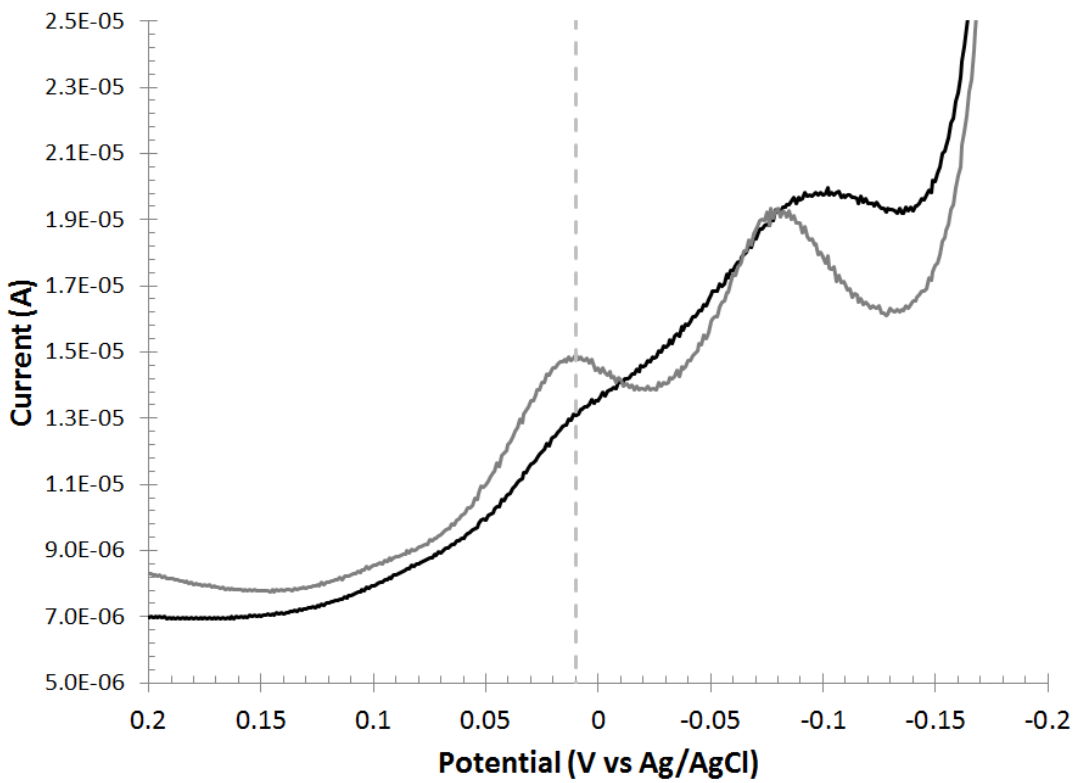

Figure 53. Overlay of subsequent headspace scans in 0.5 M H_2SO_4 through the hydrogen reduction region, 1 μM acetone in water. First pass (black) through this region reduces adsorbed acetone, while the second pass (gray) regenerates the hydrogen reduction wave.

return reductive sweep, the acetone has been fully electrolyzed to yield a butterfly consistent with only hydrogen adsorbed. The complete electrolysis of acetone is consistent with the bottom portion of the butterfly coincident on the second and fourth segments.

In Figure 54, the cyclic voltammetric response in 0.5 M H_2SO_4 is shown for analysis of headspace gas of a high concentration acetone (10 mM) immediately after the sample is introduced. The signal for the 10 mM solution differs from the 1 μM solution. In both cases for the initial segment, the first wave of the butterfly is suppressed and the second wave is altered relative to the pristine hydrogen adsorption wave. In Figure 55, the voltammetric response for the adsorbed human breath sample in 0.5 M H_2SO_4 is shown. Voltammetric characters are consistent with the responses for the acetone samples above. On the first segment, the first wave is suppressed and the second wave is altered. On the third segment, the voltammetric response is that characteristic of only hydrogen adsorbed on platinum, as for the prior samples.

6.2.1.1.3 Calibration Curve

The calibration data, shown in Table 21, are generated for solution phase acetone concentrations from 1 μM to 10 mM in decade increments. The analyzed current, $\Delta i\,(\mu A)$ is derived from the plots as the difference in the current on the first and third segments at +0.005 V. Current difference values are reported as absolute values. The calibration data are linearized as Δi versus $1/\log_{10}[acetone]$ as shown in Figure 56 by the solid markers. The linearization is observational. Temkin isotherms

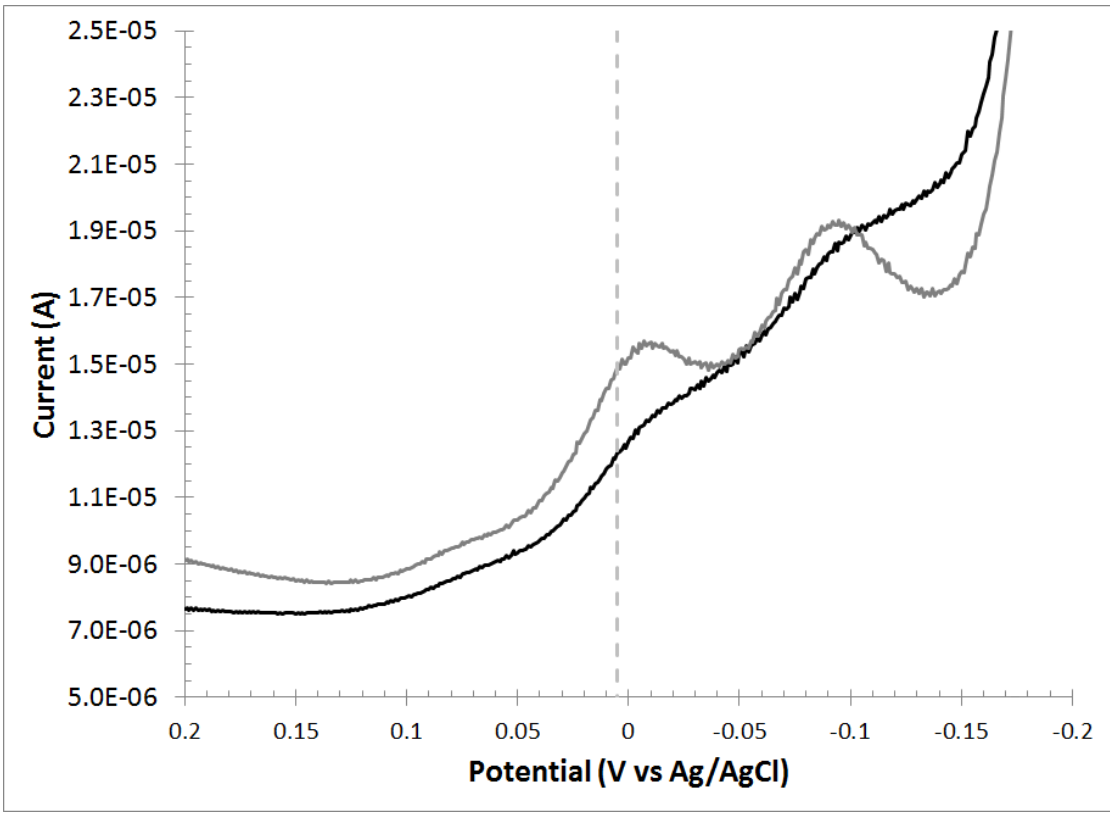

Figure 54. Overlay of subsequent headspace scans in 0.5 M H_2SO_4 through the hydrogen reduction region, 10 mM acetone in water. First pass (black) through this region reduces adsorbed acetone, while the second pass (gray) regenerates the hydrogen reduction wave.

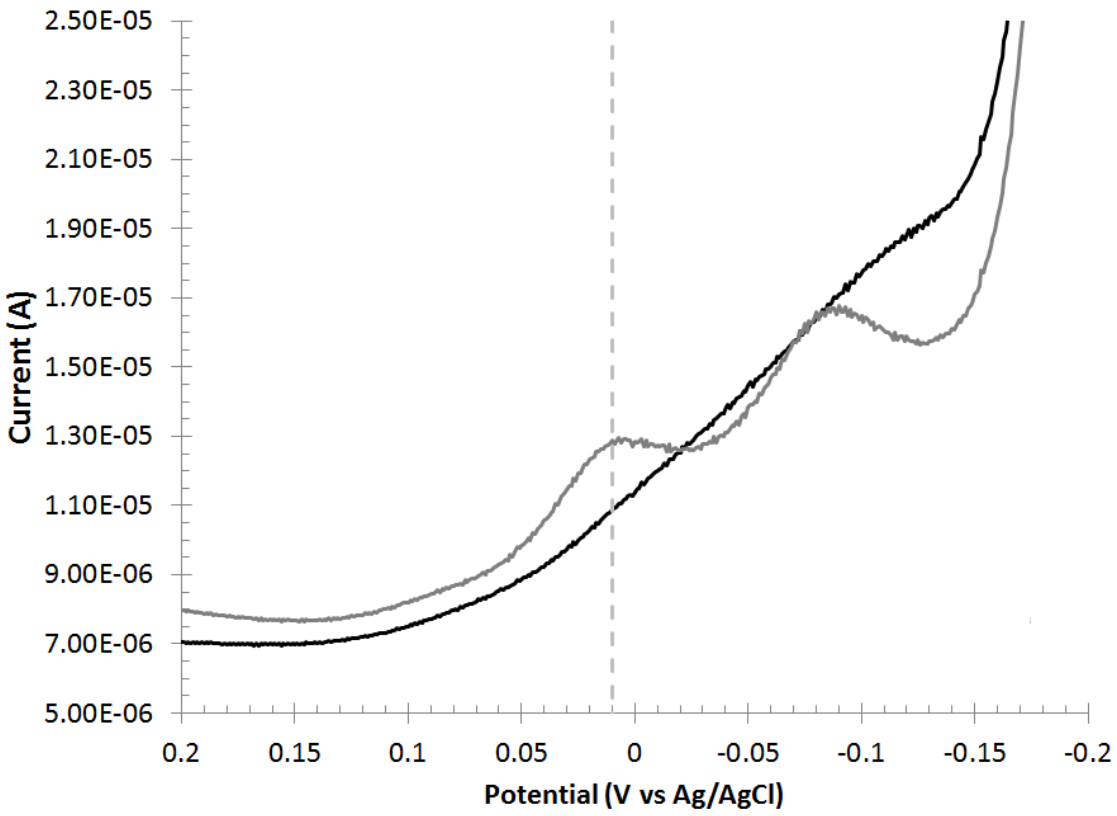

Figure 55. Overlay of subsequent human breath scans in 0.5 M H_2SO_4 through the hydrogen reduction region. First pass (black) through this region reduces adsorbed acetone, while the second pass (gray) regenerates the hydrogen reduction wave.

have a surface converage related to the logarithm of bulk concentration. Temkin isotherms included adsorbate interactions.

Table 21. Extracted current difference values for calibration and breath samples.

Sample	[acetone (M)]	-log[acetone (M)]	Δi (μA)
water vapor	0	–	1.40
1 μM	1.0E-6	6	1.40
10 μM	1.0E-5	5	1.50
100 μM	1.0E-4	4	1.60
1 mM	1.0E-3	3	1.90
10 mM	1.0E-2	2	2.40
breath	4.6×10^{-4}	3.33	**1.80**

6.2.1.2 Breath Sample

The breath sample was introduced as above and evaluated cyclic voltammetrically in 0.5 M H_2SO_4 as consistent with the calibrants. Δi for the breath sample is shown in Table 21 as 1.80 μA. From the calibration line, the breath sample correlates to an acetone concentration of 0.46 mM, a value well within the calibrant set and well within the physiological range anticipated for a fasting human. To roughly estimate the acetone levels for the subject, a Ketostix urine test strip was used to verify ketosis and correlate urine measurements of AcAc acid to breath acetone. Urine analysis determined the subject was in a mild ketotic state and fell between 5-15 mg/dL AcAc. Assuming a median value of 10 mg/dL, this converts to a value of 1 mM for a range of 0.5 to 1.5 mM. Although the sticks measure AcAc and not acetone directly, the two compounds are in equilibrium with each other at a ratio of 1:7 (acetone:AcAc) in a nonketoacidotic state. The corresponding acetone value

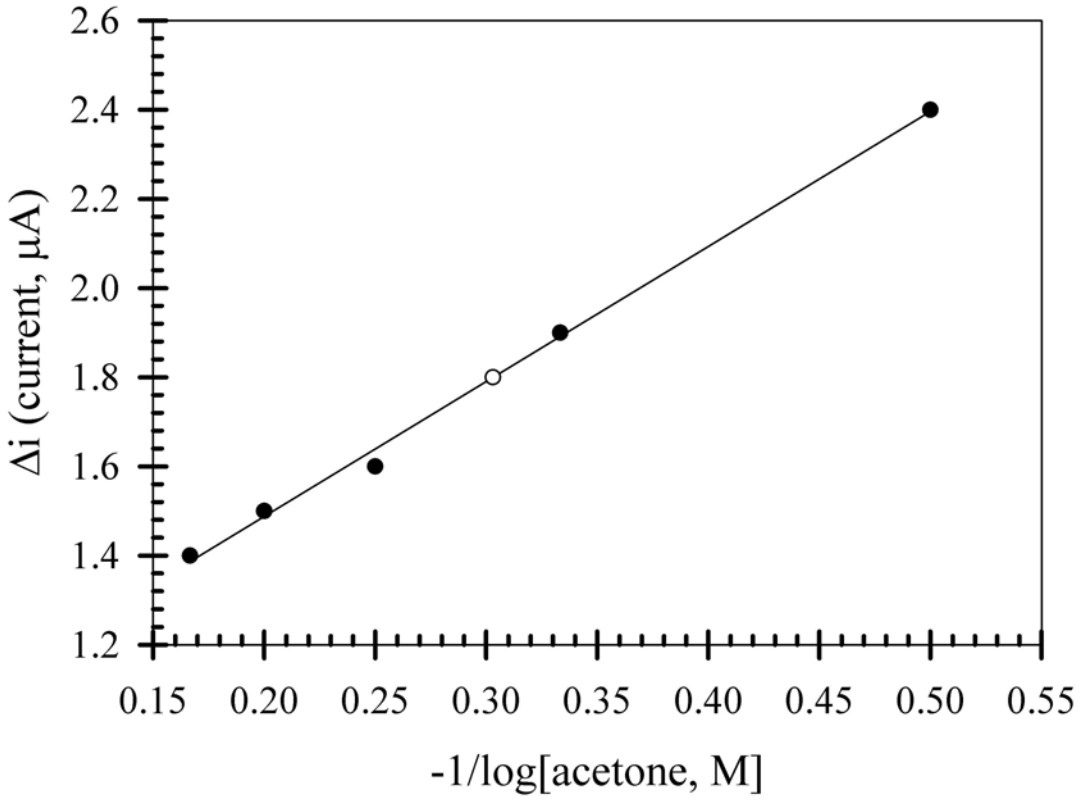

Figure 56. Calibration curve (solid circles) for headspace acetone and breath sample (open circle) analysis. The equation of the line is $y = (3.0_3 \pm 0.1_0) \times 10^{-6}x + (8.8_2 \pm 0.3) \times 10^{-7}$ with $\sigma_y = 2.6 \times 10^{-8}$and $R^2 = 0.997$. The breath sample correlates to $\sim$ 0.5 mM acetone. Standard deviations are not included because no repetitive measurements were collected.

for urine analysis is then $\sim 0.14\ mM$ for a range of 0.07 to 0.21 mM. The breath measurement and urine estimation are comparable given the uncertainties in the urine measurement and associated estimations.

6.2.1.3 Screen Printed Electrode Array

The screen printed array was a first approach to miniaturize the electrochemical cell for possible use in a hand held device. The scale and compactness of the system offer advantages over the solid working electrode, such as minimal electrolyte required, ease of cleaning, improved peak resolution, and the amount of platinum used to fabricate the SPEs is low enough that the electrode array can be considered disposable.

6.2.1.3.1 Calibration Curve

A calibration curve for the screen printed electrodes was generated by the same protocol described for the solid electrodes, with one exception. The solution volume was 100 μL instead of 10 mL. The thin layer of electrolyte was spread over the screen printed array and scans were performed as normal. The previous current difference method proved to be inadequate because the differences between scans did not always provide reliable values. Instead, peak heights were measured directly and a resultant calibration curve made. Calibration performance for the screen printed electrode proved difficult to quantify. The calibration curve in Figure 57 demonstrated large standard deviations ($n = 3$) that overlapped considerably with neighboring points. In addition, linearization required a different method than

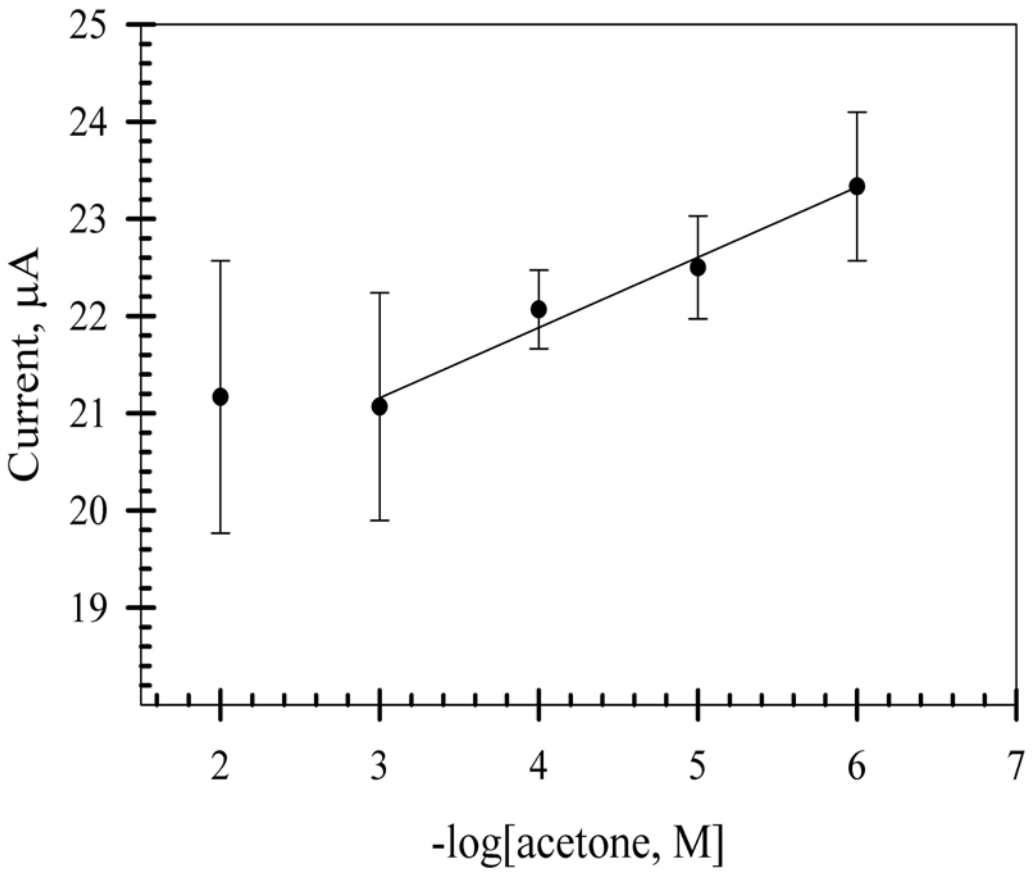

Figure 57. Calibration curve for head space acetone at a platinum screen printed electrode. The equatio of the line for the linear region is $y = (7.2_3 \pm 0.7_3)\times10^{-7}x+(1.89_9 \pm 0.03_4)\times10^{-5}$with $\sigma_y = 1.6_4\times10^{-7}$ and $R^2 = 0.980$. Standard deviations are shown for 1σ.

the solid electrodes, $-1/\log[\text{acetone}]$ versus $-\log[\text{acetone}]$, for reasons that could be related to the change in data measurement. Finally, the overall signal range between the highest concentration (10 mM) to the lowest concentration (1 μM) was $\sim$ 20 μA, which is a larger range by comparison to the solid electrode calibration presented in Figure 56. The increased current is due to the increase in surface area of the SPE versus the surface area of the solid electrode, Figure 50. No breath data was examined, as the large standard deviation would disallow a useful analysis.

6.2.2 Square Wave Voltammetry

Because of the difficulties with cyclic voltammetry, square wave voltammetry was used to acquire calibration information. The CV data lacked sufficient reproducibility and sensitivity largely due to variations in background and faradaic currents. Square wave voltammetry has higher sensitivity and better discrimination against nonfaradaic currents than cyclic voltammetry. All measurements were made with the same solid platinum disk electrode used in cyclic voltammetry measurements.

6.2.2.1 Measurement Protocol

The measurement protocol was similar to that used in CV experiments because the same phenomena of acetone blocking hydrogen adsorption sites remains the fundamental basis for the measurement. Adsorbed acetone is reduced at the electrode surface competitively with hydrogen ions. Adsorbed acetone suppresses the first hydrogen reduction peak, while the second peak is enhanced. On

subsequent reductive cycles, the first hydrogen reduction peak increases as the acetone concentration on the surface is diminished with increasing electrolysis. The electrolyte is 0.5 M H_2SO_4. Acetone calibration solutions were made the sulfuric acid electrolyte. Concentration ranges for the calibration method are the same as those used previously: 1.0 mM, 1.0×10^{-4} M, 1.0×10^{-5} M, and 1.0 μM. Unless noted otherwise, the collection sequence for the calibration curves is 1.0×10^{-5} M, 1.0 mM, 1.0 μM, and 1.0×10^{-4} M. This sequence was used to ensure signal is generated without bias of measurement made in order of concentration.

The collection procedure mimicked that used for CV measurements. The working electrode was mechanically polished with a three stage sequence of 30 second polishes at 3.0, 1.0, and 0.05 μm grit alumina polishing powders with distilled water rinse after each grit. Cyclic voltammetry in an acid only solution was used to electrochemically clean the electrode surface and to generate and verify the signature butterfly wave. Square wave voltammetry was then used to obtain a blank (acid only) measurement. The working, reference, and counter electrodes were transferred to an acetone solution and the square wave measurement was repeated. Parameters for all experiments are found in Table 20.

Once the acetone sample collection was finished, all electrodes were removed from the acetone sample and rinsed with water. The counter and reference electrodes were returned to the blank acid solution, while the working electrode was polished with 0.05 μm for 30 seconds to refresh the surface before the next acetone measurement was made. This surface refresh step was required because the electrode surface lost some acetone sensitivity over time. The quick polish was sufficient to generate a

surface for consistent measurements.

The parameters chosen for the experiment are based on suggestions of generic parameters offered by Osteryoung and O'Dea [35, 78]. The step height is generally suggested to have a value where $\Delta E_s = 10/n\ mV$ and an amplitude where $\Delta E_p = 50/n\ mV$. Assuming the two electron reduction of acetone to isopropanol, Equation 75, values of $\Delta E_s = 5\ mV$ and $\Delta E_p = 25\ mV$ would be appropriate. These are close to default parameters for the instrument, where $\Delta E_s(default) = 4\ mV$ and $\Delta E_p(default) = 25\ mV$. Consequently, the default parameters were used. Frequency is the scan rate parameter and the default value of 15 Hz was used after testing higher frequency values did not improve the measurement. With $\Delta E_s = 4\ mV$ and a frequency of 15 Hz, the effective scan rate is 60 mV/s.

A macro was written to control voltammetric sequencing and ensure consistent data collection, Appendix C.2. The collection sequence was designed to have a 10 second pause between scans. Initially, the embedded instrument control function, Repetitive Runs, was used to perform data collection with identical parameters for successive scans. However, this function does not provide a level of control sufficient for this measurement because the first scan is performed immediately with 10 sec delays between the first and second scans and then the second and third scan. This was considered problematic because of the inconsistency of start times for the first scan. Use of the function Quiet Time as a delay is possible, but the quiet time function is a potential hold time that prepolarizes the working electrode at the initial potential before starting the potential scan. The polarization hold time proved to have a negative impact on the system and was not used for the data reported here.

Instead, the user written macro included a Pause Time before each scan, including the first scan, that served as the delay between runs with no polarization hold time applied.

6.2.2.2 SWV Calibration Curves

Square wave voltammograms were analyzed based upon peak differences found in acetone/sulfuric acid solutions and solutions with acid only. Figure 58 is an overlay of three successive square wave voltammograms performed in 0.5 M sulfuric acid. A similarly generated sequence for a 1.0 mm acetone sample is shown in Figure 59. Two metrics were used to analyze acetone samples. Peak current differences were analyzed for acetone between the first and second scans, as shown in Figure 59. The second metric is based on peak potential shifts, as shown in Figure 63.

6.2.2.2.1 Current Based Calibration

Consider the peak current measurement shown in Figure 59. As acetone is reduced at the surface, the products diffuse away, and the cleared sites are replaced with hydrogen ion that adsorbs to the surface and is electrolyzed on the next scan. There is some adsorption of acetone but the newly adsorbed material is largely hydrogen because the adsorption rate and concentration of hydrogen is substantially greater than for acetone. In Figure 60, Δ (SWV ΔCurrent), is the difference in the peak current for the first wave from the first and second scans of the sample (see Figure 59) is shown as a function of the analyte concentration, $-\log[acetone]$. An increase in peak current for the first wave, peak 1, is observed and varies with

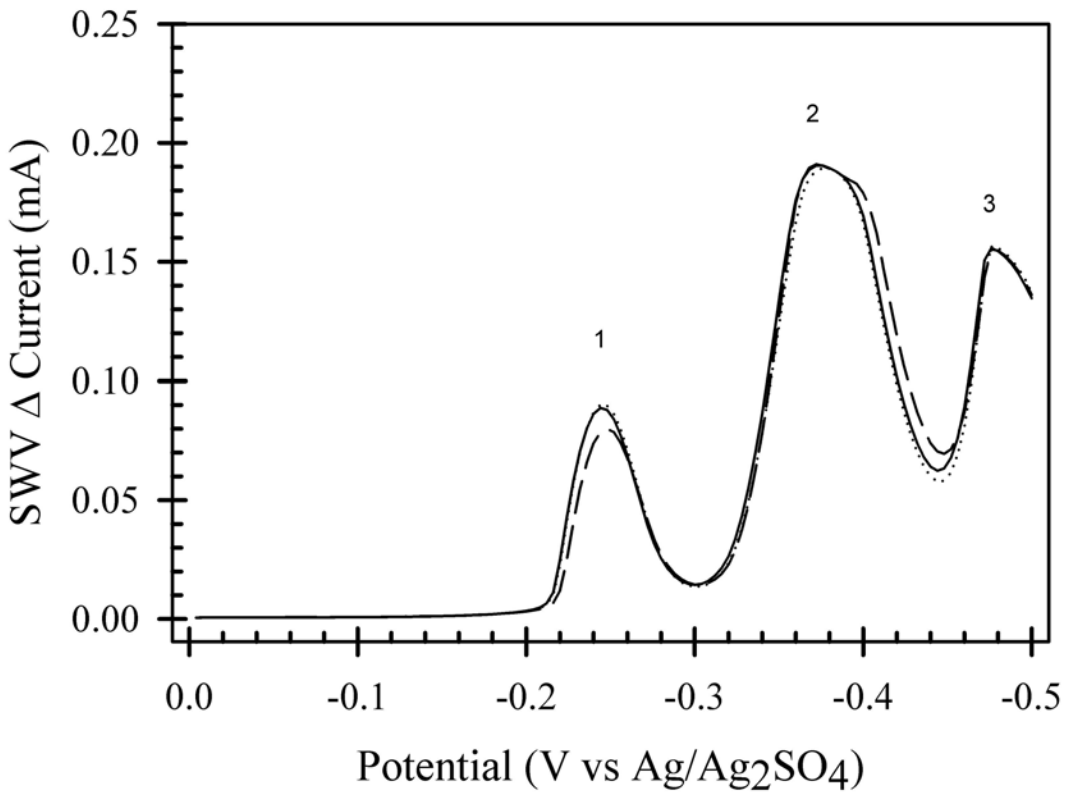

Figure 58. Overlay of SWV output for the reductive wave of the butterly region collected in 0.5 M H_2SO_4. Peaks 1 and 2 represent the standard hydrogen reduction peaks observed on platinum and Peak 3 results as potential advances into the aqueous solvent window. For an introduction of square wave voltammetry, see section 5.2.4

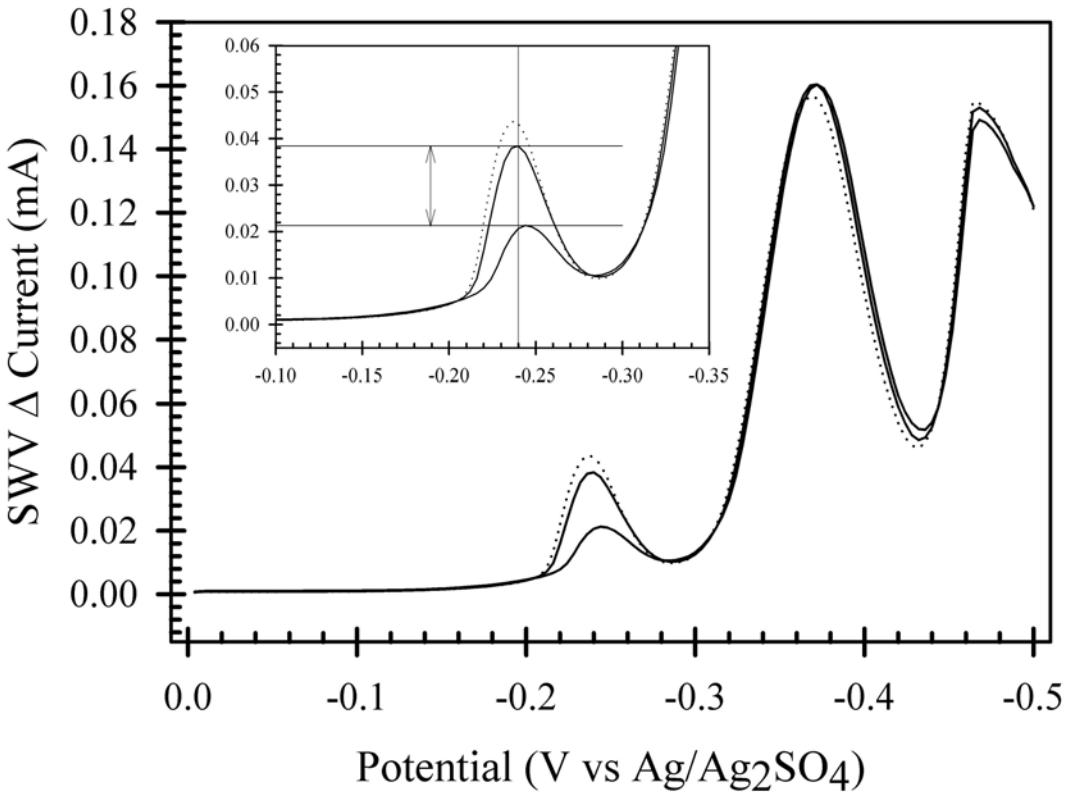

Figure 59. Overlay of square wave voltammetry scans of 1.0 mM acetone in 0.5 M H_2SO_4. The inset figure illustrates the measurement protocol for use in generating a calibration curve. The double headed arrow illustrates difference measurement performed from the peak heights between the first and second scans.

respect to acetone concentration. However, the correlation of peak current with acetone concentration had wide standard deviations. A linear relationship is found with average peak currents of multiple runs at each concentration, but the system had great variance with large standard deviations that encompass the entire data range. All attempts to utilize acetone peak currents as a metric, with respect to either a blank or the acetone sample itself, resulted in calibration curves with standard deviations too wide to allow analysis, as shown in Figure 60. In the linearization shown in Figure 60, the 1.0 mM data is excluded. It is possible that at higher concentrations the surface coverage of acetone either saturates or changes morphologically. Note that for concentrations of 10^{-4} to 10^{-6} M even decade concentration differences cannot be reliably determined because of the uncertainties, despite good linearity ($R^2 = 0.995$).

Several different techniques were also evaluated. Initially, the working electrode was polished only at the beginning with the three stage polish described previously. As data were collected, the working electrode was not polished further. This was not thought to be a problem because of the quick regeneration of the hydrogen butterfly wave in sulfuric acid, which is considered a metric of surface cleanliness. However, surface activity to acetone diminished over time. If the calibrant solutions are tested in sequence, decreasing from high to low concentrations, decreased performance over time is observed, but signal degradation is observed more clearly when randomizing the calibrant collection sequence. Decreased performance is considered to occur when the same sample that was tested first is then tested at the end and the same intensity or behavior is not observed. Second, a prepolarization potential was

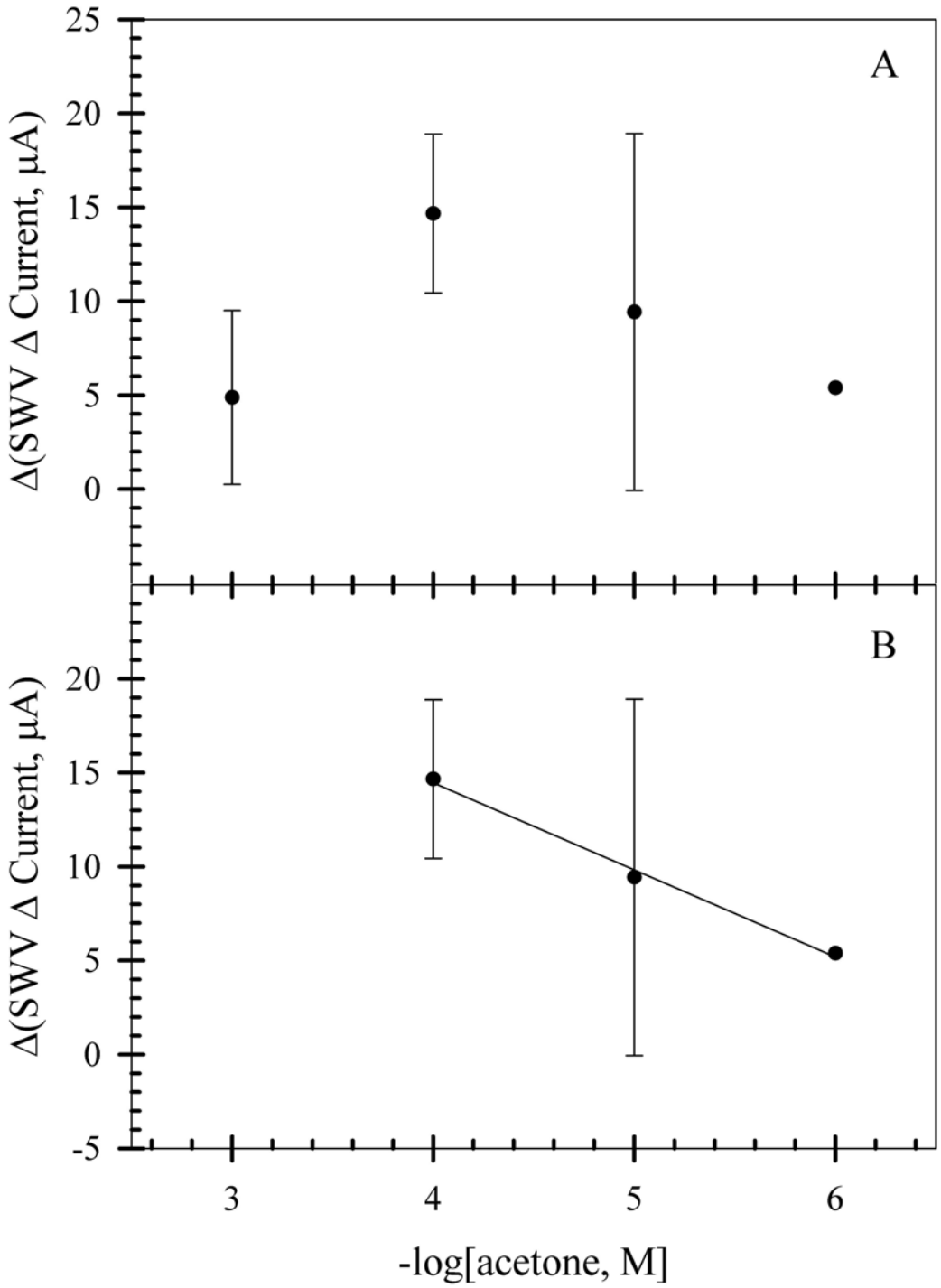

Figure 60. Calibration curve based on the peak height difference for wave 1 for the first and second sequential square wave scans. The peaks heights are calculated from zero and no baseline measured values were used. The equation of the line for the linear range is $y = (-4.6_4 \pm 0.3_4) \times 10^{-6}x + (3.3_0 \pm 0.1_7) \times 10^{-5}$ with $\sigma_y = 4._8 \times 10^{-7}$ and $R^2 = 0.995$. Standard deviations are reported for 1σ and $n = 3$ samples. The data point for 1.0 μM is reported for $n = 2$ samples.

applied to the working electrode. The intent was to sustain selectivity to acetone over time and to aid the adsorption process. A potential of 0.0 V was applied for 60 seconds for one calibration model and 10 seconds for another. In both cases, either a nonlinear relationship of peak current difference was observed or the standard deviations were too large for use. Finally, a quick polish with 0.05 μm grit alumina powder and distilled water was used to refresh the surface, as described previously. Although the quick polish was able to maintain surface activity and minimize surface aging effects, the standard deviations were again too large for use. Relative standard deviations were comparable to those shown in Figure 60.

Various data analyses were applied to data collected as well. Ratios of peak characteristics were made to attempt to find a calibration method. Peak heights were used, such as the ratio for peak 1 to peak 2 on the first scan of the same sample (Figure 61), the ratio of peak 1 acetone to peak 1 blank on the first scan (Figure 62), and then the ratio of peak 1 for the first and second sequential scans for an acetone sample. Peak areas were also used in the same manner to find a calibration method, but none of these methods proved to work with better consistency or correlation, if they worked at all. Eventually, attempts to find calibration models based on current were abandoned.

6.2.2.2.2 Potential Based Calibration

Calibration curves based on peak potential provided a superior metric. Peak shifts along the potential axis (x axis) were observed with different acetone concentrations. To demonstrate measurement stability, it was necessary to determine if the position

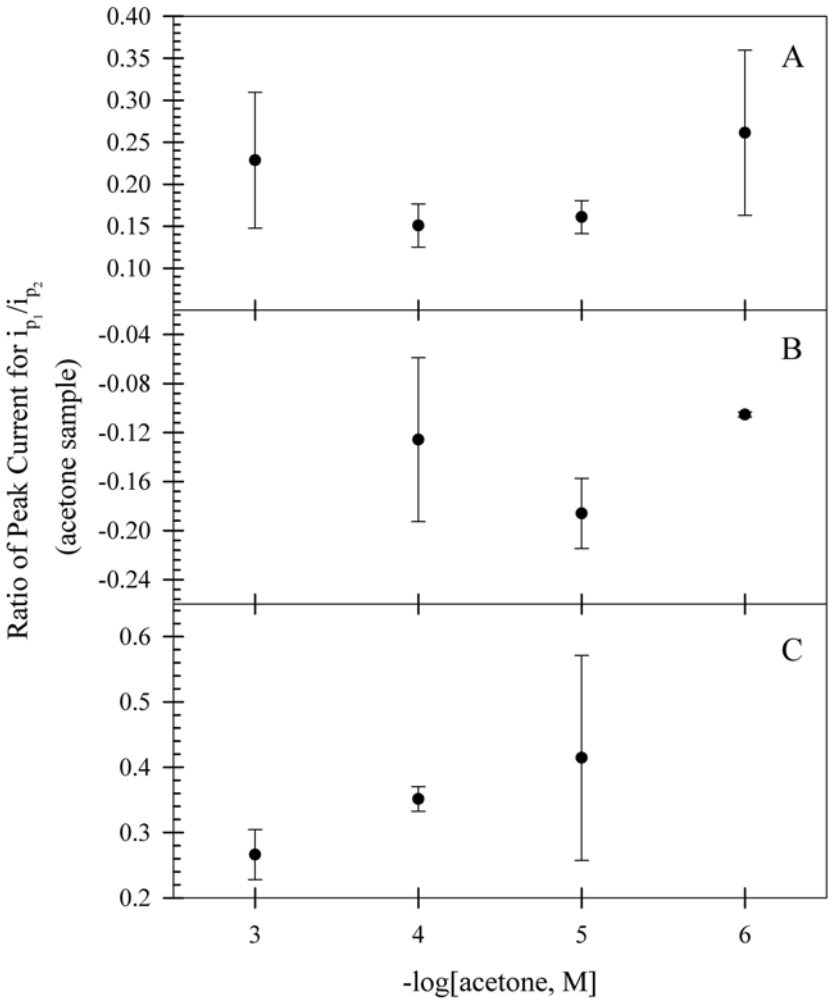

Figure 61. Calibration curves based the ratio of peak currents for peak 1 and peak 2 within the same scan. Different polarization times and minimal polishing of the electrode were used. A polarization potential of 0.0 V (vs Ag/Ag_2SO_4) was held for 60 seconds (top), 10 seconds (middle), and no polarization applied (bottom) prior to performing a scan. In all cases, the standard deviations are large or no linearization was possible with the use of a polarization time. The electrode was polished only initially by the three stage procedure described previously.

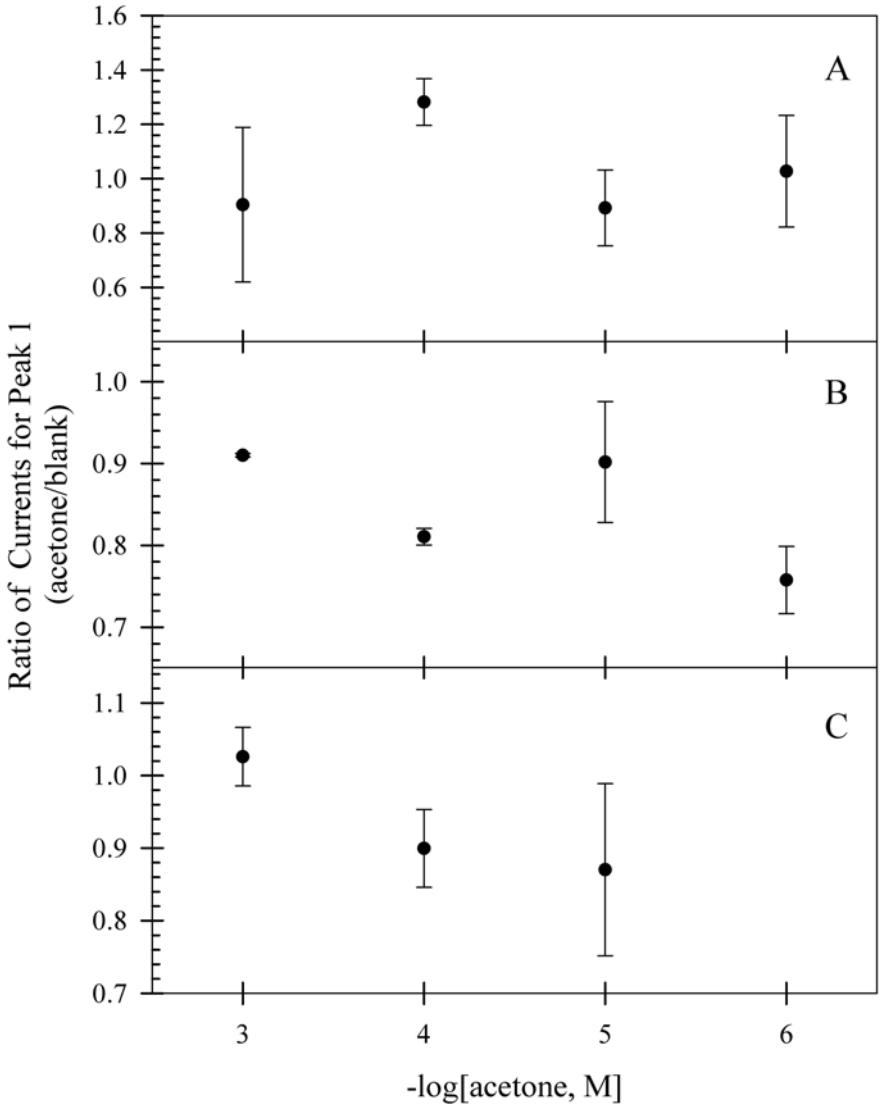

Figure 62. Calibration curves based the ratio of peak currents (acetone/blank) for Peak 1 with different polarization times and minimal polishing of the electrode. A polarization potential of 0.0 V (vs Ag/Ag_2SO_4) was held for 60 seconds (top), 10 seconds (middle), and no polarization applied (bottom) prior to performing a scan. In all cases, the standard deviations are large or no linearization was possible with the use of a polarization time. The electrode was polished only initially by the three stage procedure described previously.

of peaks 1 and 2 within a single sample move with respect to each other. Figure 63A defines ΔE_1 as the peak potential difference between peaks 1 and 2 in one sample. The stability of this measurement is necessary if comparisons of peak positions are to be made across scans performed in different solutions. Figure 64 illustrates the average values of peak positions obtained from the triplicate scan measurement performed for various acetone concentrations. The average ΔE_1 variance across all concentrations is 3.5 mV. The largest standard deviation is 6 mV. The stability of the system allows for comparison of peak potential shifting across different samples

Figure 63 illustrates the peak potential difference measurement labeled as ΔE_2. Here, ΔE_2 is defined as the peak potential difference for peak 1, on the first scan, between acetone and blank solutions.The shifted peak potential measurement is the metric for the calibration curve, Figure 65B. Because of transfer between blank and acetone samples, standard deviations are expected higher than ΔE_1, where the measurement is made in the same solution. The standard deviations for ΔE_2 are reasonable except for the 10 μM sample, where they are exceptionally large for the first sample concentration collected. These large deviations were routinely observed when initially collecting data, regardless of which concentration was collected first. Here, 10 μM was the first sample recorded and 100 μM was the last. More data scans per concentration will reduce standard deviations, but some systematic uncertainty for the first concentration remains. This method shows promise in that at least an order of magnitude estimate of concentration is possible for the concentration range between 1 μM to 100 μM.

The same protocols for calibration used in data collection for calibrations based

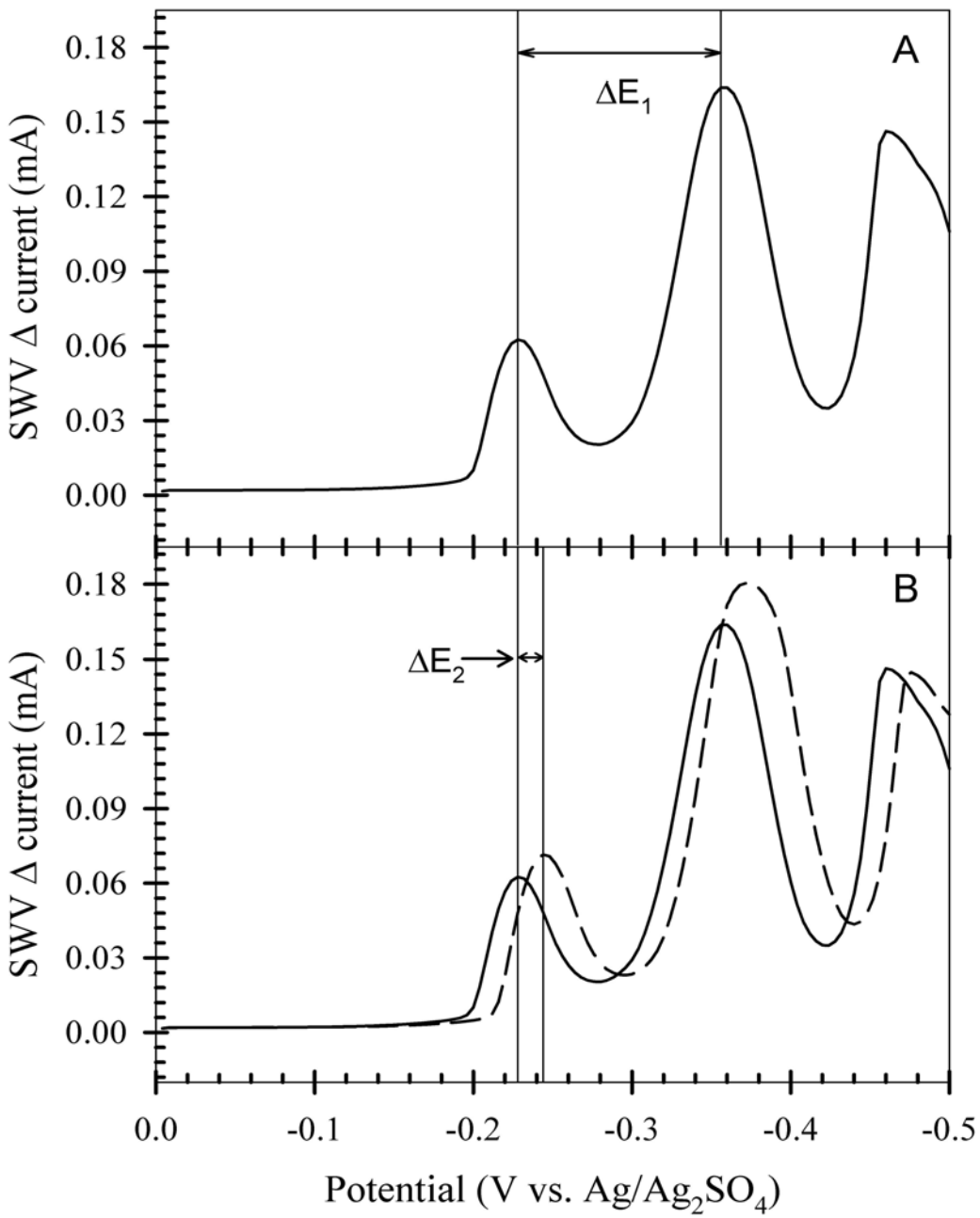

Figure 63. Illustration of peak shifting observed as a function of acetone concentration. Figure A defines ΔE_1 as the peak potential difference between peaks 1 and 2. Figure B defines ΔE_2 as peak potential difference based on the observed shift between acetone (*solid*) and blank (*dashed*) measurements. The concentration for this sample is 1.0×10^{-4} M.

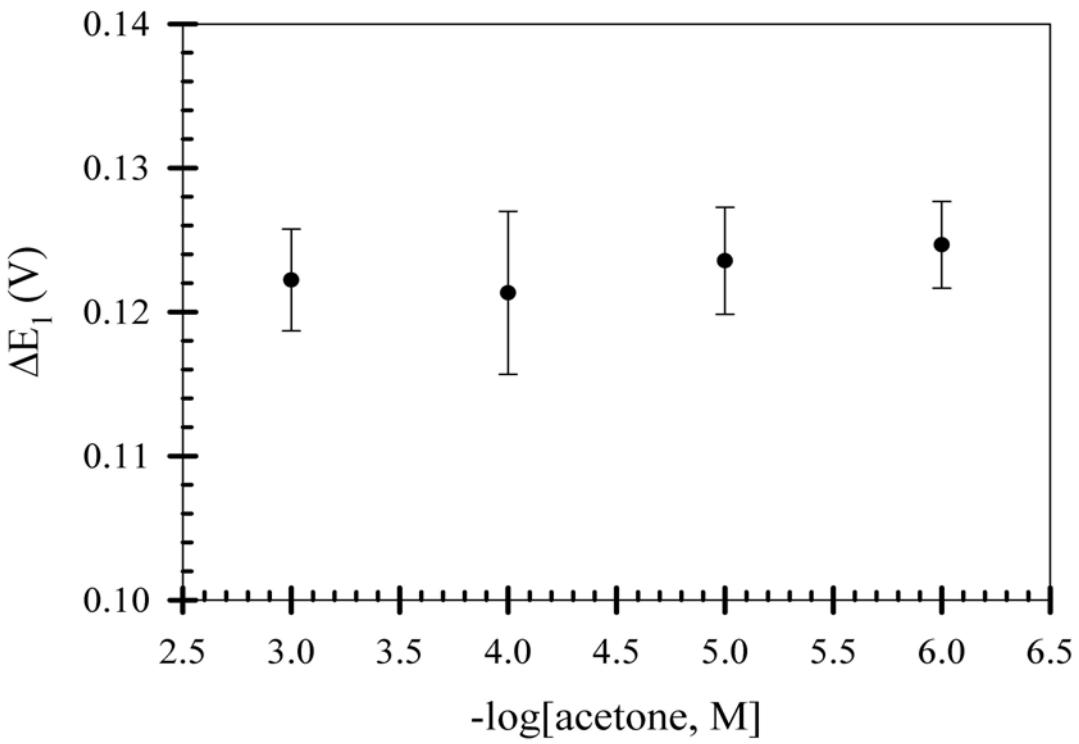

Figure 64. Evaluation of ΔE_1 for square wave voltammetry measurements in acetone solution. Average values are obtained from triplicate scans performed for each acetone solution. Variation (low to high) of the average positions was no more than 3.5 $m\dot{V}$. The largest standard deviation is 6 mV.

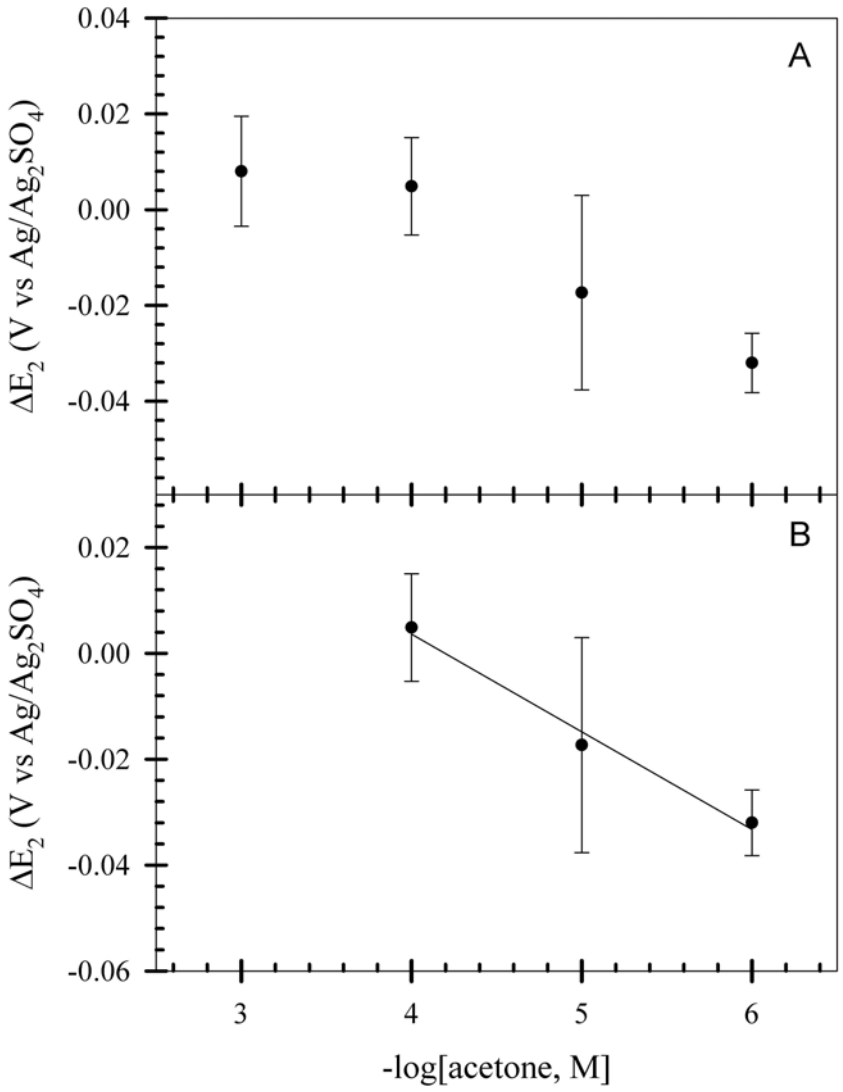

Figure 65. Calibration curve based on the potential shift of peak 1 for acetone and blank solutions. Figure A is the entire calibration range test and Figure B is the linear portion of the data set. Standard deviations are reported to 1σ for $n = 3$ repetitions. The equation of the line for linear range is $y = (-0.018_4 \pm 0.002_1)x + 0.07_7 \pm 0.01_1$ with $\sigma_y = 0.003_1$ and $R^2 = 0.986$.

on peak current were applied to peak potential data. Similarities in data variance for experiments performed with only the initial polish or electrode prepolarization were observed, Figure 66. Standard deviations were found to be too large or good linearity could not be achieved. Only when applying the quick polish to refresh the surface was the best fit found.

Other potential based metrics, in addition to differences in peak potentials observed with $\Delta E_1$and ΔE_2 measurements, were examined. It has been shown the positions of peaks 1 and 2 (ΔE_1) do not move much with respect to each other for a given sample. Because shifting between peaks 1 and 2 does not vary much, a different potential based metric between acetone/acid and acid only solutions could be made using peak 2 of an acetone signal and peak 1 of the blank, or vice versa. However, peak 2 can demonstrate greater susceptibility to an overflow current error (max value cap) if attention is not paid to instrument sensitivity settings. Consequently, the correlation used in ΔE_2 is the more consistent metric.

6.2.2.2.3 Measurement Precision

For the data in Figure 65B, the average standard deviation is $\pm 12\ mV$. Assume a Nernstian relationship of 0.05916 V per n electrons transferred. The precision of the measurement can be estimated as

$$\%\ relative\ error = \frac{E_{meas} - E_{true}}{E_{meas}} \times 100 \quad (77)$$

$$= \left| 1 - 10^{\frac{(E_{meas} - E_{true})n}{0.05916}} \right| \times 100 \quad (78)$$

where E_{meas} and E_{true} are the measured and true (actual) peak potentials. Allow

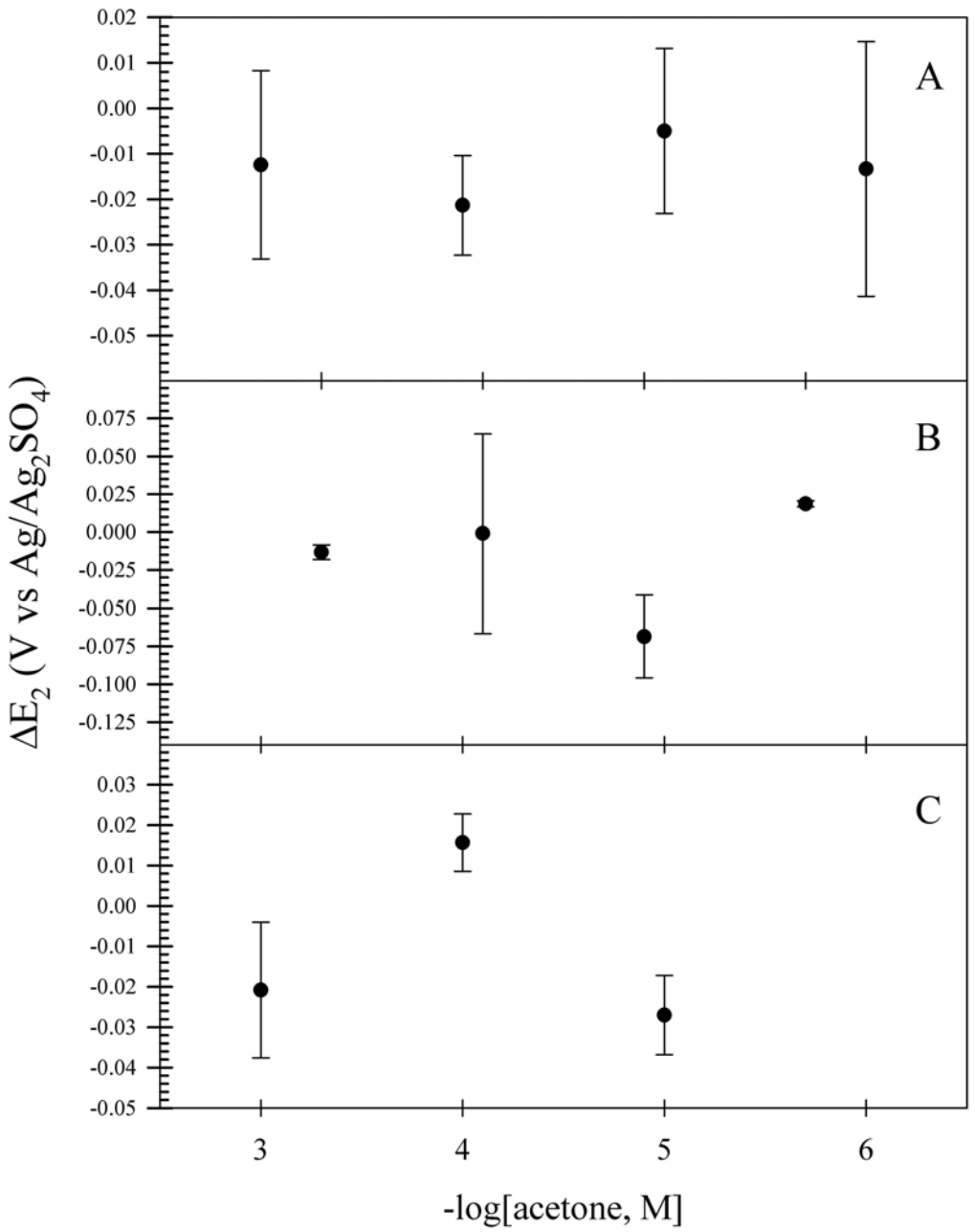

Figure 66. Calibration curves based on ΔE_2 for different polarization times and minimal polishing of the electrode. A polarization potential of 0.0 V (vs Ag/Ag_2SO_4) was held for 60 seconds (top), 10 seconds (middle), and no polarization applied (bottom) prior to performing a scan. In all cases, the standard deviations are large or no linearization was possible with the use of a polarization time. The electrode was polished only initially by the three stage procedure descried previously.

$E_{meas} - E_{true} = 0.012\ V$. From Figure 65B, the slope of the line is -0.018 ± 0.002, which translates to an approximate value of $n = 3$ for the electrons transferred $(0.05916/n)$. Equation 78 becomes

$$\%\ relative\ error = \left|1 - 10^{\frac{\pm stdev \times n}{slope}}\right| \times 100 \quad (79)$$

$$= \left|1 - 10^{\frac{\pm 0.012 \times 3}{0.05916}}\right| \times 100 \quad (80)$$

with incorporation of the slope, standard deviation, and n values. From this calculation, the ratio of $10^{-0.66} = 0.22$ yields a relative error of $\sim 80\%$. Although high, measurement within an order of magnitude is possible with the preliminary data. The measurement distinguishes between decade changes in concentration. Further development is required, but decreasing the standard deviation below 6 mV brings this relationship to $\sim 50\%$ and would allow for determination of half decade changes in concentration.

6.3 Supplemental Discussion Regarding Reproducibility Concerns

Reproducibility of signal remains the limitation for this project. There are inherent errors in any measurement but here, reproducibility is a factor regardless of how the measurement is made. Differences in the working electrode surface area and porosity impacted the measurements and required different methods for linearization. The following discussion is our current understanding of the system.

6.3.1 Adsorption

Acetone is electroactive as an adsorbate on platinum. Therein lies a major

difficulty: driving consistent acetone adsorption to platinum. Although acetone adsorbs to platinum, the adsorption kinetics from solution are slow and the initial adsorption is physisorption. To increase adsorption efficiency and rate, and to promote chemisorption, a polarizing potential is applied to the electrode when acetone is adsorbed from bulk solution [29]. During this process, acetone is chemisorbed onto the electrode surface from the physisorbed state. Chemisorbed species strongly adhere to the platinum surface and are not displaced from the surface by washing. Physisorbed species are weakly adsorbed and can be easily removed by washing. Wieckowski and coworkers demonstrated a voltage dependence on the rate of adsorption [29]. A potential of $+0.6\ V$ (vs NHE) was found to be a useable potential to increase the rate of adsorption and fractional surface coverage. The use of $0.0\ V$ vs Ag/Ag_2SO_4 is $\sim 100\ mV$ slightly positive of the value reported by Wieckowski and lies outside the butterfly region. It was also demonstrated that acetone is not consumed during the polarization step as evidenced by a lack of current flow. This voltage dependence is corraborated by de Hemptinne and Schunck based on their observation that the rate of acetone electroreduction to propane is governed by the adsorption of the molecule to the electrode. The overall process was also found to be governed by a Langmuirian type relationship and the current was found to be dependant on the adsorption rate coefficient, which is not only voltage dependent but also dependent on the electrode surface electroactivity [31]. Wieckowski and coworkers also demonstrated that water adsorbs to platinum, but does not have a potential dependence like acetone [88]. It is known that water can be displaced by organic solvents at a platinum electrode. In a study of water adsorption

from a dimethylsulfoxide (DMSO) solution, it was reported that adsorbed water is readily displaced by the stronger, voltage dependent chemisorption of DMSO [88].

This complex, voltage dependant adorption of acetone is problematic when sampling acetone from gas or liquid phases. For a solid electrode, the work presented here for headspace analysis involves disconnection of the electrode from the potentiostat, exposing the electrode surface to a gas sample, returning the electrode to solution, and then reconnecting the electrode to the potentiostat. In that time and in a bulk solution, acetone has time to desorb from a physisorbed state and diffuse away from the electrode. Work reported by Wieckowski demonstrated that surface coverage of acetone on platinum after 10 minutes of applied potential at +0.15 V (within the butterfly region) and +0.60 V (no reaction and is outside of the butterly region) differs by a factor of two [29]. The factor of two may represent different adsorbates or an electroclysis product, but acetone capture on the electrode was enhanced by polarization in the butterfly region. The sample method here did not involve polarization in the butterfly region and acetone is likely lost from the surface during gas phase sampling. Gas phase acetone samples involved acetone blown over a dry electrode surface for $\sim$ 10 seconds, which also greatly influence surface coverage of acetone. For the same electrode in solution, adsorption becomes easier because the electrode is not removed from the sample. It is possible that prepolarization within the butterly region may be useful but it would require different measurement protocols than thus far investigated.

6.3.2 Electrode Behavior

The physical differences in the screen printed and solid electrode surfaces contributed to slightly different behavior. These difference are summarized.

6.3.2.1 Screen Printed Platinum

The screen printed electrodes provided peaks in the butterfly region with greater resolution than solid electrodes. However, porosity of the working electrode made voltammetric cleaning difficult. Although easily identifiable, the peak currents never reached a consistent value. This made assessment difficult in that no constant or nearly constant peak values were sufficiently consistent to determine if an electrode was comparably clean between scans. The screen printed Ag/AgCl reference electrode behaved more like a Ag/Ag_2SO_4 reference electrode in the sulfuric acid media. This also played havoc with the system such that peak positions were not always stable from one SPE to the next. The screen printed Ag/AgCl electrode was discovered to behave more like a silver sulfate reference, when tested against a true Ag/Ag_2SO_4 reference electrode. The requirement for reference electrode stability negated use of the screen printed array in a thin layer configuration.

6.3.2.2 Solid Platinum

The solid platinum electrode offered different advantages over the SPEs but came with its own complexities. Because the solid working electrode was used with a true reference electrode, peak positions were stable. However, peak resolution was

not as good for the solid electrodes and was attributed to lesser electrode surface area, Figure 50. The solid electrode suffered from its scanning history far quicker than the screen printed electrodes. Cleaning the electrode was required after each measurement to regenerate a clean surface.

6.3.3 Alternative Gas Sampling

The nature of the gas sample itself was considered as a possible source of systematic error, specifically the presence of water vapor. Acetone samples were created by sealing appropriate aliquots of liquid acetone into an empty 1 L glass bottle with a Teflon/silicone septa and allowed to evaporate into the gas phase. Samples were collected with a valved syringe and injected into a custom built gas chamber with a screen printed electrode array. Acetone then diffused throughout the chamber and partitioned into a thin layer (150 μL) of 0.5 M H_2SO_4 distributed across the electrode array. Changes in the cyclic voltammetric signal correlated to expected changes related to acetone adsorption. However, the measured currents were again not well correlated to acetone concentration and highlight the challenge of good acetone sampling. These measurements were undertaken by Ian Blanch at Stratos Product Development (Seattle, WA) under a collaboration research agreement to develop a portable voltammetric breath sensor.

6.4 Conclusions

Several conclusions are drawn from this preliminary study. First, phenomenologically derived calibration curves of acetone concentration adsorbed onto platinum

from the vapor phase can be derived in acidic solution based cyclic voltammetric analysis. Measurements are performed based on observed changes in the voltammetric butterfly region when acetone is adsorbed to the platinum surface. Second, breath acetone sampled on human breath yields a value in the physiological range and is roughly consistent with a urine test strip. Third, square wave voltammetry allows for correlation of peak potential shifting based on acetone concentration. Peak potentials allow at least an order of magnitude estimate in acetone concentration. Finally, the protocols described here require further validation and refinement. Thus, components of a successful voltammetric and potentiometric analyses for breath acetone are apparent, but not yet refined. There are challenges of sampling, timing, electrode polarization to drive chemisorption, electrolyte volume, and electrode surfaces to be overcome.

CHAPTER 7

FUTURE WORK

This thesis has presented data and results for two unrelated projects, batteries and acetone breath analysis. Each in itself would be a full dissertation and keep a student well occupied. Consequently, this dissertation has provided a first step for what should be many more to come.

7.1 Alkaline Batteries

Incorporation of magnetic microparticles into the MnO_2 cathode has shown improved power output. However, several factors still need to be addressed. Mixing of cathode materials needs to be improved. The make shift tumbler used for these experiments does not do an adequate job to ensure homogeneity of reagents involved. The glass beads eventually served to pack the cathode powder into the crevasses of the vial or cap and eventually smooth over the surface of the loosely packed pellet. A mixer or rotating blade of some kind needs to be used to smash the clumps formed when adding KOH. This would improve homogeneity of the cathode reagents involved and ensure electrolyte is as uniformly distributed as possible.

Self discharge of the battery was a consistent problem for all batteries tested and resulted in a common shelf life of 12-24 hours. Attempts to prolong the shelf life concluded self discharge occurred across the membrane. Consequently, production and storage of numerous batteries was generally avoided. In addition, all impedance and discharge tests were performed with this fundamental flaw. This may have

been a problem during testing but attempts to minimize it were made by applying an equal and opposite open circuit potential during each impedance test and the intentional discharge rates of C/2, C/3, and C/5 are faster drains than what is oberserved for self discharge. However, the fact that self discharge prevented storage and delayed use of a battery cannot be avoided.

Issues to consider lie exclusively in the assembly of the whole cell. Open circuit voltage measurements often indicated a decrease in voltage over time and was most likely from inadequacies in assembly and electrical insulation. Disassembly of commerical cylinder batteries sometimes showed a piece of cellophane was used on the cathode side of the paper separator, depending on manufacturer, but was not present in all commercial batteries. Development of a better sealed clamshell or possible use of commercially available button cell cannisters could help minimize self discharge.Higher surface area zinc could improve discharge behavior. Formation of zincate and zinc oxide passivate the anode over time. It is possible the large zinc alloy particle size contributed to the discharge behavior by coating zinc, while a substantial amount of active material remains unused.

Further exploration of the system with electrochemical impedance spectroscopy could provide insight as well. Use of a two electrode configuration does not allow the instrument to distinguish between effects observed at the anode and cathode. The instrument can only report on the behavior of the battery as a whole cell. A three electrode impedance measurement with a reference electrode included in the clamshell would allow the instrument to distinguish effects at the anode from those at the cathode. However, the reference electrode would need to be a custom Hg/HgO

electrode because the commercially available clamshells are not suited for use with the conventional design of a commercially available Hg/HgO reference electrode. Another option would be to design a different clamshell to accommodate the use of a commercially available reference electrode. Because of these complexities, separation of the half cell components would be easier and be more useful than redesigning the clamshell and/or reference electrode for impedance measurements in the high alkaline environment.

7.2 Acetone Detection

Voltammetric and potentiometric detection of breath acetone at platinum electrodes is possible over physiologically relevant concentrations. However, much needs to be optimized. Voltammetric parameters that require attention include scan rate, surface cleaning, and characterization. Comparable parameters apply to potentiometric measurements as well. Differences in deactivated adsorption sites versus reactivated adsorption sites are easily addressed by refreshment of the electrode surface with mechanical and electrochemical cleaning, such as voltammetric cycling in H_2SO_4.

The strong correlation of applied potential toward adsorption efficiency can be exploited when sampling from the gas phase. To maximize adsorption, a potential needs to be applied to the electrode. This will require a gas sampling chamber with a complete electrochemical cell perhaps thin layer of electrolyte. Timing for these multiple steps will need to be optimized.

Sample generation should be reconsidered. The current method provides an

acetone sample in the saturated relative humidity of breath, a matrix comparable to that in the lungs. Purity of the gas sample may need to be considered. One method could be to place an aliquot of acetone within an empty jar and allow vaporization to occur within the sealed system. A second method would be to sparge acetone from a water solution and sample as required. Both methods would generate an acetone vapor sample and still contain moisture and atmospheric gases. Heating the latter mixture to body temperature would then mimic a breath sample more accurately. Samples generated by pressurizing a vacuum emptied chamber would provide the purist acetone vapor.

APPENDIX A

DATA PROCESSING MACRO FOR USE WITH MTI's BST5.0

The following computer code was written in Visual Basic within Microsoft Excel 2003. At the time of this dissertation, the code also worked with Excel 2010. The goal of this program was to process data output from MTI Corporation's battery analyzer. Although the company does provide an analytical software package, it is generally inadequate for the specific needs of this work. This code was written for version 5.0 of the software.

```
Public i, j, m, n As Integer
Public section1, section2, section3 As Integer

Sub Whole_Cell_Battery_Analyzer()
'Last modified: 3 Sept 2010 by Perry Motsegood
'Changes include:
'Addition of the column header for Capacity (mAh)

'Open data file(s).
Call OpenFileMacro

Application.ScreenUpdating = False
Call Integration
Call Performance_Table
Call Battery_Performance
Call PlotData(ActiveSheet)

'Input file save name.
FileSaveName = Application.GetSaveAsFilename(Left(Worksheets(2).Name, 9) & "Data", _
    fileFilter:="Excel Files (*.xls), *.xls", _
    Title:="Save As")

'Save file if the Cancel button is not pressed.
If FileSaveName <> False Then ActiveWorkbook.SaveAs FileSaveName

'Moved prior to saving because the last sheet was being renamed unintentionally.
Sheets("Performance").Activate

'Uncomment if you want to view a different starting sheet.
'Charts("Voltage Overlay").Activate
End Sub
```

```
Private Sub OpenFileMacro()


'This subroutine is capable of opening multiple tab delimited text files and
'condensing them into one workbook.

Dim Filter, Title, strFind, FileName As String
Dim SheetName, HomeFile As String
Dim FilterIndex As Integer
Dim FileOpenName As Variant

' Initialize counters.
m = 1

' Declare file filters
Filter = "Excel Files (*.xls),*.xls," & _
        "Text Files (*.txt),*.txt," & _
        "All Files (*.*),*.*"

    FilterIndex = 1 ' Set default filter to *.xls
    Title = "Select File(s) to Open" ' Set Dialog Caption


'Open text file(s).
    FileOpenName = Application.GetOpenFilename(Filter, FilterIndex, Title, , True)

'Exit on Cancel
If Not IsArray(FileOpenName) Then Exit Sub

'Core logic for subroutine - open files and condense to one workbook.
For i = LBound(FileOpenName) To UBound(FileOpenName)
    Workbooks.Open FileOpenName(i)

    FileName = Right(FileOpenName(i), 23)
    SheetName = Left(FileName, 19)

    If m = 1 Then HomeFile = FileName

    If m > 1 Then
        n = m - 1
        Workbooks(FileName).Worksheets(SheetName).Move _
         after:=Workbooks(HomeFile).Sheets(n)
    End If
    m = m + 1
Next i

Workbooks(HomeFile).Worksheets(1).Activate
End Sub


Private Sub Integration()

'This subroutine integrates the area under the curve and sums the data to provide
'step wise energy values and energy to a given voltage.
```

```
'Integration is performed using the trapezoid rule to numerically represent
'Energy = Current*<integral from t=0 to t=final>Voltage*dt.
'Energy is in joules. Current is changed to amps. Time is in seconds.

'Adjust idle time values to negative time. Written Feb 5

For i = 1 To Application.Sheets.Count

Sheets(i).Activate
    'Find idle time marker and data range.
    Cells.Find(what:="001[", after:=[A1], SearchDirection:=xlPrevious).EntireRow. _
        Insert shift:=xlDown
    Cells.Find(what:="001[", after:=[A1], SearchDirection:=xlPrevious).Select

    IdleRunTime = ActiveCell.Offset(0, 1)
    IdleRangeBegin = ActiveCell.Offset(2, 3).Address

    With ActiveCell 'Insert headers.
        .Offset(1, 0).EntireRow.Insert shift:=xlDown
        .Offset(1, 2).Value = "Time (min)"
        .Offset(1, 3).Value = "Adjusted Time (min)"
        .Offset(1, 4).Value = "Potential (V)"
    End With

    IdleRangeEnd = ActiveCell.Offset(2, 3).End(xlDown).Address

    'Insert column for adjusted time data.
    Range(IdleRangeBegin, IdleRangeEnd).Insert shift:=xlToRight

    'Insert formula and autofill.
    ActiveCell.Offset(2, 3).Formula = "=RC[-1]-" & IdleRunTime
    Range(IdleRangeBegin).AutoFill Destination:=Range(IdleRangeBegin, IdleRangeEnd)

    'Find discharge data beginning.
    Cells.Find(what:="002[", after:=[A1], SearchDirection:=xlPrevious).EntireRow. _
        Insert shift:=xlDown
    Cells.Find(what:="002[", after:=[A1], SearchDirection:=xlPrevious).Select

    InsertRangeBegin = ActiveCell.Offset(1, 3).Address
    InsertRangeEnd = ActiveCell.Offset(1, 3).End(xlDown).Address
    Range(InsertRangeBegin, InsertRangeEnd).Insert shift:=xlToRight

    With ActiveCell
        .Offset(1, 0).EntireRow.Insert shift:=xlDown
        .Offset(1, 2).Value = "Time (min)"
        .Offset(1, 3).Value = "C/g "
        .Offset(1, 4).Value = "Potential (V)"
        .Offset(1, 5).Value = "Current (mA)"
        .Offset(1, 6).Value = "Capacity (mAh)"

        '.Offset(1, 6).Value = "Energy (J)"
    End With

    'Determine data range.
    CoulombRangeStart = ActiveCell.Offset(2, 3).Address
    ActiveCell.Offset(2, 2).End(xlDown).Select
    CoulombRangeEnd = ActiveCell.Offset(0, 1).Address
```

```
    'Insert equations for C/g calculation.
    Range(CoulombRangeStart).Formula = "=(ABS(RC[+2])/1e3)*(RC[-1]*60)"
    Range(CoulombRangeStart).Offset(1, 0).Select
    With ActiveCell
        'Convert mA to Amps ('0.001' term) and convert minuets to seconds.
        .Formula = "=(ABS(RC[+2])/1E3*((RC[-1]-R[-1]C[-1])*60))+R[-1]C"
        If CoulombRangeStart <> CoulombRangeEnd Then _
        .AutoFill Destination:=Range(ActiveCell, CoulombRangeEnd)
    End With

    'Total area under curve provided via summation of integral data.
    Range("K8") = "=" & CoulombRangeEnd
Next i
End Sub


Private Sub Performance_Table()
'This subroutine creates the skeleton for the performance table.
'Data gets incorporated in the Battery_Performance subroutine.

Sheets.Add before:=Sheets(1), Type:=xlWorksheet
ActiveSheet.Name = "Performance"
With ActiveWindow
    .SplitRow = 1
    .SplitColumn = 3
    .FreezePanes = True
    .Zoom = 85
End With

section = 1  'variable used to separate time, capacity, and energy sections
vval = 0.8

For j = 1 To 3          'repeat for the number of sections in tables
    For k = 2 To 6      'establish column headers
        vval = 0.8 - (0.1 * (k - 6))
        If j = 1 Then
            Cells(1, 1) = "#"
            Cells(1, 2) = "Battery"
            Cells(1, 3) = "Discharge Rate"
            Cells(1, k + 2).Value = "Time (min) to " & vval & " V"
        ElseIf j = 2 Then
            If j = 2 And k = 2 Then _
            Cells(1, 8 + k).Value = "Theoretical Capacity (mAh)"
            Cells(1, 9 + k).Value = "% Capacity at " & vval & " V"
        Else
            Cells(1, 15 + k).Value = "Coulombs (C/g) at " & vval & " V"
        End If
    Next k

    With Rows("1:1")
        .WrapText = True
        .ColumnWidth = 10.5
    End With
Next j
section1 = 0 'declares marker for section1 for use later.
End Sub
```

```
Private Sub Battery_Performance()

'This subroutine will calculate consumed capacity of a battery and output
'percent efficiency.

Dim Voltage(5)

Voltage(1) = 1.2
Voltage(2) = 1.1
Voltage(3) = 1#
Voltage(4) = 0.9
Voltage(5) = 0.8

Set PERF = Sheets("Performance")

Header1 = "Time to reach " & Voltage(5) & " Volts"

'Start on Sheet5 because of overlay plots and tables.
For i = 2 To Application.Sheets.Count

    'Text to columns for experimental parameters.
    Sheets(i).Activate
    ActiveWindow.Zoom = 75

    Cells.Find(what:="002[", after:=[A1], SearchDirection:=xlPrevious).Select
    current = Abs(ActiveCell.Offset(2, 5).Value)
    battcap = Left(ActiveCell.Offset(-16, 1).Value, 5) '
    ActiveCell.Offset(2, 4).Select
    'InitialDataRow = ActiveCell.Offset(2, 3).Rows.Count
    'InitialDataColumn = ActiveCell.Offset(2, 3).Address

    With Sheets(i)
    'Create experiment run number and place for future reference
        .Cells(1, 8).Value = "Battery " & i - 1

        .Range("A9").TextToColumns DataType:=xlDelimited, _
        ConsecutiveDelimiter:=False, Space:=False, Other:=True, OtherChar:="]"

        .Range("C9").TextToColumns DataType:=xlDelimited, _
        ConsecutiveDelimiter:=True, Space:=True

        .Range("H3") = Header1
        .Range("k3") = "Discharge Rate"
        .Range("I4") = "min"
        .Range("I5") = "hrs"
        .Range("H7") = "% Capacity Used"
        .Range("K7") = "Area Under Curve"

        'Output is a %.
        .Range("H8").Formula = "=((Left($B$9, 4) * $h$5)/(Left($E$9, 5)/2))*100"

        'Shorten decimal format to two places.
        .Range("H8").NumberFormat = "0.00"
        .Range("K4").Formula = _
        "=""C/""&ROUND(IF(LEN(E$9)=5,LEFT(E$9,2),LEFT(E$9,3))/ABS(" & _
```

```
        current & ")/2,0)"

    End With

    section = 0 'reset the counter for every sheet.
    m = 1
    Do
        'Find value for the performance table.
        If ActiveCell.Value < Voltage(m) Then
            'Insert battery number within spreadsheet.
            PERF.Cells(i, 1) = i - 1
            PERF.Cells(i, 2).Value = Left(Sheets(i).Name, 13) & _
                Right(Sheets(i).Name, 2)

            'Discharge Rate
            PERF.Cells(i, 3) = Sheets(i).Range("K4")

            'Time value
            PERF.Cells(i, m + 3).Formula = "='" & Sheets(i).Name & "'!" & _
                ActiveCell.Offset(0, -2).Address
            If m = 1 Then _
            PERF.Cells(i, m + 9).Formula = "=If(LEN('" & Sheets(i).Name & _
                "'!E9)=5, Left('" & Sheets(i).Name & "'!E9,2), Left('" & _
                Sheets(i).Name & "'!E9,3))"

            'Coulomb value
            PERF.Cells(i, m + 16).Formula = "='" & Sheets(i).Name & "'!" & _
                ActiveCell.Offset(0, -1).Address

            'Capacity value
            If m = 1 Then capacity = PERF.Cells(i, m + 9).Address
            PERF.Cells(i, m + 10).Formula = _
                "=100*'" & Sheets(i).Name & "'!" & _
                ActiveCell.Offset(0, 2).Address & "/" & capacity

            m = m + 1
        Else
            ActiveCell.Offset(1, 0).Select
        End If

    Loop Until ActiveCell.Value < Voltage(5) And m = 6
Next i
    'Adjust table section formats
    With PERF
        .Range("I:I,P:P").ColumnWidth = 2
        .Range("A:Z").HorizontalAlignment = xlCenter
        .Range("K:O").NumberFormat = "0.00"
        .Range("Q:V").NumberFormat = "0.000"
        .Columns("c:e").Insert
        .Cells(1, 3) = "Type"
        .Cells(1, 4) = "Magnetic Material"
        .Cells(1, 5) = "Soak Time"
        .Range("A:E").Columns.AutoFit
    End With

End Sub
```

```
Private Sub PlotData(ActiveSheet)
'This subroutine will plot the data in the workbook generating individual
'and overlay plots.

Dim EnergyPlot, VoltagePlot As Range

Set WS = Worksheets

For i = 2 To Application.Sheets.Count
    WS(i).Activate

'Determine data range for plot.
    With WS(i)
        'Determine the data ranges automatically.
        Cells.Find(what:="002[", after:=[A1], SearchDirection:=xlPrevious).Select
        TimeRange = Range(ActiveCell.Offset(2, 2), ActiveCell.Offset(2, 2). _
            End(xlDown)).Address
        CoulombRange = Range(ActiveCell.Offset(2, 3), ActiveCell.Offset(2, 3). _
            End(xlDown)).Address
        VoltageRange = Range(ActiveCell.Offset(2, 4), ActiveCell.Offset(2, 4). _
            End(xlDown)).Address
        EnergyRange = Range(ActiveCell.Offset(2, 6), ActiveCell.Offset(3, 6). _
            End(xlDown)).Address

        'Quirckiness with the Union command requires a pre-initialization of variables
        'hence the next lines.
        Set VoltagePlot = Range(TimeRange)
        Set CoulombPlot = Range(CoulombRange)
        'Set EnergyPlot = Range(VoltageRange)

        'Merge data ranges for plotting.
        Set VoltagePlot = Application.Union(Range(TimeRange), Range(VoltageRange))
        Set CoulombPlot = Application.Union(Range(CoulombRange), Range(VoltageRange))
        'Set EnergyPlot = Application.Union(Range(VoltageRange), Range(EnergyRange))

    End With

    For j = 1 To 2
    'Add embedded V vs T chart.
    If j = 1 Then
        With WS(i).ChartObjects.Add _
            (Left:=550, Top:=150, Width:=500, Height:=350)
            .Chart.ChartType = xlXYScatterLinesNoMarkers
            .Chart.SetSourceData Source:=VoltagePlot, PlotBy:=xlColumns
            .Chart.HasTitle = True
            .Chart.ChartTitle.Text = "Voltage for " & WS(i).Name
            .Chart.HasLegend = False
        End With
    Else
        With WS(i).ChartObjects.Add _
            (Left:=550, Top:=550, Width:=500, Height:=350)
            .Chart.ChartType = xlXYScatterLinesNoMarkers
            .Chart.SetSourceData Source:=CoulombPlot, PlotBy:=xlColumns
            .Chart.HasTitle = True
            .Chart.ChartTitle.Text = "Voltage for " & WS(i).Name
            .Chart.HasLegend = False
```

```
        '.Chart.Axes(xlCategory).ReversePlotOrder = True
        '.Chart.Axes(xlCategory).MinimumScale = 0.2
    End With
End If

'Format embedded ChartObject
    WS(i).ChartObjects(j).Activate
    Call ChartParameters(ActiveChart, j)
Next j

'Create overlay plots.
If i = 2 Then
    Charts.Add.Location xlLocationAsNewSheet, "Voltage Overlay"
    Charts.Add.Location xlLocationAsNewSheet, "Coulomb Overlay"

'Incorporate data for Voltage vs Time plot.
    With Charts("Voltage Overlay")
        .ChartType = xlXYScatterLinesNoMarkers
        .SetSourceData Source:=VoltagePlot, PlotBy:=xlColumns
        .SeriesCollection(i - 1).Name = WS(i).Range("H1")
        .HasTitle = True
        .ChartTitle.Text = "Voltage overlay of battery experiments from " + _
            Left(WS(i).Name, 8)
        .Axes(xlCategory).MajorUnit = 30
        With .Axes(xlValue)
            .MaximumScale = 1.6
            .MinimumScale = 0.2
            .MajorUnit = 0.1
        End With '.Axes(xlValue)
        .Move before:=Sheets("Performance")
    End With 'Charts("Voltage Overlay")

'Incorporate data for Energy vs Time plot.
    With Charts("Coulomb Overlay")
        .ChartType = xlXYScatterLinesNoMarkers
        .SetSourceData Source:=CoulombPlot, PlotBy:=xlColumns
        .SeriesCollection(i - 1).Name = WS(i).Range("H1")
        .HasTitle = True
        .ChartTitle.Text = "Voltage overlay of battery experiments from " + _
            Left(WS(i).Name, 8)
        With .Axes(xlValue)
            .MaximumScale = 1.6
            .MinimumScale = 0.2
            .MajorUnit = 0.1
            '.ReversePlotOrder = True
        End With '.Axes(xlValue)
        .Move after:=Charts("Voltage Overlay")
    End With 'Charts("Coulomb Overlay")

    'Format axes.
    j = 1 'Adjust the passed parameter to flag for proper formatting.
    Charts("Voltage Overlay").Activate
    Call ChartParameters(ActiveChart, j)

    j = 2
    Charts("Coulomb Overlay").Activate
    Call ChartParameters(ActiveChart, j)
```

```
    Else
        With Charts("Voltage Overlay")
            .SeriesCollection.NewSeries
            .SeriesCollection(i - 1).XValues = WS(i).Range(TimeRange)
            .SeriesCollection(i - 1).Values = WS(i).Range(VoltageRange)
            .SeriesCollection(i - 1).Name = WS(i).Range("H1")
       End With 'Charts("Voltage Overlay")

       With Charts("Coulomb Overlay")
            .SeriesCollection.NewSeries
            .SeriesCollection(i - 1).XValues = WS(i).Range(CoulombRange)
            .SeriesCollection(i - 1).Values = WS(i).Range(VoltageRange)
            .SeriesCollection(i - 1).Name = WS(i).Range("H1")
        End With 'Charts("Coulomb Overlay")
    End If
Next i

'Format line styles.
Charts("Coulomb Overlay").Activate
Call OverlayFormatting(ActiveChart)

Charts("Voltage Overlay").Activate
Call OverlayFormatting(ActiveChart)
End Sub


Private Sub ChartParameters(ActiveChart, j)
'This subroutine formats axes and plot area.

With ActiveChart
    'Set titles.
    .Axes(xlValue, xlPrimary).HasTitle = True
    .Axes(xlCategory, xlPrimary).HasTitle = True

    If j = 2 Then
        '.Axes(xlValue, xlPrimary).AxisTitle.Characters.Text = "Energy (J)"
        .Axes(xlValue, xlPrimary).AxisTitle.Characters.Text = "Potential (V)"
        .Axes(xlCategory, xlPrimary).AxisTitle.Characters.Text = "C/g"
    Else
        .Axes(xlValue, xlPrimary).AxisTitle.Characters.Text = "Potential (V)"
        .Axes(xlCategory, xlPrimary).AxisTitle.Characters.Text = "Time (min)"
    End If

    'X-Axis parameters
    .Axes(xlCategory).MajorTickMark = xlTickMarkCross
    .Axes(xlCategory).MinorTickMark = xlTickMarkInside

    'Y-Axis parameters
    .Axes(xlValue).MajorTickMark = xlTickMarkCross
    .Axes(xlValue).MinorTickMark = xlTickMarkInside

    'Plot area parameters
    .PlotArea.Interior.ColorIndex = 0   'Color code for black = 0
    .Axes(xlValue).HasMajorGridlines = False
End With
End Sub
```

```
Private Sub OverlayFormatting(ActiveChart)
'This subroutine formats the line styles on the plot.

Dim Style(6), Marker(9) As Variant

'Establish LineStyle Array
Style(0) = xlNone
Style(1) = xlContinuous
Style(2) = xlDash
Style(3) = xlDot
'Style(4) = xlDashDot
'Style(5) = xlDashDotDot
'Style(6) = xlSlantDashDot

'Establish MarkerStyle Array
Marker(0) = xlNone
Marker(1) = xlMarkerStyleX
Marker(2) = xlMarkerStyleDot
Marker(3) = xlMarkerStyleDash
Marker(4) = xlMarkerStyleCircle
Marker(5) = xlMarkerStyleTriangle
Marker(6) = xlMarkerStyleSquare
Marker(7) = xlMarkerStylePlus
Marker(8) = xlMarkerStyleStar
Marker(9) = xlMarkerStyleDiamond

    With ActiveChart
        .HasLegend = True
        .Legend.Position = xlLegendPositionBottom

    If ActiveChart.Name = "Energy Overlay" Then
        With .Axes(xlCategory)
            .HasMajorGridlines = True
            .MajorGridlines.Border.ColorIndex = 15
            .MajorGridlines.Border.Weight = xlHairline
            .MajorGridlines.Border.LineStyle = xlContinuous
        End With

        With .Axes(xlValue)
            .HasMajorGridlines = True
            .MajorGridlines.Border.ColorIndex = 15
            .MajorGridlines.Border.Weight = xlHairline
            .MajorGridlines.Border.LineStyle = xlContinuous
        End With
    End If
    End With

'Setup loop for n-1 sheets. The overlay chart counts as a sheet.
limit = Application.Sheets.Count - 3

For i = 1 To limit
    ActiveChart.SeriesCollection(i).Select

    With Selection
        If i <= 3 Then
            .Border.ColorIndex = 1
```

```
            'Choices for line thickness are xlThin, xlMedium, and xlThick.
            .Border.Weight = xlMedium

            'This value is adjustable if more lines are needed.
            .Border.LineStyle = Style(i)
            .MarkerStyle = Marker(0)

        ElseIf i > 3 And i <= 9 Then
            .Border.ColorIndex = 1

            'Choices for line thickness are xlThin, xlMedium, and xlThick.
            .Border.Weight = xlMedium

            'This value is adjustable if more lines are needed.
            .Border.LineStyle = Style(0)

            'These MarkerStyles will appear as hollow objects.
            .MarkerBackgroundColorIndex = xlNone
            .MarkerForegroundColorIndex = 1
            .MarkerStyle = Marker(i)

        ElseIf i > 9 And i <= 12 Then
            'These MarkerStyles will appear as solid objects.
            .MarkerBackgroundColorIndex = 1
            .MarkerForegroundColorIndex = xlNone
            .MarkerStyle = Marker(i - 6)
        End If

        .MarkerSize = 4
        .Smooth = False
        .Shadow = False
    End With
Next i

'Copy the overlay chart and adjust the y-axis to highlight the first
'electron discharge.
If ActiveChart.Name = "Voltage Overlay" Then
    Charts("Voltage Overlay").Copy after:=Charts("Voltage Overlay")

    With Charts("Voltage Overlay (2)")
        .Axes(xlValue).MaximumScale = 1.6
        .Axes(xlValue).MinimumScale = 0.8
        .Axes(xlValue).MajorUnit = 0.1
    End With
End If

End Sub
```

APPENDIX B

DATA PROCESSING MACRO FOR USE WITH MTI's BST5.3

The following computer code was written in Visual Basic within Microsoft Excel 2003. At the time of this dissertation, the code also worked with Excel 2010. The goal of this program was to process data output from MTI Corporation's battery analyzer. Although the company does provide an analytical software package, it is generally inadequate for the specific needs of this work. Changes in the data output format were made when changing from version 5.0 to version 5.3 of the control software. This code was written to account for the new format.

```
Public HomeCell, TimeStart, TimeEnd As Variant
Public PotentialStart, PotentialEnd As Variant
Public CoulombStart, CoulombEnd As Variant
Public EnergyStart, EnergyEnd As Variant
Public i, j, m, n As Integer

Sub BatteryAnalyzer()
'This macro processes Excel files generated by the MTI Battery Analyzer v5.3 control
'software.
'Export data using the General Report option of the MTI data analyzer. The raw data
'files are in *.nda format.
'THIS PROGRAM WAS WRITTEN FOR EXCEL 2003.

Call OpenFileMacro

Application.ScreenUpdating = False

Call Integration
Call PerformanceTable
Call BatteryPerformance
Call PlotData(ActiveSheet)
Call SaveFileMacro
End Sub


Private Sub OpenFileMacro()

'This subroutine is capable of opening multiple tab delimited text files and condensing
'them into one workbook.
```

```
Dim SheetName, HomeFile, FileName As String

Dim FileOpenName As Variant

'Open text file(s)
    FileOpenName = Application.GetOpenFilename _
        ("Excel Files (*.xls), *.xls), Text Files (*.txt), *.txt, All Files (*.*), *.*", _
        1, "Select File(s) to Open", , True)

If Not IsArray(FileOpenName) Then Exit Sub 'Exit on Cancel

'Core logic for subroutine - open files and condense to one workbook
For i = LBound(FileOpenName) To UBound(FileOpenName)
    Workbooks.Open FileOpenName(i)
    Filelength = Len(FileOpenName(i))

        'Search from right to left to extract the filename from the full file path
        For j = Filelength To 1 Step -1
            If Mid(FileOpenName(i), j, 1) = "\" Then
                FileName = Right(FileOpenName(i), (Filelength - j))
                Exit For
            End If
        Next j

    SheetName = Left(FileName, (Len(FileName) - 4)) 'Remove the last characters (.txt)

    If i = 1 Then
        HomeFile = FileName
    Else
        n = i - 1
        Workbooks(FileName).Worksheets(1).Move _
         after:=Workbooks(HomeFile).Sheets(n)
    End If

    'Rename the sheet name if too long and insert a counter into the name so similar
    'files can be combined.
    If Len(SheetName) >= 31 Then
        SheetName = Left(SheetName, 29)
    End If
    'Add count to sheet name if neeeded. Remove marker before & to activate.
    Sheets(i).Name = Replace(SheetName, " ", "") '& i
Next i

Workbooks(HomeFile).Worksheets(1).Activate 'Activate the first sheet
End Sub


Private Sub SaveFileMacro()

'Input file save name.
FileSaveName = Application.GetSaveAsFilename(Left(Worksheets(2).Name, 9) & "Data", _
    fileFilter:="Excel Files (*.xls), *.xls", _
    Title:="Save As")
```

```
If FileSaveName <> False Then ActiveWorkbook.SaveAs FileSaveName

'Moved prior to saving because the last sheet was being renamed unintentionally.
Sheets("Performance").Activate

'The following can be uncommented if a different initial sheet is desired.
'Sheets(1).Activate
'Charts("Voltage Overlay").Activate
End Sub


Private Sub Integration()
'This subroutine modifies the data layout and inserts headers and formulas for adjusted
'time and voltage

For i = 1 To Application.Sheets.Count

Sheets(i).Activate
Range("A3").Value = "Battery " & i

    Rows("2:2").Copy
    'Find discharge time marker and data range.
    Cells.Find(what:="CC_DChg", after:=[A1], SearchDirection:=xlPrevious).EntireRow.Insert _
        shift:=xlDown
    Cells.Find(what:="CC_DChg", after:=[A1], SearchDirection:=xlPrevious).Select

    HomeCell = Selection.Address 'Set a home position.

    'Copy original data headers and insert at end of first section.
    Rows("3:3").Copy
    ActiveCell.Offset(1, 0).EntireRow.Insert shift:=xlDown

    'Insert new colums for unit conversions
    Range("E:E").Insert shift:=xlToRight
    Range("G:G").Insert shift:=xlToRight
    Range("I:I").Insert shift:=xlToRight

    With ActiveCell 'Insert headers.
        .Offset(1, 2).Value = "Time (min)"
        .Offset(2, 2).FormulaR1C1 = "=RC[-1]/60"
        .Offset(1, 4).Value = "Potential (V)"
        .Offset(2, 4).FormulaR1C1 = "=RC[-1]/1000"
        .Offset(1, 6).Value = "C/g"
        .Offset(2, 6).FormulaR1C1 = "=abs(RC[-1]/1e3)*RC[-5]"
        .Offset(3, 6).FormulaR1C1 = "=R[-1]C+abs(RC[-1]/1e3)*(RC[-5]-R[-1]C[-5])"
    End With

    'Determine time data range.
    TimeStart = ActiveCell.Offset(2, 2).Address
    ActiveCell.Offset(2, 1).End(xlDown).Select
    TimeEnd = ActiveCell.Offset(0, 1).Address

    'Format number format. Change if necessary.
    'Range(TimeStart, TimeEnd).NumberFormat = "0.000"

    Range(HomeCell).Select  'Return to home position.
```

```
    'Determine voltage data range.
    PotentialStart = ActiveCell.Offset(2, 4).Address
    ActiveCell.Offset(2, 3).End(xlDown).Select
    PotentialEnd = ActiveCell.Offset(0, 1).Address

    Range(HomeCell).Select

    'Determine voltage data range.
    CoulombStart = ActiveCell.Offset(2, 6).Address
    EnergyStart = ActiveCell.Offset(2, 10).Address
    AdjustedCoulombStart = ActiveCell.Offset(3, 6).Address
    ActiveCell.Offset(2, 5).End(xlDown).Select
    CoulombEnd = ActiveCell.Offset(0, 1).Address
    EnergyEnd = ActiveCell.Offset(0, 5).Address


    'Check to verify the batteries were not duds and Autofill formulas
    If TimeStart <> TimeEnd Then _
        Range(TimeStart).AutoFill Destination:=Range(TimeStart, TimeEnd)

    If PotentialStart <> PotentialEnd Then _
        Range(PotentialStart).AutoFill Destination:=Range(PotentialStart, PotentialEnd)

    If CoulombStart <> CoulombEnd Then _
        Range(AdjustedCoulombStart).AutoFill Destination:=Range(AdjustedCoulombStart, _
        CoulombEnd)

Next i
End Sub


Private Sub PerformanceTable()
'This subroutine creates the skeleton for the performance table.
'Data gets incorporated in the Battery_Performance subroutine.

Sheets.Add before:=Sheets(1), Type:=xlWorksheet
ActiveSheet.Name = "Performance"
With ActiveWindow
    .SplitRow = 1
    .SplitColumn = 3
    .FreezePanes = True
    .Zoom = 85
End With

section = 1  'variable used to separate time, capacity, and energy sections
vval = 0.8

For j = 1 To 3          'repeat for the number of sections in tables
    For k = 2 To 8      'establish column headers
        vval = 0.8 - (0.1 * (k - 8))
        If j = 1 Then
            Cells(1, 1) = "#"
            Cells(1, 2) = "Battery"
            Cells(1, 3) = "Discharge Rate"
            Cells(1, k + 2).Value = "Time (min) to " & vval & " V"
            Cells(1, 10 + k).Value = "Coulombs (C/g) at " & vval & " V"
            Cells(1, 18 + k).Value = "Energy (mWh) at " & vval & " V"
```

```
        End If
    Next k

    With Rows("1:1")
        .WrapText = True
        .ColumnWidth = 10.5
    End With
Next j
section1 = 0 'declares marker for section1 for use later.
End Sub


Private Sub BatteryPerformance()
'This subroutine will calculate consumed capacity of a battery and
'output percent efficiency.

Dim Voltage(7)

Voltage(1) = 1.4
Voltage(2) = 1.3
Voltage(3) = 1.2
Voltage(4) = 1.1
Voltage(5) = 1#
Voltage(6) = 0.9
Voltage(7) = 0.8

Set PERF = Sheets("Performance")

Header1 = "Time to reach " & Voltage(7) & " Volts"

'Start on Sheet5 because of overlay plots and tables.
For i = 2 To Application.Sheets.Count

    'Text to columns for experimental parameters.
    Sheets(i).Activate
    ActiveWindow.Zoom = 75

    Range(HomeCell).Select
    current = Abs(ActiveCell.Offset(2, 5).Value)
    ActiveCell.Offset(2, 4).Select
    section = 0 'reset the counter for every sheet.
    m = 1
    Do
'Find value for the performance table.
        If ActiveCell.Value < Voltage(m) Then
    'Insert battery number within spreadsheet.
            PERF.Cells(i, 1) = i - 1
            PERF.Cells(i, 2).Value = Left(Sheets(i).Name, 13) & Right(Sheets(i).Name, 2)
            'PERF.Cells(i, 3) = Sheets(i).Range("K4") 'Discharge Rate

            'Time value
            PERF.Cells(i, m + 3).Formula = "='" & Sheets(i).Name & "'!" & _
            ActiveCell.Offset(0, -2).Address

            If m = 1 Then _
            PERF.Cells(i, m + 9).Formula = _
            "=If(LEN('" & Sheets(i).Name & "'!E9)=5, Left('" & Sheets(i).Name & _
```

```
            "'!E9,2), Left('" & Sheets(i).Name & "'!E9,3))"

            'Coulomb value
            PERF.Cells(i, m + 11).Formula = "='" & Sheets(i).Name & "'!" & _
            ActiveCell.Offset(0, 2).Address

            'Energy value
            PERF.Cells(i, m + 19).Formula = "='" & Sheets(i).Name & "'!" & _
            ActiveCell.Offset(0, 6).Address

            m = m + 1
        Else
            ActiveCell.Offset(1, 0).Select
        End If

    'Loop Until Sheets(i).Cells(InitialDataRow, InitialDataColumn).Value < Cutoff1
    Loop Until ActiveCell.Value < Voltage(7) And m = 8
Next i
    'Adjust table section formats
    With PERF
        .Range("K:K,S:S").ColumnWidth = 2
        .Range("A:AA").HorizontalAlignment = xlCenter
        .Range("D:J").NumberFormat = "0.00"
        .Range("L:S").NumberFormat = "0.00"
        .Range("U:AA").NumberFormat = "0.000"
        .Columns("C:E").Insert
        .Cells(1, 3) = "Type"
        .Cells(1, 4) = "Magnetic Material"
        .Cells(1, 5) = "Soak Time"
        .Range("A:E").Columns.AutoFit
    End With
End Sub


Private Sub PlotData(ActiveSheet)
'This subroutine will plot the data in the workbook generating individual
'and overlay plots.

Dim EnergyPlot, VoltagePlot As Range

Set WS = Worksheets

For i = 2 To Application.Sheets.Count
    WS(i).Activate

'Determine data range for plot.
    With WS(i)
        TimeRange = Range(TimeStart, TimeEnd).Address
        PotentialRange = Range(PotentialStart, PotentialEnd).Address
        EnergyRange = Range(EnergyStart, EnergyEnd).Address

        'Quirckiness with the Union command requires a pre-initialization of variables
        'hence the next lines.
        Set VoltagePlot = Range(TimeRange)

        'Set CoulombPlot = Range(CoulombRange)
        Set EnergyPlot = Range(PotentialRange)
```

```
    'Merge data ranges for plotting.
    Set VoltagePlot = Application.Union(Range(TimeRange), Range(PotentialRange))

    'Set CoulombPlot = Application.Union(Range(CoulombRange), Range(VoltageRange))
    Set EnergyPlot = Application.Union(Range(PotentialRange), Range(EnergyRange))
End With

For j = 1 To 2
'Add embedded V vs T chart.
If j = 1 Then
    With WS(i).ChartObjects.Add _
        (Left:=550, Top:=150, Width:=500, Height:=350)
        .Chart.ChartType = xlXYScatterLinesNoMarkers
        .Chart.SetSourceData Source:=VoltagePlot, PlotBy:=xlColumns
        .Chart.HasTitle = True
        .Chart.ChartTitle.Text = "Voltage for " & WS(i).Name
        .Chart.HasLegend = False
    End With
Else
    With WS(i).ChartObjects.Add _
        (Left:=550, Top:=550, Width:=500, Height:=350)
        .Chart.ChartType = xlXYScatterLinesNoMarkers
        .Chart.SetSourceData Source:=EnergyPlot, PlotBy:=xlColumns
        .Chart.HasTitle = True
        .Chart.ChartTitle.Text = "Energy for " & WS(i).Name
        .Chart.HasLegend = False
        .Chart.Axes(xlCategory).ReversePlotOrder = True
        .Chart.Axes(xlCategory).MinimumScale = 0.2
    End With
End If

'Format embedded ChartObject
    WS(i).ChartObjects(j).Activate
    Call ChartParameters(ActiveChart, j)
Next j

'Create overlay plots.
If i = 2 Then
    Charts.Add.Location xlLocationAsNewSheet, "Voltage Overlay"
    Charts.Add.Location xlLocationAsNewSheet, "Energy Overlay"

'Incorporate data for Voltage vs Time plot.
    With Charts("Voltage Overlay")
        .ChartType = xlXYScatterLinesNoMarkers
        .SetSourceData Source:=VoltagePlot, PlotBy:=xlColumns
        .SeriesCollection(i - 1).Name = WS(i).Range("A3")
        .HasTitle = True
        .ChartTitle.Text = "Voltage overlay of battery experiments from " + _
            Left(WS(i).Name, 8)
        .Axes(xlCategory).MajorUnit = 30
        With .Axes(xlValue)
            .MaximumScale = 1.6
            .MinimumScale = 0.2
            .MajorUnit = 0.1
        End With '.Axes(xlValue)
        .Move before:=Sheets("Performance")
```

```
        End With 'Charts("Voltage Overlay")

    'Incorporate data for Energy vs Time plot.
        With Charts("Energy Overlay")
            .ChartType = xlXYScatterLinesNoMarkers
            .SetSourceData Source:=EnergyPlot, PlotBy:=xlColumns
            .SeriesCollection(i - 1).Name = WS(i).Range("A3")
            .HasTitle = True
            .ChartTitle.Text = "Energy overlay of battery experiments from " + _
                Left(WS(i).Name, 8)
            .Axes(xlCategory).ReversePlotOrder = True
            'With .Axes(xlValue)
                '.MaximumScale = 1.6
                '.MinimumScale = 0.2
                '.MajorUnit = 0.1
                '.ReversePlotOrder = True
            'End With '.Axes(xlValue)
            .Move after:=Charts("Voltage Overlay")
        End With 'Charts("Energy Overlay")

        'Format axes.
        j = 1 'Adjust the passed parameter to flag for proper formatting.
        Charts("Voltage Overlay").Activate
        Call ChartParameters(ActiveChart, j)

        j = 2
        Charts("Energy Overlay").Activate
        Call ChartParameters(ActiveChart, j)
    Else
        With Charts("Voltage Overlay")
            .SeriesCollection.NewSeries
            .SeriesCollection(i - 1).XValues = WS(i).Range(TimeRange)
            .SeriesCollection(i - 1).Values = WS(i).Range(PotentialRange)
            .SeriesCollection(i - 1).Name = WS(i).Range("A3")
       End With 'Charts("Voltage Overlay")

       With Charts("Energy Overlay")
            .SeriesCollection.NewSeries
            .SeriesCollection(i - 1).XValues = WS(i).Range(PotentialRange)
            .SeriesCollection(i - 1).Values = WS(i).Range(EnergyRange)
            .SeriesCollection(i - 1).Name = WS(i).Range("A3")
        End With 'Charts("Energy Overlay")
    End If
Next i

'Format line styles.
Charts("Energy Overlay").Activate
Call OverlayFormatting(ActiveChart)

Charts("Voltage Overlay").Activate
Call OverlayFormatting(ActiveChart)
End Sub


Private Sub ChartParameters(ActiveChart, j)
'This subroutine formats axes and plot area.
```

```
With ActiveChart
    'Set titles.
    .Axes(xlValue, xlPrimary).HasTitle = True
    .Axes(xlCategory, xlPrimary).HasTitle = True

    If j = 2 Then
        .Axes(xlValue, xlPrimary).AxisTitle.Characters.Text = "Energy (mWh)"
        .Axes(xlCategory, xlPrimary).AxisTitle.Characters.Text = "Potential (V)"
        '.Axes(xlValue, xlPrimary).AxisTitle.Characters.Text = "Potential (V)"
        '.Axes(xlCategory, xlPrimary).AxisTitle.Characters.Text = "C/g"
    Else
        .Axes(xlValue, xlPrimary).AxisTitle.Characters.Text = "Potential (V)"
        .Axes(xlCategory, xlPrimary).AxisTitle.Characters.Text = "Time (min)"
    End If

    'X-Axis parameters
    .Axes(xlCategory).MajorTickMark = xlTickMarkCross
    .Axes(xlCategory).MinorTickMark = xlTickMarkInside

    'Y-Axis parameters
    .Axes(xlValue).MajorTickMark = xlTickMarkCross
    .Axes(xlValue).MinorTickMark = xlTickMarkInside

    'Plot area parameters
    .PlotArea.Interior.ColorIndex = 0   'Color code for black = 0
    .Axes(xlValue).HasMajorGridlines = False
End With
End Sub

Private Sub OverlayFormatting(ActiveChart)
'This subroutine formats the line styles on the plot.

Dim Style(6), Marker(9) As Variant

'Establish LineStyle Array
Style(0) = xlNone
Style(1) = xlContinuous
Style(2) = xlDash
Style(3) = xlDot
'Style(4) = xlDashDot
'Style(5) = xlDashDotDot
'Style(6) = xlSlantDashDot

'Establish MarkerStyle Array
Marker(0) = xlNone
Marker(1) = xlMarkerStyleX
Marker(2) = xlMarkerStyleDot
Marker(3) = xlMarkerStyleDash
Marker(4) = xlMarkerStyleCircle
Marker(5) = xlMarkerStyleTriangle
Marker(6) = xlMarkerStyleSquare
Marker(7) = xlMarkerStylePlus
Marker(8) = xlMarkerStyleStar
Marker(9) = xlMarkerStyleDiamond

    With ActiveChart
        .HasLegend = True
```

```
        .Legend.Position = xlLegendPositionBottom

'Uncomment the following section to incorporate major gridlines
'for the Energy Plot.
'    If ActiveChart.Name = "Energy Overlay" Then
'        With .Axes(xlCategory)
'            .HasMajorGridlines = True
'            .MajorGridlines.Border.ColorIndex = 15
'            .MajorGridlines.Border.Weight = xlHairline
'            .MajorGridlines.Border.LineStyle = xlContinuous
'        End With

'        With .Axes(xlValue)
'            .HasMajorGridlines = False
'            .MajorGridlines.Border.ColorIndex = 15
'            .MajorGridlines.Border.Weight = xlHairline
'            .MajorGridlines.Border.LineStyle = xlContinuous
'        End With
'    End If
    End With

'Setup loop for n-1 sheets. The overlay chart counts as a sheet.
limit = Application.Sheets.Count - 3

For i = 1 To limit
    ActiveChart.SeriesCollection(i).Select

    With Selection
        If i <= 3 Then
            .Border.ColorIndex = 1

            'Choices for line thickness are xlThin, xlMedium, and xlThick.
            .Border.Weight = xlMedium

            'This value is adjustable if more lines are needed.
            .Border.LineStyle = Style(i)
            .MarkerStyle = Marker(0)

        ElseIf i > 3 And i <= 9 Then
            .Border.ColorIndex = 1

            'Choices for line thickness are xlThin, xlMedium, and xlThick.
            .Border.Weight = xlMedium

            'This value is adjustable if more lines are needed.
            .Border.LineStyle = Style(0)

            'These MarkerStyles will appear as hollow objects.
            .MarkerBackgroundColorIndex = xlNone
            .MarkerForegroundColorIndex = 1
            .MarkerStyle = Marker(i)

        ElseIf i > 9 And i <= 12 Then
            'These MarkerStyles will appear as solid objects.
            .MarkerBackgroundColorIndex = 1
            .MarkerForegroundColorIndex = xlNone
            .MarkerStyle = Marker(i - 6)
```

```
        End If

        .MarkerSize = 4
        .Smooth = False
        .Shadow = False
    End With
Next i

'Copy the overlay chart and adjust the y-axis to highlight the first
'electron discharge.
If ActiveChart.Name = "Voltage Overlay" Then
    Charts("Voltage Overlay").Copy after:=Charts("Voltage Overlay")

    With Charts("Voltage Overlay (2)")
        .Axes(xlValue).MaximumScale = 1.6
        .Axes(xlValue).MinimumScale = 0.8
        .Axes(xlValue).MajorUnit = 0.1
    End With
Else
    With Charts("Energy Overlay")
        .Axes(xlCategory).MaximumScale = 1.6
        .Axes(xlCategory).MinimumScale = 0.8
        .Axes(xlCategory).MajorUnit = 0.1
    End With
End If

End Sub
```

APPENDIX C

CONTROL MACROS FOR CH INSTRUMENTS MODEL 760B

The following macro code was written for controlling the CH Instruments Model 760B Potentiostat/Galvanostat to perform impedance spectroscopy with a multiplexer or single channel configuration. The macro code is a variant of BASIC with minimized capabilities. See the CH Instruments Model 760B User Manual for more information.

C.1 Electrochemical Impedance Spectroscopy

multichannel macro

```
tech = imp
for = 8
mchn
eio
fh = 100000
fl = 0.01
amp = 0.01
qt = 1
impautosens
run
folder: c:\Path\to\data\directry\
save = <insert filename>.bin
next
end
```

single channel macro

```
tech = imp
eio
fh = 100000
fl = 0.05
amp = 0.01
qt = 2
impautosens
```

```
run

folder: c:\Path\to\data\directry\
save = <insert filename>.bin
end
```

C.2 Acetone Square Wave Voltammetry

```
tech = swv
for = 3
delay = 10
ei = 0
ef = -0.5
incre = 0.004
amp = 0.025
freq = 15
qt = 2
sens = 1e-5
run
folder: c:\Path\to\data\directry\
save = <insert filename>.bin
tsave = <insert filename>.txt
next
end
```

REFERENCES

[1] Holdings, I. E. "Annual Report", Technical Report, Energizer Holdings, Inc, 2011.

[2] Bailey, M. R.; Denman, J. A.; King, B. V.; Donne, S. W. *Journal of The Electrochemical Society* **2012,** *159,* A158-A165.

[3] Kriegsmann, J. J.; Cheh, H. Y. *Journal of Power Sources* **1999,** *77,* 127-135.

[4] Rühling, K.; Winsel, A. *Journal of Applied Electrochemistry* **1989,** *19,* 553-558.

[5] Inoue, H.; Kakiuchi, H. US Patent 6,689,506, Sealed Alkaline Storage Battery With Safety Vent Unit, 10 Feb 2004.

[6] Cheiky, M.; Robles, G. US Patent 6,641,949, Battery Vent and Method of Assembly, 4 Nov 2003.

[7] Bouffard, R. L.; Lewis, P. M.; Li, H.; Eldson, J. P. R.; Sweet, W. E.; Wu, J. X. US Patent 7,195,839, Battery Cell With Improved Pressure Relief Vent, 27 March 2007.

[8] Kozawa, A. *Electrochemistry of Manganese Dioxide and Production and Properties of Electrolytic Manganese Dioxide (EMD);* Vol. 1 of *Batteries, Manganese Dioxide* Marcel Dekker, Inc.: New York, 1974.

[9] Kordesch, K.; Weissenbacher, M. *Journal of Power Sources* **1994,** *51,* 61-78.

[10] Kordesch, K.; Gsellmann, J.; Peri, M.; Tomantschger, K.; Chemelli, R. *Electrochimica Acta* **1981,** *26,* 1495-1504.

[11] Raghuveer, V.; Manthiram, A. *Electrochem. Commun.* **2005,** *7,* 1329.

[12] Manickam, M.; Singh, P.; Issa, T. B.; Thurgate, S.; Marco, R. D. *J. Power Sources* **2004,** *130,* 254.

[13] Minteer, S. D. *Magnetic Field Effects on Electron Transfer Reactions,* Ph.D. thesis, University of Iowa, 2000.

[14] Gellett, W. L. *Magnetic Microparticles on Electrodes: Polymer Electrolyte Membrane Fuel Cells, Carbon Monoxide Oxidation, and Transition Metal Complex Electrochemistry,* Ph.D. thesis, University of Iowa, 2004.

[15] Lee, H. C. *Magnetic Field Effects on Electron Transfer Reactions: Heterogeneous Photoelectrochemical Hydrogen Evolution and Homogeneous Self Exchange Reaction,* Ph.D. thesis, University of Iowa, 2011.

[16] Ward, C. B.; Walker, A. I.; Taylor, A. R. *Prog. Batt. Batt. Mater.* **1992,** *11,*.

[17] Kozawa, A.; Yeager, J. F. *Journal of The Electrochemical Society* **1968,** *115,* 1003-1007.

[18] Kozawa, A.; Powers, R. A. *Journal of The Electrochemical Society* **1966,** *113,* 870-878.

[19] Arumugam, P. U.; Fakunle, E. S.; Anderson, E. C.; Evans, S. R.; King, K. G.; Aguilar, Z. P.; Carter, C. S.; Fritsch, I. *Journal of The Electrochemical Society* **2006,** *153,* E185-E194.

[20] Anderson, E. C.; Fritsch, I. *Analytical Chemistry* **2006,** *78,* 3745-3751.

[21] Buchachenko, A. *Russ. Chem. Rev.* **1976,** *45,* 375-390.

[22] Leventis, N.; Gao, X. *Anal. Chem.* **2001,** *73,* 3981-3992.

[23] Fahidy, T. *J. Appl. Electrochem.* **1983,** *13,* 553-563.

[24] Ragsdale, S. R.; Lee, J.; Gao, X.; White, H. S. *Journal of Physical Chemistry* **1996,** *100,* 5913-5922.

[25] Ragsdale, S.; Lee, J.; White, H. *Anal. Chem.* **1997,** *69,* 2072-2076.

[26] Leventis, N.; Gao, X. *J. Am. Chem. Soc.* **2002,** *124,* 1079-1088.

[27] Leddy, J.; Amarasinghe, S.; Zook, L. A.; Tinoco, F. Magnetic Ion Exchange Polymer Composites: Transport Enhancements Driven by Non-Uniform Magnetic Fields and Magnetic Moments of Transported Species. in *Proceedings of the 37th Power Sources Conference*; United States Army Research Laboratory: 1996 pages 93–95.

[28] Amarasinghe, S.; Minteer, S.; Zook, L. A.; Dunwoody, D. C.; Spolar, C.; Chung, H.; Leddy, J. US Patent Application, Field Enhanced Composite Materials and Methods for Making and Using the Same, 29 October 1999.

[29] Wieckowski, A.; Zelenay, P.; Szklarczyk, M.; Sobkowski, J. *Journal of Electroanalytical Chemistry and Interfacial Electrochemistry* **1982,** *135,* 285-299.

[30] Bänsch, B.; Härtung, T.; Baltruschat, H.; Heitbaum, J. *Journal of Electroanalytical Chemistry and Interfacial Electrochemistry* **1989,** *259,* 207-215.

[31] de Hemptinne, X.; Schunck, K. *Transactions of the Faraday Society* **1969,** *65,* 591-597.

[32] Kozawa, A.; Powers, R. A. *Journal of The Electrochemical Society* **1968,** *115,* 122-126.

[33] Kozawa, A.; Yeager, J. F. *Journal of The Electrochemical Society* **1965,** *112,* 959-963.

[34] Kozawa, A.; Kalnoki-Kis, T.; Yeager, J. F. *Journal of The Electrochemical Society* **1966,** *113,* 405-409.

[35] Bard, A.; Faulkner, L. *Electrochemical Methods;* John Wiley & Sons, Inc.: New York, Second ed.; 2001.

[36] Salikhov, K.; Molin, Y.; Sagdeev, R.; Buchachenko, A. *Spin Polarization and Magnetic Effects in Radical Reactions;* Vol. 22 of *Studies in Physical and Theoretical Chemistry* Elsevier: New York, NY, 1984.

[37] White, H. S.; Leddy, J.; Bard, A. J. *J. Am. Chem. Soc.* **1982,** *104,* 4811-4817.

[38] Dunwoody, D. C. *Magnetically Modified Polymer Electrolyte Fuel Cells and Low Temperature Effects on Polymer Electrolyte Nafion,* Ph.D. thesis, University of Iowa, 2003.

[39] Dahms, H. *J. Phys. Chem.* **1968,** *72,* 362-364.

[40] Ruff, I.; Friedrich, V. *J. Phys. Chem.* **1971,** *75,* 3297-3302.

[41] Ruff, I.; Friedrich, V.; Demeter, K.; Csillag, K. *J. Phys. Chem.* **1971,** *75,* 3303-3309.

[42] Ruff, I.; Korosi-Odor, I. *Inorg. Chem.* **1970,** *9,* 186-188.

[43] Wolff, P. M. D. *Acta. Cryst.* **1959,** *12,* 341.

[44] Baur, W. *Acta Crystallographica Section B* **1976,** *32,* 2200-2204.

[45] Byström, A. M. *Acta Chemica Scandinavica* **1949,** *3,* 169-173.

[46] Fleischer, M.; Richmond, W. E.; Jr, H. T. E. *The American Mineralogist* **1962,** *47,* 47-58.

[47] Cahoon, C. N.; Heise, G. W. *The Primary Battery;* Vol. 2 of *The Electrochemical Society Series* Wiley and Sons: New York, 1976.

[48] Faulring, G. *The American Mineralogist* **1965,** *50,* 170-179.

[49] Magnetic Susceptibility of the Elements and Inorganic Compounds, in *CRC Handbook of Chemsitry and Physics*, 85 ed.; Lide, D., Ed.; CRC Press: 2004.

[50] Selwood, P. W.; Eischens, R. P.; Ellis, M.; Wethington, K. *Journal of the American Chemical Society* **1949,** *71,* 3039-3043.

[51] Tesene, J. P. *Magnetically-Treated Electrolytic Manganese Dioxide in Alkaline Electrolyte,* Thesis, University of Iowa, 2005.

[52] Villars, P.; Calvert, L. *Pearson's Handbook of Crystallographic Data for Intermetallic Phases;* Vol. 4 ASM International: Materials Park, OH, 1991.

[53] Will, G. *Acta Crystallographica* **1965,** *19,*.

[54] Caminti, R.; Marongiu, G.; Paschina, G. *Zeitschrift fur Naturforschung* **1982,** *A37,* 581-586.

[55] Barsoukov, E.; Macdonald, J. R. *Impedance Spectroscopy: Theory, Experiment, and Applications;* Wiley-Interscience: Hoboken, N.J., 2005.

[56] Randles, J. E. B. *Disc. Faraday Soc.* **1947,** *1,* 11-19.

[57] Leddy, J.; Tesene, J. P. Published US Patent Application, Publication Number 20070009771, Batteries and battery components with magnetically modified manganese dioxide, 11 January 2007.

[58] Ünlü, M. *Coated Magnetic Particles In Electrochemical Systems: Synthesis, Modified Electrodes, Alkaline Batteries, and Paste Electrodes,* Ph.D. thesis, The University of Iowa, 2008.

[59] Linden, D. *Linden's Handbook of Batteries;* McGraw-Hill, Inc.: New York, 4 ed.; 2011.

[60] Minakshi, M. *Electrochemistry of Cathode Materials in Aqueous Lithium Hydroxide Electrolyte,* Thesis, Murdoch University, 2006.

[61] Minakshi, M.; Ionescu, M. *International Journal of Hydrogen Energy* **2010,** *35,* 7618-7622.

[62] Laffel, L. *Diabetes Metab Res Rev* **1999,** *15,* 412-426.

[63] Kalapos, M. P. *Biochimica et Biophysica Acta* **2003,** *1621,* 122-139.

[64] Phillips, M. *Analytical Biochemistry* **1997,** *247,* 272-278.

[65] Dills, R. L.; Ackerlund, W. S.; Kalman, D. A.; Morgan, M. S. *J. of Exposure Analysis and Epidemiology* **1993,** *3,* 471-489.

[66] Wang, G.; Maranelli, G.; Perbellini, L.; Raineri, E.; Brugone, F. *International Archives of Occupational and Environmental Health* **1994,** *65,* 285-289.

[67] Dills, R. L.; Ackerlund, W. S.; Kalman, D. A.; Morgan, M. S. *J. of Exposure Analysis and Environmental Epidemiology* **1994,** *4,* 229-245.

[68] Basak, S. C.; Mills, D.; El-Masri, H. A.; Mumtaz, M. M.; Hawkins, D. M. *Environmental Toxicology and Pharmacology* **2004,** *16,* 45-55.

[69] Dills, R. L.; Enderlein, C.; Ackerlund, W. S.; Kalman, D. A.; Morgan, M. S. *J. of Exposure Analysis and Environmental Epidemiology* **1994,** *4,* 343-353.

[70] Owen, O. E.; Trapp, V. E.; Skutches, C. L.; Mozzoli, M. A.; Hoeldtke, R. D.; Boden, G.; Reichard, G. A. *Diabetes* **1982,** *31,* 242-248.

[71] Phillips, M.; Herrera, J.; Krishnan, S.; Zain, M.; Greenberg, J.; Cataneo, R. N. *J. Chromatography B* **1999,** *729,* 75-88.

[72] Dahnke, H.; Kahl, J.; Schüler, G.; Boland, W.; Urban, W.; Kuhnemann, F. *Appl. Phys. B* **2000,** *70,* 275-280.

[73] Kundu, S. K.; Bruzek, J. A.; Nair, R.; Judilla, A. M. *Clinical Chemistry* **1993,** *39,* 87-92.

[74] Leddy, J.; Haverhals, L. M. Published US Patent Application, Publication Number 20060130557, Breath-based sensors for non-invasive molecular detection, 22 June 2006.

[75] Leddy, J.; Haverhals, L. M. Published US Patent Application, Publication Number 20050214169, Multicomponent analysis of volatile organic compositions in vapor samples, 29 September 2005.

[76] Haverhals, L. *Fuel Cells as Power Sources and Sensors,* Thesis, The University of Iowa, 2008.

[77] Kissinger, P. T.; Heineman, W. R. *Journal of Chemical Education* **1989,** *60,* 702-706.

[78] Osteryoung, J.; O'Dea, J. J. *Journal of Electroanalytical Chemistry* **1986,** 209-308.

[79] Lovric, M.; Komorsky-Lovric, S.; Murray, R. W. *Electrochimica Acta* **1988,** *33,* 739-744.

[80] Osteryoung, J.; O'Dea, J. J. *Journal of Physical Chemistry* **1990,** *94,* 3628-3636.

[81] Guo, X.; Yun, Y.; Sanov, V. N.; Halsall, B.; Heineman, W. R. *Electroanalysis* **2011,** *23,* 1252-1259.

[82] Yue, W.; Riehl, B. L.; Pantelic, N.; Schlueter, K. T.; Johnson, J. M.; Wilson, R. A.; Guo, X.; King, E. E.; Heineman, W. R. *Electroanalysis* **2012,** *Ahead of Print.,*.

[83] Hardcastle, J. L.; Compton, R. G. *Electroanalysis* **2002,** *14,* 753-759.

[84] Wang, Y.; Laborda, E.; Compton, R. G. *Journal of Electroanalytical Chemistry* **2012,** *670,* 56-61.

[85] Bowden, F. *Proc. Roy. Soc.* **1929,** *A125,*.

[86] Giner, J. *Z. Elektrochem.* **1959,** *63,*.

[87] Will, F. G. *Journal of The Electrochemical Society* **1965,** *112,* 451-455.

[88] Wieckowski, A.; Szklarczyk, M.; Sobkowski, J. *Journal of Electroanalytical Chemistry* **1980,** *113,* 79-97.